University of Alberta

Cryo-electron microscopy of SERCA interacting with oligomeric phospholamban and oligomeric sarcolipin

by

John Paul Glaves

A thesis submitted to the Faculty of Graduate Studies and Research
in partial fulfillment of the requirements for the degree of

Doctor of Philosophy

Biochemistry

Fall 2011
Edmonton, Alberta

Dedicated to my grandfather Joseph Glaves,

your heart was stronger than it let on.

Abstract

In 2007, heart disease was the second leading cause of death in Canadians. In heart muscle cells, calcium (Ca^{2+}) is released from the sarcoplasmic reticulum (SR) during contraction and must be replenished for relaxation to occur. Three proteins restore Ca^{2+} to the SR following contraction: the sarco(endo)plasmic reticulum ATPase (SERCA) and its regulatory binding partners, phospholamban (PLB) and sarcolipin (SLN). The importance and sensitivity of SERCA regulation has been highlighted by identified human mutations in PLB and SLN that lead to heart disease and heart failure. This thesis aims to provide upstream biochemical insights into regulatory complexes formed between SERCA and PLB and between SERCA and SLN for the development of heart disease therapies. The structural information suggests novel interactions between SERCA and its regulatory binding partners.

We studied SERCA-PLB and SERCA-SLN complexes using electron microscopy (EM) of two-dimensional co-crystals. Cryo-EM of SERCA and PLB co-crystals revealed a novel mode of binding between the PLB pentamer and SERCA. The binding site involved the third transmembrane helix of SERCA and represented a site distinct from the SERCA binding site for monomeric PLB. Cryo-EM of SERCA and SLN co-crystals suggested that SLN can also bind the third transmembrane helix of SERCA. The functional mutation of PLB affected co-crystal frequency and the structure of PLB in the projection maps. The co-crystal frequency was directly related to the functional state of PLB. The structure of PLB was also influenced by phosphorylation, but the interaction was maintained between the phosphorylated PLB pentamer and SERCA. Combined, the results support an active, functional interaction between pentamers of PLB and SERCA. The function of the pentameric interaction is proposed to deliver monomeric PLB to its inhibitory interaction with SERCA at a different binding site.

Acknowledgements

The Young lab has been a tremendous experience. Howard provided endless support and stability. I have learned a great amount from following your lead and thank you for a great graduate experience. Thanks for keeping the door open.

Cathy Trieber was a pillar of unyielding help and experience. Cathy provided me with some of my first training in the lab and her continuous good nature and good knowledge continued teaching me things to the very end. Thanks!

Other members of the Young lab have been absolutely critical to this thesis. Michael, Maria, Karine and Jen were the welcoming committee and made my early experience most enriching. I have had the pleasure of working with Delaine, Gina, Grant and Shem as fellow graduate students. Their work has been inspiring and their friendship invaluable. There were many times when they provided a leg to stand on. I have had the pleasure of mentoring some talented undergraduate research students that have contributed to the work present herein. Lily, Jeff and Joe all deserve a big thank you. The current and past members of the lab have always made work a lot easier: Angela, Leah, Ghazelah, Paramita and Ludovic. Thank you.

I would like to thank my examining committee. Dr. Larry Fliegel and Dr. Mark Glover have been insightful members of my supervisory committee. Special thanks to Dr. James Young and Dr. Francesca Marassi for taking valuable time out of their schedules to partake in my examination.

I am indebted to the NINT EM group led by Marek Malac. Julie, Peng, Xiongyao and Jian have all been a great help. I would also like to acknowledge members of the Westaway group and the Jhamandas group for their help and collaboration.

I have met some wonderful people along the way. Some have moved on and some remain. Oliver Kent, Dave Arthur, Steve Chaulk, Jason Lamoreaux and Dave Hau were welcoming veterans in the Department. I'm not sure if I won an argument against Ryan Hoffman, but I still enjoyed every one. Victor Cheng and Quang Tran are great friends that share my passions for membrane proteins and hockey. Jeff Odenbach, Charles Leung and Steven Campbell were great neighbours. Jonny Lacasse has always brought the good times. Mike Shopik was a quiet source of inspiration in the lab, on the ice, and on the slopes. Olivier Julien never turned down a scientific discussion and was an endless source

for advice. Ian Robertson has been a great friend and optimist. Dustin Ritchie feels more like a brother than someone I met 7 years ago.

There has been a huge amount of support outside of the lab. The IceBears and Watchmen have been rivals on the ice, but a common catalyst of hockey fun. Kim, Sue-Ann, Rob, Maureen, Anders, Janelle, Angela, Dara, Greg, Brandie, Rohit, and Tito have been great friends. I consider some of these people family. My Edmonton sister, Renee, had not done one nice thing for me ever until she mothered my Edmonton niece, Harper. My Edmonton parents, J.J. and Bret, have retired to Beaumont but still continue to look out for me.

My family has been outstanding in their support. Janette provided me with a warm start to life in Edmonton and, along with Aarron and Baden, has continued to be an important source of family away from home. My in-laws continue to defy all stereotypes and have been an awesome addition to my family. Ken, Lynn and Kevin, thank you. My parents, Gerry and Germaine, have always encouraged me. Your love has always been strong, even miles from home. Sarah, Gerry, Jason and Dez have been the greatest siblings one could ask. Matthew, Jamison, Megan, Emily and Acaydia have been wonders to be around and unbearable to leave.

My wife, Mel, has been most excellent. You have been an inspiration in every aspect of my life since we met. I cannot thank you enough. You have all of my love.

Table of Contents

List of Tables

List of Figures

Chapter 2.

Chapter 3.

Chapter 4.

Chapter 5.

Chapter 6.

Appendix I.

Appendix II.

List of Abbreviations

Ca^{2+}	calcium
Mg^{2+}	magnesium
H^{+}	proton
ATP	adenosine triphosphate
SERCA	sarco(endo)plasmic reticulum Ca^{2+} ATPase
PLB	phospholamban
SLN	sarcolipin
SR	sarcoplasmic reticulum
EM	electron microscopy
ADP	adenosine diphosphate
P-domain	phosphorylation domain
N-domain	nucleotide-binding domain
A-domain	actuator domain

PKA	protein kinase A
CaMKII	Ca^{2+}-calmodulin-dependent protein kinase
TG	thapsigargin
BHQ	dibutyl-dihydroxybenzene
CPA	cyclopiazonic acid
NMR	nuclear magnetic resonance
EPR	electron paramagnetic resonance
FRET	fluorescence resonance energy transfer
TM	transmembrane domain
TM(num)	transmembrane helix number (num)
pdb	Protein Data Bank (www.rcsb.org/pdb/) identifier
EBI	European Bioinformatics Institute
V_{max}	maximum reaction rate
K_{Ca}	apparent Ca^{2+} affinity
AFA-PLB	PLB with cysteines 36, 41 and 46 mutated to alanines
PLB-tm	PLB residues 34 to 52
SLN-tm	SLN residues 11 to 31
$C_{12}E_8$	octaethylene glycol monododecyl ether
EYPC	egg yolk phosphatidyl choline
EYPA	egg yolk phosphatidic acid
EYPE	egg yolk phosphatidyl ethanolamine
EDTA	ethylene diamine tetraacetic acid

EGTA	ethylene glycol tetraacetic acid
wt	wild-type
ctrl	control
TEV	tobacco etch virus
IPTG	isopropyl beta-D-1-thiogalactopyranoside
GdnHCl	guanidine hydrochloride
HPLC	high-pressure liquid chromatography
ER	endoplasmic reticulum
CFP	cyan fluorescent protein
YFP	yellow fluorescent protein
BeF_3^-	beryllium fluoride
FITC	fluoroscein isothiocyanate
BMH	1,6-bismaleimidohexane
AMP	adenosine monophosphate
AMPPCP	5'-adenylyl (beta, gamma-methylene) diphosphonate
TNP-AMP	(2',3'-(2,4,6-trinitrophenyl-AMP
PrP	prion protein
PrP^c	cellular form of PrP
PrP^{Sc}	scrapie form of PrP
PrP(106-126)	peptide of PrP residues 106 to 126
PrP(127-147)	peptide of PrP residues 127 to 147
TSE	transmissible spongiform encephalopathy

CJD	Cruetzfeldt-Jakob disease
BSE	bovine spongiform encephalopathy
CWD	chronic wasting disease
GSS	Gertsmann-Straussler-Schienker syndrome
ThT	thioflavin T
AFM	atomic force microscopy
MTT	3-(4,5-Dimethylthiazol-2-yl)-2,5-diphenyltetrazolium bromide
LB	Luria broth
OD_{600}	optical density at 600 nm
TrisHCl	trishydroxymethylaminomethane hydrochloride
TBS	tris buffer saline
PBS	phosphate buffer saline
TCA	trichloroacetic acid
HRP	horse radish peroxidase
MALDI-TOF	multi-absorption laser de-ionization time-of-flight
SDS-PAGE	sodium dodecyl sulphate polyacrylamide gel electrophoresis
kDa	kilo Dalton
DTT	dithiolthreitol
SEM	standard error of the mean
mRNA	messenger ribonucleic acid
DNA	deoxyribonucleic acid
PCR	polymerase chain reaction

2D	two-dimensional
3D	three-dimensional
Min	minimum
Max	maximum

Standard Amino Acids

Glycine	Gly	G
Alanine	Ala	A
Valine	Val	V
Leucine	Leu	L
Isoleucine	Ile	I
Methionine	Met	M
Proline	Pro	P
Phenylalanine	Phe	F
Tryptophan	Trp	W
Serine	Ser	S
Threonine	Thr	T
Tyrosine	Tyr	Y
Asparagine	Asn	N
Glutamine	Gln	Q
Cysteine	Cys	C
Lysine	Lys	K
Arginine	Arg	R
Histidine	His	H
Aspartic Acid	Asp	D
Glutamic Acid	Glu	E

Chapter 1.

Introduction.

"Chemistry is not something you can manufacture".

-Oprah Winfrey

Chapter 1. Introduction.

1-1. Thesis rationale.

In 2007, heart disease was the second leading cause of death among men and women in Canada with an estimated economic burden of over $20 billion (Statistics Canada – www.statcan.gc.ca). This thesis aims to provide insights into molecular mechanisms directly and intimately involved in human heart disease. By understanding these mechanisms in greater detail we can provide a framework for the development of therapies aimed at ameliorating this devastating disease.

1-2. Calcium, calcium, calcium!!!

The movement of ions and molecules across membranes is vital for many cellular processes. Calcium (Ca^{2+}) is central to a number of cellular processes including neurotransmission, neurosecretion, egg fertilization, and excitation-contraction coupling in muscle tissue[1, 2]. These processes rely on the maintenance of low cytosolic Ca^{2+} concentrations within the cell.

Excitation-contraction coupling in muscle cells requires a temporary increase in cytosolic Ca^{2+} following depolarization, known as the Ca^{2+} transient. The Ca^{2+} transient activates the contractile apparatus leading to muscle cell shortening. For relaxation to occur, the cytoplasmic Ca^{2+} concentration must be lowered to its resting concentration. This is primarily achieved by the activity of the sarcoplasmic reticulum Ca^{2+}-ATPase (SERCA). At the expense of ATP, SERCA transports two cytoplasmic Ca^{2+} ions[3] into the sarcoplasmic reticulum (SR) lumen against its concentration gradient. As a result, SERCA determines the intracellular Ca^{2+} store that is available for the next contraction. Thus, SERCA activity is fundamental to rates of muscle relaxation and Ca^{2+} transient amplitudes that determine the strength of contraction.

1-3. SERCA as a model P-type ATPase.

P-type ATPases are a family of ion pumps central to cellular transport in archaea, bacteria and eukaryotes, named for the formation of a phosphorylated intermediate during their transport cycle[4, 5]. The first identified P-type ATPase was the Na^+-K^+ ATPase in 1957 by Nobel Laureate Jens Christian Skou[6]. Members of the P-type ATPase family now include SERCA, the Na^+-K^+ ATPase, the H^+-K^+ ATPase, the H^+-ATPase and heavy-metal transporters. P-type ATPases share structural similarities and, although they transport different substrates, are thought to use common molecular mechanisms[5].

SERCA was the first P-type ATPase to have its three-dimensional structure determined[7] and currently we have atomic resolution structures of almost every intermediate in the SERCA transport cycle[2]. We have an excellent structural understanding of how SERCA binds ATP and Ca^{2+}, details of the conformational changes that occur during transport, and even how small molecules can function to inhibit SERCA activity. As such, SERCA is the best characterized member of the P-type ATPase family and provides a framework for the study of other members of the P-type ATPase family. *However, despite the wealth of information available for SERCA, we still do not have a full grasp on how SERCA couples the hydrolysis of ATP to the transport of* Ca^{2+}.

1-4. The role of SERCA in human heart disease.

Three genes encode SERCA (SERCA1, SERCA2, and SERCA3) and splice variants of these three genes are differentially expressed in human tissues[8]. SERCA1 is expressed in fast-twitch skeletal muscle, SERCA2 in cardiac and smooth muscle, and SERCA3 is expressed in low amounts in a variety of tissues[8]. Ten splice variants of SERCA have been identified, which are also regulated during development[9]. For example, SERCA1b is the predominant isoform in developing fast-twitch skeletal muscle and SERCA1a is the predominant isoform in adult fast-twitch skeletal muscle[8]. SERCA2a is the predominant isoform in adult cardiac muscle and SERCA2b is the predominant isoform in smooth muscle. SERCA2a is identical to SERCA2b, except the 4 C-terminal residues of SERCA1a are replaced by an additional 49 residue "tail" in SERCA2b.

Altered Ca^{2+}-handling is a hallmark of human heart failure[10] and many studies agree that SERCA2a levels are decreased in human heart failure[9, 11]. Recently, contractile function in failing heart muscle was improved using SERCA gene transfer[9, 12]. SERCA2a was

over-expressed by adenoviral gene transfer into cardiac myocytes from patients with end-stage heart failure. The over-expression of SERCA2a enhanced contraction and rates of relaxation[9, 12]. *Such evidence suggests SERCA holds potential as a therapeutic target for human disease.*

1-5. Dysregulation of SERCA by phospholamban and sarcolipin in heart disease.

Phospholamban (PLB) is a small SR protein that regulates SERCA in cardiac and smooth muscle. PLB binds and inhibits SERCA by lowering its apparent Ca^{2+} affinity. Studies of mouse atrial and ventricular muscle have shown that differentially expressed levels of PLB reflect their different rates of force development and relaxation[13]. Mouse atrial muscle, which has a relatively low PLB to SERCA ratio compared to ventricular muscle, has faster rates of contraction and relaxation. PLB knockout mice also exhibit enhanced ventricular contractility compared to wild-type mice. These results suggest the relative PLB to SERCA ratio is a critical determinant of myocardial contractility[13]. Genetic expression studies have suggested that alterations in the ratio of PLB to SERCA might be a hallmark of human heart failure[14]. *For this reason, PLB has become a target for the development of therapeutic strategies for the clinical improvement of contractility in failing hearts[14].*

The importance of PLB in cardiac function is underscored by the identification of PLB mutations that cause human heart disease. The PLB mutation $Arg^{9}Cys$ causes inherited dilated cardiomyopathy with an average age of death of 25 years in affected individuals[15]. Recapitulated in transgenic mice, the PLB-$Arg^{9}Cys$ mutation altered PLB phosphorylation, an important mechanism in relieving inhibition of SERCA[15]. A PLB truncation, $Leu^{39}stop$, was attributed to recessive dilated cardiomyopathy causing heart failure in the second decade of life[16]. Characterized by heterologous expression, PLB-$Leu^{39}stop$ caused protein instability and mis-targeting of PLB localization[16]. A third PLB mutation, deletion of Arg^{14} (ΔArg^{14}), led to hereditary heart failure of heterozygous individuals in a large family[17]. Similar to the PLB-$Arg^{9}Cys$ mutation, the ΔArg^{14} mutation also resulted in dilated cardiomyopathy. Recapitulated in transgenic mice, the PLB-ΔArg^{14} mutation caused cardiomyopathy and premature death. Characterized by heterologous expression, PLB-ΔArg^{14} resulted in super-inhibition of SERCA that was not fully relieved by phosphorylation[17]. *Since the dysregulation of SERCA by PLB can*

adversely affect cardiac function, manipulation of PLB could be a therapeutic approach to improve cardiac function in failing hearts.

Sarcolipin (SLN) is a small SR protein that regulates SERCA in fast-twitch skeletal muscle and the atria of the heart. Aberrant expression of SLN in ventricular muscle has been described in Tako-Tsubo cardiomyopathy patients[18]. Tako-Tsubo cardiomyopathy is also known as "broken heart syndrome" and causes contractile dysfunction following emotional or physical stress. *Therefore, SLN could be another important therapeutic target for improving cardiac function.*

There are a number of avenues to target SERCA regulation by PLB and SLN, such as gene transfer to directly alter the SERCA to PLB (or SLN) ratio, or altering or disrupting functional interactions between SERCA and PLB (or SLN). These target avenues stem from an incomplete understanding of the molecular mechanisms used by PLB and SLN to regulate SERCA. *For this reason, furthering our knowledge of PLB and SLN will be important for developing heart disease therapies. Even if we do not directly target PLB and SLN, understanding their interactions with SERCA in greater detail will aid in the targeting of SERCA activity.*

1-6. Structural insights into the molecular mechanisms of SERCA regulation by PLB and SLN.

The central aims of this thesis are to further our understanding of PLB and SLN, the physiological regulators of SERCA in cardiac muscle. We currently have an incomplete understanding of how PLB and SLN interact with SERCA. Our understanding is limited due to a lack of high-resolution structures of SERCA bound to PLB, or SERCA bound to SLN, making it difficult to delineate their molecular mechanisms. We address this using cryo-electron crystallography of SERCA-PLB co-crystals and SERCA-SLN co-crystals. Structural information from these co-crystals describes a novel interaction of PLB and SLN with SERCA. We propose PLB and SLN bind as oligomers to SERCA and this interaction is important for SERCA regulation.

We are also only beginning to understand SLN. It has long been assumed that SLN acts similar to PLB because of a high degree of sequence homology, however, evidence is mounting that this is not the case. We have functionally characterized residues in SLN in the first extensive study with SERCA in a purified system, which highlights key differences between SLN and PLB. Understanding SLN in greater detail has become an

important goal with recent evidence that SLN is expressed in the atria[19-23]. SLN works with PLB to regulate SERCA in the atria and, thus, insights into SLN mechanisms will aid in development of heart disease therapies.

This thesis is organized as follows. Chapter 2 begins with a chronological exploration of Ca^{2+} transport, culminating in atomic resolution structures of SERCA transport intermediates. The physiological regulators of SERCA are then introduced with a review of our current understanding of PLB and SLN. Chapters 3, 4, and 5 address some of the discrepancies and gaps in our understanding by contributing novel insights into the molecular mechanisms of PLB and SLN.

1-7. References.

1. Carafoli E. Calcium signaling: A tale for all seasons. Proc Natl Acad Sci U S A 2002 FEB 5;99(3):1115-22.

2. Moller JV, Olesen C, Winther AL, Nissen P. The sarcoplasmic Ca2+-ATPase: Designof a perfect chemi-osmotic pump. Q Rev Biophys 2010 NOV;43(4):501-66.

3. Inesi G, Kurzmack M, Coan C, Lewis DE. Cooperative calcium-binding and atpase activation in sarcoplasmic-reticulum vesicles. J Biol Chem 1980;255(7):3025-31.

4. Moller JV, Juul B, leMaire M. Structural organization, ion transport, and energy transduction of P-type ATPases. Biochimica Et Biophysica Acta-Reviews on Biomembranes 1996 MAY 6;1286(1):1-51.

5. Kuhlbrandt W. Biology, structure and mechanism of P-type ATPases. Nature Reviews Molecular Cell Biology 2004 APR;5(4):282-95.

6. Skou JC. The influence of some cations on an adenosine triphosphatase from peripheral nerves. Biochim Biophys Acta 1957;23(2):394-401.

7. Toyoshima C, Nakasako M, Nomura H, Ogawa H. Crystal structure of the calcium pump of sarcoplasmic reticulum at 2.6 angstrom resolution. Nature 2000 JUN 8;405(6787):647-55.

8. Simmerman HKB, Jones LR. Phospholamban: Protein structure, mechanism of action, and role in cardiac function. Physiol Rev 1998 OCT;78(4):921-47.

9. Periasamy M, Kalyanasundaram A. SERCA pump isoforms: Their role in calcium transport and disease. Muscle Nerve 2007 APR;35(4):430-42.

10. Morgan JP. Mechanisms of disease - abnormal intracellular modulation of calcium as a major cause of cardiac contractile dysfunction. N Engl J Med 1991 AUG 29;325(9):625-32.

11. MacLennan DH, Kranias EG. Phospholamban: A crucial regulator of cardiac contractility. Nature Reviews Molecular Cell Biology 2003 JUL;4(7):566-77.

12. del Monte F, Harding SE, Schmidt U, Matsui T, Kang ZB, Dec W, Gwathmey JK, Rosenzweig A, Hajjar RJ. Restoration of contractile function in isolated cardiomyocytes from failing human hearts by gene transfer of SERCA2a. Circulation 1999 DEC 7;100(23):2308-11.

13. Koss KL, Grupp IL, Kranias EG. The relative phospholamban and SERCA2 ratio: A critical determinant of myocardial contractility. Basic Res Cardiol 1997;92:17-24.

14. Koss KL, Kranias EG. Phospholamban: A prominent regulator of myocardial contractility. Circ Res 1996 DEC;79(6):1059-63.

15. Schmitt JP, Kamisago M, Asahi M, Li GH, Ahmad F, Mende U, Kranias EG, MacLennan DH, Seidman JG, Seidman CE. Dilated cardiomyopathy and heart failure caused by a mutation in phospholamban. Science 2003 FEB 28;299(5611):1410-3.

16. Haghighi K, Kolokathis F, Pater L, Lynch RA, Asahi M, Gramolini AO, Fan GC, Tsiapras D, Hahn HS, Adamopoulos S, Liggett SB, Dorn GW, MacLennan DH, Kremastinos DT, Kranias EG. Human phospholamban null results in lethal dilated cardiomyopathy revealing a critical difference between mouse and human. J Clin Invest 2003 MAR;111(6):869-76.

17. Haghighi K, Kolokathis F, Gramolini AO, Waggoner JR, Pater L, Lynch RA, Fan GC, Tsiapras D, Parekh RR, Dorn GW, MacLennan DH, Kremastinos DT, Kranias EG. A mutation in the human phospholamban gene, deleting arginine 14, results in lethal, hereditary cardiomyopathy. Proc Natl Acad Sci U S A 2006 JAN 31;103(5):1388-93.

18. Nef HM, Moellmann H, Troidl C, Kostin S, Voss S, Hilpert P, Behrens CB, Rolf A, Rixe J, Weber M, Hamm CW, Elsaesser A. Abnormalities in intracellular Ca2+ regulation contribute to the pathomechanism of tako-tsubo cardiomyopathy. Eur Heart J 2009 SEP;30(17):2155-64.

19. Minamisawa S, Wang YB, Chen J, Ishikawa Y, Chien KR, Matsuoka R. Atrial chamber-specific expression of sarcolipin is regulated during development and hypertrophic remodeling. J Biol Chem 2003 MAR 14;278(11):9570-5.

20. Vangheluwe P, Schuermans M, Zador E, Waelkens E, Raeymaekers L, Wuytack F. Sarcolipin and phospholamban mRNA and protein expression in cardiac and skeletal muscle of different species. Biochem J 2005 JUL 1;389:151-9.

21. Babu GJ, Bhupathy P, Carnes CA, Billman GE, Periasamy M. Differential expression of sarcolipin protein during muscle development and cardiac pathophysiology. J Mol Cell Cardiol 2007 AUG;43(2):215-22.

22. Babu GJ, Bhupathy P, Timofeyev V, Petrashevskaya NN, Reiser PJ, Chiamvimonvat N, Periasamy M. Ablation of sarcolipin enhances sarcoplasmic reticulum calcium transport and atrial contractility. Proc Natl Acad Sci U S A 2007 NOV 6;104(45):17867-72.

23. Bhupathy P, Babu GJ, Periasamy M. Sarcolipin and phospholamban as regulators of cardiac sarcoplasmic reticulum Ca2+ ATPase. J Mol Cell Cardiol 2007 MAY;42(5):903-11.

Chapter 2.

SERCA structure and regulation circa 2011.

in·hib·it·ed/

Adjective: Unable to act in a relaxed and natural way because of self-consciousness or mental restraint.

-Dictionary.com

Chapter 2. SERCA structure and regulation circa 2011.

2-1. E1-E2 models of enzymatic transport.

Before we begin a detailed exploration of SERCA structure, it is worthwhile to cover some history of intermediates in enzymatic transport. Unlike channels, transporters undergo conformational changes to carry ions or molecules across the lipid bilayer. Early active transport models were based on two conformations of the transporting enzyme, E1 and E2[1, 2]. The E1 state presented a high affinity binding site for the transported substrate to one side of the membrane, and the E2 state presented a low affinity site to the opposite side. By interconversion between the E1 and E2 states, the transporting enzyme produces vectorial transport across a membrane. The E1-E2 model for active transport was initially used to describe transport by the Na^+/K^+-ATPase[1, 2] and later for transport by SERCA[3]. It was proposed that different transporters used common mechanisms to transport a wide variety of ions and molecules[1].

Early E1-E2 models involved more intermediates, specifically well-established phosphorylated states that couple the hydrolysis of ATP to transport[1-3]. In such a way, the transport of ions or molecules across a membrane and to a higher electrochemical potential was achieved at an energetic cost. The concentration gradient resulting from substrate transport serves as a potential energy source for other cellular work[1]. These additional states were denoted E1-P and E2-P to reflect their phosphorylated states[1-3]. The complete cycle of E1 to E1-P to E2-P to E2 and conversion to E1 to begin the cycle anew, became known as the Post-Albers Cycle[4]. We will begin with the Post-Albers cycle for the transport of Ca^{2+} by SERCA as it was described in 1979[3].

SERCA, embedded in the sarcoplasmic reticulum membrane, begins the cycle in the E1 state, with a high affinity site for Ca^{2+} facing the cytoplasm. The affinity of the E1 site for Ca^{2+} is experimentally 0.2 to 2 μM at pH 7.0[3]. Following Ca^{2+} binding at the cytoplasmic surface, the terminal γ-phosphate of ATP is transferred to an aspartyl residue, forming an acyl-phosphate in the E1-P state. This autophosphorylation event requires ATP complexed with magnesium (Mg^{2+}) and facilitates transition to the E2-P state. Ca^{2+} is released from the E2-P state prior to hydrolysis of the phosphoenzyme to the E2 state[3]. The affinity of the E2 site for Ca^{2+} is experimentally 1 to 3 mM at pH 7.0[3]. Thus, the Ca^{2+} affinity of the E2 state is approximately 1000-fold lower than the Ca^{2+} affinity of the E1 state. It was postulated that interconversion of intermediates in the Ca^{2+} transport cycle should involve conformational changes in SERCA and ample evidence was building for such conformational changes[3].

Our current understanding of the Post-Albers cycle is more detailed[4, 5]. Most notably, it is well established that the low-affinity E2 state has a high-affinity for a counter-transported ion. In the case of SERCA, two to three protons are counter-transported from the SR lumen into the cytoplasm[5-8]. As well, occluded states are proposed to alternate between openings of the binding sites to different sides of the membrane[5, 9]. For these reasons, our present definition of E1 and E2 do not define the binding sites as opened to the cytoplasm or lumen, but rather refer to conformational states with high-affinity for Ca^{2+} (E1) or H^+ ions (E2)[5]. Finally, it is generally agreed that nucleotide (ATP or ADP) is bound SERCA throughout the transport cycle under physiological conditions[5].

A general overview of the SERCA transport cycle is shown in Figure 2.1. Two cytoplasmic Ca^{2+} ions bind to the high-affinity E1-ATP state forming $(Ca^{2+})_2$-E1-ATP. The binding of Ca^{2+} leads to autophosphorylation by Mg^{2+}-ATP at Asp^{351} and formation of the $(Ca^{2+})_2$-E1-P-ADP high-energy intermediate (Figure 2.1). At this point in the cycle, Ca^{2+} is in an occluded state and is not accessible from the cytoplasm or lumen. Transition to the $(Ca^{2+})_2$-E2-P-ADP state lowers the Ca^{2+}-affinity and ADP is exchanged for ATP[5]. The Ca^{2+} ions remain occluded in the $(Ca^{2+})_2$-E2-P-ATP state. Luminal opening occurs during the transition to the $(H^+)_n$-E2-P-ATP state when two Ca^{2+} ions are released into the SR lumen and two to three luminal H^+ bind. The protons are released to the cytoplasm accompanied by dephosphorylation. Back in the E1-ATP state the ion-binding site is now available to bind two cytoplasmic Ca^{2+} ions and begin the cycle anew (Figure 2.1).

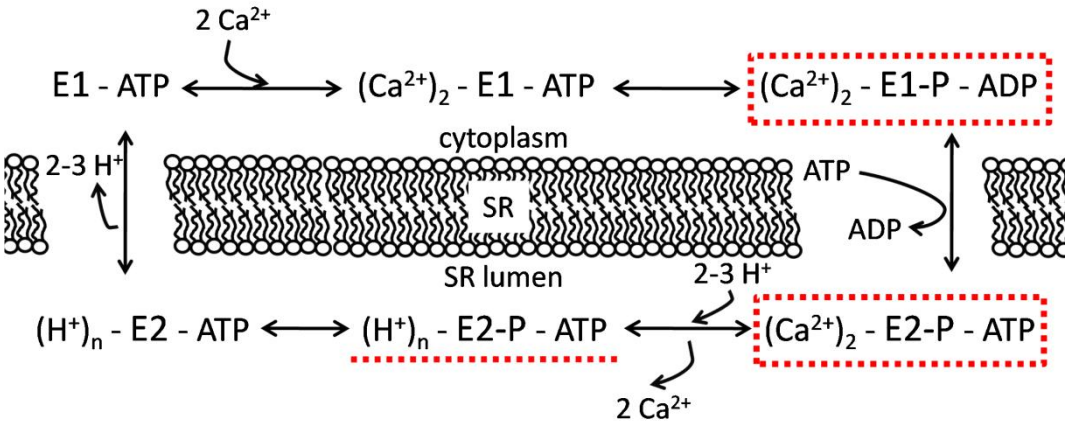

Figure 2.1. Schematic of the Post-Albers cycle for SERCA. The two conformations of SERCA are denoted as E1 and E2. The E1 state has a high-affinity for Ca^{2+} and the E2 state has a high-affinity for H^+. Intermediates with occluded binding sites are indicated by dashed red boxes. The $(H^+)_n$-E2-P-ATP state is underlined in red because high resolution crystal structures have been determined in both occluded and lumen-accessible conformations. The direction of arrows associated with Ca^{2+} and H^+ ions indicate the sidedness of binding or release with respect to the SR membrane. The exchange of ATP for ADP occurs in the cytoplasmic domains of SERCA.

2-2. Milestones in P-type ATPase structure: Structural studies of SERCA reveal transport intermediate conformations at the atomic level.

2-2.1. The structure of SERCA to 8 Å resolution.

In the early 1990s, researchers were anxious to visualize the structure of SERCA. Mutagenesis had identified many functional sites in the enzyme[10-13] and the involvement of transmembrane helices 4, 5, 6, and 8 (TM4, TM5, TM6 and TM8) in the binding of Ca^{2+} ions[14]. In addition, the predicted secondary structure of SERCA led to the proposal of ten transmembrane helices[15]. But how did all of these residues fit together in three-dimensional space?

In 1993, the SERCA field was granted its first view of SERCA by cryo-electron microscopy. There was structural information about SERCA at this time, but it was primarily limited to low resolution information of the cytoplasmic domain[16, 17]. Electron microscopy of frozen-hydrated specimens of tubular crystals provided the first view of the entire SERCA structure to 14 Å resolution[18]. The SERCA tubular crystals were grown in the presence of vanadate, which had previously produced two-dimensional (2D) crystals of the Na^+-K^+ ATPase[19] and 2D crystals of SERCA[20]. It was later shown that decavanadate was a key component for crystal formation[21]. As had been observed previously[16, 17, 20], the SERCA molecules crystallized in an anti-parallel dimer ribbon. Although "unexpectedly thin"[18], the nearly continuous density of the membrane bilayer allowed the density within to be assigned as the transmembrane domain. The large cytoplasmic head of SERCA and the transmembrane domain were linked by a 25 Å "stalk". The cytoplasmic domain resembled the "head" and "beak" of a bird with the "stalk" as the neck (Figure 2.2). The cytoplasmic portion accounted for ~70% of the total mass of SERCA and its asymmetric appearance. It would later be shown that the "head" is composed of two domains; the phosphorylation domain (P-domain) and the nucleotide-binding domain (N-domain)[22]. The "beak" is composed of a third cytoplasmic domain, the actuator domain (A-domain)[22]. Strands of each dimer ribbon were linked by interactions between the large cytoplasmic heads and neighbouring dimer ribbons were linked by the luminal portions of SERCA. A distinct channel between two of the transmembrane segments at the luminal side of the membrane was hypothesized to serve as a Ca^{2+} exit pathway[18]. This would be consistent with reports that tubular crystals of SERCA are composed of the E2 state[20, 23].

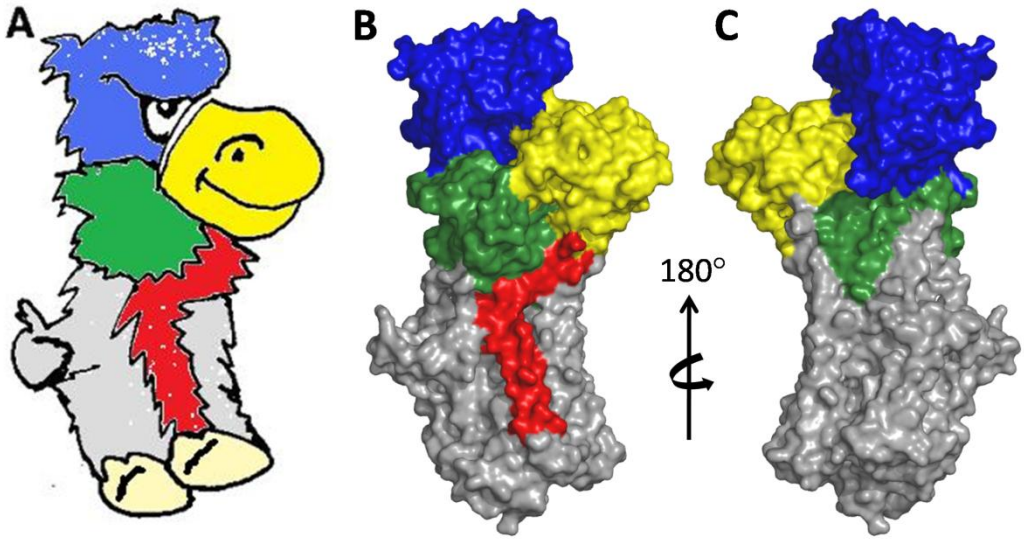

Figure 2.2. The asymmetric bird-like appearance of SERCA by cryo-electron microscopy of tubular crystals. Panel A, an artist's rendering of the bird-like appearance of SERCA. **Panel B,** a surface representation of SERCA from tubular crystals formed with bound TG and decavanadate (pdb: 1KJU)[24]. The three cytoplasmic domains of SERCA form the head and beak: the P-domain is green, the N-domain is blue and the A-domain is yellow. The transmembrane domain is coloured grey with TM3 highlighted in red. **Panel C,** rotation of panel B by 180° along the y-axis as indicated.

In 1998, a more detailed view of the transmembrane domain was accomplished by improving the SERCA structure to 8 Å resolution[25]. Using cryo-electron microscopy of tubular SERCA crystals, the structure was improved by including a fluorescent derivative of thapsigargin (TG), a high-affinity small molecule inhibitor of SERCA. Overall, the structure was similar with the "head" and "beak" cytoplasmic arrangement connected to the transmembrane domain. However, rather than split into segments, the transmembrane domain was now observed as ten transmembrane helices consistent with the proposed model[15]. Tentative sequence assignments for the transmembrane helices were made[25] to predict the locations of the Ca^{2+}-binding residues identified by mutagenesis studies[14, 26-29]. These tentative assignments would require higher resolution information to be verified. At this point, our understanding of SERCA structure would benefit most if we could reach atomic resolution to discern side chain orientations and interactions. This was, no doubt, a very lofty goal.

2-2.2. The high-resolution structure of SERCA in the $(Ca^{2+})_2$-E1 state.

Within two years, our view of SERCA reached atomic resolution with the publication of the x-ray crystal structure of SERCA bound to two Ca^{2+} ions by Toyoshima and coworkers[22]. The new SERCA structure represented the $(Ca^{2+})_2$-E1 intermediate and, when combined with the 8 Å resolution E2-TG structure, permitted structural comparison of E1 and E2 transport intermediates. Upon its publication, the 2.6 Å SERCA structure provided answers to many of the outstanding questions about SERCA structure and function.

All 994 residues of SERCA could be identified in the final electron density from the Ca^{2+}-bound x-ray crystal structure and were assigned to specific structural regions of the enzyme. The cytoplasmic headpiece was split into three well-separated domains; the P-domain, N-domain, and A-domain (Figure 2.3a). This well-separated arrangement of the three cytoplasmic domains differed from the more compact arrangement observed in the low-resolution SERCA structures by EM. The conserved phosphorylation site, Asp^{351}, is located on the central P-domain and is well separated from the N-domain containing the bound nucleotide analog TNP-AMP (2',3'-(2,4,6-trinitrophenyl)-AMP). Thus, the P-domain and the N-domain are splayed apart in the $(Ca^{2+})_2$-E1 crystal structure (Figure 2.3a). This observation provided a structural explanation for the long-standing debate as to which domain was responsible for nucleotide-binding and phosphorylation. The crystal

structure showed that it was not the activity of a single domain, but these activities were shared by the P-domain and N-domain and would thus require their co-ordination. The third cytoplasmic domain, the A-domain, was also well-separated from the central P-domain and the N-domain (Figure 2.3a).The SERCA x-ray crystal structure also resolved the transmembrane domain into ten transmembrane helices. TM7 to TM10 exist as a separated platform, distinct from the central part of the enzyme (Figure 2.3a). The central part of the transmembrane domain contains most of TM4, TM5, TM6 and TM8 which form the Ca^{2+}-binding sites. TM4 and TM5 extend from the membrane and serve as the "stalk" between the transmembrane and cytoplasmic domains.

The Ca^{2+}-binding sites merit special discussion. As mentioned, the residues composing the Ca^{2+}-binding sites had been predicted from mutational studies, but the exact nature of the sites was revealed from the SERCA x-ray crystal structure. Both Ca^{2+}-binding sites (named site I and site II) are at similar heights with respect to the membrane and 5.7 Å away from each other (Figure 2.3b). Site I is located between TM5 and TM6, with distal contributions from TM8, and is composed solely of side-chain oxygen atoms. Site II is mainly formed by TM4 main-chain carbonyl and side-chain oxygen atoms. Experimentally it has been demonstrated that Ca^{2+} binding occurs in steps; first a Ca^{2+} ion binds to site II and is then passed to site I and, subsequently, a second Ca^{2+} ion binds co-operatively to site II[30]. Of particular interest, is the unwinding and disruption of helical secondary structure in TM4 around the calcium-binding sites (Figure 2.3b). This unwinding is necessary for residues close in sequence to contribute to the Ca^{2+}-binding sites. Excitingly, this mode of helix-unwinding may be a common mechanism used for cation co-ordination as unwound helices are also observed in the Na^{+}-H^{+} exchanger from prokaryotes[31] and in nuclear magnetic resonance (NMR) studies of isolated hydrophobic helices of the human Na^{+}-H^{+} exchanger[32, 33].

Comparison of the $(Ca^{2+})_2$-E1 crystal structure of SERCA with the E2-TG tubular crystal structure suggested large-scale movements of the cytoplasmic domains. The most striking difference is the splayed apart nature of the N-domain and P-domains in the $(Ca^{2+})_2$-E1 state that contrasts with the compact "head" in the E2-TG state (Figure 2.4). In the $(Ca^{2+})_2$-E1 state, the P-domain phosphorylation site (Asp^{351}) is more than 25 Å away from the TNP-AMP bound in the N-domain. Thus, the P-domain and the N-domain must come together for efficient auto-phosphorylation and presumably adopt a compact conformation similar to E2-TG state.

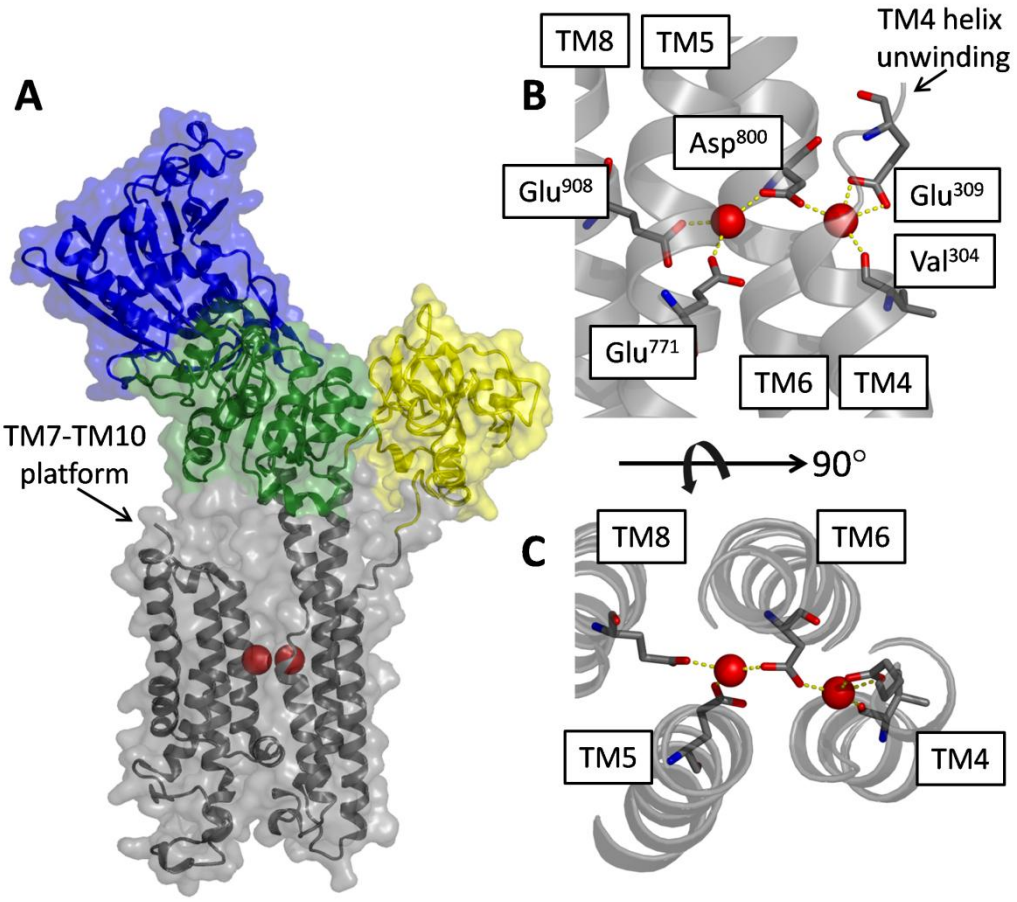

Figure 2.3. The 2.6 Å structure of SERCA bound to two Ca^{2+} ions. Panel A, the $(Ca^{2+})_2$-E1 state of SERCA shown as a cartoon representation with a transparent surface (pdb: 1SU4)[22]. The cytoplasmic domains are coloured as in Figure 2.2 (the P-domain is green, the N-domain is blue and the A-domain is yellow). The transmembrane domain is coloured grey. The two bound Ca^{2+} ions are shown as red spheres. Transmembrane helices 3, 5 and 6 have been removed for clarity of the Ca^{2+} ions. **Panel B,** a close-up view of the Ca^{2+}-binding sites in the same orientation as panel A (site I is on the *left* and site II is on the *right*). Select ligating residues and transmembrane helices are labelled. Co-ordination of the Ca^{2+} ions by atoms in SERCA is indicated by yellow dashed lines. For clarity, transmembrane helices not involved in Ca^{2+} co-ordination have been removed and not all of the ligating residues are shown. **Panel C,** rotation of panel B by 90° around the x-axis as indicated. Labelled as in panel A with the backbone atoms of Glu^{309} removed for clarity.

Although the x-ray crystal structure of SERCA in the calcium-bound state provided us with a lot of answers, it also raised a lot of new questions, particularly about the nature of the large-scale conformational changes between SERCA intermediates. In particular, how these changes in the cytoplasmic domains might translate to changes in the transmembrane domain and the Ca^{2+}-binding sites. The field anxiously awaited a second high-resolution structure of SERCA that might directly answer these questions, but how long would we have to wait?

2-2.3. "We eagerly await future crystals structures of the various reaction intermediates"[24]

Following the Ca^{2+}-bound SERCA structure at atomic resolution, Stokes and coworkers improved the resolution of SERCA in the E2-TG state. The resolution was improved from 8 Å to 6 Å by increasing the number of tubular crystals in the structure calculation. This improvement allowed a better comparison of the $(Ca^{2+})_2$-E1 and E2-TG states than the domain fitting performed after the initial release of the $(Ca^{2+})_2$-E1 crystal structure. Overall, the improved model involved conformational changes similar to the original model. The authors also reported the E2-TG structure bound to decavanadate was more similar to E2-P than E2, because the proteolytic sensitivity of decavanadate-bound SERCA more closely resembled that of E2-P[24, 34]. A structure was also determined for fluoroscein isothiocyanate (FITC)-labelled SERCA, which covalently attaches to Lys^{515} in the nucleotide-binding pocket and prevents ATP binding[24, 35]. The primary reason for determining the FITC-SERCA structure was to investigate the contributions of decavanadate to the E2-TG SERCA structure. The density at the intersection of the cytoplasmic domains assigned to bound decavanadate[22] was absent in the FITC-labelled structure[24]. Overall, the FITC-SERCA structure was similar to the decavanadate-bound E2-TG structure, suggesting that the E2-TG structure is not artefactually influenced by decavanadate and likely represents an E2 conformation in the SERCA transport cycle[24].

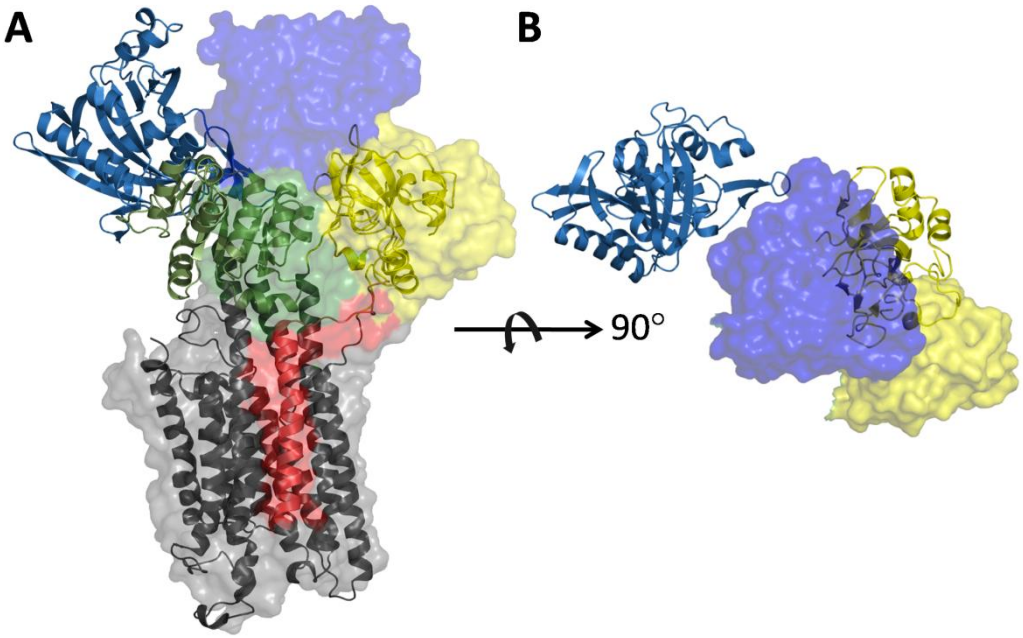

Figure 2.4. Large-scale conformational changes of the cytoplasmic domains of SERCA between the (Ca^{2+})2-E1 and E2-TG states. Panel A, alignment of the $(Ca^{2+})_2$-E1 state (pdb: 1SU4)[22] and the E2-TG state (pdb: 1KJU)[24] along SERCA TM7 to TM10. The $(Ca^{2+})_2$-E1 state is shown in cartoon representation with the E2-TG state shown in transparent surface. The cytoplasmic domains are coloured as in Figure 2.2 (the P-domain is green, the N-domain is blue and the A-domain is yellow). The transmembrane domain is coloured grey with TM3 highlighted in red. Alignment was performed using PyMOL (The PyMOL Molecular Graphics System, Version 0.99, Schrödinger, LLC.). **Panel B,** rotation of panel A by 90° around the x-axis as indicated. The presented view would be normal to the cytoplasmic surface of the SR membrane. The P-domain and transmembrane domain have been removed for clarity.

2-2.4. The high-resolution structure of SERCA in the E2-TG state.

Fortunately, we wouldn't have to wait very long for a second high-resolution structure of SERCA. In 2002, the second high-resolution x-ray crystal structure of SERCA representing the E2-TG state was solved by Toyoshima's group to 3.1 Å resolution[36]. The new structure allowed a direct comparison with the Ca^{2+}-bound SERCA crystal structure on a per-residue basis. To form the compact headpiece in the E2-TG intermediate, the cytoplasmic domains splayed apart in the $(Ca^{2+})_2$-E1 intermediate must come together. Based on comparison of the high resolution structures, the movements of the cytoplasmic domains between the $(Ca^{2+})_2$-E1 and the E2-TG states were more dramatic than originally modeled (Figure 2.5). The N-domain inclines nearly 90° towards the P-domain and the membrane, moving a distance of more than 50 Å in the process. The P-domain also inclines by about 30° with respect to the membrane assuming a more upright position. The A-domain, originally modeled to rotate by 90°, rotates 110° between the two states. Interestingly, despite the large conformational changes, the structure of each cytoplasmic domain remains very similar between the $(Ca^{2+})_2$-E1 and E2-TG states. The conformational changes that occur are mainly restricted to hinge regions between the domains.

The new E2-TG SERCA structure permitted visualization of movements in the transmembrane helices surrounding the Ca^{2+}-binding sites. The movements involve TM1 to TM6, while TM7 to TM10 remain relatively immobile. Interestingly, the movements are not restricted to the TM helices that compose the Ca^{2+}-binding sites (TM4, TM5, TM6, and TM8). Overall, the movements are complex; some TM helices (TM1 and TM2) move upward with respect to the membrane, some TM helices (TM3 and TM4) move downward, and also include lateral movements and kinking of helices. The "stalk" TM helices (TM4 and TM5) link movements between the transmembrane domain and the P-domain. The authors suggest these conformational changes cause a "domino effect" between SERCA TM helices, with the movement of one TM helix compensated by the movement of another, transducing movements throughout the enzyme[36]. The high-resolution E2-TG SERCA crystal structure also provided mechanistic details for the dissociation of Ca^{2+}. Site I is re-arranged mainly due to movements of the side chains of residues on TM6, which rotate 90° away from their co-ordination geometry in the Ca^{2+}-bound structure (Figure 2.6). Site II, which is primarily formed by TM4, is disrupted by the downwards movement of TM4 (Figure 2.6).

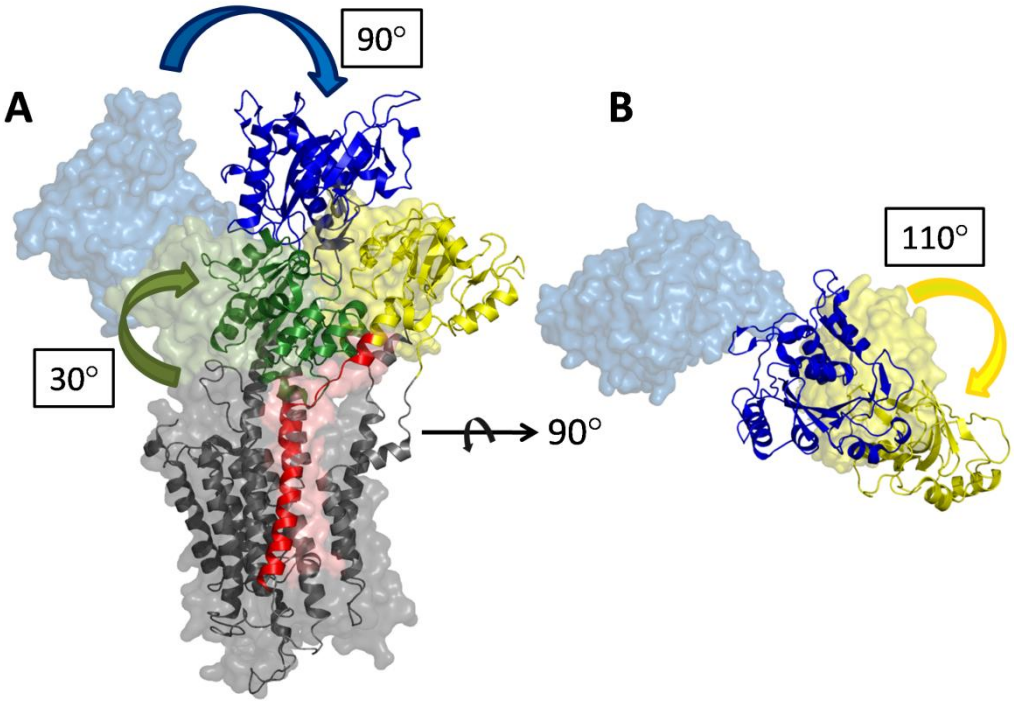

Figure 2.5. Conformational changes of SERCA cytoplasmic domains from high-resolution crystals structures of the (Ca^{2+})2-E1 and E2-TG states. Panel A, alignment of the (Ca^{2+})$_2$-E1 state (pdb: 1SU4)[22] and the E2-TG state (pdb: 1IWO)[36] along SERCA TM7 to TM10. The E2-TG state is shown in cartoon representation with the (Ca^{2+})$_2$-E1 state shown in transparent surface. The cytoplasmic domains are coloured as in Figure 2.2 (the P-domain is green, the N-domain is blue and the A-domain is yellow). The transmembrane domain is coloured grey with TM3 highlighted in red. Movements of the individual cytoplasmic domains are indicated by similar coloured arrows. The domain movements are more dramatic between the high-resolution SERCA crystal structures than previously modeled using the E2-TG structure from cryo-electron microscopy (as in Figure 2.4). Alignment was performed using PyMOL (The PyMOL Molecular Graphics System, Version 0.99, Schrödinger, LLC.). **Panel B,** rotation of panel A by 90° around the x-axis as indicated. The presented view would be normal to the cytoplasmic surface of the SR membrane. The P-domain and transmembrane domain have been removed for clarity.

Another highlight of the high-resolution E2-TG structure was the co-ordination of TG. Highly selective for SERCA enzymes, TG inhibits in the sub-nanomolar range. The TG-binding site had been previously characterized by mutation and shown to involve TM3[37, 38], but the exact details awaited a high-resolution structure. The new structure revealed that TG binds to a cavity formed by TM3, TM5 and TM7, near the cytoplasmic side of the membrane. The TG binding site was consistent with mutation studies that identified Phe^{256} as a critical residue for TG inhibition[37, 38]. The remainder of the TG binding site involved bulky hydrophobic side-chains contributed from TM3, TM5 and TM7.

2-2.5. Binding of ATP analogs to SERCA occludes the Ca^{2+} entry pathway.

In 2004, the SERCA field was spoiled with new crystal structures representing two intermediates bound to ATP analogs and an intermediate mimicking the phosphorylation transition-state[39, 40]. Bound to Ca^{2+}, the SERCA structures represented the $(Ca^{2+})_2$-E1-ATP and $(Ca^{2+})_2$-E1-P-ADP states. These structures had a compact cytoplasmic headpiece with a slightly different arrangement than the E2-TG state. With these new structures, we could now follow cytoplasmic domain conformational changes from the $(Ca^{2+})_2$-E1 state to one of its neighbouring intermediates, $(Ca^{2+})_2$-E1-ATP. We could also more directly visualize how the splayed $(Ca^{2+})_2$-E1 cytoplasmic domains gather to co-ordinate auto-phosphorylation of Asp^{351} in the P-domain using the bound ATP analog AMPPCP (5'-adenylyl-beta,gamma-methylene-diphosphonate).

The key observations show movement of the A-domain occludes the Ca^{2+} entry pathway around TM3, TM4, and TM6 from the cytoplasmic side[39]. A 90° rotation of the N-domain towards the P-domain allows binding of AMPPCP at an interface formed between the two domains. N-domain residues stabilize a bent conformation of AMPPCP that allows the 3'-OH to hydrogen-bond to the β–phosphate, while a Mg^{2+} ion and P-domain residues co-ordinate the γ–phosphate. The Mg^{2+} ion also co-ordinates the Asp^{351} side-chain into a rotamer different than the $(Ca^{2+})_2$-E1 and E2-TG states. The A-domain rotates towards the P-domain as well, and physically caps one side of the nucleotide binding site. This A-domain rotation strains pulls TM1 and TM2 upwards as a pair. The movement causes the cytoplasmic end of TM1 to kink and "plug" the cytoplasmic Ca^{2+} entry channel and prevents the backflow of Ca^{2+} into the cytoplasm. The P-domain undergoes subtle shifts in arrangement between the $(Ca^{2+})_2$-E1 and $(Ca^{2+})_2$-E1-ATP states.

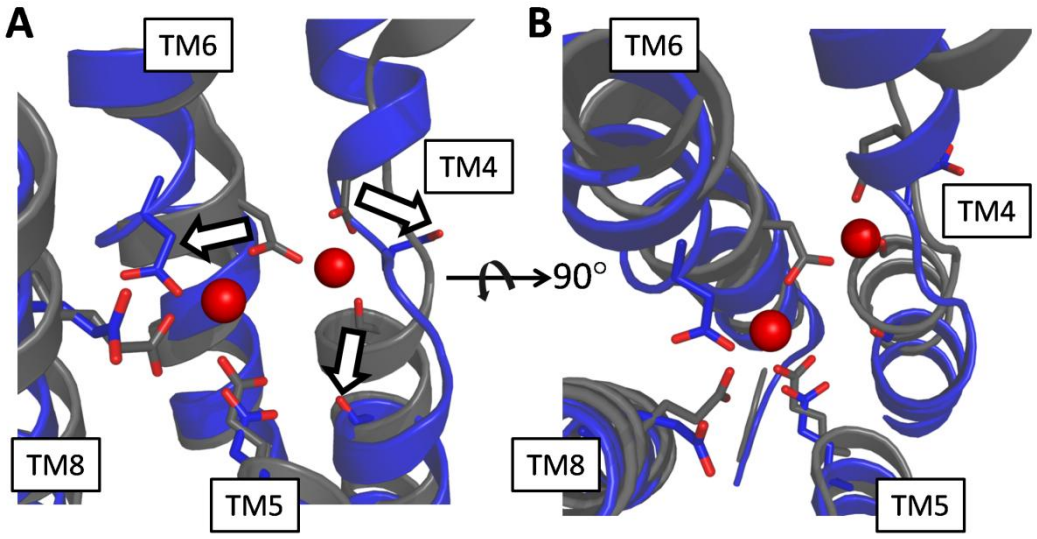

Figure 2.6. Conformational changes around the Ca^{2+} binding sites between the high-resolution (Ca^{2+})2-E1 and E2-TG structures of SERCA. Panel A, Ca^{2+} co-ordination in the $(Ca^{2+})_2$-E1 state (pdb: 1SU4 in *grey*)[22] is disrupted in the E2-TG state (pdb: 1IWO in *blue*)[36]. Of particular note is the downward shift of TM4 which changes the position of its unwound region near site II including Glu^{309}. Large conformational changes in site II ligating residues are indicated by arrows. The transmembrane domains involved in Ca^{2+} binding are labelled. Other transmembrane helices have been removed for clarity. **Panel B,** rotation of panel A by 90° along the x-axis as indicated.

The AlF_4^- in the $(Ca^{2+})_2$-E1-AlF_4^--ADP structure is found equidistant (~2.0 Å) from the β–phosphate of ADP and Asp^{351} supporting its validity as a representation of the $(Ca^{2+})_2$-E1-P-ADP intermediate. There are some important differences between the $(Ca^{2+})_2$-E1-ATP and $(Ca^{2+})_2$-E1-P-ADP states, represented by the $(Ca^{2+})_2$-E1-AMPPCP and the $(Ca^{2+})_2$-E1-AlF_4^--ADP structures, respectively. One difference in the $(Ca^{2+})_2$-E1-AlF_4^--ADP structure is a second Mg^{2+} ion co-ordinating the α–phosphate and β–phosphate of ADP. The conformation of the phosphoryl oxygens in the $(Ca^{2+})_2$-E1-AMPPCP structure are not in a proper orientation to co-ordinate a second Mg^{2+} ion. The structural changes between the $(Ca^{2+})_2$-E1-ATP state and the $(Ca^{2+})_2$-E1-P-ADP transition state are minimal, but their experimental Ca^{2+} occlusion rates differ, suggesting important differences. The $(Ca^{2+})_2$-E1-AMPPCP form of the enzyme is less effective at occluding Ca^{2+} than the transition-state $(Ca^{2+})_2$-E1-AlF_4^--ADP form[39].

2-2.6. And boom goes the database.

As a field, and as scientists in general, we have been spoiled by the structural studies of SERCA spanning the last few decades, in particular with the atomic resolution SERCA structures beginning in 2000[22]. To date, we have a near complete structural understanding of intermediates in the SERCA transport cycle[5]. In addition to those already discussed, many representative structures of SERCA transport intermediates have recently been published, including: the Ca^{2+}-bound E1-P-ADP state[41], the E2-P state[41, 42], the H^+-bound E2-P-ADP state[41-43] and the H^+-bound E2-ATP state[44]. With these determined structures, the only remaining unknown structure in the SERCA transport cycle is the Ca^{2+}-bound E2-P-ATP intermediate[5].

One unique observation was a structural view of the open luminal ion pathway observed in one of the E2-P structures bound to beryllium fluoride (BeF_3^-)[41]. The pathway resulted from pair-wise movements of TM1-TM2 and TM3-TM4 with respect to TM5-TM10. However, the open luminal ion pathway was not observed in the other E2-P structure also determined with BeF_3^- bound[42], which raises two very important points concerning our interpretation of SERCA crystal structures. The first is that most of the SERCA crystal structures require substrate mimics bound within the context of a crystal lattice and, for this reason, we do not know how well they represent actual SERCA transport intermediates[5]. Secondly, the recent SERCA crystal structures have provided the first

examples of different crystal conditions resulting in different structures using identical substrate analogs[5, 41, 42].

Despite a wealth of SERCA structural information (45 structures are currently deposited in the Protein Data Bank - www.rcsb.org/pdb), we still do not have complete understanding of the SERCA transport cycle. For example, it remains unknown how the phosphorylation of SERCA is transmitted through the enzyme to induce Ca^{2+} transport[5]. We also do not know the basis for the apparent release of cytoplasmic domain interactions upon Ca^{2+}-binding[5]. The interested reader would enjoy the excellent review by Moller and coworkers on SERCA structure, transport and energetics[5].

2-2.7. Small molecule inhibitors of SERCA use different mechanisms of inhibition.

We have already discussed TG as a small molecule inhibitor of SERCA. The TG inhibitory mechanism is proposed to involve immobilization of TM3, TM5 and TM7 where it binds (Figure 2.7a)[36]. Although TM7 does not appear to move to a large degree during transitions of SERCA intermediates, by immobilizing TM3 and TM5, TG favours the E2 form of SERCA and stabilizes SERCA in E2-like intermediates. As such, SERCA is inhibited from transitioning between different conformations and completing its transport cycle.

The structure of SERCA with dibutyldihydroxybenzene (BHQ) revealed a second mode of inhibition by a small molecule[45]. Like TG, BHQ is a high-affinity inhibitor of SERCA, binding with a K_d of approximately 20 nm[46]. However, BHQ has a distinct binding site from TG and uses a different mechanism of inhibition. BHQ bridges TM1 and TM4 with hydrogen-bonds to its two hydroxyl groups and van der Waals contacts to its butyl groups[45] (Figure 2.7b). This is consistent with previous observations that the butyl groups are critical portions of BHQ for its inhibitory activity[46]. The position of TM1 in the BHQ-bound structure is similar to the TG-bound SERCA structure, suggesting BHQ also stabilizes the E2-state. An important difference observed in the BHQ-bound SERCA structure compared to the TG-bound structure is the orientation of residue Glu^{309}. This residue is thought to act as the gating residue for site II[12, 39, 40, 47], allowing Ca^{2+} to enter from the cytoplasmic side of the membrane or occluding Ca^{2+} depending on its orientation. In the SERCA-BHQ structure, Glu^{309} is pointed towards site II in contrast to the SERCA-TG structure where Glu^{309} is pointed away from site II. In the SERCA-BHQ

structure, BHQ physically sits above Glu^{309} and occupies the space Glu^{309} would occupy if it was pointed outwards. As such, Ca^{2+} is physically blocked from accessing its binding site by the bound BHQ.

The physical blocking of gating-residue Glu^{309} is used by a second small molecule SERCA inhibitor, cyclopiazonic acid (CPA)[48]. CPA, an indole tetramic acid, is a metabolite of fungi that can contaminate food, acting as a toxin at high concentrations. CPA is highly-specific inhibitor of SERCA, binding with a K_d of approximately 120 nm[49-51]. The structure of SERCA in complex with CPA was solved by our laboratory in 2007[48]. CPA binds approximately 4 Å above Glu^{309} and stabilizes TM1 and TM2 in a locked conformation against TM4. The binding of CPA is stabilized by a polar pocket that surrounds the tetramic acid moiety and a hydrophobic platform that supports the indole portion of the molecule (Figure 2.7c). The indole ring of CPA bridges TM1 and TM4, whereas TM2 is displaced by interactions with the tetramic acid[48]. In this conformation, the positions of TM1 and TM2 are incompatible with Ca^{2+} binding. Thus, CPA blocks the Ca^{2+} access channel, like BHQ, and also immobilizes a subset of transmembrane helices using a mechanism similar, but distinct from TG. Thus, small molecule inhibitors of SERCA (TG, BHQ, and CPA) use different mechanisms to inhibit the Ca^{2+} transport cycle. One might be inspired to ask, what mechanisms are used to physiologically regulate SERCA?

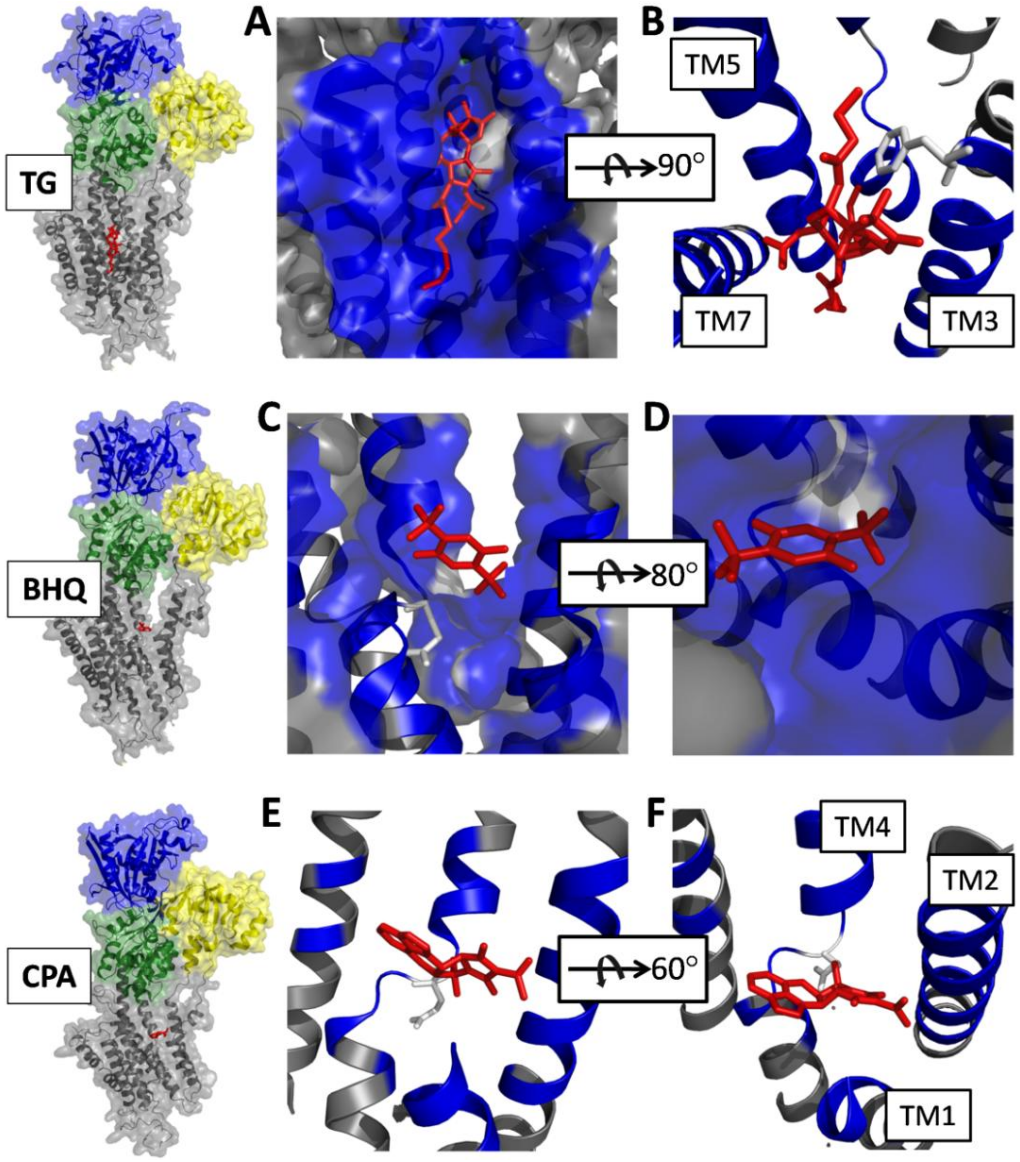

Figure 2.7. High-resolution complexes of SERCA with small molecule inhibitors reveal different mechanisms. For full SERCA views the cytoplasmic domains are coloured as in Figure 2.2 (the P-domain is green, the N-domain is blue, the A-domain is yellow and the transmembrane domain is grey). The small molecule inhibitors are red sticks. For clarity, TM3 has been removed for BHQ and CPA. **Panel A,** the binding of TG to SERCA (pdb: 1IWO)[36]. The surface within 10 Å of TG is coloured *blue*. Phe[256] is shown in *white*. **Panel B,** rotation of panel A by 90° around the x-axis as indicated. **Panel C,** the binding of BHQ to SERCA (pdb: 2AGV)[45]. The surface within 10 Å of BHQ is coloured *blue*. Glu[309] is shown in *white*. **Panel D,** rotation of panel C by 80° around the x-axis as indicated. **Panel E,** the binding of CPA to SERCA with part of TM1 removed for clarity (pdb: 2OJ9)[48]. The surface within 10 Å of CPA is coloured *blue*. Glu[309] is shown in white. **Panel F,** rotation of panel E by 60° around the x-axis as indicated.

2-3. Physiological inhibitors of SERCA: phospholamban and sarcolipin.

As discussed, we have a detailed structural understanding of SERCA intermediates in the Ca^{2+} transport cycle and the mechanisms used by small molecule inhibitors. However, our structural understanding of mechanisms used by physiological regulators of SERCA is still lacking important details. Physiologically, SERCA activity is regulated by differential expression of SERCA isoforms and also by interactions between SERCA and small regulatory SR transmembrane peptides. Two of these SR peptides, PLB and SLN, are key regulators of SERCA in cardiac muscle and will be the major focus of this thesis.

2-3.1. An introduction to PLB.

Initially described as a 22 kDa protein and later as a pentamer of lower molecular weight subunits[52-56], PLB is the predominant regulator of SERCA in cardiac, smooth and slow-twitch skeletal muscle[56-59]. As a 52-residue type I integral membrane protein, PLB binds to SERCA and lowers the apparent Ca^{2+} affinity of the enzyme. PLB was first identified as a major target of cAMP-dependent protein kinase (PKA) in cardiac microsomes and named for its ability to be phosphorylated (phosphorus and lambano are Latin for "to receive phosphate")[56, 60].

The regulation of SERCA by PLB is a dynamic process that is tightly coupled to the cytosolic Ca^{2+} concentration[61] and the phosphorylation states of PLB[62]. PLB inhibits SERCA in a dephosphorylated state under sub-micromolar cytosolic Ca^{2+} concentrations. PLB inhibition is relieved by micromolar cytosolic Ca^{2+} or PLB phosphorylation. PLB can be phosphorylated at two sites in its cytoplasmic domain; Ser^{16} by PKA or Thr^{17} by Ca^{2+}-calmodulin-dependent protein kinase (CaMKII)[63, 64]. The inhibition of SERCA can also be relieved using antibodies against PLB[62, 65], although this bears little physiological relevance.

2-3.2. PLB structure and dynamics: order and disorder in the cytoplasmic domain.

Structural studies of PLB were hampered by its hydrophobic nature and, as a result, initial structural studies were based on biochemical and mutational analyses. The first structural model of PLB accompanied its amino acid sequence[64, 66]. PLB contained an amphipathic helix long enough to cross a membrane and a positively-charged cytoplasmic region. The proposed PLB pentamer had hydrophobic residues facing the exterior lipid and hydrophilic residues lining the monomer interfaces[64]. This model was refined by a mutational study that identified residues critical for PLB pentamer formation[67]. The critical residues occurred in overlapping leucine-zipper-like heptad repeats and the offset of repeats suggested hydrophobic inter-helix interactions. The critical residues (Leu^{37}, Ile^{40}, Leu^{44}, Ile^{47}, and Leu^{51}) were located in the transmembrane domain and became known as the PLB leucine zipper. It was hypothesized that these residues faced the interior of the pentamer promoting a coiled-coil pore structure[67].

Different models for the arrangement of the PLB pentamer, based on mutation[67] or molecular dynamics[68], were in agreement with respect to a coiled-coil pentamer structure, but varied in the contacts between PLB monomers. To resolve this discrepancy, labelling studies were performed on the reactivity of the three Cys residues in PLB, which are all located in the transmembrane domain[69]. The study reported Cys^{41} as buried and the other two Cys residues (Cys^{36} and Cys^{46}) as readily accessible to labelling in pentameric states of PLB. The final model, refined by molecular dynamics, suggested that residues of the leucine zipper from one helix (Leu^{37}, Leu^{44}, and Leu^{51}) interdigitate with leucine zipper residues of the neighbouring helix (Ile^{40} and Ile^{47})[69] in agreement with the leucine zipper model[67].

In addition to its hydrophobic nature, the different possible oligomeric states of PLB also complicate its study. For this reason, initial structural studies used monomeric forms of PLB. Early NMR studies of a PLB fragment and the monomeric PLB-Cys^{41}Phe mutant in organic solvents reported an overall α–helical structure[70, 71]. The studies agreed that PLB contained an unstructured "hinge" region around residues 17 to 21 that separated PLB into three sub-domains: cytoplasmic domains Ia and Ib (residues 1 to 20 and residues 21 to 30, respectively) and transmembrane domain II (residues 31 to 52). Overall, this structure would be consistent with future NMR studies (Figure 2.8)[72, 73].

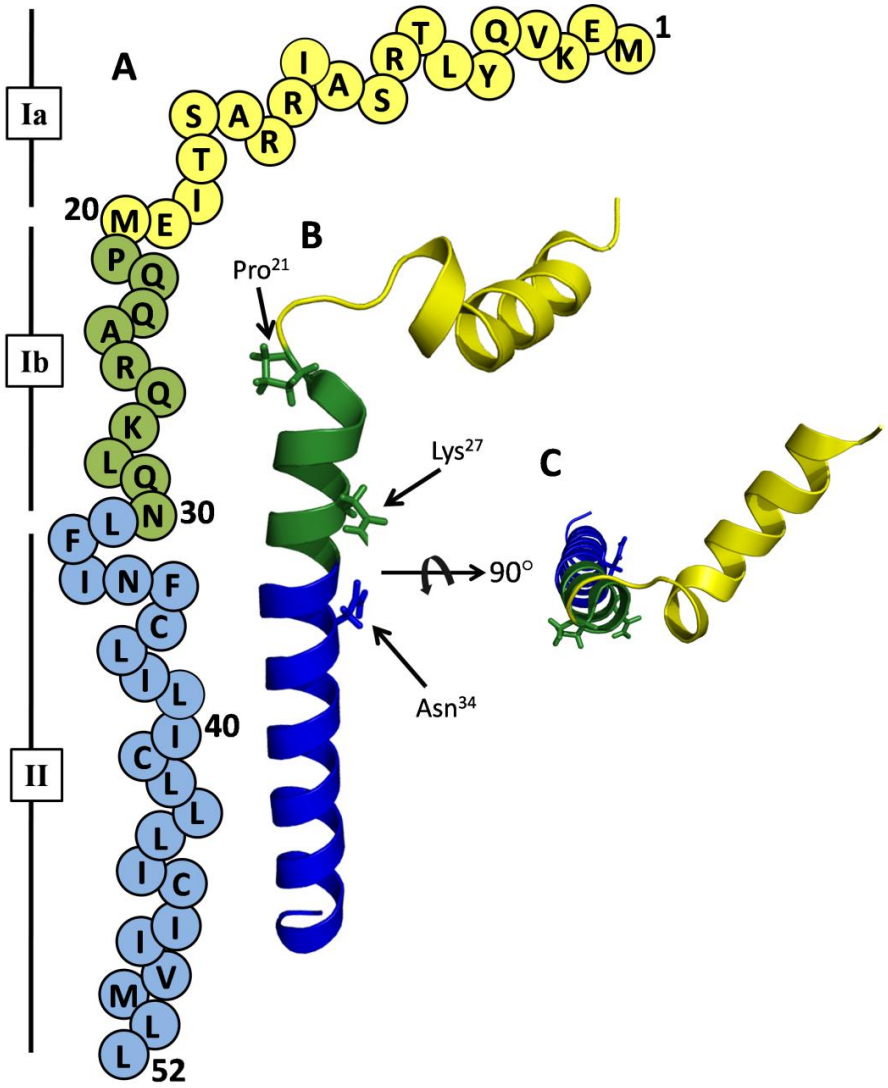

Figure 2.8. PLB sequence and structure. Panel A, the sequence of PLB as a schematic representation of its structure. Domain Ia is *yellow* (residues 1 to 20), domain Ib is *green* (residues 21 to 30) and domain II is *blue* (residues 31 to 52). **Panel B,** cartoon representation of the PLB monomer structure (pdb: 1N7L)[74]. Domains Ia, Ib and II are coloured as in panel A. Pro^{21} of the hinge region, Lys^{27} and Asn^{34} are shown as sticks. **Panel C,** rotation of panel A by 90° along the x-axis as indicated. The presented view would be normal to the cytoplasmic surface of the SR membrane.

An important step in our structural understanding of PLB occurred with the NMR solution-state structure of the PLB pentamer by Oxenoid and Chou[73]. The pentamer formed a channel-like structure in lipid micelles with a minimum "pore" radius of 1.8 Å[73]. The coiled-coil arrangement agreed with the current PLB leucine zipper model[67, 69] with the transmembrane helices adopting a curved conformation (Figure 2.9). The structure of each PLB monomer in the pentamer resembles the NMR structures with one important exception; the PLB cytoplasmic Ia domains in the pentamer were interacting with each other and pointing away from the membrane. This arrangement of the PLB pentamer was described as a "bellflower"[73] with the transmembrane domain acting as the stem and the cytoplasmic Ia domains clustered to form the bellflower (Figure 2.9). However, the "bellflower" model of the PLB pentamer has fallen to mounting evidence supporting the "pinwheel" model with the cytoplasmic Ia domains interacting with the membrane[75-77]. In the "pinwheel" model, the cytoplasmic regions are lying on the membrane surface rather than pointing away from the membrane and, viewed from above and normal to the membrane resembles the "pinwheel" toy that spins in the wind (Figure 2.9)[75]. Along with the "bellflower" PLB pentamer NMR structure, Oxenoid and Chou suggested binding of the PLB pentamer to SERCA could provide initial recognition[73]. This is an early suggestion that the PLB pentamer does not sit idly by as an inactive storage form. However, this hypothesis was based on the NMR structure of the PLB pentamer without any experimental evidence about its SERCA binding site[73].

At this time, it was also apparent that phosphorylation changed the oligomeric state of PLB in lipid membranes from EPR spectroscopy[78]. This result was in contrast to SDS-PAGE, which does not show a difference in the oligomeric states of non-phosphorylated and phosphorylated PLB[78, 79]. Phosphorylation was shown to increase the oligomeric states of wild-type PLB and a monomeric mutant, PLB-Leu^{37}Ala, in lipid membranes[78]. Similar results would be observed in NMR[80] and fluorescence resonance energy transfer (FRET) studies[81] using the phospho-mimetic PLB-Ser^{16}Glu mutant. As such, the authors suggested that PLB exists in a dynamic equilibrium in the SR membrane between pentamers and monomers[78].

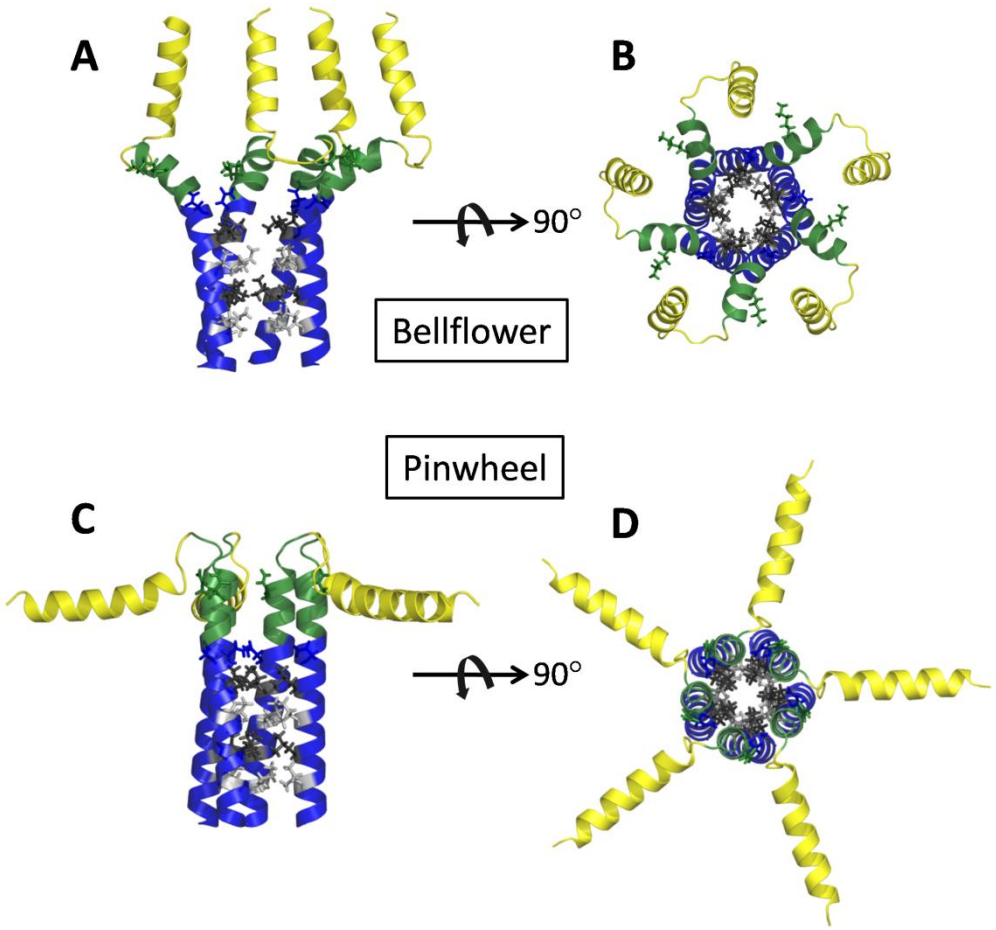

Figure 2.9. Models for the structure of the PLB pentamer. Panel A, the bellflower model of the PLB pentamer (pdb: 1ZLL)[73]. The foreground monomer has been removed for clarity. Domain Ia is *yellow*, domain Ib is *green* and domain II is *blue*. Lys^{27} is shown in green sticks and Asn^{34} is shown in yellow sticks. Residues of the leucine zipper are shown in *grey*. Leucine zipper residues from on helix (*dark grey*) interdigitate with leucine zippers from the neighbouring helix (*light grey*). **Panel B,** rotation of panel A by 90° along the x-axis as indicated. The presented view would be normal to the cytoplasmic surface of the SR membrane. **Panel C,** the pinwheel model of the PLB pentamer (pdb: 2KYV)[82]. The foreground monomer has been removed for clarity. Domains and residues are indicated as in panel A. **Panel D,** rotation of panel C by 90° along the x-axis as indicated. The presented view would be normal to the cytoplasmic surface of the SR membrane.

Spectroscopic studies of a labelled monomeric mutant of PLB, called AFA-PLB (PLB-Cys^{36}Ala, Cys^{41}Phe, Cys^{46}Ala), concluded that the cytoplasmic domain of PLB is in a dynamic equilibrium between ordered and disordered states in lipid vesicles[83]. The ordered state of the cytoplasmic PLB domain directly contacts the membrane, whereas the dynamic disordered state is detached from the membrane (Figure 2.10). The different dynamic states of the cytoplasmic domain were attributed to the "hinge" region of PLB domain I[83]. Ordered and disordered states of PLB were also supported by NMR studies[84, 85]. Interestingly, the dynamic equilibrium of the cytoplasmic domain could be modulated by $MgCl_2$. High concentrations of $MgCl_2$ increased the PLB disordered state and this was not observed with KCl, leading the authors to suggest that Mg^{2+} ions specifically compete with the positively-charged PLB cytoplasmic domain for binding sites on the lipid surface[83]. More recent spectroscopic studies suggest phosphorylation of labelled AFA-PLB influenced the order-disorder equilibrium in favour of the disordered state[86]. The dynamics of AFA-PLB were not affected by increased concentrations of Ca^{2+}, suggesting that relief of PLB inhibition by phosphorylation and micromolar Ca^{2+} could involve different mechanisms[86]. These findings were later supported by NMR studies[85, 87].

2-3.3. Important insights into PLB inhibition of SERCA are based on heterologous co-expression studies.

A number of important mechanisms of PLB inhibition of SERCA have been revealed through co-expression studies in heterologous systems. Indeed, the co-expression of SERCA and PLB in COS-1 cells helped define PLB as an inhibitor of SERCA[88]. Co-expression of the three different SERCA genes with PLB showed PLB could decrease the apparent Ca^{2+} affinity of SERCA1a and SERCA2a, but had no effect on SERCA3[89].

Co-expression studies also permitted mutagenesis of PLB to investigate contributions of individual residues to the inhibitory mechanism. PLB mutant co-expression studies identified a number of residues that result in loss-of-function or gain-of-function relative to wild-type PLB, with respect to lowering the apparent Ca^{2+}-affinity of SERCA. Combined, such co-expression studies have identified residues throughout the sequence of PLB that are functionally important for SERCA inhibition, including residues in all three structural domains (cytoplasmic domains Ia and Ib and transmembrane domain II)[90-92]. These data resolved debates as to which domains of PLB are responsible for SERCA inhibition by identifying functional residues in all domains of PLB.

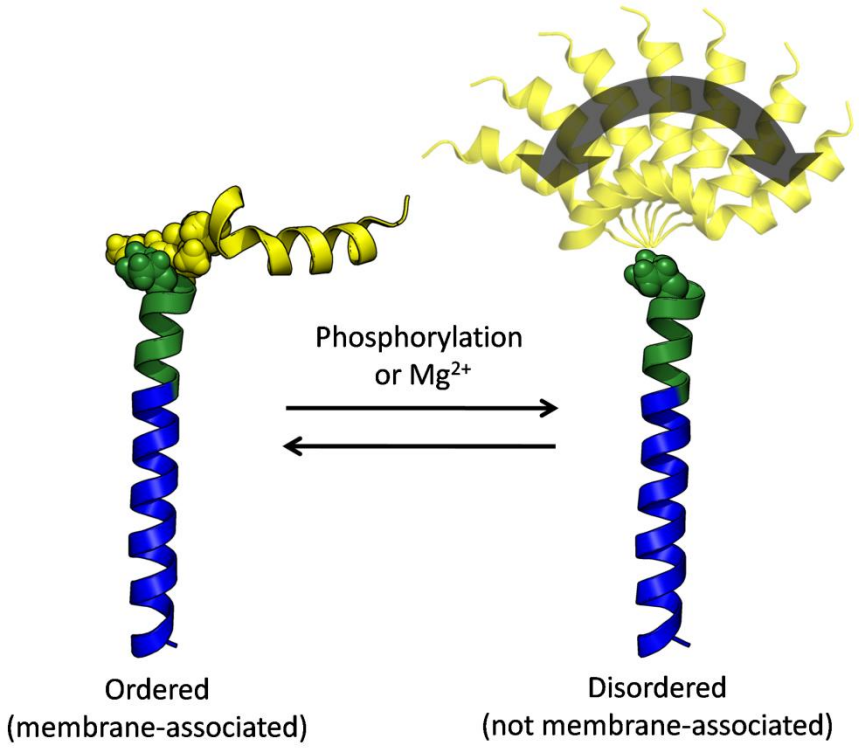

Figure 2.10. The order-disorder equilibrium of the PLB cytoplasmic domain. Cartoon representations of PLB with domain Ia in *yellow*, domain Ib in *green* and domain II in *blue* (pdb: 1N7L)[74]. Pro^{21} of the hinge region is indicated in green spheres. *Left panel*, residues 18 to 21 in the hinge region are shown as spheres.

Co-expression studies inspired two important hypotheses from MacLennan and coworkers that have since dominated literature descriptions of how PLB inhibits SERCA[59, 93]. The first is the two-faced helix model of PLB which states that residues on one face of the PLB transmembrane helix are responsible for stabilizing pentamers and residues on the other side interact with SERCA (Figure 2.11a)[91]. Future studies would support some overlap of these two faces, such that residues important for stabilizing the pentamer are also important for interaction with SERCA (Figure 2.11a)[94]. The second hypothesis was that PLB pentamers must depolymerise to interact with and inhibit SERCA (Figure 2.11b)[91, 92], with the corollary that the PLB monomer was the active inhibitory species[91]. This hypothesis was driven by observations that some gain-of-function mutants of PLB had a much higher ratio of monomer-to-pentamer relative to wild-type PLB in SDS-PAGE[91]. The mechanism for the gain-of-function mutants was attributed to mass action with an increase in the inhibitory monomeric PLB species driving SERCA inhibition[92]. From this point of view, the speculation was made that the PLB pentamer is an inactive storage form.

It is critical to point out that some PLB mutants in these co-expression studies did not agree with the mass action mechanism. For example, a number of PLB mutants had a larger fraction of monomers than wild-type PLB, but were normal or loss-of-function (see Table I in Kimura JBC 1997 and Table I in Kimura JBC 1998). Most dramatically, two of the largest gain-of-function PLB mutants ever reported, $Lys^{27}Ala$ and $Asn^{30}Ala$, form pentamers to a similar (PLB-$Lys^{27}Ala$) or greater (PLB-$Asn^{30}Ala$) degree than wild-type PLB[92]. This discrepancy was addressed by MacLennan and coworkers by suggesting that multiple mechanisms are involved in PLB inhibition of SERCA[92]. The authors proposed some mutants may stabilize interactions between SERCA and PLB as a mode of gain-of-inhibition and this mechanism works in addition to PLB mass action[92]. However, the PLB mass action mechanism has won out in terms of popularity and there is little structural evidence to suggest how PLB mutants stabilize SERCA interactions in the alternative mechanism. For this reason, we do not have a complete understanding of the multiple mechanisms used by PLB to inhibit SERCA.

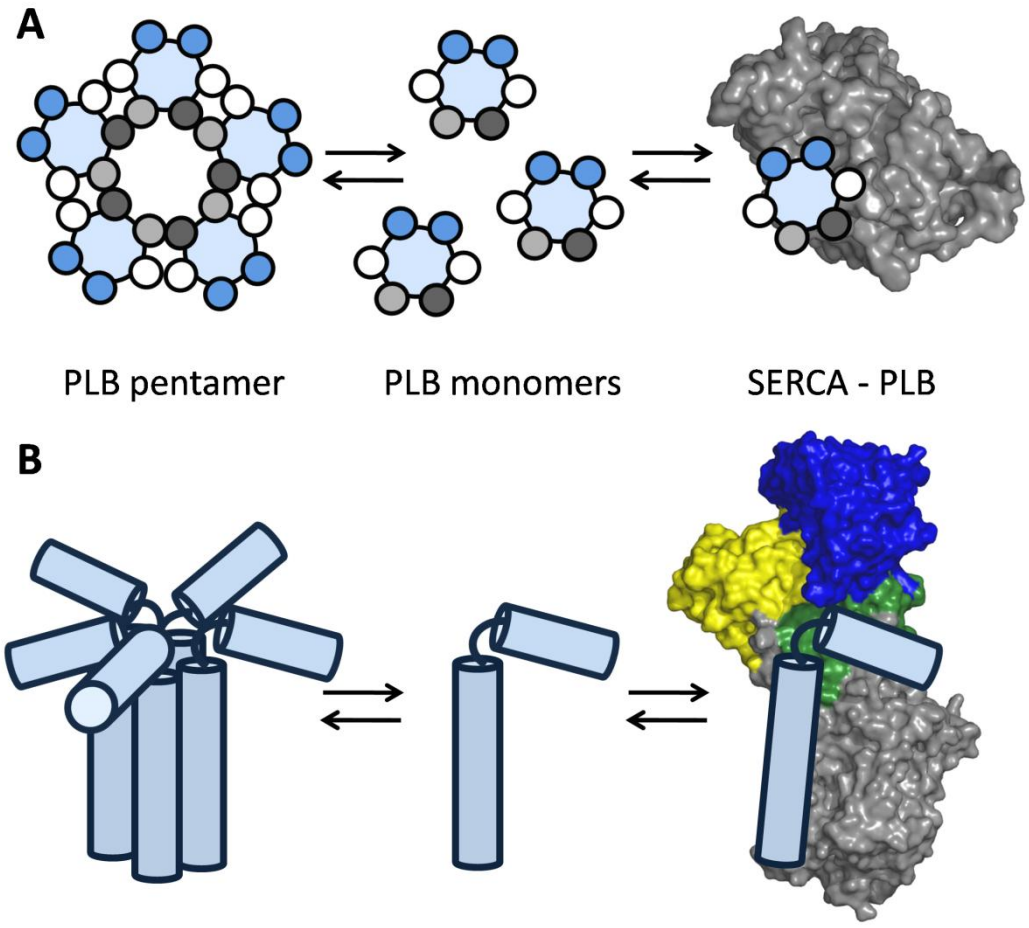

Figure 2.11. Proposed mechanisms for PLB inhibition of SERCA based on heterologous co-expression. PLB pentamers (*left*) and monomers (*middle*) are in dynamic equilibrium and the PLB monomer can bind and inhibit SERCA (in surface on *right*; pdb: 1KJU)[24]. **Panel A,** the PLB two-faced helix model for interaction with SERCA. The presented view would be normal to the cytoplasmic surface of the SR membrane and highlights residues in the PLB transmembrane domain. Pentamers of PLB are stabilized by leucine zipper residues (coloured in *grey*) on one face of the helix. The other face of the helix, exposed in the pentameric state, contains functionally important residues for interaction with SERCA (coloured in *blue*). Recent studies have suggested the two faces overlap[94]. Figure adapted from Figure 7 in Cornea et al. 2000[94]. **Panel B,** model for the PLB monomer as the active inhibitory species. PLB must depolymerise into monomers to bind and inhibit SERCA. The PLB pentamer is speculated to be an inactive storage form. Figure adapted from Figure 3 in MacLennan et al. 2003[59].

It is also important to keep in mind that the PLB mutant monomer-to-pentamer ratio was determined by SDS-PAGE. Cornea and coworkers[94] re-examined the leucine zipper of PLB and concluded that SDS-PAGE is not a fair representation of PLB oligomeric stabilities. Thus, it is unlikely that SDS-PAGE reflects the oligomeric state or distribution of PLB in membrane environments. In contrast to the hypothesis of PLB monomer as the active species, they conclude:

> "several PLB mutants with hydrophobic amino acid substitutions at the Leu/Ile zipper region retain the ability to form pentamers but at the same time give the same or even stronger inhibition of the Ca^{2+}-pump than do mutants that are more completely monomeric"[94].

In contrast to the popular mass action mechanism of inhibition by PLB, the degree of destabilization of the PLB pentamer did not correlate with SERCA2a inhibition[94].

2-3.4. PLB physically interacts with SERCA.

Initially, a number of models were proposed for the mechanisms used by PLB to regulate SERCA. For example, one early model suggested the positively-charged PLB cytoplasmic domain, which can be modulated by phosphorylation, plays an important electrostatic role affecting the local concentration of ions near the SR membrane[95]. Another postulated that channel activity of PLB itself influences ion transport across the SR membrane[64]. However, evidence for a physical interaction between the PLB and SERCA led to the predominance of models involving PLB binding to SERCA.

The first evidence of a physical interaction between PLB and SERCA was the cross-linking of the two proteins using a hetero-bifunctional reagent reported by James and coworkers[96]. The ε–amino group of the single Lys present in canine PLB (Lys^3) was linked to the photo-activatable, cleavable hetero-bifunctional Denny-Jaffe reagent. The reagent-modified PLB formed pentamers to the same extent as non-labelled PLB, suggesting the modification did not dramatically affect PLB structure. When the labelled PLB was light activated and incubated with purified cardiac SR, a complex was formed. The formation of this complex was prevented by 100 μM Ca^{2+} and phosphorylation of PLB by PKA. The crosslinked partner of PLB in the complex was proposed to be SERCA based on FITC-labelling of SERCA and subsequent formation of the PLB-crosslinked complex[96]. Overall, the results supported an interaction between non-

phosphorylated PLB and SERCA in the E2 state. The authors went on to determine the nature of the cross-linked residue in SERCA using radiolabelled Denny-Jaffe reagent. The cross-linked residues in SERCA, Lys^{397} and Lys^{400}, were just downstream of the phosphorylated Asp^{351} residue leading the authors to propose PLB might interfere with formation of the SERCA acyl-phosphate intermediate[96].

Although it has proven difficult to reproduce this initial cross-linking result[97, 98], more support for a physical interaction between SERCA and PLB has come from subsequent cross-linking studies. Cys-scanning mutagenesis of PLB identified an interaction between Asn^{30} of PLB and Cys^{318} of SERCA2a[97]. Using the homo-bifunctional thiol cross-linking reagent BMH (1,6-bismaleimidohexane), Jones and coworkers crosslinked PLB-Asn^{30}Cys with high efficiency to SERCA2a co-expressed in insect cell microsomes. The PLB-Asn^{30}Cys mutant was the only PLB mutant to cross-link to SERCA2a among twelve Cys-mutants scanning PLB residues 30 to 41 on a Cys-less background (with the three native Cys residues of PLB mutated to Ala). Phosphorylation of PLB by PKA decreased crosslinking by 50%. The crosslink between PLB-Asn^{30}Cys and SERCA did not form in micromolar Ca^{2+} and did not form in the presence of TG, CPA or the anti-PLB antibody 2D12[97]. The observed crosslinking required micromolar concentrations of ATP or ADP which, combined with the absence of crosslinking in micromolar Ca^{2+}, suggested that the observed interaction involved a nucleotide-bound E2 state of SERCA[97]. The determination of Cys^{318} of SERCA as the crosslinked residue positioned the observed PLB interaction site near TM4[97]. To note, the PLB-Asn^{30}Cys mutant migrated primarily as a monomer, with very little pentamer, in SDS-PAGE conditions where wild-type PLB migrates primarily as a pentamer[97].

A similar study extended the region of Cys-scanning beyond residues 30 to 41 to include residue 27 of PLB[98]. Cys-mutants of residues 27 and 30 of PLB were specifically and efficiently crosslinked to Lys^{328} of SERCA2a in the nucleotide-bound E2 state when co-expressed in insect cell microsomes[98]. Overall, the results were consistent with the previous study[97]. Another pair-wise interaction between PLB and SERCA2a was identified between PLB-Leu^{31}Cys and SERCA2a-Thr^{317}Cys using insect cell co-expression[99]. Using BMH, a high efficiency of crosslinking was observed between PLB and SERCA2a Cys-variants, positioning residue 31 of PLB within 10 Å of residue 317 in

SERCA. In contrast to previous models, these results provided evidence that a PLB loss-of-function mutant could still bind to SERCA2a without causing inhibition[99].

These cross-linking studies culminated in a model of PLB bound to the high-resolution SERCA (E2-TG) structure[36, 100]. The SERCA-PLB model involved more crosslinking results; between PLB-Lys^{27}Cys and SERCA-Leu^{321}Cys near TM4 and between PLB-Val^{49}Cys and SERCA-Val^{89}Cys near TM2. The SERCA-PLB model was constrained by the PLB two-faced helical model of SERCA interaction based on mutational studies[91] and the cross-linking of PLB-Lys^{3} to Lys^{397} and Lys^{400} in SERCA[96]. The structure of PLB was constructed from the solution-state NMR structures[70, 71]. The model had PLB bound to a groove in SERCA formed by TM2, TM4, TM6 and TM9. The α–helical structure of PLB was disrupted near the cytoplasmic side by TM4 causing unwinding such that the N-terminus could interact with Lys^{397} and Lys^{400} in the N-domain of SERCA. PLB bound to SERCA (E2-TG) in the model assumed a position similar to TM2 in the Ca^{2+}-bound SERCA-E1 structure[22]. Accordingly, the Ca^{2+}-bound SERCA-E1 state does not contain the groove for PLB-binding. The authors proposed the transition from E2 to E1 closed the groove and physically pushes PLB out of its binding site[100]. A summary of the cross-linking data is presented in Figure 2.11 with the modeled PLB binding site highlighted.

2-3.5. Studies of SERCA-PLB complexes suggest PLB remains associated with SERCA under non-inhibitory conditions.

As cross-linking evidence mounted that PLB physically interacts with SERCA[89, 96-99, 101], studies of the SERCA-PLB complex provided further insights into the regulation of SERCA by PLB. Spectroscopic studies suggested relief of PLB inhibition by phosphorylation increased the rotational mobility of SERCA[102]. SERCA activity was related to its rotational mobility, which was influenced by SERCA self-association[103-106] and an increase in SERCA rotational mobility would be related to an increase in activity. As such, it was proposed that PLB holds SERCA in a kinetically unfavourable state and that SERCA is freed upon phosphorylation of PLB[102]. An NMR study hinted at possible consequences of the interaction with SERCA using labelled monomeric AFA-PLB to follow residue-specific changes upon titration with SERCA[72]. The dynamic equilibrium between the ordered and disordered states of PLB was influenced by SERCA, where SERCA altered the ordered state to favour the disordered state and promote interaction[72].

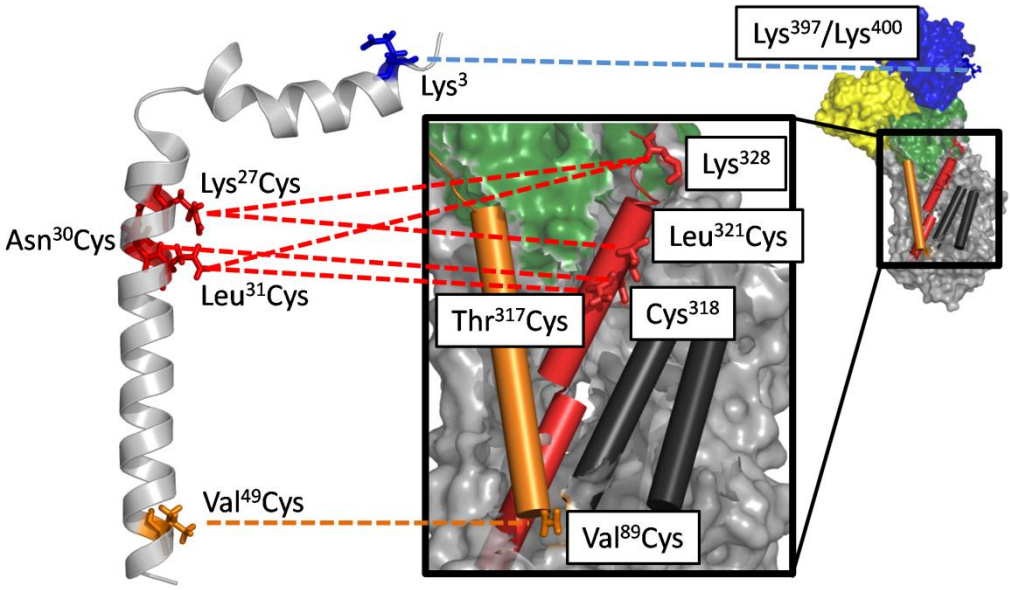

Figure 2.12. The proposed SERCA interaction site for the PLB monomer based on cross-linking and mutational studies. Panel A, summary of cross-linking studies between PLB and SERCA. A cartoon ribbon representation of PLB in *grey* with cross-linked residues shown as sticks. The PLB residues are coloured based on the colour of their cross-linking partner in SERCA with the residue or mutation indicated. The proposed PLB binding groove[100]of TM2 (*orange*), TM4 (*red*), TM6 (*dark grey*) and TM9 (*dark grey*) is highlighted as cylinders in the full view of SERCA (P-domain in *green*, N-domain in *blue*, A-domain in *yellow* and transmembrane domain in *grey*). A close-up of the proposed PLB binding groove from the full enzyme view is presented for clarity. Dashed lines linking cross-linking partners from PLB to SERCA are coloured based on the location of the SERCA residue. SERCA residues or mutations are indicated in boxes.

Fluorescence energy transfer studies confirmed that, similar to its migration in SDS-PAGE, PLB forms oligomers in lipid bilayers[107]. In support of a physical interaction between SERCA and PLB, it was shown that SERCA depolymerised PLB oligomers in lipid bilayers. Co-reconstituted SERCA increased the fraction of PLB monomers, supporting an interaction between SERCA and monomeric PLB. However, since SERCA was able to depolymerise PLB into monomers and smaller oligomers, the interaction between SERCA and monomeric PLB is preferred, but SERCA must also interact with oligomeric PLB in order to change the structure of PLB[107]. There is little evidence to suggest how SERCA interacts with oligomeric forms of PLB.

The nature and stoichiometry of SERCA and PLB interactions have also been studied using FRET by Thomas and coworkers[108]. These studies suggested the affinity of PLB for SERCA was very high, such that PLB acts as a subunit of SERCA and does not dissociate. The relief of PLB inhibition by micromolar Ca^{2+} concentrations was proposed to result from a structural rearrangement of the SERCA-PLB complex as opposed to physical dissociation[108]. A number of other observations are also in favour of PLB remaining associated with SERCA, including spectroscopic[86] and NMR studies[87]. Thomas and coworkers also concluded that the stoichiometry of binding is one PLB per SERCA. It is worth noting that these studies were performed using the "monomeric" PLB-Ile[40]Ala monomer and at relatively high lipid to protein ratios (between 0.18 and 1.4 SERCA per 1000 lipids). Also, the one PLB per SERCA stoichiometry was determined by the intersection of extrapolated lines fit to the slope of the initial and final energy transfer rates. Careful examination of the data (see Figure 8 in Mueller et al. 2004[108]) reveals that FRET continues to increase beyond a ratio of one PLB per SERCA, and does not reach a maximal energy transfer plateau until a ratio of approximately five PLB per SERCA.

A study using fluorescence resonance energy transfer (FRET) and photo-bleaching studied interactions between cyan-fluorescent protein (CFP) labelled SERCA and yellow-fluorescent protein (YFP) labelled PLB in the ER of AAV-293 cells[109]. The results indicated a rapid exchange between CFP-SERCA and YFP-PLB with an upper time constant limit of 1.4 s for PLB binding and unbinding. Although this appears to contradict models involving the constant association of PLB with SERCA, the authors propose the high concentration of SERCA and PLB in muscle SR exceeds the

dissociation constant of the complex, leading to most SERCA molecules being associated with PLB in the steady state. A secondary result of this study was the expression of CFP-PLB and YFP-PLB in the plasma membrane that allowed for the study of the exchange rate of PLB pentamers. The results suggest that PLB exchanges very slowly from pentamers, with oligomeric interactions showing stability on the order of minutes[109]. A caveat of this experiment was the very low apparent concentration of PLB expressed in the plasma membrane of the AAV-293 cells, which may not accurately reflect exchange rates of PLB pentamers in the muscle SR.

With prominent emerging themes of order-to-disorder in the PLB cytoplasmic domain and the influence of phosphorylation and SERCA on these dynamics, it was of interest to study the relationship between structural changes in PLB and its inhibition of SERCA. To this point it had been assumed that disordering of the cytoplasmic domain of PLB, which was favoured by phosphorylation, was associated with a loss of inhibition. However, SERCA also promoted the disordered state to promote binding[72], a requirement for regulation by PLB. Veglia and coworkers set out to directly study the relationship between PLB structural dynamics and SERCA inhibition[110]. They suggest the dynamics of PLB play an important role in the regulation of SERCA and modulation of PLB dynamics finely "tunes" the inhibition of SERCA[110]. Mutations were centered on Pro^{21} in the "hinge" region of the cytoplasmic domain to influence PLB ordered and disordered states. Veglia and coworkers determined that PLB mutants with an increased ordered state had a decreased binding affinity for SERCA and were also loss-of-function[110].

The most popular intermediates in proposed models for the regulation of SERCA by PLB from heterologous co-expression[91, 92] and spectroscopy studies[72, 81, 86, 108, 109] are concentrated in Figure 2.13. This thesis aims to determine a structure of PLB bound to SERCA. The results suggest the concentrated scheme in Figure 2.13 is incomplete.

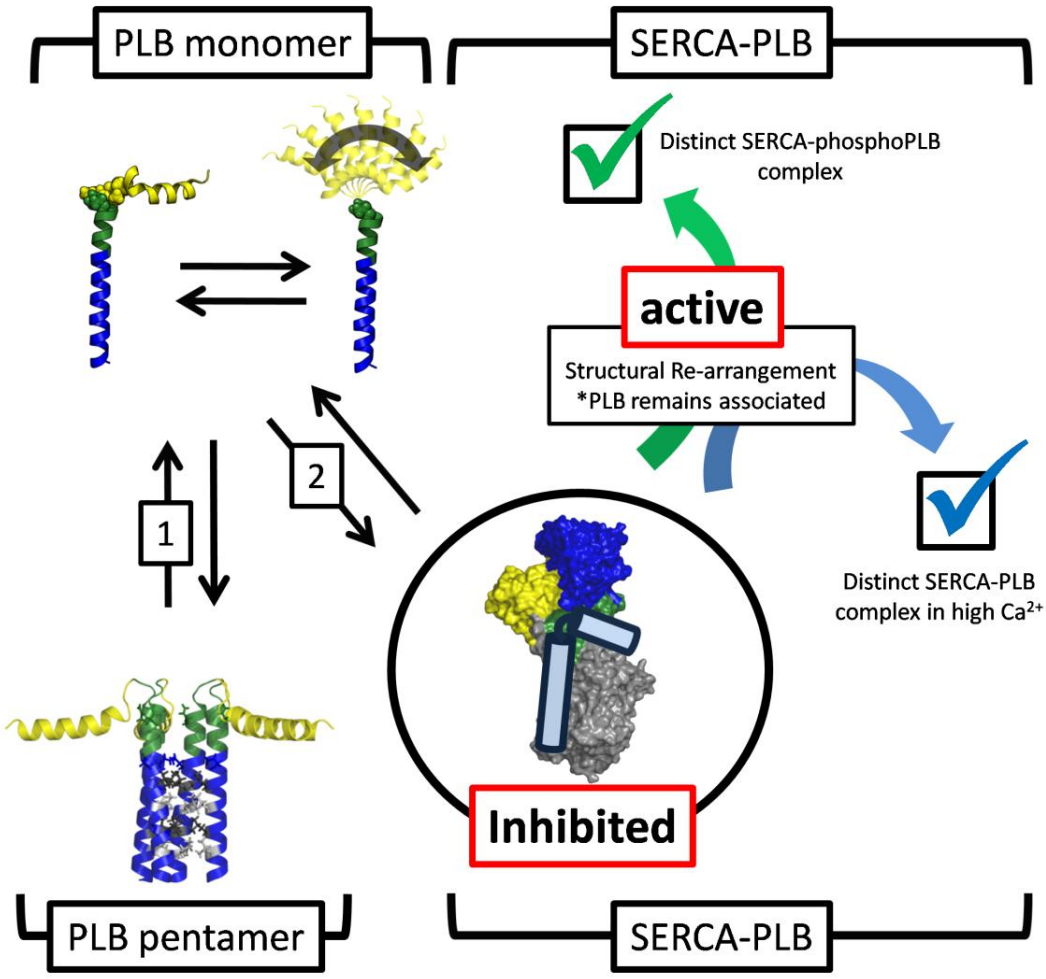

Figure 2.13. Summary of proposed intermediates in the inhibition of SERCA by PLB. Common models for PLB inhibition of SERCA from heterologous co-expression[91, 92] and spectroscopic studies[72, 81, 86, 108, 109] are concentrated into a single scheme. The arrow labelled 1 is the dissociation of the PLB pentamer associated with the "mass action" PLB mechanism. The arrow labelled 2 is the association of PLB with SERCA associated with the "enhanced interaction" PLB mechanism. Evidence for higher-order interactions (i.e. SERCA self-association) are not included, but represent ternary complexes with apparent functional consequences. This thesis proposes that the interaction between pentameric PLB and SERCA is involved as a regulatory intermediate. The results suggest the PLB pentamer actively engages SERCA.

2-3.6. Structural characterization of SERCA and PLB binding sites.

If SERCA and PLB were physically interacting and influencing the oligomeric states of each other, then where were the two proteins contacting each other? Was the current model with PLB bound to TM2, TM4, TM6 and TM9 correct? What was the actual molecular nature of their binding sites? A high-resolution structure of PLB bound to SERCA would be an excellent way to corroborate the current model, but such information of the SERCA-PLB complex has been curiously absent.

In contrast to the TM2, TM4, TM6 and TM9 groove as the PLB-binding site, a different interaction site between PLB and SERCA was proposed from cryo-electron microscopy of tubular co-crystals[111]. Using three different variants of PLB (wild-type PLB, PLB-Lys^{27}Ala, and PLB-Leu^{37}Ala), Young and coworkers identified TM3 as the PLB interaction site with SERCA in the co-crystals. However, the density for the PLB transmembrane domain was discontinuous and difficult to assign, perhaps due to a SERCA crystal contact involving TM3 disrupting the interaction with PLB[111]. This, unfortunately, limited the resolution of the SERCA-PLB complex.

In 2006, we reported the 10 Å projection structure obtained from two-dimensional co-crystals of SERCA and PLB-Ile^{40}Ala[112]. The co-crystals contained the well-characterized SERCA dimer ribbons observed in the tubular crystals used to calculate previous cryo-EM structures of SERCA. Interspersed between the SERCA dimer ribbons were smaller densities that were attributed to PLB[112]. To our surprise, these densities, although much smaller than the SERCA density, were too large to be PLB monomers[112]. Despite using a gain-of-function mutant of PLB that was thought to be primarily monomeric, the structure demonstrated that an oligomer of PLB was capable of binding to SERCA. The size of the PLB density was comparable to the dimensions of the recently published PLB pentamer NMR structure[73]. For this reason, we constructed a model of PLB pentamers bound to SERCA dimer ribbons (Figure 2.14)[112]. Interestingly, the site of interaction between SERCA and the PLB pentamer was TM3, the same site of interaction identified previously using tubular co-crystals of SERCA and PLB[111]. Unfortunately, the current resolution of the SERCA and PLB co-crystals could not determine if a PLB monomer was present or absent in its predicted TM2, TM4, TM6 and TM9 binding groove. It was later confirmed by FRET studies that PLB-Ile^{40}Ala is capable of forming stable pentamers in the membrane environment[76, 109].

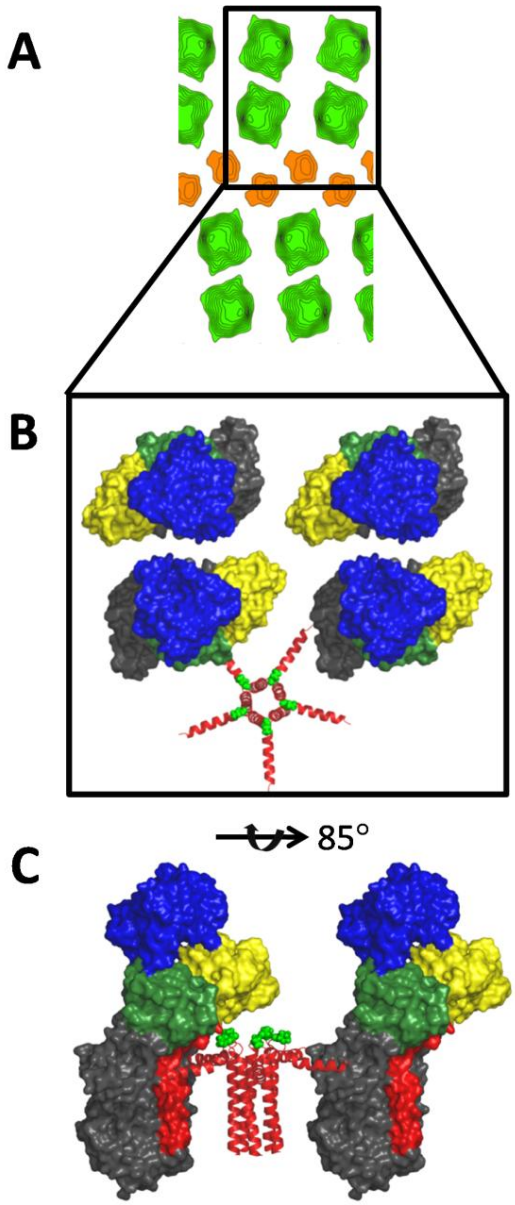

Figure 2.14. Interactions between the PLB pentamer and SERCA based on two-dimensional co-crystals of SERCA and PLB-Ile40Ala. Figure adapted from Stokes et al. 2006[112]. **Panel A,** 10 Å projection map from cryo-electron microscopy of SERCA and PLB-Ile^{40}Ala co-crystals. Positive contours are coloured for the characteristic anti-parallel SERCA dimer ribbons (*green*) and the associated oligomeric PLB densities (*orange*). **Panel B,** model for the interaction of SERCA (pdb: 1KJU)[24] with pentameric (pdb: 2KYV)[82] based on the projection map from 2D co-crystals. SERCA and PLB are in surface and cartoon, respectively. The cytoplasmic domains of SERCA are coloured as in Figure 2.2 (the P-domain is green, the N-domain is blue and the A-domain is yellow). The SERCA transmembrane domain is grey with TM3 highlighted in red. PLB is coloured red with Pro^{21} in green spheres. **Panel C,** rotation of panel B by 85° along the x –axis as indicated.

Could PLB oligomers interact with SERCA at a site distinct from the site modeled for the interaction of the PLB monomer with SERCA? If a PLB pentamer was binding to SERCA, did this influence subsequent interactions between the two proteins? Was the PLB pentamer really an inactive storage form for PLB, as was currently speculated, or did the pentamer have some active role in the regulation of SERCA?

2-3.7. Animal models reveal key aspects of PLB regulation of SERCA.

A number of studies have investigated the expression of super-inhibitory, gain-of-function PLB mutants in the mouse heart. The first investigated the effects of cardiac-specific over-expression of a super-inhibitory pentameric mutant, PLB-Lys^{27}Ala, in transgenic mice with a wild-type PLB background[113]. The over-expression of PLB-Lys^{27}Ala caused depressed contractile parameters and induced slight cardiac hypertrophy. In contrast to wild-type PLB cardiomyocytes, the PLB-Lys^{27}Ala over-expressing cardiomyocytes were not fully relieved from inhibition upon isoproterenol treatment, a β–adrenergic agonist that causes downstream PKA activation and phosphorylation of PLB. Importantly, the levels of phosphorylation were similar between wild-type PLB and PLB-Lys^{27}Ala. As such, the mutation Lys^{27}Ala in PLB did not prevent phosphorylation and, thus, phosphorylation cannot overcome the effects of the Lys^{27}Ala mutation on SERCA inhibition[113]. A second study investigated the effects of cardiac-specific over-expression of super-inhibitory monomeric mutants of PLB (Leu^{37}Ala and Ile^{40}Ala) and compared the effects to over-expression of wild-type PLB[114]. The over-expression of PLB-Leu^{37}Ala and PLB-Ile^{40}Ala caused depressed contractile parameters with induction of cardiac hypertrophy[114]. Interestingly, the authors found an apparent compensatory mechanism of increased phosphorylation in the transgenic mice over-expressing the super-inhibitory monomeric PLB mutants[114].

The generation of the PLB-knockout mouse confirmed many aspects of PLB regulation of SERCA and also produced some surprising results[115]. The PLB-knockout mice had increased SERCA affinity for Ca^{2+} which was attributed to the ablation of PLB in their hearts[115]. The PLB-knockout mice also exhibited enhance myocardial performance without significant changes in heart rate. These enhanced parameters of the PLB-knockout mouse hearts were not affected by isoproterenol treatment and their baseline levels were similar to the isoproterenol-stimulated parameters of their wild-type littermates[115]. Amazingly, the heart weight of the PLB-knockout mice was identical to

wild-type littermates, and the PLB-knockout mice did not develop any cardiomyopathies. So, why has PLB evolved as a regulatory mechanism in the heart? It is worth noting that there is a major difference in this respect between mice and humans. In humans, there has not been a documented PLB-knockout phenotype suggesting that PLB is crucial for fetal development[59]. A mimic of a PLB-knockout phenotype does exist in humans as the mutation PLB-Leu[39]stop which causes truncation and mis-targeting of PLB[116]. This mutation causes dilated cardiomyopathy and heart failure in affected individuals[116].

A study using PLB knockout mice was aimed at determining the functional PLB unit *in vivo*[117]. This study was an extension of previous studies using transgenic mice expressing mutant PLB on a wild-type PLB expression background[118]. On a PLB knockout background, the cardiac-specific expression of wild-type PLB and a monomeric PLB (Cys[41]Phe) had similar SERCA Ca^{2+} affinities in SR transport assays[117]. However, wild-type PLB caused greater depression of cardiac function in whole mouse hearts than did PLB-Cys[41]Phe, relative to the enhanced relaxation parameters of PLB knockout mice. Importantly, the expression levels were similar for wild-type PLB and the PLB-Cys[41]Phe mutant. Thus, although both pentameric wild-type PLB and monomeric PLB-Cys[41]Phe had similar inhibitory properties in transport assays using purified SR membrane vesicles, the overall regulation of SERCA in the whole mouse heart was dependent on the apparent oligomeric state of PLB. Such evidence would suggest that the regulation of SERCA is not achieved simply by inhibition of SERCA transport in whole hearts.

Animal studies have confirmed the importance of PLB regulation of SERCA for proper cardiac function, which is further supported by PLB mutations that cause human heart disease. Importantly, animal models have also highlighted the importance of PLB oligomerization for SERCA regulation[117]. Although the PLB monomer is proposed to be the active inhibitory species, the PLB pentamer plays an important role in physiological SERCA regulation. Such observations argue against the current speculation of the PLB pentamer as an inactive storage form.

2-3.8. An introduction to SLN.

Sarcolipin was first described as a low molecular-weight proteolipid that co-purified with preparations of SERCA[119] and named to describe its origin (sarcoplasmic reticulum) and properties (proteolipid)[120]. SLN is the predominant regulator of SERCA1a in fast-twitch skeletal muscle[120-122]. Recently, it has been shown that SLN is also expressed in the atria of the heart[123-125], where it can interact with PLB and cause super-inhibition of SERCA[126, 127]. SLN is a 31-resdiue type I integral membrane protein with a transmembrane domain homologous to the transmembrane domain of PLB[121, 122]. For this reason, it is hypothesized that SLN inhibits SERCA by binding and lowering the apparent Ca^{2+} affinity of the enzyme in a PLB-like manner[122]. Current models propose SLN and PLB might also use a common binding surface on SERCA to inhibit the enzyme[127, 128].

2-3.9. SLN inhibition of SERCA: In light or shadow of PLB studies?

SLN inhibition of SERCA is less well-characterized than PLB and only beginning to be understood[129]. It was proposed that SLN inhibits SERCA in a similar manner as PLB. However, as we learn more about SLN, we are finding that SLN inhibits SERCA differently than PLB. For example, it is generally accepted that SLN inhibition is not relieved by increased cytosolic Ca^{2+} concentrations[93]. Some studies report a small decrease in the maximum reaction rate (V_{max}) of SERCA by SLN at micromolar Ca^{2+} concentrations[126, 130], whereas other studies report that SLN can increase the V_{max} of SERCA at micromolar Ca^{2+} concentrations[122, 131]. In addition, it is not well established if phosphorylation of SLN is an important physiological mechanism and those supporting SLN phosphorylation are split on the identity of the responsible protein kinase[132, 133]. SLN migrates primarily as a monomer in SDS-PAGE, although evidence exists that SLN can oligomerize in detergent and lipid environments[131].

Similar to PLB, heterologous co-expression studies with SERCA have made important contributions to our understanding of SLN. Alanine-scanning mutagenesis of ten SLN residues identified only two gain-of-function mutants (Thr^{5}Ala and Tyr^{29}Ala). The remaining sampled residues were neutral or loss-of-function and the phospho-mimetic SLN-Thr^{5}Glu was a complete loss-of-function[122]. Co-expression of SERCA and SLN also identified the C-terminal (Arg^{27}-Ser-Tyr-Gln-Tyr^{31}) luminal tail of SLN as an important site of interaction[134]. Solid-state NMR has verified the importance of the C-

terminus of SLN for interaction with SERCA[130]. In particular, the two C-terminal SLN tyrosines (Tyr^{29} and Tyr^{31}) were demonstrated to specifically interact with SERCA1a[130]. As well, very high concentrations of a synthetic peptide mimicking the five C-terminal residues of SLN was reported to affect SERCA1a activity, suggesting the SLN C-terminal luminal tail has a functional role[130]. The hydrophilic luminal tail of SLN (Arg^{27}-Ser-Tyr-Gln-Tyr^{31}) is different than the hydrophobic luminal tail of PLB (Met^{50}-Leu-Leu^{51}) and perfectly conserved among mammals.

Co-immunoprecipitation studies with SERCA1a have compared residues in SLN to previously characterized residues in PLB[127]. With respect to binding SERCA1a, residues in SLN did not recapitulate the same effects as their equivalent residues in PLB. Most notably, SLN-Leu^{8}Ala had no effect on binding to SERCA1a (the equivalent PLB-Leu^{31}Ala decreased binding by 73%) and SLN-Ile^{17}Ala decreased binding by 18% (the equivalent PLB-Ile^{40}Ala increased binding by 145%)[135]. Overall, the SLN mutants had much less of an effect on the binding to SERCA1a compared to their PLB equivalents[127]. Mutation of residues in TM6 of SERCA1a had some effect on SLN binding suggesting that SLN binds in a similar region as PLB[127]. For this reason, the modeled site of interaction between SLN and SERCA is the same TM2, TM4, TM6 and TM9 groove as the monomer-binding site for PLB[127]. However it is worth noting that the effects of SERCA1a mutation were not the same between PLB and SLN. Taken together, these results suggest that SLN binding is different to some degree from that of PLB. Thus, their respective molecular mechanisms may also differ.

2-3.10. Structural studies of SLN.

Similar to functional studies of SLN, there have been few structural studies of SLN relative to PLB. The 3D structure of SLN has been determined in detergent and lipid environments by NMR (Figure 2.15)[136]. SLN forms a transmembrane α–helix (residues 9 to 27) with a short disordered N-terminal cytoplasmic region (residues 1 to 8) and a disordered C-terminal luminal region (residues 28 to 31)[136]. Solid-state NMR data was consistent with a perpendicular orientation of SLN to the membrane plane[136]. It was later determined that SLN can adopt a second distinct orientation and forms a mixed population between the two orientations[137].

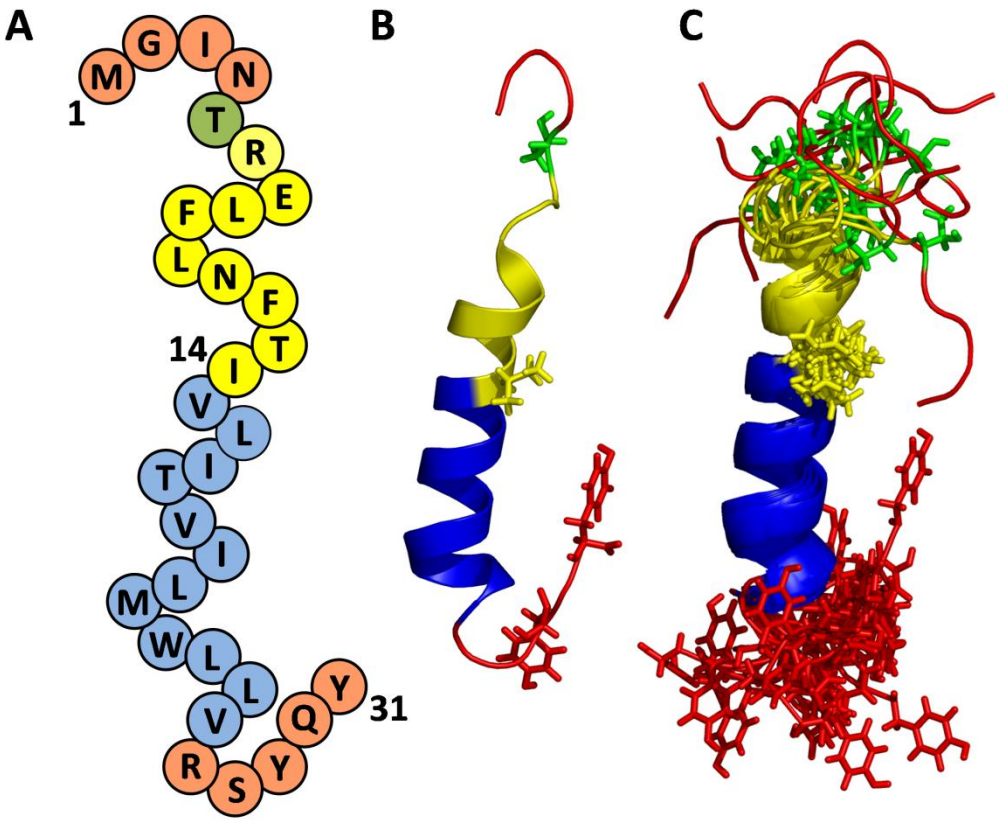

Figure 2.15. Sequence and structure of SLN. Panel A, the sequence of SLN as a schematic representation of its structure. The residues are coloured to highlight their dynamics with the N-terminus and C-terminus in *red* (dynamic), residues 6 to 14 in *yellow* (less dynamic) and residues 15 to 26 in *blue* (rigid). The potential SLN phosphorylation site, Thr^{5}, is indicated in *green* sticks. Residues Ile^{14}, Tyr^{29} and Tyr^{31} are also shown as sticks. **Panel B,** cartoon representation of the SLN structure by NMR (pdb: 1JDM)[136]. SLN residues are coloured as in panel A. **Panel C,** cartoon representation of SLN dynamics from the 16 deposited NMR states (pdb: 1JDM)[136]. SLN residues are coloured as in panel A.

A subsequent NMR study[138] determined a similar SLN structure with a minor extension of the transmembrane α-helix towards the N-terminus (starting at residue 6 compare to residue 8 in the previous structure). As well, SLN dynamics suggested the small protein is split into four sub-domains (Figure 2.15). The N-terminus and C-terminus were still disordered as previously described, but the transmembrane α-helix was dissected into two different domains based on their different dynamics (Figure 2.15). The more hydrophilic portion (residues 6 to 14) of the transmembrane domain was more dynamic than the hydrophobic portion (residues 15 to 27)[138]. The different dynamics of the SLN transmembrane α-helix mirrored differences between domain Ib and domain II in PLB. The authors also characterized the effect of SERCA on the structure of SLN[138]. The results suggest the relatively rigid transmembrane domain anchors SLN to SERCA and undergoes minor helix unwinding. The more dynamic SLN termini undergo more complex structural changes in the presence of SERCA[137].

A surprising channel-like activity has recently been reported for SLN reconstituted into tethered bilayer lipid membranes[139, 140]. The SLN channel-like activity was selective for small inorganic anions, such as Cl^- and phosphate, and impermeable to inorganic cations[139, 140]. This channel-like activity could be abolished by the SLN-Thr[18]Ala mutation in the SLN transmembrane α-helix[140]. Interestingly, the SLN channel-like activity was also modulated by ATP and ADP, in which the conductivity is stimulated by ATP and inhibited by ADP[140]. A regulatory role for the SLN channel activity was proposed on the activity of SERCA, which would require the SLN channels to come into close proximity with SERCA to exert their regulatory effects[140]. The observed channel-like activity of SLN under the experimental conditions would require SLN to oligomerize, consistent with previous cross-linking experiments[131]. There are no reported structural details of a SLN oligomer.

2-3.11. Transgenic approaches to study the regulation of SERCA by SLN in cardiac tissue.

In the mouse heart, SLN messenger RNA (mRNA) is specifically expressed in the atria and not detected in the ventricles[123]. SLN mRNA expression in the mouse atria was also shown to increase during development. A specific SLN mRNA signal was also demonstrated in human atria[123]. SLN protein expression in the atria of mice and rats was later demonstrated[93, 124]. With respect to the role of SLN in disease, SLN mRNA

expression is down-regulated in human hearts with chronic atrial fibrillation[141]and down-regulated in a transgenic mouse model of cardiac hypertrophy over-expressing Ras[123].

To investigate the role of SLN in the heart, transgenic mice were created on a PLB-knockout background with cardiac-specific over-expression of SLN[132]. Cardiomyocytes from the transgenic mice had altered contractility and Ca^{2+} transient amplitudes. However, there was no observed *in vivo* effect of cardiac-specific SLN over-expression. This study supported SLN phosphorylation and suggested Ser/Thr kinase 16 as a candidate kinase[132]. The candidate kinase for SLN phosphorylation has been proposed to be CaMKII by other studies[133, 142].

The SLN-knockout mouse quickly followed[143]. In the atria, the loss of SLN resulted in increased apparent Ca^{2+} affinity of SERCA, increased Ca^{2+} transient amplitudes and increased contractility. The SLN-knockout mice did not develop any heart disease phenotypes[143]. SLN phosphorylation was proposed based on the blunted response of SLN-knockout atria to isoproterenol stimulation. Combined, these data suggest SLN has a critical role in proper cardiac function in addition to PLB.

2-4. Thesis outline.

2-4.1. PLB and SLN bind as oligomers to SERCA in two-dimensional co-crystals.

In chapter 3 we introduce mutations into SLN to better characterize its regulation of SERCA. A number of residues in the short cytoplasmic domain increase SERCA inhibition upon mutation suggesting the cytoplasmic domain of SLN might be critical to fine-tuning its inhibitory mechanism. By increasing the similarity of the transmembrane domain of SLN to PLB, we shifted the equilibrium of SLN oligomerization towards a more oligomeric state. Concurrently, we also observed a loss-of-inhibition. These results parallel the mass action model of PLB regulation where destabilization of PLB pentamers causes a gain-of-inhibition.

In chapter 4, we characterize the interaction between SERCA and pentameric PLB observed by electron crystallography. The results support an active regulatory role for this interaction and argue against the long-held speculation that the PLB pentamer is an inactive storage form.

In chapter 5, we shift our focus to the interaction between SERCA and SLN. We observe a similar mode of interaction between SLN oligomers and SERCA as was observed between PLB pentamers and SERCA. This similarity highlights a previously undescribed mechanism used by both PLB and SLN to interact with SERCA.

In chapter 6, we conclude the main body of the thesis with a short discussion of its major contributions and the promise these hold for future studies of SERCA regulation by PLB and SLN.

2-4.2. Studying fragments of the prion protein to provide insights into the species transmission barrier phenomena of prion diseases.

In appendix I, we end with a short jaunt through prion research and potential applications of electron microscopy to the study of prion misfolding. The study focuses on the transmission of prion disease between species, the mechanisms of which are currently not well understood. In particular, the species bovine and elk were chosen because their associated diseases (bovine spongiform encephalopathy and chronic wasting disease, respectively) have been identified in Alberta within the last decade. The results highlight a potential source of variation between misfolded prions of different species and implications about the misfolding of the full-length prion protein are discussed.

2-5. References.

1. Albers RW. Biochemical aspects of active transport. Annu Rev Biochem 1967;36:727.

2. Post RL, Kume S, Hegyvary C. Activation by adenosine-triphosphate in phosphorylation kinetics of sodium and potassium ion transport adenosine-triphosphatase. J Biol Chem 1972;247(20):6530.

3. Demeis L, Vianna AL. Energy interconversion by the Ca2+-dependent atpase of the sarcoplasmic-reticulum. Annu Rev Biochem 1979;48:275-92.

4. Kuhlbrandt W. Biology, structure and mechanism of P-type ATPases. Nature Reviews Molecular Cell Biology 2004 APR;5(4):282-95.

5. Moller JV, Olesen C, Winther AL, Nissen P. The sarcoplasmic Ca2+-ATPase: Designof a perfect chemi-osmotic pump. Q Rev Biophys 2010 NOV;43(4):501-66.

6. Cornelius F, Moller JV. Electrogenic pump current of sarcoplasmic-reticulum Ca-2+-ATPase reconstituted at high lipid protein ratio. FEBS Lett 1991 JUN 17;284(1):46-50.

7. Levy D, Seigneuret M, Bluzat A, Rigaud JL. Evidence for proton countertransport by the sarcoplasmic-reticulum Ca-2+-ATPase during calcium-transport in reconstituted proteoliposomes with low ionic permeability. J Biol Chem 1990 NOV 15;265(32):19524-34.

8. Yu X, Carroll S, Rigaud JL, Inesi G. H+ countertransport and electrogenicity of the sarcoplasmic-reticulum Ca-2(+) pump in reconstituted proteoliposomes. Biophys J 1993 APR;64(4):1232-42.

9. Tanford C. Translocation pathway in the catalysis of active-transport. Proceedings of the National Academy of Sciences of the United States of America-Biological Sciences 1983;80(12):3701-5.

10. Clarke DM, Loo TW, Maclennan DH. Functional consequences of alterations to amino-acids located in the nucleotide binding domain of the Ca-2+-ATPase of sarcoplasmic-reticulum. J Biol Chem 1990 DEC 25;265(36):22223-7.

11. Clarke DM, Maruyama K, Loo TW, Leberer E, Inesi G, Maclennan DH. Functional consequences of glutamate, aspartate, glutamine, and asparagine mutations in the stalk sector of the Ca-2+-ATPase of sarcoplasmic-reticulum. J Biol Chem 1989 JUL 5;264(19):11246-51.

12. Vilsen B, Andersen JP, Clarke DM, Maclennan DH. Functional consequences of proline mutations in the cytoplasmic and transmembrane sectors of the Ca-2+-ATPase of sarcoplasmic-reticulum. J Biol Chem 1989 DEC 15;264(35):21024-30.

13. Andersen JP, Vilsen B, Leberer E, Maclennan DH. Functional consequences of mutations in the beta-strand sector of the Ca-2+-ATPase of sarcoplasmic-reticulum. J Biol Chem 1989 DEC 15;264(35):21018-23.

14. Clarke DM, Loo TW, Inesi G, Maclennan DH. Location of high-affinity Ca-2+-binding sites within the predicted transmembrane domain of the sarcoplasmic-reticulum ca-2+-atpase. Nature 1989 JUN 8;339(6224):476-8.

15. Maclennan DH, Brandl CJ, Korczak B, Green NM. Amino-acid-sequence of a Ca-2(+) + Mg-2+-dependent ATPase from rabbit muscle sarcoplasmic-reticulum, deduced from its complementary-dna sequence. Nature 1985;316(6030):696-700.

16. Taylor KA, Dux L, Martonosi A. 3-dimensional reconstruction of negatively stained crystals of the Ca-2+-ATPase from muscle sarcoplasmic-reticulum. J Mol Biol 1986 FEB 5;187(3):417-27.

17. Castellani L, Hardwicke PMD, Vibert P. Dimer ribbons in the 3-dimensional structure of sarcoplasmic-reticulum. J Mol Biol 1985;185(3):579-94.

18. Toyoshima C, Sasabe H, Stokes DL. 3-dimensional cryoelectron microscopy of the calcium-ion pump in the sarcoplasmic-reticulum membrane. Nature 1993 APR 1;362(6419):469-71.

19. Skriver E, Maunsbach AB, Jorgensen PL. Formation of two-dimensional crystals in pure membrane-bound na+,k+-atpase. FEBS Lett 1981;131(2):219-22.

20. Dux L, Martonosi A. Two-dimensional arrays of proteins in sarcoplasmic-reticulum and purified Ca-2+-ATPase vesicles treated with vanadate. J Biol Chem 1983;258(4):2599-603.

21. Maurer A, Fleischer S. Decavanadate is responsible for vanadate-induced 2-dimensional crystals in sarcoplasmic-reticulum. J Bioenerg Biomembr 1984;16(5-6):491-505.

22. Toyoshima C, Nakasako M, Nomura H, Ogawa H. Crystal structure of the calcium pump of sarcoplasmic reticulum at 2.6 angstrom resolution. Nature 2000 JUN 8;405(6787):647-55.

23. Stokes DL, Lacapere JJ. Conformation of Ca2+-ATPase in 2 crystal forms - effects of Ca2+, thapsigarin, adenosine 5'-(beta,gamma-methylene)triphosphate), and chromium(iii)-atp on crystallization. J Biol Chem 1994 APR 15;269(15):11606-13.

24. Xu C, Rice WJ, He WZ, Stokes DL. A structural model for the catalytic cycle of Ca2+-ATPase. J Mol Biol 2002 FEB 8;316(1):201-11.

25. Zhang PJ, Toyoshima C, Yonekura K, Green NM, Stokes DL. Structure of the calcium pump from sarcoplasmic reticulum at 8-angstrom resolution. Nature 1998 APR 23;392(6678):835-9.

26. MacLennan DH, Rice WJ, Green NM. The mechanism of Ca2+ transport by sarco(endo)plasmic reticulum Ca2+-ATPases. J Biol Chem 1997 NOV 14;272(46):28815-8.

27. Rice WJ, MacLennan DH. Scanning mutagenesis reveals a similar pattern of mutation sensitivity in transmembrane sequences M4, M5, and M6, but not in M8, of the Ca2+-ATPase of sarcoplasmic reticulum (SERCA1a). J Biol Chem 1996 DEC 6;271(49):31412-9.

28. Chen L, Sumbilla C, Lewis D, Zhong LL, Strock C, Kirtley ME, Inesi G. Short and long range functions of amino acids in the transmembrane region of the sarcoplasmic reticulum ATPase - A mutational study. J Biol Chem 1996 MAY 3;271(18):10745-52.

29. Andersen JP. Dissection of the functional domains of the sarcoplasmic reticulum Ca2+-ATPase by site-directed mutagenesis. Biosci Rep 1995 OCT;15(5):243-61.

30. Lee AG, East JM. What the structure of a calcium pump tells us about its mechanism. Biochem J 2001 JUN 15;356:665-83.

31. Hunte C, Screpanti E, Venturi M, Rimon A, Padan E, Michel H. Structure of a Na+/H+ antiporter and insights into mechanism of action and regulation by pH. Nature 2005 JUN 30;435(7046):1197-202.

32. Ding J, Rainey JK, Xu C, Sykes BD, Fliegel L. Structural and functional characterization of transmembrane segment VII of the Na+/H+ exchanger isoform 1. J Biol Chem 2006 OCT 6;281(40):29817-29.

33. Lee BL, Li X, Liu Y, Sykes BD, Fliegel L. Structural and functional analysis of transmembrane XI of the NHE1 isoform of the Na+/H+ exchanger. J Biol Chem 2009 APR 24;284(17):11546-56.

34. Danko S, Daiho T, Yamasaki K, Kamidochi M, Suzuki H, Toyoshima C. ADP-insensitive phosphoenzyme intermediate of sarcoplasmic reticulum Ca2+-ATPase has a compact conformation resistant to proteinase K, V8 protease and trypsin. FEBS Lett 2001 FEB 2;489(2-3):277-82.

35. Pick U, Karlish SJD. Indications for an oligomeric structure and for conformational-changes in sarcoplasmic-reticulum Ca-2+-ATPase labeled selectively with fluorescein. Biochim Biophys Acta 1980;626(1):255-61.

36. Toyoshima C, Nomura H. Structural changes in the calcium pump accompanying the dissociation of calcium. Nature 2002 AUG 8;418(6898):605-11.

37. Yu MH, Zhang LL, Rishi AK, Khadeer M, Inesi G, Hussain A. Specific substitutions at amino acid 256 of the sarcoplasmic/endoplasmic reticulum Ca2+ transport ATPase mediate resistance to thapsigargin in thapsigargin-resistant hamster cells. J Biol Chem 1998 FEB 6;273(6):3542-6.

38. Hua SM, Inesi G. Synthesis of a radioactive azido derivative of thapsigargin and photolabeling of the sarcoplasmic reticulum ATPase. Biochemistry (N Y) 1997 SEP 30;36(39):11865-72.

39. Sorensen TLM, Moller JV, Nissen P. Phosphoryl transfer and calcium ion occlusion in the calcium pump. Science 2004 JUN 11;304(5677):1672-5.

40. Toyoshima C, Mizutani T. Crystal structure of the calcium pump with a bound ATP analogue. Nature 2004 JUL 29;430(6999):529-35.

41. Olesen C, Picard M, Winther AL, Gyrup C, Morth JP, Oxvig C, Moller JV, Nissen P. The structural basis of calcium transport by the calcium pump. Nature 2007 DEC 13;450(7172):1036-U5.

42. Toyoshima C, Norimatsu Y, Iwasawa S, Tsuda T, Ogawa H. How processing of aspartylphosphate is coupled to lumenal gating of the ion pathway in the calcium pump. Proc Natl Acad Sci U S A 2007 DEC 11;104(50):19831-6.

43. Olesen C, Sorensen TLM, Nielsen RC, Moller JV, Nissen P. Dephosphorylation of the calcium pump coupled to counterion occlusion. Science 2004 DEC 24;306(5705):2251-5.

44. Jensen AL, Sorensen TL, Olesen C, Moller JV, Nissen P. Modulatory and catalytic modes of ATP binding by the calcium pump. EMBO J 2006 JUN 7;25(11):2305-14.

45. Obara K, Miyashita N, Xu C, Toyoshima L, Sugita Y, Inesi G, Toyoshima C. Structural role of countertransport revealed in Ca2+ pump crystal structure in the absence of Ca2+. Proc Natl Acad Sci U S A 2005 OCT 11;102(41):14489-96.

46. Khan YM, Wictome M, East JM, Lee AG. Interactions of dihydroxybenzenes with the Ca2+-ATPase - separate binding-sites for dihydroxybenzenes and sesquiterpene. Biochemistry (N Y) 1995 NOV 7;34(44):14385-93.

47. Inesi G, Ma HL, Lewis D, Xu C. Ca2+ occlusion and gating function of Glu(309) in the ADP-fluoroaluminate analog of the Ca2+-ATPase phosphoenzyme intermediate. J Biol Chem 2004 JUL 23;279(30):31629-37.

48. Moncoq K, Trieber CA, Young HS. The molecular basis for cyclopiazonic acid inhibition of the sarcoplasmic reticulum calcium pump. J Biol Chem 2007 MAR 30;282(13):9748-57.

49. Soler F, Plenge-Tellechea F, Fortea I, Fernandez-Belda F. Cyclopiazonic acid effect on Ca2+-dependent conformational states of the sarcoplasmic reticulum ATPase. implication for the enzyme turnover. Biochemistry (N Y) 1998 MAR 24;37(12):4266-74.

50. Ma HL, Zhong LL, Inesi G, Fortea I, Soler F, Fernandez-Belda F. Overlapping effects of S3 stalk segment mutations on the affinity of Ca2+-ATPase (SERCA) for thapsigargin and cyclopiazonic acid. Biochemistry (N Y) 1999 NOV 23;38(47):15522-7.

51. Seidler NW, Jona I, Vegh M, Martonosi A. Cyclopiazonic acid is a specific inhibitor of the Ca-2+-ATPase of sarcoplasmic-reticulum. J Biol Chem 1989 OCT 25;264(30):17816-23.

52. Tada M, Kirchberger MA, Li HC. Phosphoprotein phosphatase-catalyzed dephosphorylation of 22,000 dalton phosphoprotein of cardiac sarcoplasmic-reticulum. J Cyclic Nucleotide Res 1975;1(6):329-38.

53. Tada M, Kirchberger MA, Katz AM. Phosphorylation of a 22,000-dalton component of cardiac sarcoplasmic-reticulum by adenosine 3'-5'-monophosphate-dependent protein kinase. J Biol Chem 1975;250(7):2640-7.

54. Jones LR, Besch HR, Fleming JW, Mcconnaughey MM, Watanabe AM. Separation of vesicles of cardiac sarcolemma from vesicles of cardiac sarcoplasmic-reticulum - comparative biochemical-analysis of component activities. J Biol Chem 1979;254(2):530-9.

55. Bidlack JM, Shamoo AE. Adenosine 3',5'-monophosphate-dependent phosphorylation of a 6000 and a 22000 dalton protein from cardiac sarcoplasmic-reticulum. Biochim Biophys Acta 1980;632(2):310-25.

56. Koss KL, Kranias EG. Phospholamban: A prominent regulator of myocardial contractility. Circ Res 1996 DEC;79(6):1059-63.

57. Kranias EG, Nakamura J, Schwartz A. Phospholamban, the regulator of the cardiac sarcoplasmic-reticulum calcium-pump, does not copurify with the Ca-2+-ATPase enzyme. Biochim Biophys Acta 1983;749(1):62-8.

58. Ambudkar IS, Fanfarillo DT, Shamoo AE. Phospholamban involvement in the maintenance of basal calcium-transport in cardiac sarcoplasmic-reticulum. Membr Biochem 1986;6(4):327-46.

59. MacLennan DH, Kranias EG. Phospholamban: A crucial regulator of cardiac contractility. Nature Reviews Molecular Cell Biology 2003 JUL;4(7):566-77.

60. Tada M, Kirchber.Ma, Repke DI, Katz AM. Stimulation of calcium-transport in cardiac sarcoplasmic-reticulum by adenosine 3'-5'-monophosphate-dependent protein kinase. J Biol Chem 1974;249(19):6174-80.

61. Asahi M, McKenna E, Kurzydlowski K, Tada M, MacLennan DH. Physical interactions between phospholamban and sarco(endo)plasmic reticulum Ca2+-ATPases are dissociated by elevated Ca2+, but not by phospholamban phosphorylation, vanadate, or thapsigargin, and are enhanced by ATP. J Biol Chem 2000 MAY 19;275(20):15034-8.

62. Antipenko AY, Spielman AI, Sassaroli M, Kirchberger MA. Comparison of the kinetic effects of phospholamban phosphorylation and anti-phospholamban monoclonal antibody on the calcium pump in purified cardiac sarcoplasmic reticulum membranes. Biochemistry (N Y) 1997 OCT 21;36(42):12903-10.

63. Tada M, Inui M, Yamada M, Kadoma M, Kuzuya T, Abe H, Kakiuchi S. Effects of phospholamban phosphorylation catalyzed by adenosine 3'-5'-monophosphate-dependent and calmodulin-dependent protein-kinases on calcium-transport atpase of cardiac sarcoplasmic-reticulum. J Mol Cell Cardiol 1983;15(5):335-46.

64. Simmerman HKB, Collins JH, Theibert JL, Wegener AD, Jones LR. Sequence-analysis of phospholamban - identification of phosphorylation sites and 2 major structural domains. J Biol Chem 1986 OCT 5;261(28):3333-41.

65. Morris GL, Cheng HC, Colyer J, Wang JH. Phospholamban regulation of cardiac sarcoplasmic-reticulum (Ca2+-Mg2+)-atpase - mechanism of regulation and site of monoclonal-antibody interaction. J Biol Chem 1991 JUN 15;266(17):11270-5.

66. Fujii J, Kadoma M, Tada M, Toda H, Sakiyama F. Characterization of structural unit of phospholamban by amino-acid sequencing and electrophoretic analysis. Biochem Biophys Res Commun 1986 AUG 14;138(3):1044-50.

67. Simmerman HKB, Kobayashi YM, Autry JM, Jones LR. A leucine zipper stabilizes the pentameric membrane domain of phospholamban and forms a coiled-coil pore structure. J Biol Chem 1996 MAR 8;271(10):5941-6.

68. Adams PD, Arkin IT, Engelman DM, Brunger AT. Computational searching and mutagenesis suggest a structure for the pentameric transmembrane domain of phospholamban. Nat Struct Biol 1995 FEB;2(2):154-62.

69. Karim CB, Stamm JD, Karim J, Jones LR, Thomas DD. Cysteine reactivity and oligomeric structures of phospholamban and its mutants. Biochemistry (N Y) 1998 SEP 1;37(35):12074-81.

70. Pollesello P, Annila A, Ovaska M. Structure of the 1-36 amino-terminal fragment of human phospholamban by nuclear magnetic resonance and modeling of the phospholamban pentamer. Biophys J 1999 APR;76(4):1784-95.

71. Lamberth S, Schmid H, Muenchbach M, Vorherr T, Krebs J, Carafoli E, Griesinger C. NMR solution structure of phospholamban. Helv Chim Acta 2000;83(9):2141-52.

72. Zamoon J, Nitu F, Karim C, Thomas DD, Veglia G. Mapping the interaction surface of a membrane protein: Unveiling the conformational switch of phospholamban in calcium pump regulation. Proc Natl Acad Sci U S A 2005 MAR 29;102(13):4747-52.

73. Oxenoid K, Chou JJ. The structure of phospholamban pentamer reveals a channel-like architecture in membranes. Proc Natl Acad Sci U S A 2005 AUG 2;102(31):10870-5.

74. Zamoon J, Mascioni A, Thomas DD, Veglia G. NMR solution structure and topological orientation of monomeric phospholamban in dodecylphosphocholine micelles. Biophys J 2003 OCT;85(4):2589-98.

75. Robia SL, Flohr NC, Thomas DD. Phospholamban pentamer quaternary conformation determined by in-gel fluorescence anisotropy. Biochemistry (N Y) 2005 MAR 22;44(11):4302-11.

76. Kelly EM, Hou Z, Bossuyt J, Bers DM, Robia SL. Phospholamban oligomerization, quaternary structure, and sarco(endo) plasmic reticulum calcium ATPase binding measured by fluorescence resonance energy transfer in living cells. J Biol Chem 2008 MAY 2;283(18):12202-11.

77. Traaseth NJ, Verardi R, Torgersen KD, Karim CB, Thomas DD, Veglia G. Spectroscopic validation of the pentameric structure of phospholarnban. Proc Natl Acad Sci U S A 2007 SEP 11;104(37):14676-81.

78. Cornea RL, Jones LR, Autry JM, Thomas DD. Mutation and phosphorylation change the oligomeric structure of phospholamban in lipid bilayers. Biochemistry (N Y) 1997 MAR 11;36(10):2960-7.

79. Wegener AD, Simmerman HKB, Liepnieks J, Jones LR. Proteolytic cleavage of phospholamban purified from canine cardiac sarcoplasmic-reticulum vesicles - generation of a low resolution model of phospholamban structure. J Biol Chem 1986 APR 15;261(11):5154-9.

80. Oxenoid K, Rice AJ, Chou JJ. Comparing the structure and dynamics of phospholamban pentamer in its unphosphorylated and pseudo-phosphorylated states. Protein Science 2007 SEP;16(9):1977-83.

81. Hou Z, Kelly EM, Robia SL. Phosphomimetic mutations increase phospholamban oligomerization and alter the structure of its regulatory complex. J Biol Chem 2008 OCT 24;283(43):28996-9003.

82. Verardi R, Shi L, Traaseth NJ, Walsh N, Veglia G. Structural topology of phospholamban pentamer in lipid bilayers by a hybrid solution and solid-state NMR method. Proc Natl Acad Sci U S A 2011 MAY 31;108(22):9101-6.

83. Karim CB, Kirby TL, Zhang ZW, Nesmelov Y, Thomas DD. Phospholamban structural dynamics in lipid bilayers probed by a spin label rigidly coupled to the peptide backbone. Proc Natl Acad Sci U S A 2004 OCT 5;101(40):14437-42.

84. Metcalfe EE, Zamoon J, Thomas DD, Veglia G. H-1/N-15 heteronuclear NMR spectroscopy shows four dynamic domains for phospholamban reconstituted in dodecylphosphocholine micelles. Biophys J 2004 AUG;87(2):1205-14.

85. Metcalfe E, Traaseth N, Veglia G. Serine 16 phosphorylation induces an order-to-disorder transition in monomeric phospholamban RID B-4751-2010. Biochemistry (N Y) 2005 MAR 22;44(11):4386-96.

86. Karim CB, Zhang ZW, Howard EC, Torgersen KD, Thomas DD. Phosphorylation-dependent conformational switch in spin-labeled phospholamban bound to SERCA. J Mol Biol 2006 MAY 12;358(4):1032-40.

87. Traaseth NJ, Thomas DD, Veglia G. Effects of Ser16 phosphorylation on the allosteric transitions of phospholamban/Ca2+-ATPase complex. J Mol Biol 2006 MAY 12;358(4):1041-50.

88. Fujii J, Maruyama K, Tada M, Maclennan DH. Coexpression of slow-Twitch/cardiac muscle Ca2+-atpase (SERCA2) and phospholamban. FEBS Lett 1990 OCT 29;273(1-2):232-4.

89. Toyofuku T, Kurzydlowski K, Tada M, Maclennan DH. Identification of regions in the Ca2+-ATPase of sarcoplasmic-reticulum that affect functional association with phospholamban. J Biol Chem 1993 FEB 5;268(4):2809-15.

90. Toyofuku T, Kurzydlowski K, Tada M, Maclennan DH. Amino-acids glu(2) to ile(18) in the cytoplasmic domain of phospholamban are essential for functional association with the Ca2+-ATPase of sarcoplasmic-reticulum. J Biol Chem 1994 JAN 28;269(4):3088-94.

91. Kimura Y, Kurzydlowski K, Tada M, MacLennan DH. Phospholamban inhibitory function is activated by depolymerization. J Biol Chem 1997 JUN 13;272(24):15061-4.

92. Kimura Y, Asahi M, Kurzydlowski K, Tada M, MacLennan DH. Phospholamban domain ib mutations influence functional interactions with the Ca2+-ATPase

isoform of cardiac sarcoplasmic reticulum. J Biol Chem 1998 JUN 5;273(23):14238-41.

93. Periasamy M, Bhupathy P, Babu GJ. Regulation of sarcoplasmic reticulum Ca2+ ATPase pump expression and its relevance to cardiac muscle physiology and pathology. Cardiovasc Res 2008 JAN 15;77(2):265-73.

94. Cornea RL, Autry JM, Chen ZH, Jones LR. Reexamination of the role of the leucine/isoleucine zipper residues of phospholamban in inhibition of the Ca2+ pump of cardiac sarcoplasmic reticulum. J Biol Chem 2000 DEC 29;275(52):41487-94.

95. Chiesi M, Schwaller R. Involvement of electrostatic phenomena in phospholamban-induced stimulation of Ca uptake into cardiac sarcoplasmic-reticulum. FEBS Lett 1989 FEB 13;244(1):241-4.

96. James P, Inui M, Tada M, Chiesi M, Carafoli E. Nature and site of phospholamban regulation of the Ca-2+ pump of sarcoplasmic-reticulum. Nature 1989 NOV 2;342(6245):90-2.

97. Jones LR, Cornea RL, Chen ZH. Close proximity between residue 30 of phospholamban and cysteine 318 of the cardiac Ca2+ pump revealed by intermolecular thiol cross-linking. J Biol Chem 2002 AUG 2;277(31):28319-29.

98. Chen ZH, Stokes SL, Rice WJ, Jones LR. Spatial and dynamic interactions between phospholamban and the canine cardiac Ca2+ pump revealed with use of heterobifunctional cross-linking agents. J Biol Chem 2003 NOV 28;278(48):48348-56.

99. Chen ZH, Stokes DL, Jones LR. Role of leucine 31 of phospholamban in structural and functional interactions with the Ca2+ pump of cardiac sarcoplasmic reticulum. J Biol Chem 2005 MAR 18;280(11):10530-9.

100. Toyoshima C, Asahi M, Sugita Y, Khanna R, Tsuda T, MacLennan DH. Modeling of the inhibitory interaction of phospholamban with the Ca2+ ATPase. Proc Natl Acad Sci U S A 2003 JAN 21;100(2):467-72.

101. Young EF, Mckee MJ, Ferguson DG, Kranias EG. Structural characterization of phospholamban in cardiac sarcoplasmic-reticulum membranes by cross-linking. Membr Biochem 1989;8(2):95-106.

102. Voss J, Jones LR, Thomas DD. The physical-mechanism of calcium-pump regulation in the heart. Biophys J 1994 JUL;67(1):190-6.

103. Squier TC, Thomas DD. Relationship between protein rotational-dynamics and phosphoenzyme decomposition in the sarcoplasmic-reticulum Ca-ATPase. J Biol Chem 1988 JUL 5;263(19):9171-7.

104. Squier TC, Hughes SE, Thomas DD. Rotational-dynamics and protein-protein interactions in the Ca-ATPase mechanism. J Biol Chem 1988 JUL 5;263(19):9162-70.

105. Squier TC, Bigelow DJ, Thomas DD. Lipid fluidity directly modulates the overall protein rotational mobility of the Ca-ATPase in sarcoplasmic-reticulum. J Biol Chem 1988 JUL 5;263(19):9178-86.

106. Birmachu W, Thomas DD. Rotational-dynamics of the Ca-ATPase in sarcoplasmic-reticulum studied by time-resolved phosphorescence anisotropy. Biochemistry (N Y) 1990 APR 24;29(16):3904-14.

107. Reddy LG, Jones LR, Thomas DD. Depolymerization of phospholamban in the presence of calcium pump: A fluorescence energy transfer study. Biochemistry (N Y) 1999 MAR 30;38(13):3954-62.

108. Mueller B, Karim CB, Negrashov IV, Kutchai H, Thomas DD. Direct detection of phospholamban and sarcoplasmic reticulum Ca-ATPase interaction in membranes using fluorescence resonance energy transfers. Biochemistry (N Y) 2004 JUL 13;43(27):8754-65.

109. Robia SL, Campbell KS, Kelly EM, Hou Z, Winters DL, Thomas DD. Forster transfer recovery reveals that phospholamban exchanges slowly from pentamers but rapidly from the SERCA regulatory complex. Circ Res 2007 NOV 26;101(11):1123-9.

110. Ha KN, Traaseth NJ, Verardi R, Zamoon J, Cembran A, Karim CB, Thomas DD, Veglia G. Controlling the inhibition of the sarcoplasmic Ca2+-ATPase by tuning phospholamban structural dynamics. J Biol Chem 2007 DEC 21;282(51):37205-14.

111. Young HS, Jones LR, Stokes DL. Locating phospholamban in co-crystals with Ca2+-ATPase by cryoelectron microscopy. Biophys J 2001 AUG;81(2):884-94.

112. Stokes DL, Pomfret AJ, Rice WJ, Glaves JP, Young HS. Interactions between Ca2+-ATPase and the pentameric form of phospholamban in two-dimensional co-crystals. Biophys J 2006 JUN;90(11):4213-23.

113. Zhai J, Schmidt AG, Hoit BD, Kimura Y, MacLennan DH, Kranias EG. Cardiac-specific overexpression of a superinhibitory pentameric phospholamban mutant enhances inhibition of cardiac function in vivo. J Biol Chem 2000 APR 7;275(14):10538-44.

114. Zvaritch E, Backx PH, Jirik F, Kimura Y, de Leon S, Schmidt AG, Hoit BD, Lester JW, Kranias EG, MacLennan DH. The transgenic expression of highly inhibitory monomeric forms of phospholamban in mouse heart impairs cardiac contractility. J Biol Chem 2000 MAY 19;275(20):14985-91.

115. Luo WS, Grupp IL, Harrer J, Ponniah S, Grupp G, Duffy JJ, Doetschman T, Kranias EG. Targeted ablation of the phospholamban gene is associated with markedly enhanced myocardial-contractility and loss of beta-agonist stimulation. Circ Res 1994 SEP;75(3):401-9.

116. Haghighi K, Kolokathis F, Pater L, Lynch RA, Asahi M, Gramolini AO, Fan GC, Tsiapras D, Hahn HS, Adamopoulos S, Liggett SB, Dorn GW, MacLennan DH, Kremastinos DT, Kranias EG. Human phospholamban null results in lethal dilated cardiomyopathy revealing a critical difference between mouse and human. J Clin Invest 2003 MAR;111(6):869-76.

117. Chu GX, Li L, Sato Y, Harrer JM, Kadambi VJ, Hoit BD, Bers DM, Kranias EG. Pentameric assembly of phospholamban facilitates inhibition of cardiac function in vivo. J Biol Chem 1998 DEC 11;273(50):33674-80.

118. Chu GX, Dorn GW, Luo WS, Harrer JM, Kadambi VJ, Walsh RA, Kranias EG. Monomeric phospholamban overexpression in transgenic mouse hearts. Circ Res 1997 OCT;81(4):485-92.

119. Maclenna.Dh, Seeman P, Iles GH, Yip CC. Resolution of enzymes of biological transport .2. membrane formation by adenosine triphosphatase of sarcoplasmic reticulum. J Biol Chem 1971;246(8):2702,&.

120. Wawrzynow A, Theibert JL, Murphy C, Jona I, Martonosi A, Collins JH. Sarcolipin, the proteolipid of skeletal-muscle sarcoplasmic-reticulum, is a unique, amphipathic, 31-residue peptide. Arch Biochem Biophys 1992 NOV 1;298(2):620-3.

121. Odermatt A, Taschner PEM, Scherer SW, Beatty B, Khanna VK, Cornblath DR, Chaudhry V, Yee WC, Schrank B, Karpati G, Breuning MH, Knoers N, MacLennan DH. Characterization of the gene encoding human sarcolipin (SLN), a proteolipid associated with SERCA1: Absence of structural mutations in five patients with brody disease. Genomics 1997 NOV 1;45(3):541-53.

122. Odermatt A, Becker S, Khanna VK, Kurzydlowski K, Leisner E, Pette D, MacLennan DH. Sarcolipin regulates the activity of SERCA1, the fast-twitch skeletal muscle sarcoplasmic reticulum Ca2+-ATPase. J Biol Chem 1998 MAY 15;273(20):12360-9.

123. Minamisawa S, Wang YB, Chen J, Ishikawa Y, Chien KR, Matsuoka R. Atrial chamber-specific expression of sarcolipin is regulated during development and hypertrophic remodeling. J Biol Chem 2003 MAR 14;278(11):9570-5.

124. Vangheluwe P, Schuermans M, Zador E, Waelkens E, Raeymaekers L, Wuytack F. Sarcolipin and phospholamban mRNA and protein expression in cardiac and skeletal muscle of different species. Biochem J 2005 JUL 1;389:151-9.

125. Babu GJ, Bhupathy P, Carnes CA, Billman GE, Periasamy M. Differential expression of sarcolipin protein during muscle development and cardiac pathophysiology. J Mol Cell Cardiol 2007 AUG;43(2):215-22.

126. Asahi M, Kurzydlowski K, Tada M, MacLennan DH. Sarcolipin inhibits polymerization of phospholamban to induce superinhibition of sarco(endo)plasmic reticulum Ca2+-ATPases (SERCAs). J Biol Chem 2002 JUL 26;277(30):26725-8.

127. Asahi M, Sugita Y, Kurzydlowski K, De Leon S, Tada M, Toyoshima C, MacLennan DH. Sarcolipin regulates sarco(endo)plasmic reticulurn Ca2+-ATPase (SERCA) by binding to transmembrane helices alone or in association with phospholamban. Proc Natl Acad Sci U S A 2003 APR 29;100(9):5040-5.

128. Morita T, Hussain D, Asahi M, Tsuda T, Kurzydlowski K, Toyoshima C, MacLennan DH. Interaction sites among phospholamban, sarcolipin, and the sarco(endo)plasmic reticulum Ca2+-ATPase. Biochem Biophys Res Commun 2008 APR 25;369(1):188-94.

129. Periasamy M, Kalyanasundaram A. SERCA pump isoforms: Their role in calcium transport and disease. Muscle Nerve 2007 APR;35(4):430-42.

130. Hughes E, Clayton JC, Kitmitto A, Esmann M, Middleton DA. Solid-state NMR and functional measurements indicate that the conserved tyrosine residues of sarcolipin are involved directly in the inhibition of SERCA1. J Biol Chem 2007 SEP 7;282(36):26603.

131. Hellstern S, Pegoraro S, Karim CB, Lustig A, Thomas DD, Moroder L, Engel J. Sarcolipin, the shorter homologue of phospholamban, forms oligomeric structures in detergent micelles and in liposomes. J Biol Chem 2001 AUG 17;276(33):30845-52.

132. Gramolini AO, Trivieri MG, Oudit GY, Kislinger T, Li WP, Patel MM, Emili A, Kranias EG, Backx PH, MacLennan DH. Cardiac-specific overexpression of sarcolipin in phospholamban null mice impairs myocyte function that is restored by phosphorylation. Proc Natl Acad Sci U S A 2006 FEB 14;103(7):2446-51.

133. Bhupathy P, Babu GJ, Ito M, Periasamy M. Threonine-5 at the N-terminus can modulate sarcolipin function in cardiac myocytes. J Mol Cell Cardiol 2009 NOV;47(5):723-9.

134. Gramolini AO, Kislinger T, Asahi M, Li WP, Emili A, MacLennan DH. Sarcolipin retention in the endoplasmic reticulum depends on its C-terminal RSYQY sequence and its interaction with sarco(endo)plasmic Ca2+-ATPases. Proc Natl Acad Sci U S A 2004 NOV 30;101(48):16807-12.

135. Asahi M, Kimura Y, Kurzydlowski R, Tada M, MacLennan DH. Transmembrane helix M6 in sarco(endo)plasmic reticulum Ca2+-ATPase forms a functional interaction site with phospholamban - evidence for physical, interactions at other sites. J Biol Chem 1999 NOV 12;274(46):32855-62.

136. Mascioni A, Karim C, Barany G, Thomas DD, Veglia G. Structure and orientation of sarcolipin in lipid environments. Biochemistry (N Y) 2002 JAN 15;41(2):475-82.

137. Buffy JJ, Traaseth NJ, Mascioni A, Gor'kov PL, Chekmenev EY, Brey WW, Veglia G. Two-dimensional solid-state NMR reveals two topologies of sarcolipin in oriented lipid bilayers. Biochemistry (N Y) 2006 SEP 12;45(36):10939-46.

138. Buffy JJ, Buck-Koehntop BA, Porcelli F, Traaseth NJ, Thomas DD, Veglia G. Defining the intramembrane binding mechanism of sarcolipin to calcium ATPase using solution NMR spectroscopy. J Mol Biol 2006 APR 28;358(2):420-9.

139. Becucci L, Guidelli R, Karim CB, Thomas DD, Veglia G. An electrochemical investigation of sarcolipin reconstituted into a mercury-supported lipid bilayer. Biophys J 2007 OCT;93(8):2678-87.

140. Becucci L, Guidelli R, Karim CB, Thomas DD, Veglia G. The role of sarcolipin and ATP in the transport of phosphate ion into the sarcoplasmic reticulum. Biophys J 2009 Nov 18;97(10):2693-9.

141. Uemura N, Ohkusa T, Hamano K, Nakagome M, Hori H, Shimizu M, Matsuzaki M, Mochizuki S, Minamisawa S, Ishikawa Y. Down-regulation of sarcolipin mRNA expression in chronic atrial fibrillation. Eur J Clin Invest 2004 NOV;34(11):723-30.

142. Bhupathy P, Babu GJ, Periasamy M. Sarcolipin and phospholamban as regulators of cardiac sarcoplasmic reticulum Ca2+ ATPase. J Mol Cell Cardiol 2007 MAY;42(5):903-11.

143. Babu GJ, Bhupathy P, Timofeyev V, Petrashevskaya NN, Reiser PJ, Chiamvimonvat N, Periasamy M. Ablation of sarcolipin enhances sarcoplasmic reticulum calcium transport and atrial contractility. Proc Natl Acad Sci U S A 2007 NOV 6;104(45):17867-72.

Chapter 3.

The cytoplasmic domain of the calcium pump inhibitor sarcolipin functionally mimics domain Ib of phospholamban.

Acknowledgements: J. Douglas cloned the human SLN gene and generated the MBP-SLN expression plasmid. Dr. C. Trieber purified SERCA for the co-reconstitutions. J. Primeau and P. Gorski both played important roles in the purification of the numerous SLN mutants and provided technical expertise for reverse-phase high pressure liquid chromatography.

Chapter 3. The cytoplasmic domain of the calcium pump inhibitor sarcolipin functionally mimics domain Ib of phospholamban.

3-1. Introduction.

Sarcolipin (SLN) is a small integral membrane protein that regulates the sarco(endo)plasmic reticulum ATPase (SERCA) in fast-twitch skeletal muscle and cardiac muscle. SLN was originally identified as a physiological regulator of SERCA1a in fast-twitch skeletal muscle[1-3], and more recently as a regulator of SERCA2a in the atria of the heart[4-8]. To regulate calcium (Ca^{2+}) transport, SLN binds to SERCA and lowers the apparent Ca^{2+} affinity of the enzyme. The critical fine-tuning of this regulatory mechanism is evident in SLN over-expression models that impair muscle contraction[9-13]. Indeed, SLN expression has been shown to be altered in human disease[14-16] and may be an important target of stress responses in the heart[17, 18]. NMR studies of SLN[19, 20] split the small protein into 3 regions: a short unstructured, cytoplasmic domain (residues 1-6), a transmembrane helical domain (residues 7-26) and a short unstructured, luminal tail (residues 27-31). The transmembrane helix of SLN can be further split into a dynamic N-terminal region (residues 6-14) and a more rigid C-terminal region (residues 15-27) (Figures 3.1 and 3.2)[20]. It has been proposed that the dynamics of the different regions of SLN play a role in binding to SERCA[20].

Functionally, the regions of SLN have overlapping and distinctive roles. The transmembrane helix is thought to be primarily responsible for the inhibitory properties

of SLN because of homology to the transmembrane helix of phospholamban (PLB), a related SERCA inhibitor in cardiac and smooth muscle. Mutations in the transmembrane domain of PLB dramatically alter its functional state leading to both gain-of-function and loss-of-function[32]. However, homologous mutations in the transmembrane domain of SLN do not cause any gain-of-function with respect to SERCA inhibition[3]. The luminal tail of SLN is critical for proper SLN function[3, 21] and proper targeting[2222] through interaction with SERCA[22]. More specifically, residues Tyr^{29} and Tyr^{31} of SLN have been highlighted by co-expression[3] and solid-state NMR[21] to be critical for proper inhibition of SERCA. The C-terminal five residues (Arg^{27}-Ser-Tyr-Gln-Tyr^{31}) and SERCA co-expression are required for localization to the endoplasmic reticulum (ER) of HEK-293 cells[22]. Highlighting the importance of the SLN tail is the absolute conservation of this region between species. In the cytoplasmic region of SLN, Thr^5 is involved in inhibition[3] and phosphorylation of Thr^5 might influence SLN activity[1313]. Two kinases have been proposed to phosphorylate SLN: serine/threonine kinase 16[13] and Ca^{2+}-calmodulin dependent kinase II[8]. Interestingly, the SLN mutation Thr-5 to Ala leads to a gain-of-function, whereas the phosphorylation-mimicking SLN mutation, Thr^5Glu, causes a complete loss-of-function[3]. Thus, if phosphorylation of SLN is physiologically relevant, it likely disrupts inhibition of SERCA as has been observed for phosphorylation of PLB. Aside from Thr^5 as an important residue in SLN function and a potential site of phosphorylation, little is known about the functional contribution of other cytoplasmic SLN residues.

Herein, we report the functional activities of cytoplasmic and transmembrane mutants of SLN in co-reconstituted proteoliposomes with SERCA. In a controlled, purified system, the functional consequences of SLN mutations on its regulation of SERCA can be observed in the absence of other proteins. As well, reconstitution allows for low lipid-to-protein in the final proteoliposomes, mimicking the SR environment for SERCA and SLN. We observe gain-of-function mutants localized to the cytoplasmic domain (Asn^4Ala, Thr^5Ala) and the more dynamic, hydrophilic region of the transmembrane domain (Glu^7Ala). We do not observe any gain-of-function mutants in a sampling of residues in the more rigid hydrophobic region of the transmembrane domain. The results show the short cytoplasmic domain of SLN, and the neighbouring dynamic region of the transmembrane domain, are critical for its functional inhibition of SERCA.

A

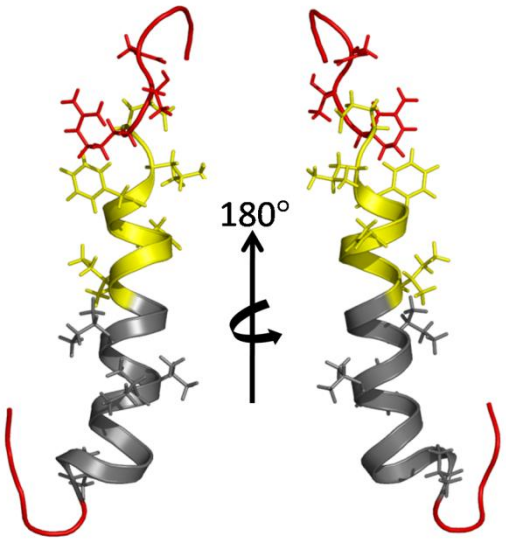

B

```
SLN  1    MGINTRELFLNFTIVLITVILMWLLVRSYQY 31
PLB 21 PQQARQKLQNLFINFCLILICLLLICIIVMLL-- 52
                :**:**  ::**  ::*:  ::*
```

Figure 3.1. Cartoon and surface structural representations of SLN. Panel A, The structure of SLN was determined in SDS micelles by NMR (pdb: 1JDM)[19]. The different regions of SLN are coloured based on their relative dynamics[20]; red – dynamic, yellow – less dynamic, grey – rigid. Cartoon SLN with residues mutated in this study (to alanine) shown as sticks. The right-side is a 180° rotation of the left-side along the y-axis as indicated. **Panel B,** Sequence alignment of SLN and PLB. Asterisks (*) are identical residues and colons (:) are similar residues (ClustalW hosted at EBI - www.ebi.ac.uk).

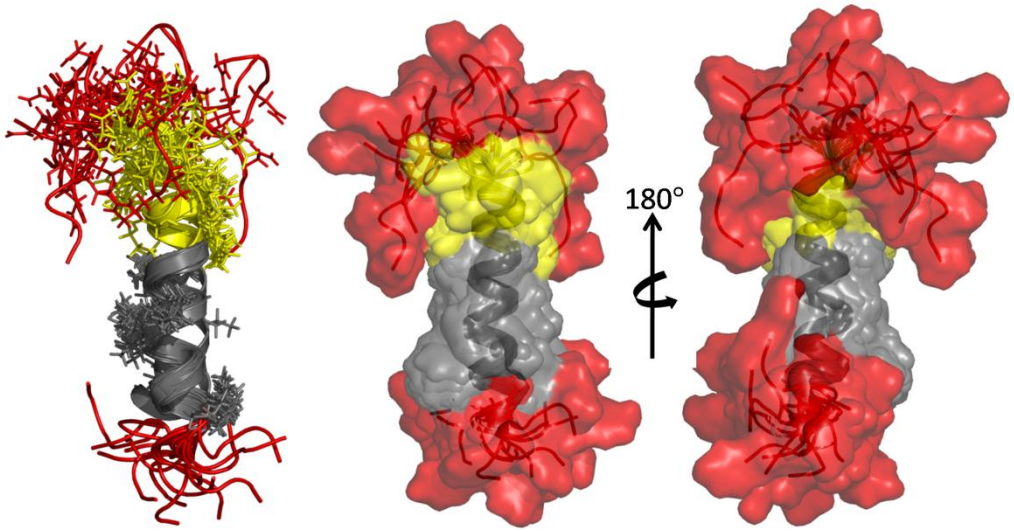

Figure 3.2. Cartoon and surface renderings of SLN to highlight dynamics. Deposited NMR ensemble for SLN in SDS micelles (pdb: 1JDM)[19]. The different dynamic regions of SLN are coloured as in Figure 3.1 (red – dynamic, yellow – less dynamic, grey – rigid)[20]. The surface representation on the right-side is a 180° rotation of the left-side surface representation along the y-axis as indicated.

3-2. Results and Discussion.

3-2.1. Co-reconstitution of SERCA and SLN.

Co-reconstitution for the study of SERCA and SLN provides a number of advantages for the functional study of mutants. The lipid to protein ratio can be controlled, such that low ratios reflecting an SR-like environment are possible. As well, the addition of purified components allows the observation of SERCA and SLN in the absence of any binding partners or containments. The relative levels of purified SERCA and SLN can be adjusted such that the amounts of protein co-reconstituted are normalized between different mutants. Finally, our co-reconstitution approach has provided a number of important functional insights into the regulation of SERCA by PLB[23-25].

3-2.2. SERCA activity in the absence and presence of wild-type SLN.

We investigated the Ca^{2+}-dependent ATPase activity of SERCA to measure the apparent Ca^{2+} affinity of the enzyme after reconstitution with and without SLN. In the absence of SLN, the apparent Ca^{2+} affinity of SERCA is 0.39 μM. The apparent Ca^{2+} affinity is decreased by the incorporation of wild-type SLN to 0.72 μM (Figure 3.3). The observed activity of wild-type SLN in our purified reconstitutions is consistent with previous reports of SLN activity by reconstitution[26-28] and heterologous co-expression with SERCA[3, 29, 30]. The wild-type SLN activity was used as a benchmark for the functional comparison of alanine-substituted mutants sampling the cytoplasmic and transmembrane regions of SLN (Figure 3.4).

3-2.3. Mutations in the rigid hydrophobic region of the SLN transmembrane domain were neutral or loss-of-function.

Alanine-substitution of residues in the rigid region (residues 15 to 26) of the SLN transmembrane domain was insensitive to mutation or resulted in a loss-of-function. The insensitive mutants ($Ile^{17}Ala$, $Ile^{20}Ala$ and $Val^{26}Ala$) had inhibitory activity similar to wild-type SLN. The SLN mutant, $Val^{19}Ala$, was a loss-of-function relative to wild-type SLN (Figure 3.4). No gain-of-function alanine substitutions were identified in the rigid C-terminal region of SLN.

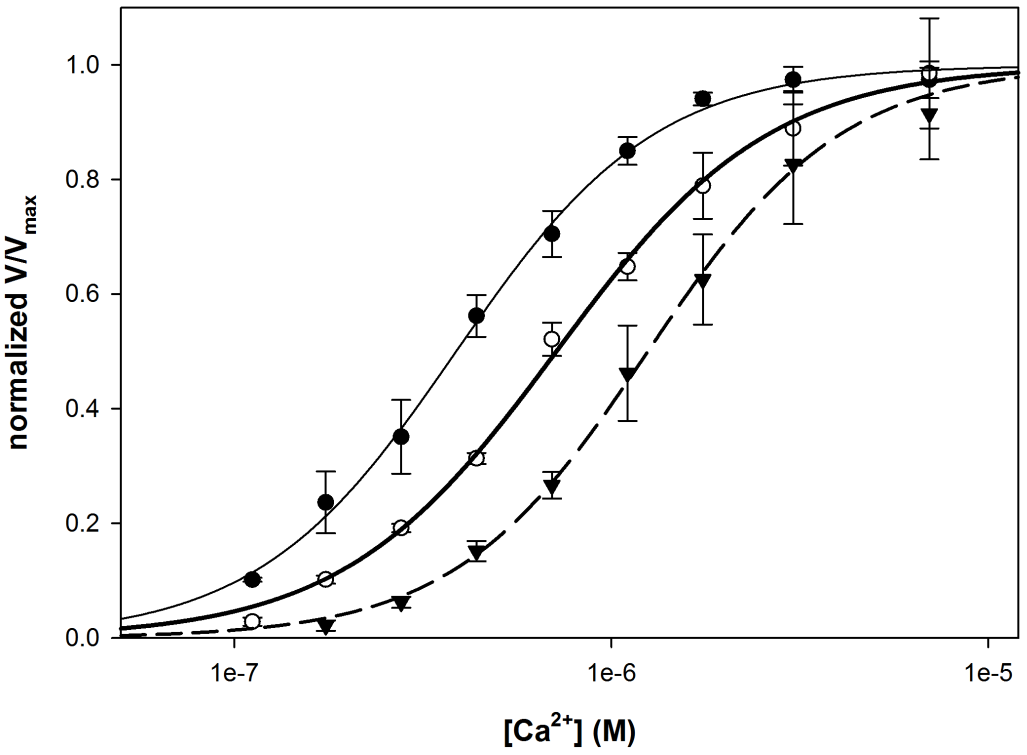

Figure 3.3. Ca^{2+}-dependent ATPase activity for SERCA in the absence of SLN, the presence of wild-type SLN and the presence of SLN-Asn4Ala. SERCA was co-reconstituted in the absence (*closed circles*) and in the presence of wild-type SLN (*open circles*). SERCA was also co-reconstituted in the presence of SLN-Asn^4Ala (*inverted triangles*). The data are plotted as normalized ATPase activity (μmol mg^{-1} mL^{-1}) to the Hill equation. The presence of wild-type SLN lowers the apparent Ca^{2+} affinity of SERCA alone (0.39 μM) to 0.72 μM. The SLN mutant Asn^4Ala causes a gain-of-function and lowers the apparent Ca^{2+} affinity of SERCA further to 1.20 μM. Error bars represent the standard error of the mean (SEM) for a minimum of three experiments.

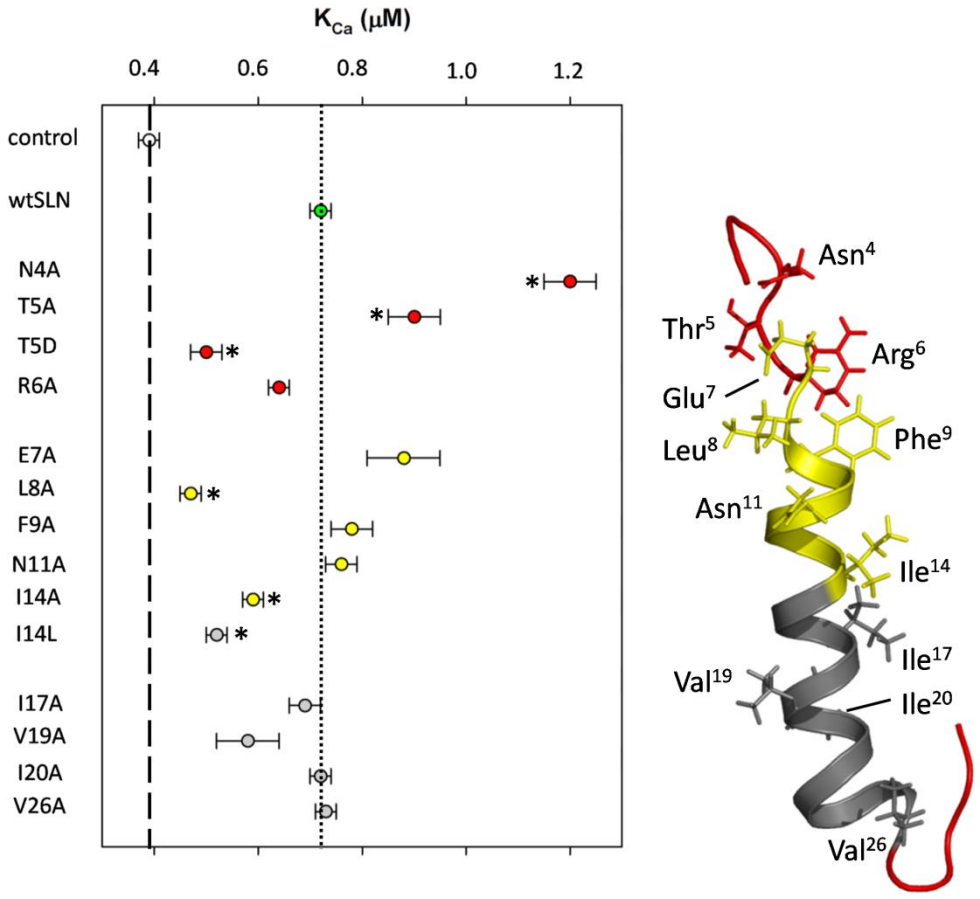

Figure 3.4. Effects of wild-type SLN and SLN mutants on the apparent Ca^{2+}-affinity of SERCA. ATPase activity was plotted for each SLN mutant and fit to the Hill equation to obtain the apparent Ca^{2+} affinity for the co-reconstitution (K_{Ca}). The long dashed line indicates the K_{Ca} of the control (SERCA alone; 0.39 μM) and the short dashed line indicates the K_{Ca} in the presence of wild-type SLN (0.72 μM). The data points are coloured based on the location of the residue in the four dynamic regions of SLN as highlighted in Figure 3.2 (red – dynamic, yellow – less dynamic, grey – rigid)[20]. Error bars represent the SEM for a minimum of three experiments. The inset cartoon structure for SLN displays sticks for residues mutated in this study. Asterisks (*) indicate statistically different K_{Ca} values from wtSLN (Tukey's HSD post hoc test; $p < 0.01$).

3-2.4. Mutations in the hydrophilic region of the SLN transmembrane domain had variable functional effects.

Mutation of residues in the more dynamic region of the SLN transmembrane domain had varying functional effects. Mutation of SLN-Ile^{14} bordering the dynamic and rigid regions of the transmembrane domain, known as the hinge residue, resulted in a loss-of-function (Figure 3.4). Alanine substitution of SLN-Leu^{8} close to the dynamic cytosolic region also resulted in loss-of-function. Mutant SLN-Glu^{7}Ala increased the inhibition of SERCA relative to wild-type SLN and was the only gain-of-function mutant identified in the SLN transmembrane domain (Figure 3.4).

3-2.5. Mutations in the SLN cytoplasmic domain were neutral or gain-of-function.

Alanine substitution of the residue bordering the cytoplasmic domain and the dynamic region of the transmembrane domain, Arg^{6}Ala, had little effect on SLN functional activity and was similar to wild-type SLN inhibition. The largest gain-of-function mutant in the study, Asn^{4}Ala, lowered the apparent Ca^{2+} affinity of SERCA to 1.20 μM, relative to 0.39 μM in the absence of SLN and 0.72 μM in the presence of wild-type SLN (Figure 3.3). Mutation of its neighbouring residue, Thr^{5}Ala, also resulted in gain-of-function lowering the apparent Ca^{2+} affinity of SERCA to 0.90 μM (Figure 3.4). Interestingly, Thr^{5} corresponds to the predicted phosphorylation site in the SLN cytoplasmic region. Introduction of a negative-charge in place of this residue, Thr^{5}Asp, results in a near complete loss-of-function (Figure 3.4).

3-2.6. It's not the size of the domain in the function, it's the size of the function in the domain.

In this study, we have mutated a number of residues in SLN that have not been previously functionally characterized, including: Asn^{4}, Arg^{6}, Glu^{7}, Phe^{9} and Ile^{20}. Two of these residues were gain-of-function (Asn^{4}Ala and Glu^{7}Ala), whereas the remaining residues were neutral. We have also characterized two novel mutations of residues (Thr^{5}Asp and Ile^{14}Leu) that have previously been characterized using different mutations[3]. Our selection of residues focused on the cytoplasmic region of SLN for two reasons: first, previous reports have only looked at a single residue (Thr^{5}) in the cytoplasmic region, and second, the cytoplasmic region of SLN aligns with domain Ib in PLB that has a critical role in PLB inhibition[23, 31]. Thus, even though the cytoplasmic domain of SLN is

predicted to be short with six residues sticking out of the SR membrane, we predicted this small region had an important role in SLN inhibition. Our results suggest the cytoplasmic region of SLN is critical for balancing the inhibition of SERCA such that the apparent Ca^{2+} affinity is finely tuned by wild-type SLN.

For the following discussion, the simple interpretation of our data will be as follows: loss-of-function mutants will be considered critical to the SLN inhibitory mechanism and gain-of-function mutants will be considered necessary for balancing SLN inhibition. SLN inhibitory mechanisms will not be proposed based on our functional data, but the results will be discussed in the context of proposed PLB inhibitory mechanisms[31, 32]. In light of this discussion, our results suggest one similarity and one difference in the mechanisms used by SLN and PLB to inhibit SERCA.

3-2.7. Comparison of co-reconstituted SERCA and SLN with heterologous co-expression of SERCA and SLN.

This study is only the second report to functionally characterize residues in SLN by site-directed mutagenesis. The first by Odermatt and colleagues[3] investigated the mutation of SLN in heterologous co-expression with SERCA. Figure 3.5 compares like residues studied by mutation of SLN herein and by Odermatt and coworkers. Normalized to an absolute change in the apparent Ca^{2+}-affinity of SERCA (ΔK_{Ca}) relative to SERCA in the absence of SLN (control), the studies share a similar overall trend and are in general agreement (Figure 3.5a). However, the absolute ΔK_{Ca} was generally larger in our co-reconstitution system compared to heterologous co-expression. For example, wild-type SLN increased the apparent K_{Ca} of SERCA by 0.33 μM in co-reconstitution, whereas wild-type SLN increased the K_{Ca} by 0.16 μM in heterologous co-expression.

Since the ΔK_{Ca} difference was consistent between the two experimental systems, we plotted a comparison of the results on a relative ΔK_{Ca} scale, such that each residue is indicated as a fold change in K_{Ca} relative to wild-type SLN (set to 1) (Figure 3.5b). Such a comparison highlights the relative effect of each mutation within its respective experimental system (co-reconstitution herein or heterologous co-expression by Odermatt and coworkers). By comparing the studies in this manner, the effects of mutation nearly overlay with two notable exceptions. The first, SLN-Asn^{11}Ala, was a neutral mutation in

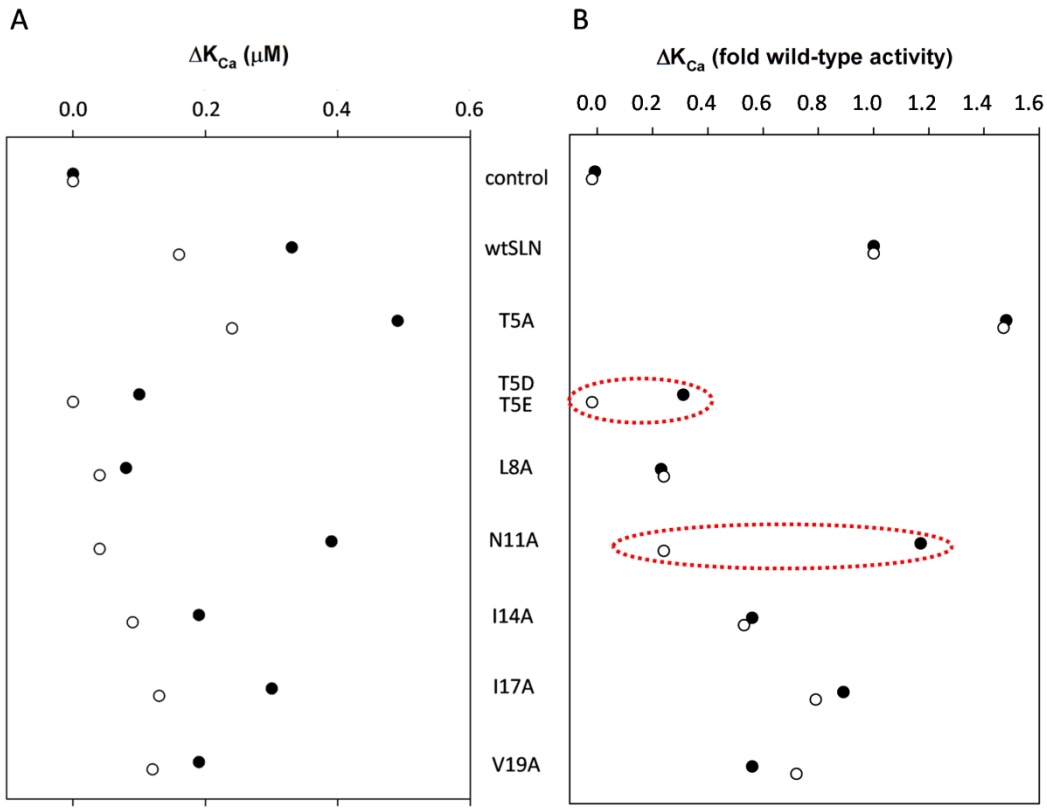

Figure 3.5. Comparison of the functional effects of SLN mutation in co-reconstitution and heterologous co-expression with SERCA. Panel A, the absolute change in the apparent Ca^{2+} affinity (ΔK_{Ca}) for SLN mutants common to this study and heterologous co-expression studies[3]. The overall trend is similar between the two studies. **Panel B,** the change in the apparent Ca^{2+} affinity (ΔK_{Ca}) for SLN mutants normalized as fold-activity of wild-type SLN. The two studies agree very well except for two mutants at positions Thr^{5} and Asn^{11} (dashed red circles; see section 3-2.7 of the text for discussion).

our hands (1.17-fold wild-type activity), but was a near complete loss-of-function in heterologous co-expression (0.24-fold wild-type activity). Mutation of the homologous residue in PLB ($Asn^{34}Ala$) was reported as a complete loss-of-function in both systems, suggesting that Asn^{11} is a critical residue in SLN. The second exception is observed between SLN-$Thr^{5}Asp$ in this study, which was a near complete loss-of-function (0.31-fold wild-type activity), and SLN-$Thr^{5}Glu$ in heterologous co-expression, which was a complete loss-of-function. The expression of SLN-$Thr^{5}Glu$ in heterologous co-expression was very weak and a lack of SLN protein would be an apparent complete loss-of-function. For this reason, and because the compared mutations are not identical, the minor difference observed is negligible and will not be discussed further.

3-2.8. Comparison of SLN mutations to homologous mutations characterized in PLB.

The homology between PLB and SLN is reason to support similar mechanisms between the two regulatory proteins. Indeed, we have found SLN residues in the cytoplasmic domain reflect the homologous residue in PLB domain Ib, with respect to the functional effects of alanine substitution (Figure 3.6a). This comparison includes PLB functional co-reconstitution data from our lab[23, 24] and heterologous co-expression studies[31]. PLB-$Lys^{27}Ala$ ($Asn^{4}Ala$) and PLB-$Asn^{30}Ala$ ($Glu^{7}Ala$) are gain-of-function. A third gain-of-function mutant is located between these residues in SLN ($Thr^{5}Ala$) and PLB ($Gln^{29}Ala$), although offset by a single position in homology sequence alignments. Mutations in PLB domain Ib motivated the enhanced interaction mechanism proposed by MacLennan and coworkers, which stated that some PLB domain Ib mutants increase the inhibition of SERCA by enhancing interaction[31]. Since the homologous mutations in SLN have similar functional effects (Fig 3.6a), it suggests the SLN cytoplasmic domain mechanistically mimics PLB Ib.

An important difference between SLN and PLB occurs in the comparison of mutants in their respective transmembrane domains (Figure 3.6b). Classic "monomeric" mutants in PLB (including $Leu^{37}Ala$, $Ile^{40}Ala$ and $Leu^{43}A$) provided the basis for the mass action mechanism proposed by MacLennan and coworkers, whereby mutants that destabilize PLB pentamers form an increased fraction of PLB monomers available to inhibit SERCA[32]. Mutation of certain Leu and Ile residues in the transmembrane domain of PLB caused dissociation of the PLB pentamer under SDS-PAGE and also caused greater

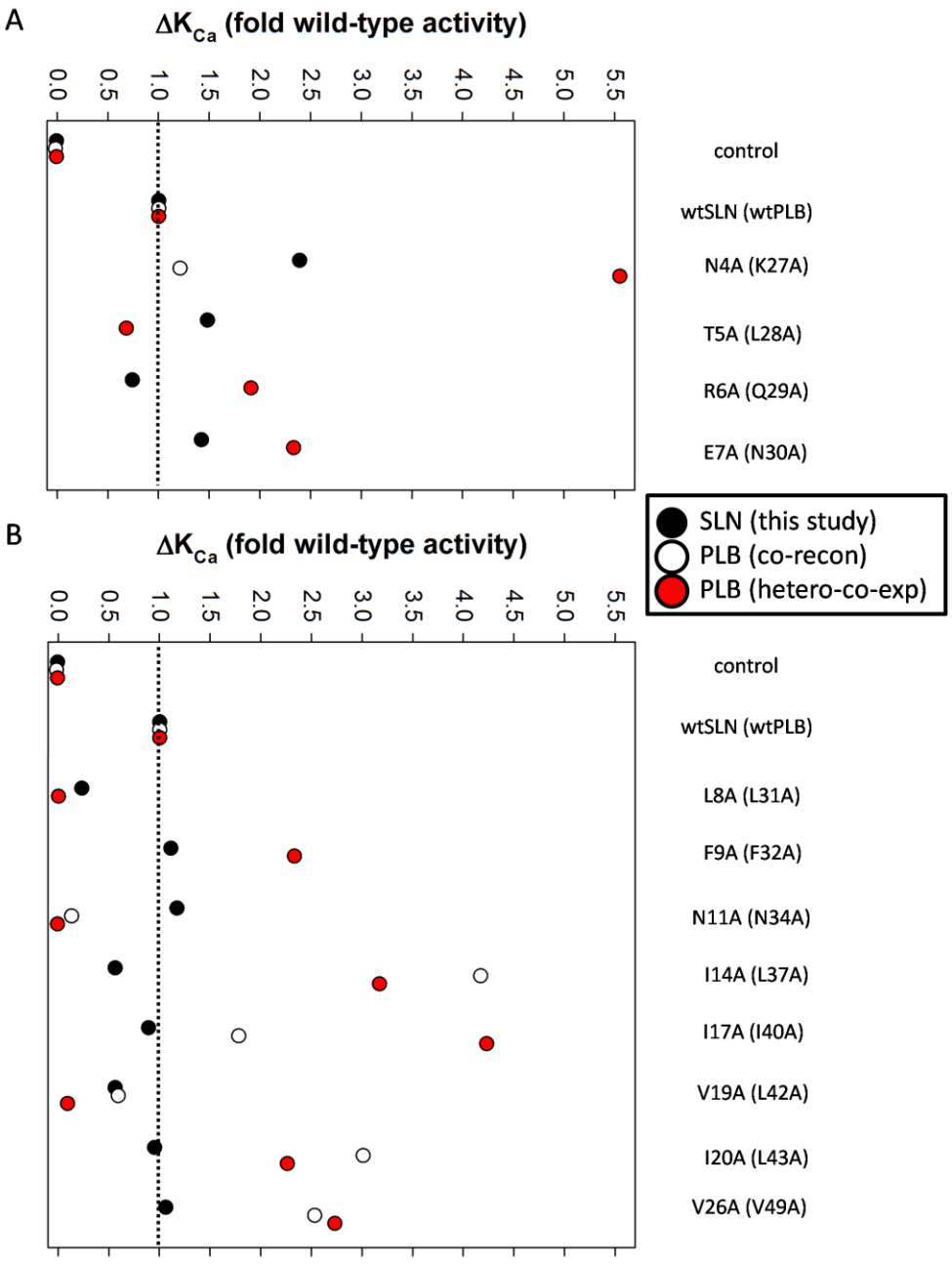

Figure 3.6. Comparison of SLN mutations to the homologous PLB residues characterized by mutation in co-reconstitution and heterologous co-expression. SLN mutants (*black circles*) are plotted against aligning residues in PLB mutated in similar co-reconstitutions (*white circles*)[23, 24] or PLB mutated in heterologous co-expression studies (*red circles*)[31, 32]. The data are plotted as the change in the apparent Ca^{2+} affinity (ΔK_{Ca}) for SLN mutants normalized as fold-activity of wild-type SLN or wild-type PLB. The dotted line represents wild-type activity (set to 1). **Panel A,** SLN mutants aligning with domain Ib of PLB follow a similar trend. **Panel B,** SLN mutants aligning with the transmembrane domain of PLB.

inhibition of SERCA than wild-type PLB (which is primarily pentameric in SDS-PAGE). Thus, the now classic "monomeric" PLB mutants, such as $Ile^{40}Ala$, caused increased SERCA inhibition and were among the largest gain-of-function PLB mutants. Herein, we did not identify any residues in the SLN transmembrane domain that resulted in gain-of-function. Notably, the residues sampled in this study are homologous to many of the classic "monomeric" mutants that led to the proposal of the mass action mechanism ($Ile^{14}Ala$, $Ile^{17}Ala$ and $Ile^{20}Ala$ are homologous to $Leu^{37}Ala$, $Ile^{40}Ala$ and $Leu^{43}Ala$, respectively). We characterized the mutant SLN-$Ile^{14}Leu$, because a similar switch in PLB, $Leu^{37}Ile$, leads to gain-of-function[33]. However, the SLN-$Ile^{14}Leu$ mutant was a loss-of-function and similar to the alanine-substituted $Ile^{14}Ala$ mutant. In contrast to PLB, SLN does not appear to use a mass action driven mechanism in the co-reconstitutions. It is worth noting that SLN forms inherently weak oligomers[26] relative to the stability of PLB pentamers.

In conclusion, mutations in the cytoplasmic domain of SLN are similar to enhanced interaction PLB mutants. This suggests the nature of the amino acids in the short, dynamic SLN cytoplasmic domain may be critical for balancing wild-type SLN inhibition. The cytoplasmic domain of SLN is the most variable region between species and the distribution of charged residues in the cytoplasmic region is variable between humans, rabbits and mice[2]. In fact, only Met^{1} and Thr^{5} are conserved in the first six residues between these three species[2]. Asn^{4} in human SLN is Ser^{4} in both rabbit and mouse SLN.

3-3. Materials and Methods.

3-3.1. Materials.

The following reagents were of the highest purity available: octaethylene glycol monododecyl ether ($C_{12}E_8$; Barnet Products, Englewood Cliff, NJ); egg yolk phosphatidylcholine (EYPC), phosphatidylethanolamine (EYPE) and phosphatidic acid (EYPA) (Avanti Polar Lipids, Alabaster, AL); reagents used in the coupled enzyme assay (Sigma-Aldrich, Oakville, ON Canada).

3-3.2. Expression and purification of recombinant SLN.

Oligonucleotide and DNA purification kits were purchased from Qiagen (Mississauga, ON, Canada) and DNA sequencing was performed by the DNA Core Services Laboratory

in the Department of Biochemistry, University of Alberta. Restriction enzymes were purchased from Invitrogen (Carlsbad, CA, USA). The MBP-fusion plasmid pMal-c2x and amylose resin were purchased from New England Biolabs. Active TEV (AcTEV) protease was purchased from Invitrogen.

The wild-type SLN construct with a Gly-Ser-His_8 N-terminal extension was generated previously in our laboratory and inserted into the pMal-c2x plasmid[28]. Site-directed mutants of SLN were generated directly by PCR if the mutations were near the ends of the gene, or by megaprimer mutagenesis[34] if the mutations were near the middle of the gene. Products were then cloned into the pMal-SLN plasmid with *Bam*HI and *Eco*RI, replacing the wild-type gene. All mutations were confirmed by DNA sequencing.

Recombinant SLN was expressed and purified as previously described[28] with an additional organic extraction step. *Escherichia coli* DH5α cells were transformed with MBP-SLN fusion expression plasmids. A 50 mL culture of LB growth media with 100 μg/mL ampicillin was inoculated with a single colony and incubated overnight at 37°C with shaking. The overnight culture was diluted into 1 L of minimal M9 media with 100 μg/mL ampicillin and grown at 37°C until OD_{600} ~0.6 (about 2-3 h). The incubation temperature was reduced to 22°C and following equilibration, expression of MBP-SLN was induced with 1 mM IPTG. Cells were harvested at 4°C after 48 h of induction and washed with 50 mM Tris HCl buffer (pH 8.0). Cell pellets were stored at -20°C.

Cell pellets from 1 L of culture were resuspended in 50 mL lysis buffer (20 mM phosphate, pH 8.0, 120 mM NaCl, 1 mM EDTA, 0.5% glycerol, 0.5% Triton X-100, 0.1 mM dithiothreitol). The resuspension was sonicated in a Branson digital sonifier 250 (Branson Ultrasonics, Danbury, CT, USA). The sonicated suspension was centrifuged at 50,000g for 25 min at 4°C in a Beckman Ti-45 rotor. The supernatant containing MBP-SLN fusion protein was subjected to amylose-affinity chromatography column. The column was washed with 5 column volumes of equilibration buffer (20 mM phosphate, pH 8.0, 120 mM NaCl, 1 mM EDTA, and 0.02% azide). The MBP-SLN fusion protein was eluted with equilibration buffer containing 40 mM maltose. The purified MBP-SLN fusion protein was cleaved with AcTEV protease at 10U/mg with 1 mM dithiothreitol for 24 h in a 16°C water bath. A second addition of AcTEV protease was added with fresh dithiothreitol and incubated for an additional 24 h.

Following protease digestion of the maltose-binding protein and SLN fusion protein, trichloroacetic acid was added to a final concentration of 1% (check value). This mixture was incubated on ice for 20 minutes. The precipitate was collected by centrifugation at 4°C and subsequently homogenized in a mixture of chloroform : isopropanol : water (4 : 4 : 1) and incubated at room temperature for 3 hours. The organic phase, highly enriched in recombinant SLN, was removed, dried to a thin film under nitrogen gas and resuspended in 7 M (guanidine hydrochloride) GdnHCl. The addition of the organic extraction step to the purification of recombinant SLN was inspired by purifications of proteolipid from rabbit skeletal muscle[35, 36].

The extracted SLN in 7 M GdnHCl was centrifuged at 10,000g for 20 min at 4°C in a C0650 rotor to eliminate insoluble material. Reverse-phase high-pressure liquid chromatography (HPLC) was performed as described[28]. Solvent A was HPLC-grade distilled water and solvent B was HPLC-grade isopropanol with 0.05% TFA. The 7 M GdnHCl supernatant was applied to a Zorbax 300 SB-C8 column with a Zorbax C3 guard column (Agilent Technologies, Palo Alto, CA, USA) equilibrated at 20% solvent B. A gradient was run from 20% to 80% solvent B. Fractions were collected and analyzed by mass spectrometry and SDS-PAGE. Fractions containing pure SLN were combined and the protein concentration determined by the amido black protein assay. Aliquots of 75 μg were dried by speed-vac, lyophilized to dryness and stored at -80°C.

3-3.3. Co-reconstitution of SLN with SERCA.

Lyophilized SLN (75 μg) was resuspended in a 75 μL mixture of chloroform : trifluroethanol (2 : 1) and mixed with lipids (360 μg EYPC; 40 μg EYPA) from stock chloroform solutions. The peptide-lipid mixture was dried to a thin film under nitrogen gas and dried under vacuum overnight. The peptide-lipid mixture was hydrated in buffer (20 mM imidazole pH 7.0; 100 mM KCl; 0.02% NaN_3) at 37 °C for 10 min, cooled to room temperature, and detergent-solubilised by the addition of $C_{12}E_8$ (0.2 % final concentration) and vigorous vortexing. Detergent-solubilized SERCA was added (300 μg in a total volume of 200 μL) and the reconstitution was stirred gently at room temperature. Detergent was slowly removed by the addition of SM-2 biobeads (Bio-Rad, Hercules, CA) over a 4-hour time course (final ratio of 25 biobeads: 1 detergent w/w). Following detergent removal, the reconstitution was centrifuged over a sucrose-gradient for 1 h at 100,000g. The resultant layer of reconstituted proteoliposomes was removed,

flash-frozen in liquid-nitrogen and stored at -80 °C. The final approximate molar ratios were 120 lipid : 5 SLN : 1 SERCA[23].

3-3.4. ATPase activity assays of SERCA and SLN co-reconstitutions.

ATPase activity of the co-reconstituted proteoliposomes was measured over a range of Ca^{2+} concentrations from 0.1 μM to 10 μM by a coupled-enzyme assay[23, 37]. The K_{ca} (apparent calcium affinity) was determined by fitting the data to the Hill equation (Sigma Plot software, SPSS Inc., Chicago, IL). Errors were calculated as the standard error of the mean for a minimum of three independent reconstitutions.

3-4. References.

1. Wawrzynow A, Theibert JL, Murphy C, Jona I, Martonosi A, Collins JH. Sarcolipin, the proteolipid of skeletal-muscle sarcoplasmic-reticulum, is a unique, amphipathic, 31-residue peptide. Arch Biochem Biophys 1992 NOV 1;298(2):620-3.

2. Odermatt A, Taschner PEM, Scherer SW, Beatty B, Khanna VK, Cornblath DR, Chaudhry V, Yee WC, Schrank B, Karpati G, Breuning MH, Knoers N, MacLennan DH. Characterization of the gene encoding human sarcolipin (SLN), a proteolipid associated with SERCA1: Absence of structural mutations in five patients with brody disease. Genomics 1997 NOV 1;45(3):541-53.

3. Odermatt A, Becker S, Khanna VK, Kurzydlowski K, Leisner E, Pette D, MacLennan DH. Sarcolipin regulates the activity of SERCA1, the fast-twitch skeletal muscle sarcoplasmic reticulum Ca2+-ATPase. J Biol Chem 1998 MAY 15;273(20):12360-9.

4. Minamisawa S, Wang YB, Chen J, Ishikawa Y, Chien KR, Matsuoka R. Atrial chamber-specific expression of sarcolipin is regulated during development and hypertrophic remodeling. J Biol Chem 2003 MAR 14;278(11):9570-5.

5. Vangheluwe P, Schuermans M, Zador E, Waelkens E, Raeymaekers L, Wuytack F. Sarcolipin and phospholamban mRNA and protein expression in cardiac and skeletal muscle of different species. Biochem J 2005 JUL 1;389:151-9.

6. Babu GJ, Bhupathy P, Timofeyev V, Petrashevskaya NN, Reiser PJ, Chiamvimonvat N, Periasamy M. Ablation of sarcolipin enhances sarcoplasmic reticulum calcium transport and atrial contractility. Proc Natl Acad Sci U S A 2007 NOV 6;104(45):17867-72.

7. Babu GJ, Bhupathy P, Carnes CA, Billman GE, Periasamy M. Differential expression of sarcolipin protein during muscle development and cardiac pathophysiology. J Mol Cell Cardiol 2007 AUG;43(2):215-22.

8. Bhupathy P, Babu GJ, Ito M, Periasamy M. Threonine-5 at the N-terminus can modulate sarcolipin function in cardiac myocytes. J Mol Cell Cardiol 2009 NOV;47(5):723-9.

9. Tupling AR, Asahi M, MacLennan DH. Sarcolipin overexpression in rat slow twitch muscle inhibits sarcoplasmic reticulum Ca2+ uptake and impairs contractile function. J Biol Chem 2002 NOV 22;277(47):44740-6.

10. Asahi M, Otsu K, Nakayama H, Hikoso S, Takeda T, Gramolini AO, Trivieri MG, Oudit GY, Morita T, Kusakari Y, Hirano S, Hongo K, Hirotani S, Yamaguchi O, Peterson A, Backx PH, Kurihara S, Hori M, MacLennan DH. Cardiac-specific overexpression of sarcolipin inhibits sarco(endo)plasmic reticulum Ca2+ ATPase (SERCA2a) activity and impairs cardiac function in mice. Proc Natl Acad Sci U S A 2004 JUN 22;101(25):9199-204.

11. Babu GJ, Zheng ZL, Natarajan P, Wheeler D, Janssen PM, Periasamy M. Overexpression of sarcolipin decreases myocyte contractility and calcium transient. Cardiovasc Res 2005 JAN 1;65(1):177-86.

12. Babu GJ, Bhupathy P, Petrashevskaya NN, Wang HL, Raman S, Wheeler D, Jagatheesan G, Wieczorek D, Schwartz A, Janssen PML, Ziolo MT, Periasamy M. Targeted overexpression of sarcolipin in the mouse heart decreases sarcoplasmic reticulum calcium transport and cardiac contractility. J Biol Chem 2006 FEB 17;281(7):3972-9.

13. Gramolini AO, Trivieri MG, Oudit GY, Kislinger T, Li WP, Patel MM, Emili A, Kranias EG, Backx PH, MacLennan DH. Cardiac-specific overexpression of

sarcolipin in phospholamban null mice impairs myocyte function that is restored by phosphorylation. Proc Natl Acad Sci U S A 2006 FEB 14;103(7):2446-51.

14. Nef HM, Moellmann H, Troidl C, Kostin S, Voss S, Hilpert P, Behrens CB, Rolf A, Rixe J, Weber M, Hamm CW, Elsaesser A. Abnormalities in intracellular Ca2+ regulation contribute to the pathomechanism of tako-tsubo cardiomyopathy. Eur Heart J 2009 SEP;30(17):2155-64.

15. Vittorini S, Storti S, Parri MS, Cerillo AG, Clerico A. SERCA2a, phospholamban, sarcolipin, and ryanodine receptors gene expression in children with congenital heart defects. Molecular Medicine 2007 JAN-FEB;13(1-2):105-11.

16. Uemura N, Ohkusa T, Hamano K, Nakagome M, Hori H, Shimizu M, Matsuzaki M, Mochizuki S, Minamisawa S, Ishikawa Y. Down-regulation of sarcolipin mRNA expression in chronic atrial fibrillation. Eur J Clin Invest 2004 NOV;34(11):723-30.

17. Shimura M, Minamisawa S, Yokoyama U, Umemura S, Ishikawa Y. Mechanical stress-dependent transcriptional regulation of sarcolipin gene in the rodent atrium. Biochem Biophys Res Commun 2005 SEP 2;334(3):861-6.

18. Gupta SC, Varian KD, Bal NC, Abraham JL, Periasamy M, Janssen PML. Pulmonary artery banding alters the expression of Ca2+ transport proteins in the right atrium in rabbits. American Journal of Physiology-Heart and Circulatory Physiology 2009 JUN;296(6):H1933-9.

19. Mascioni A, Karim C, Barany G, Thomas DD, Veglia G. Structure and orientation of sarcolipin in lipid environments. Biochemistry (N Y) 2002 JAN 15;41(2):475-82.

20. Buffy JJ, Buck-Koehntop BA, Porcelli F, Traaseth NJ, Thomas DD, Veglia G. Defining the intramembrane binding mechanism of sarcolipin to calcium ATPase using solution NMR spectroscopy. J Mol Biol 2006 APR 28;358(2):420-9.

21. Hughes E, Clayton JC, Kitmitto A, Esmann M, Middleton DA. Solid-state NMR and functional measurements indicate that the conserved tyrosine residues of sarcolipin

are involved directly in the inhibition of SERCA1. J Biol Chem 2007 SEP 7;282(36):26603.

22. Gramolini AO, Kislinger T, Asahi M, Li WP, Emili A, MacLennan DH. Sarcolipin retention in the endoplasmic reticulum depends on its C-terminal RSYQY sequence and its interaction with sarco(endo)plasmic Ca2+-ATPases. Proc Natl Acad Sci U S A 2004 NOV 30;101(48):16807-12.

23. Trieber CA, Douglas JL, Afara M, Young HS. The effects of mutation on the regulatory properties of phospholamban in co-reconstituted membranes. Biochemistry (N Y) 2005 MAR 8;44(9):3289-97.

24. Trieber CA, Afara M, Young HS. Effects of phospholamban transmembrane mutants on the calcium affinity, maximal activity, and cooperativity of the sarcoplasmic reticulum calcium pump. Biochemistry (N Y) 2009 OCT 6;48(39):9287-96.

25. Glaves JP, Trieber CA, Ceholski DK, Stokes DL, Young HS. Phosphorylation and mutation of phospholamban alter physical interactions with the sarcoplasmic reticulum calcium pump. J Mol Biol 2011 JAN 21;405(3):707-23.

26. Hellstern S, Pegoraro S, Karim CB, Lustig A, Thomas DD, Moroder L, Engel J. Sarcolipin, the shorter homologue of phospholamban, forms oligomeric structures in detergent micelles and in liposomes. J Biol Chem 2001 AUG 17;276(33):30845-52.

27. Buck B, Zamoon J, Kirby TL, DeSilva TM, Karim C, Thomas D, Veglia G. Overexpression, purification, and characterization of recombinant Ca-ATPase regulators for high-resolution solution and solid-state NMR studies. Protein Expr Purif 2003 AUG;30(2):253-61.

28. Douglas JL, Trieber CA, Afara M, Young HS. Rapid, high-yield expression and purification of Ca2+-ATPase regulatory proteins for high-resolution structural studies. Protein Expr Purif 2005 MAR;40(1):118-25.

29. Asahi M, Sugita Y, Kurzydlowski K, De Leon S, Tada M, Toyoshima C, MacLennan DH. Sarcolipin regulates sarco(endo)plasmic reticulurn Ca2+-ATPase (SERCA) by

binding to transmembrane helices alone or in association with phospholamban. Proc Natl Acad Sci U S A 2003 APR 29;100(9):5040-5.

30. Asahi M, Nakayama H, Tada M, Otsu K. Regulation of sarco(endo)plasmic reticulum Ca2+ adenosine triphosphatase by phospholamban and sarcolipin: Implication for cardiac hypertrophy and failure. Trends Cardiovasc Med 2003 MAY;13(4):152-7.

31. Kimura Y, Asahi M, Kurzydlowski K, Tada M, MacLennan DH. Phospholamban domain ib mutations influence functional interactions with the Ca2+-ATPase isoform of cardiac sarcoplasmic reticulum. J Biol Chem 1998 JUN 5;273(23):14238-41.

32. Kimura Y, Kurzydlowski K, Tada M, MacLennan DH. Phospholamban inhibitory function is activated by depolymerization. J Biol Chem 1997 JUN 13;272(24):15061-4.

33. Cornea RL, Autry JM, Chen ZH, Jones LR. Reexamination of the role of the leucine/isoleucine zipper residues of phospholamban in inhibition of the Ca2+ pump of cardiac sarcoplasmic reticulum. J Biol Chem 2000 DEC 29;275(52):41487-94.

34. Sarkar G, Sommer S. The megaprimer method of site-directed mutagenesis. BioTechniques 1990 APR;8(4):404-7.

35. Maclenna.Dh, Yip CC, Iles GH, Seeman P. Isolation of sarcoplasmic reticulum proteins. Cold Spring Harb Symp Quant Biol 1973;37:469-77.

36. Ohnoki S, Martonosi A. Purification and characterization of the proteolipid of rabbit sarcoplastic reticulum. Biochim Biophys Acta 1980;626(1):170-8.

37. Warren GB, Toon PA, Birdsall NJ, Lee AG, Metcalfe JC. Reconstitution of a calcium-pump using defined membrane components. Proc Natl Acad Sci U S A 1974;71(3):622-6.

Chapter 4.

Phosphorylation and mutation of phospholamban alter physical interactions with the sarcoplasmic reticulum calcium pump.

"How can you say that your truth is better than ours?"

-Mumford and Sons

A version of this chapter is published as:

Glaves JP, Trieber CA, Ceholski DK, Stokes DL, Young HS. (2011).

Phosphorylation and mutation of phospholamban alter physical interactions with the sarcoplasmic reticulum calcium pump.

Journal Molecular Biology **405**(3):707-23.

Acknowledgements: Dr. C. Trieber purified SERCA and characterized PLB ATPase activities. D. Ceholski generated the PLB mutant $Arg^{14}Ala$ and characterized its activity. Images were recorded by Dr. H. Young and J.P. Glaves. Dr. H. Young and J.P. Glaves wrote the manuscript.

Chapter 4. Phosphorylation and mutation of phospholamban alter physical interactions with the sarcoplasmic reticulum calcium pump.

4-1. Introduction.

Cation transport by the P-type ion pumps is an essential process in all eukaryotic cells, where changes in intracellular cation concentrations are linked to precise physiological responses. The best understood members of this transport family include the sarcoplasmic reticulum calcium ATPase (SERCA) found in muscle cells and the plasma membrane sodium-potassium ATPase (Na^+-K^+ pump) found in all cell types. These two P-type ion pumps are particularly important in cardiac contractility and are major drug targets for the clinical improvement of heart disease. An extensive series of X-ray and electron crystallographic studies[1-14] have resulted in structures of a variety of SERCA reaction intermediates, thus revealing how ATP hydrolysis is coupled to calcium (Ca^{2+}) transport across the sarcoplasmic reticulum (SR) membrane in order to achieve muscle relaxation. These studies show that SERCA is composed of a transmembrane domain that contains the Ca^{2+} binding sites and three cytosolic domains that are responsible for nucleotide binding, phosphorylation, and communication with the transmembrane domain. It has been shown that the intermediate states (Ca^{2+} binding, phosphorylation, Ca^{2+} transport,

dephosphorylation, and proton counter-transport) involve coupled domain movements that link the cation binding sites with the phosphorylation state of the enzyme.

Despite this wealth of structural information, the regulation of the Ca^{2+} pump in cardiac muscle remains an elusive target of study. In cardiac and smooth muscle, SERCA is regulated by phospholamban (PLB), a 52-residue integral membrane protein. PLB engages in an inhibitory interaction with SERCA that reduces its apparent Ca^{2+} affinity. This is a dynamic process that depends on the cytosolic Ca^{2+} concentration, as well as the phosphorylation and oligomeric states of PLB. PLB is in dynamic equilibrium between monomeric and homo-oligomeric states, with pentameric forms being dominant in SDS polyacrylamide gels[15, 16]. Mutation of key leucine and isoleucine residues in the transmembrane domain of PLB destabilizes the pentameric structure and has been shown to shift this equilibrium in favor of the monomer. These pentamer-disrupting mutations correlate with increased inhibition of SERCA, leading to the speculation that the PLB monomer is the active inhibitory species[17-19] and that the pentamer is an inactive storage form[20, 21]. Unfortunately, it has not been possible to directly test this model with well defined PLB oligomeric states within a lipid membrane. In any case, SERCA inhibition by the PLB monomer can be reversed either by elevated cytoplasmic Ca^{2+} concentrations or by phosphorylation of PLB. The primary physiological mechanism for relieving SERCA inhibition is through the phosphorylation of PLB at Ser^{16} by cAMP-dependent protein kinase (PKA), but PLB can also be phosphorylated at Thr^{17} by either Ca^{2+}/calmodulin-dependent protein kinase II[22] or Akt[23].

While the functional effect of PLB phosphorylation on SERCA regulation is clear, the mechanism for this effect is less certain. The original model for SERCA regulation suggested that monomeric PLB binds to and inhibits SERCA, while phosphorylation disrupts this inhibitory complex[24, 25]. However, there is contradictory evidence about whether PLB physically dissociates from SERCA following phosphorylation. Fluorescence energy transfer experiments suggest that PLB inhibits and aggregates SERCA, and that phosphorylation reverses this process and causes dissociation of PLB and SERCA[26]. Similarly, cross-linking experiments indicate that phosphorylation weakens PLB's physical association with SERCA and makes the complex more susceptible to dissociation by sub-saturating Ca^{2+} concentrations[27, 28]. In contrast, studies using co-immunoprecipitation[29], fluorescence[30, 31] and EPR spectroscopy[32] all suggest that PLB remains associated with SERCA following phosphorylation. Rather than

dissociation of PLB from SERCA after phosphorylation, EPR and NMR studies point to a transition from order to disorder in the cytoplasmic domain of PLB[32, 33]. Such a transition is consistent with a variety of biophysical studies showing that phosphorylation causes a partial unwinding and disordering of PLB's N-terminal α-helix around the Ser^{16} phosphorylation site[34-38]. While regulation by phosphorylation is thought to occur in the context of a complex between monomeric PLB and SERCA, it has been suggested that the PLB pentamer is necessary for regulation of cardiac contractility in a physiological context[39] and a direct interaction has been proposed between the PLB pentamer and SERCA[40-42]. EPR measurements of boundary lipids suggest that phosphorylation of PLB shifts the population towards the oligomeric state[15]. These results raise questions about the role of PLB oligomeric states in the regulation of SERCA.

In previous work, we have observed a direct interaction between an oligomeric form of PLB and SERCA in two-dimensional crystals[41]. Specifically, we characterized co-crystals of SERCA and a super-inhibitory mutant of PLB (Ile^{40}-to-Ala)[41]. While SDS-PAGE indicated that this mutant of PLB was monomeric[17], our projection map revealed that PLB-Ile^{40}Ala formed an oligomer. The propensity of Ile^{40}Ala to form oligomers was later supported by fluorescence resonance energy transfer experiments[43, 44] reinforcing the conclusion of Jones and co-workers[18], that while SDS-PAGE may indicate the relative stability of PLB oligomers, it is not a definitive means of assessing the oligomeric species adopted by PLB within the lipid bilayer. A three-dimensional model based on our projection map suggested that PLB pentamers interact with SERCA at two potential sites – one near transmembrane segment TM3 and another near the C-terminus. These contact sites are distinct from the inhibitory site occupied by the PLB monomer, which is adjacent to TM2, TM4, and TM6 of SERCA according to mutagenesis and cross-linking studies[45-49]. Herein, we have investigated the effects of PLB phosphorylation and mutation on the interaction between a PLB oligomer and SERCA in the context of two-dimensional crystals. Our results show a correlation between PLB function and crystal formation, suggesting that the physical interactions that stabilize the crystals are sensitive to physiologically relevant perturbations. Our data are also consistent with an order-to-disorder transition in PLB's cytoplasmic domain, where the inhibitory forms of PLB (e.g. wild-type and the gain-of-function mutant Lys^{27}-to-Ala) retain an ordered state in the crystals and the non-inhibitory forms of PLB (phosphorylated wild-type and a loss-of-function mutant Asn^{34}-to-Ala) adopt a disordered state.

4-2. Results and Discussion.

4-2.1. Co-Reconstitution of SERCA and PLB.

Methods for co-reconstituting SERCA and PLB have been previously established for both functional[50, 51] and structural[41, 52, 53] studies. Co-reconstituted proteoliposomes have been shown to have a lipid-to-protein molar ratio of approximately 120:1 and a 3.5:1 PLB-to-SERCA molar ratio[41, 50]. These conditions mimic cardiac SR and, under the appropriate buffer conditions, they promote formation of two-dimensional crystals. Measurements of ATPase activity have been used to demonstrate the regulatory interactions between wild-type and mutants forms of PLB and SERCA. For the current studies, wild-type PLB, a gain-of-function mutant (Lys^{27}-to-Ala), a partial loss-of-function mutant (Arg^{14}-to-Ala), and a complete loss-of-function mutant (Asn^{34}-to-Ala) were chosen to represent different functional forms of PLB[17, 19, 50, 52, 54, 55]. Importantly, the oligomeric stabilities of the mutants used for two-dimensional crystallization were similar to that of wild-type PLB, despite differences in their abilities to regulate SERCA[17, 54]. Measurements of ATPase activity were used to determine the apparent Ca^{2+} affinity of SERCA in the absence and presence of PLB (Table 4.1). Reconstituted SERCA in the absence of PLB yielded a K_{Ca} of 0.41 ± 0.01 μM, while co-reconstituted SERCA in the presence of wild-type PLB yielded a K_{Ca} of 0.69 ± 0.01 μM. The K_{Ca} values in the presence of mutant forms of PLB were 1.00 ± 0.03 μM for Lys^{27}Ala, 0.59 ± 0.03 μM for Arg^{14}Ala, and 0.46 ± 0.03 μM for Asn^{34}Ala.

Table 4.1. Apparent Ca^{2+} affinities (K_{Ca}) determined for SERCA in the absence and presence of wild-type, mutant, and phosphorylated forms of PLB.

	K_{Ca} (μM Ca^{2+})	ΔK_{Ca} [a]
SERCA	0.41 ± 0.01 (n = 28)	
PLB_{wt}	0.69 ± 0.01 (n = 9)	0.28
phospho-PLB_{wt}	0.43 ± 0.02 (n = 3)	0.02
K27A	1.00 ± 0.03 (n = 7)	0.59
phospho-K27A	0.65 ± 0.03 (n = 3)	0.24
R14A	0.59 ± 0.03 (n = 3)	0.18
N34A	0.46 ± 0.03 (n = 6)	0.05

[a] The change in Ca^{2+} concentration at half-maximal ATPase activity of SERCA in the presence of wild-type, mutant, and phosphorylated forms of PLB; calculated as the difference in K_{Ca} values for SERCA in the absence and presence of PLB.

We also tested the effect of PKA phosphorylation on the inhibitory capacity of PLB. After co-reconstitution, phosphorylation of wild-type PLB restored the apparent Ca^{2+} affinity of SERCA to control levels (Figure 4.1a and Table 4.1). However, phosphorylation of the $Lys^{27}Ala$ mutant by PKA did not completely restore the apparent Ca^{2+} affinity of SERCA (Figure 4.2a and Table 1). The K_{Ca} values in the presence of phosphorylated forms of PLB were 0.43 ± 0.02 μM for wild-type [nearly complete (93%) reversal of inhibition] and 0.65 ± 0.03 μM for $Lys^{27}Ala$ [partial (59%) reversal of inhibition]. Both SDS-PAGE (Figures 4-1b and 4-2b) and MALDI-TOF (data not shown) were used to demonstrate stoichiometric phosphorylation of wild-type and $Lys^{27}Ala$ PLB. Neither $Arg^{14}Ala$ nor $Asn^{34}Ala$ mutants were treated with PKA because the former is not recognized by PKA[56] and the latter (loss-of-function) is not affected by phosphorylation. Finally, our observation that phosphorylated $Lys^{27}Ala$ remains partially inhibitory (Figure 4.2A) is consistent with previous work demonstrating that phosphorylated N27C also retains its inhibitory capacity and can be cross-linked to SERCA[28]. Note that residue 27 is lysine in the human protein (used herein) and asparagine in the canine protein[28].

4-2.2. Co-crystallization of SERCA and PLB.

We next tested the ability of wild-type, mutant and phosphorylated forms of PLB to interact with SERCA in large 2D co-crystals[41]. The proteoliposomes described above were capable of forming crystals after treatment with decavanadate, EGTA, and a freeze-thaw procedure to enhance fusion and crystal growth. However, the PLB mutants varied markedly in their ability to form co-crystals**.** In order to identify the effect of mutation and phosphorylation on crystal formation, care was taken to ensure crystallization conditions were equivalent between samples. The number of crystals per grid square (2500 μm^2) were counted in negatively stained samples (Table 4.2). Wild-type PLB produced a moderate frequency of ~3 crystals per grid square and other samples revealed a correlation between the functional state of PLB and the SERCA co-crystal frequency. For example, the $Lys^{27}Ala$ gain-of-function mutant formed ~5 crystals per grid square, while the $Asn^{34}Ala$ loss-of-function mutant formed ~1 crystal per grid square. This was not performed for the $Arg^{14}Ala$ mutant. Despite changes in crystal frequency and order, the crystal morphology and lattice parameters were similar to one another and to those previously reported[41]. In particular, all crystals exhibited $p22_12_1$ plane group symmetry with approximate lattice dimensions of a = 345 Å and b = 70 Å (γ = 90 °).

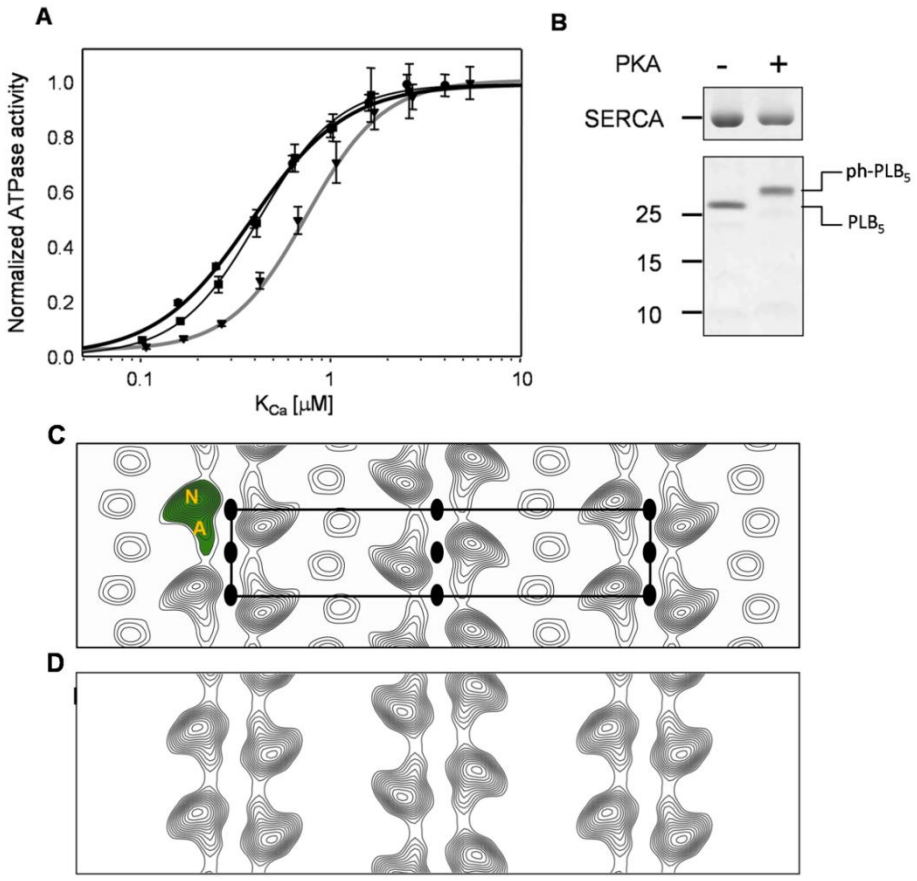

Figure 4.1. Co-reconstitution and co-crystallization of SERCA with non-phosphorylated and phosphorylated wild-type PLB. Panel A, ATPase activity of SERCA reconstituted in the absence (●) and presence of wild-type (▼) and phosphorylated wild-type (■) PLB. The Ca^{2+} affinities (K_{Ca}) are reported in the text, and all curves have been normalized to the maximal activity (V/V_{max}). **Panel B,** Shown is an example of a Coomassie-stained SDS-PAGE of the co-reconstituted proteoliposomes used in the crystallization studies. SERCA and the wild-type PLB pentamer (PLB_5) are labeled. Co-reconstituted proteoliposomes were run on 10% (top panel) and 16% (bottom panel) polyacrylamide gels. A 5-fold larger amount of sample was loaded on the 16% gel for display purposes. A characteristic shift was observed in the mobility of the PLB pentamer after phosphorylation (ph-PLB_5) with protein kinase A (PKA). **Panel C,** Projection map from negatively stained co-crystals of SERCA in the presence of wild-type PLB. A single unit cell (a ≈ 350 Å, b ≈ 71 Å) and symmetry operators are indicated for the $p22_12_1$ plane group. The green densities indicate a single SERCA molecule, where the negative stain reveals only the cytoplasmic domain. The relative locations of the actuator (A) and nucleotide binding (N) domains are indicated. The densities associated with PLB are interspersed between the SERCA dimer ribbons. **Panel D,** Projection map from negatively stained co-crystals of SERCA in the presence of phosphorylated wild-type PLB. The projection maps (panels C and D) are contoured showing all negative (< 0; dashed lines) and positive (≥ 0; solid lines) densities; each contour level corresponds to 0.25 σ.

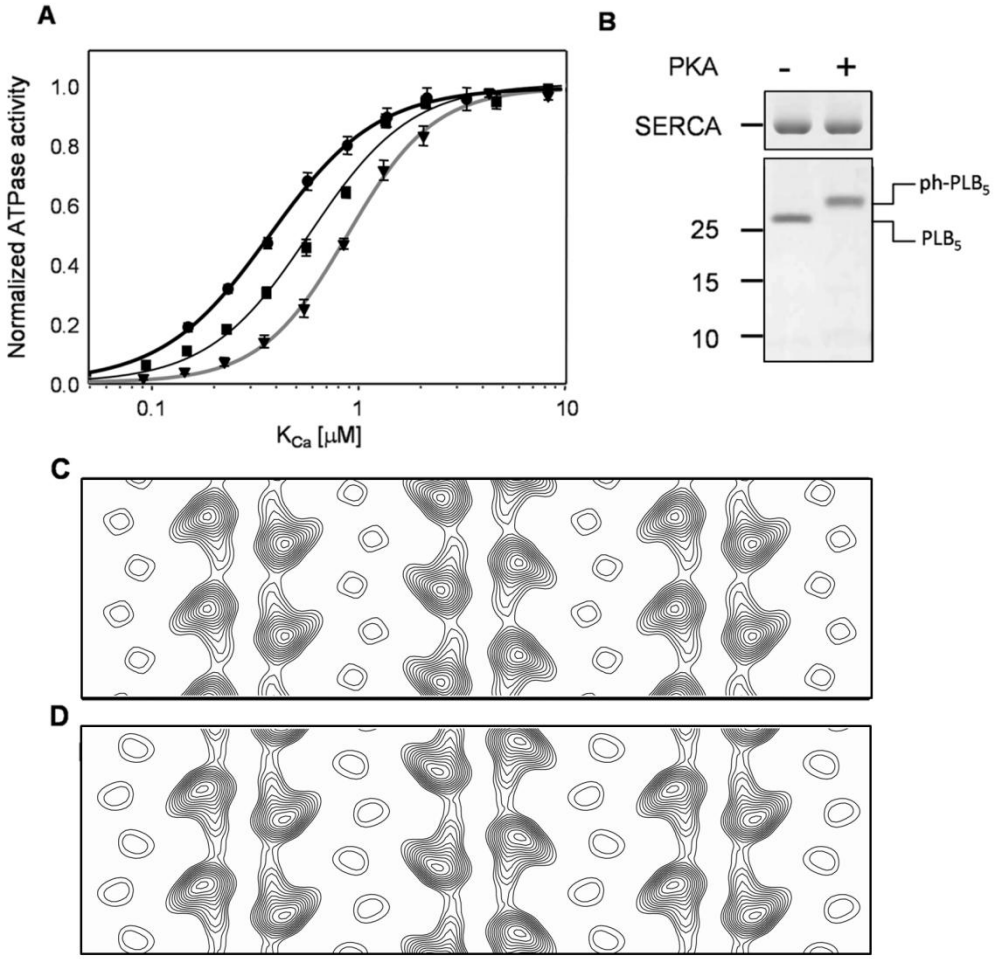

Figure 4.2. Co-reconstitution and co-crystallization of SERCA with non-phosphorylated and phosphorylated Lys27Ala PLB. Panel A, ATPase activity of SERCA reconstituted in the absence (●) and presence of $Lys^{27}Ala$ (▼) and phosphorylated $Lys^{27}Ala$ (■) PLB. The Ca^{2+} affinities (K_{Ca}) are reported in the text, and all curves have been normalized to the maximal activity (V/V_{max}). **Panel B,** Shown is an example of a Coomassie-stained SDS-PAGE of the co-reconstituted proteoliposomes used in the crystallization studies. SERCA and the $Lys^{27}Ala$ PLB pentamer (PLB_5) are labeled. Co-reconstituted proteoliposomes were run on 10% (*top panel*) and 16% (*bottom panel*) polyacrylamide gels. A 5-fold larger amount of sample was loaded on the 16% gel for display purposes. A characteristic shift was observed in the mobility of the PLB pentamer after phosphorylation (ph-PLB_5) with PKA. **Panel C,** Projection map from negatively stained co-crystals of SERCA in the presence of $Lys^{27}Ala$ PLB. **Panel D,** Projection map from negatively stained co-crystals of SERCA in the presence of phosphorylated $Lys^{27}Ala$ PLB. The projection maps (panels C and D) are contoured showing only positive (solid lines) densities; each contour level corresponds to 0.25 σ.

Table 4.2. Lattice parameters and crystal propensity for negatively stained crystals of SERCA with and without phospholamban.

		$p22_12_1$ lattice parameters				
	characteristics	a	b	γ	crystal frequency [a]	crystal quality
PLB	pentamer, inhibitory	341.3 ± 2.7	70.3 ± 0.3	90.2 ± 0.5	3.1 ± 0.5 (*n* = 7)	intermediate
phospho-PLB	pentamer, non-inhibitory	341.6 ± 6.2	70.2 ± 0.9	90.1 ± 1.0	1.4 ± 0.4 (*n* = 7)	poor
K27A	pentamer, gain-of-function	344.9 ± 4.2	70.9 ± 0.9	85.6 ± 1.5	5 ± 1 (*n* = 6)	high
phospho-K27A	pentamer, inhibitory	339.5 ± 1.5	71.3 ± 0.5	90.1 ± 0.4	1.7 ± 0.5 (*n* = 7)	poor to intermediate
N34A	pentamer, loss-of-function	339.1 ± 2.0	70.6 ± 0.7	89.5 ± 0.5	1 ± 0.4 (*n* = 7)	poor

[a] The average number of crystals observed per grid square (400 mesh grids) for a minimum of six independent co-reconstitutions and crystallization trials ($n \geq 6$). This was not done for the R14A mutant of PLB. For each independent co-reconstitution and crystallization trial (*n*), at least 30 grid squares were examined for crystal frequency.

4-2.3. Projection maps from negatively stained two-dimensional co-crystals.

For each form of PLB, projection maps of negatively stained samples were calculated after averaging Fourier data from five different crystal images at a resolution of ~20 Å. To rule out differences in negative staining, 2-3 projection maps were calculated for each form of PLB, where each projection map represented an independent co-reconstitution, crystallization, and negative stain EM grid. Typical projection maps are shown for non-phosphorylated and phosphorylated wild-type PLB (Figure 4.1). As previously observed[41], the projection maps were dominated by rows of twofold related densities that corresponded to anti-parallel dimer arrays of SERCA. In the presence of wild-type PLB, additional densities were interspersed between the SERCA arrays consistent with the presence of PLB oligomers (Figure 4.1c). These extra densities were relatively small in the maps of negatively stained crystals, due to the low contrast generated by negative stain within the lipid bilayer and the small size of PLB's cytoplasmic domain relative to SERCA. Nonetheless, the PLB densities in the projection maps were similar to those previously reported[41]. Upon phosphorylation of Ser^{16} with PKA, these PLB densities were no longer present, consistent with disordering of the cytoplasmic domain (Figure 4.1d). As mentioned above, phosphorylation of wild-type PLB also reduced the frequency of co-crystal formation (Table 4.2).

We also studied the effect of phosphorylation on the co-crystals with Lys^{27}Ala PLB, which has the same oligomeric state as wild-type PLB[17, 54]. Like wild-type PLB, the projection maps of non-phosphorylated Lys^{27}Ala co-crystals show the PLB densities

lying between the anti-parallel dimer ribbons of SERCA (Figure 4.2). The frequency of the $Lys^{27}Ala$ co-crystals is higher than wild-type, reflecting the fact that the $Lys^{27}Ala$ mutation produces a super-inhibitory PLB molecule (gain of function). Interestingly, phosphorylation of $Lys^{27}Ala$ had no effect on these PLB densities (compare Figures 4-1d and 4-2d). This behavior is consistent with the fact that stoichiometric phosphorylation of $Lys^{27}Ala$ is unable to fully reverse its inhibition of SERCA (Figure 4.2a and 4-2b). We reasoned that if phosphorylation disrupted a crystal contact or altered contrast produced by negative stain (e.g. by adding negative charge to the cytoplasmic domain), then phosphorylation of $Lys^{27}Ala$ co-crystals should produce a similar result to wild-type PLB (Figure 4.1c and 4-1d). However, if co-crystallization relies on a functional interaction between PLB and SERCA, then the inhibitory properties of the phosphorylated $Lys^{27}Ala$ mutant should correlate with its behavior during co-crystallization. Based on our observations, we believe that the cytoplasmic domain of wild-type PLB becomes disordered upon phosphorylation, whereas the cytoplasmic domain of $Lys^{27}Ala$ does not. This comparison also rules out the possibility that the disappearance of the PLB densities was a result of simply adding the negative charge (PO_4^{2-}) to its cytoplasmic domain.

4-2.4. Additional mutants of PLB.

Since the phosphorylation of wild-type PLB reverses SERCA inhibition and alters densities in the two-dimensional co-crystals, we tested the effects of (i) mutation of a charged residue (Arg^{14}) proximal to the phosphorylation site (Ser^{16}); and (ii) a well-characterized loss-of-function mutant ($Asn^{34}Ala$). As reported previously[17, 56], $Arg^{14}Ala$ retains substantial inhibitory capacity (Figure 4.3a), whereas $Asn^{34}Ala$ is a complete loss-of-function mutant (Figure 4.4a). The $Arg^{14}Ala$ mutant changes the net charge of PLB's cytoplasmic domain adjacent to the phosphorylated residue Ser^{16}, while the $Asn^{34}Ala$ mutant is located at the interface between the membrane and the cytosol. In projection maps of negatively stained co-crystals with $Arg^{14}Ala$ PLB, additional densities were observed in between the rows of SERCA molecules (Figure 4.3b). However, in co-crystals with $Asn^{34}Ala$ PLB, these additional densities were absent (Figure 4.4b). These results further support the idea that the functional state, rather than the net charge of the cytoplasmic domain, determines the stability of co-crystals and whether PLB-associated densities are visible in the projection maps. Interestingly, the $Asn^{34}Ala$ mutation appears to cause a disordering of the cytoplasmic domain that is similar to the effect of phosphorylation of wild-type PLB.

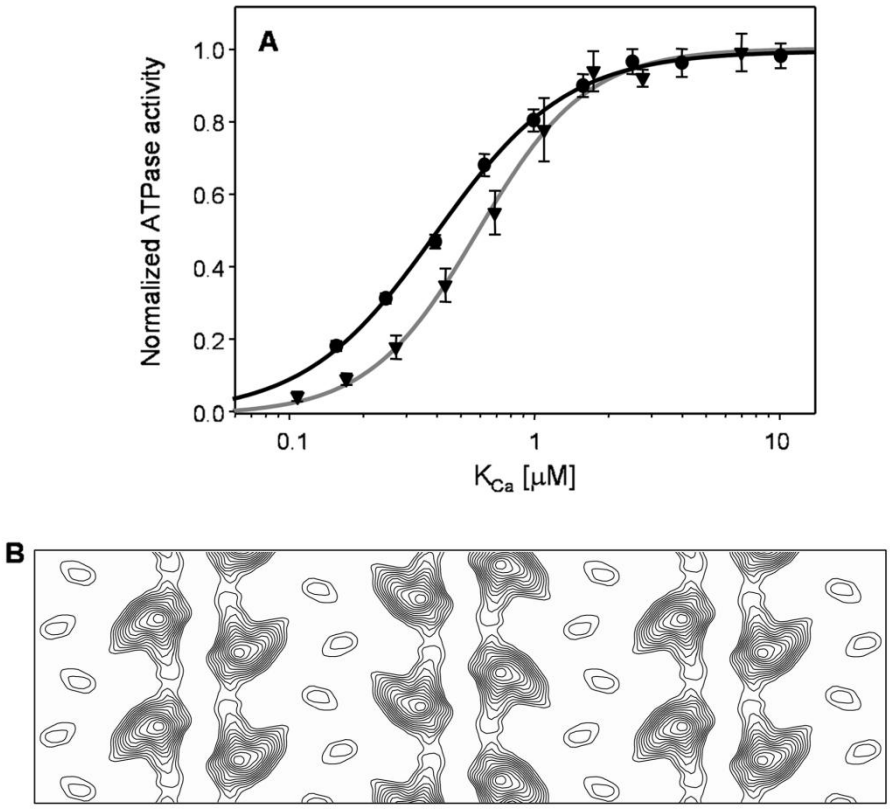

Figure 4.3. Co-reconstitution and co-crystallization of SERCA with Arg14Ala PLB. Panel A, ATPase activity of SERCA reconstituted in the absence (●) and presence of $Arg^{14}Ala$ (▼) PLB. The Ca^{2+} affinities (K_{Ca}) are reported in the text, and all curves have been normalized to the maximal activity (V/V_{max}). **Panel B,** Projection map from negatively stained co-crystals of SERCA in the presence of $Arg^{14}Ala$ PLB. The projection map is contoured showing only positive (solid lines) densities; each contour level corresponds to 0.25 σ.

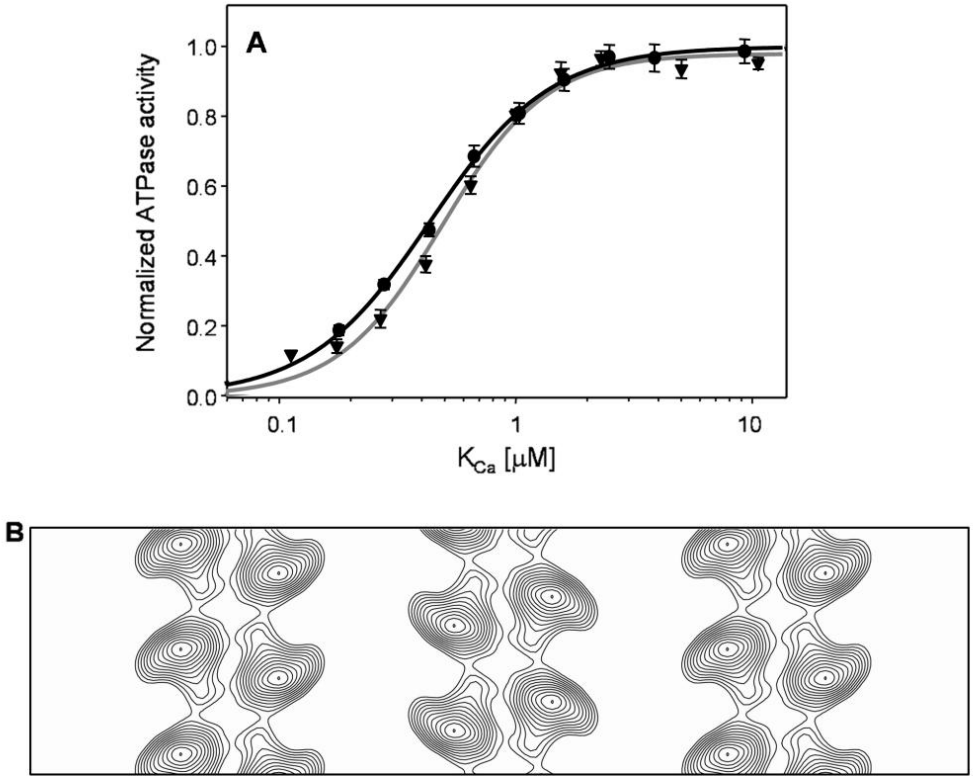

Figure 4.4. Co-reconstitution and co-crystallization of SERCA with Asn34Ala PLB. Panel A, ATPase activity of SERCA reconstituted in the absence (●) and presence of $Asn^{34}Ala$ (▼) PLB. The Ca^{2+} affinities (K_{Ca}) are reported in the text, and all curves have been normalized to the maximal activity (V/V_{max}). **Panel B,** Projection map from negatively stained co-crystals of SERCA in the presence of $Asn^{34}Ala$ PLB. The projection map is contoured showing all only positive (solid lines) densities; each contour level corresponds to 0.25 σ.

4-2.5. Projection maps from frozen-hydrated two-dimensional co-crystals.

Our observations of negatively stained crystals indicated that the co-crystallization of PLB and SERCA was negatively impacted by PLB phosphorylation and that the cytoplasmic domain of PLB tended to become disordered. To test if this disordering affected the transmembrane domain of PLB, we imaged the co-crystals in the frozen-hydrated, unstained state. Based on molecular models for PLB[40, 57, 58], the density associated with PLB in projection maps from frozen-hydrated co-crystals is dominated by the pentameric transmembrane coiled-coil. This is due to the alignment of the transmembrane helices along the imaging direction, which produces very strong densities in the corresponding projection maps. Therefore, comparison of the densities observed in negatively stained co-crystals with those observed in frozen-hydrated crystals allows us to evaluate the relative ordering of the cytoplasmic and transmembrane domains, respectively. In particular, if phosphorylation disorders primarily the cytoplasmic domain of PLB as predicted[32], densities attributable to PLB should be weak in the negatively stained samples and unaffected in frozen-hydrated samples. For this comparison, projection maps were calculated from images of frozen-hydrated co-crystals with wild-type PLB before and after PKA phosphorylation. Following merging and averaging of data from at least five crystal images, diffraction amplitudes with high signal-to-noise ratios and low phase residuals were observed for all resolution shells to a resolution of 10 Å (Table 4.3). The resulting maps were nearly identical, both containing anti-parallel dimer ribbons of SERCA molecules interspersed with densities consistent with pentameric PLB (Figure 4.5). This similarity suggests that intramembrane interactions between SERCA and the transmembrane domain of PLB mediate contacts in the crystals and that these contacts persist after phosphorylation of PLB's cytoplasmic domain. Loss of density for these cytoplasmic domains suggests that they are disordered and thus not strongly bound to SERCA after phosphorylation. Given the negative effect of phosphorylation on crystal order, PLB's cytoplasmic domain probably provides additional interactions in the non-phosphorylated state.

Table 4.3. Summary of crystallographic data for frozen-hydrated co-crystals of SERCA and phospholamban.

	Phospholamban	
	I40A*	K27A
Number of images	5	15
Cell parameters	a = 359.2 Å	a = 346.5 Å
	b = 71.9 Å	b = 70.7 Å
	γ = 90.3°	γ = 89.7°
Overall weighted phase residual ¶	16.8°	16.1°

* Data from Stokes et al. (2006).

¶ Including data to IQ7.

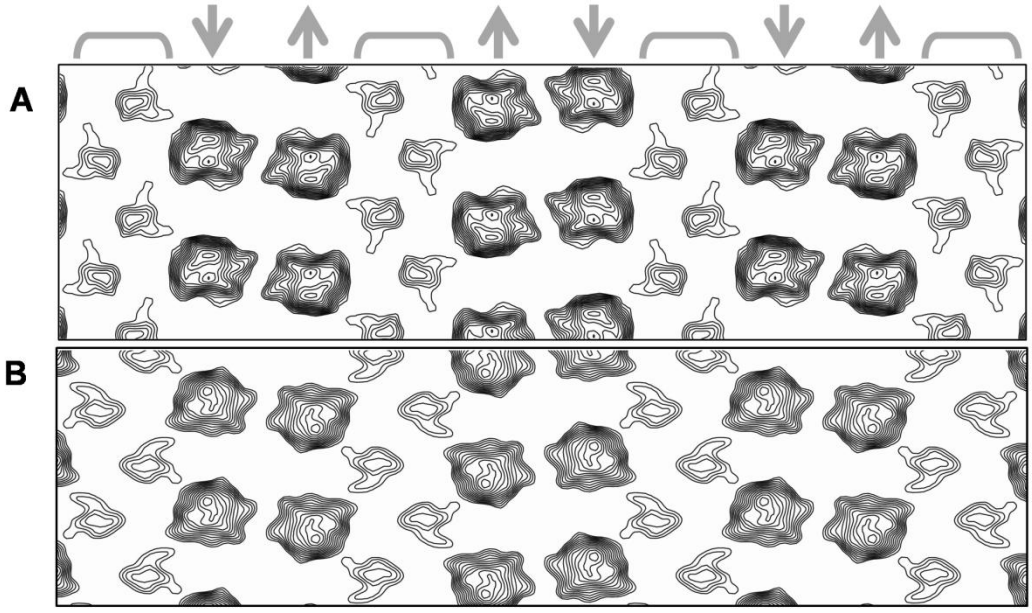

Figure 4.5. Projection maps from frozen-hydrated co-crystals of SERCA in the presence of wild-type (Panel A) and phosphorylated wild-type (Panel B) PLB. Statistics for merging five crystal images indicated that phase residuals were <35° to a resolution of approximately 10 Å. The region of the map shown is approximately 600 Å by 159 Å. The relative locations and orientations of SERCA molecules are indicated by *arrows* and the locations of the PLB densities are indicated by *brackets*. The projection maps are contoured showing only positive (solid lines) densities.

4-2.6. What is the oligomeric state of PLB in the co-crystals?

To further characterize the physical interaction between SERCA and PLB and to evaluate its oligomeric state in the co-crystals, we have used frozen-hydrated preparations to improve the resolution of the existing projection map[41]. We chose to image co-crystals of Lys^{27}Ala PLB because the relative abundance and high quality of these crystals facilitated data collection. Images from frozen-hydrated co-crystals displayed computed diffraction to a resolution of approximately 15 Å. Following merging and averaging of data from 15 crystal images, diffraction amplitudes with high signal-to-noise ratios and low phase residuals were observed for all resolution shells to a resolution of 8 Å (Figure 4.6 and Table 4.3).

The resulting projection map for SERCA in the presence of Lys^{27}Ala PLB is similar to that previously determined for SERCA in the presence of Ile^{40}Ala PLB[41]. The size and shape of the additional densities seen in our projection maps were consistent with the pentamer, which is the principle oligomeric form of PLB seen by SDS-PAGE. However, neither map from frozen-hydrated co-crystals (Ile^{40}Ala reported previously[41] or Lys^{27}Ala reported herein) provided direct evidence of pentameric assembly of PLB, presumably due to limited resolution. To address this issue, the high resolution terms of the projection map were enhanced by applying a negative 500 $Å^2$ *B*-factor (temperature factor)[59]. The truncation of Fourier data at 8 Å resolution ensured that the contribution of noise in our map was minimal. This procedure improved contrast and detail for the densities associated with both SERCA and PLB (Figure 4.7). Significantly, the density assigned to the PLB oligomer resolved into a five-lobed density consistent with the PLB pentamer. However, rather than the symmetric structure predicted by NMR structural models[40, 58], our density resembles a distorted pentamer (Figure 4.7b-d), where two of the five observed lobes are stronger and better delineated than the others. Although the shape of the pentamer may be affected by the increased noise in the "sharpened" projection map, a physical distortion of the pentamer would be consistent with its asymmetric interaction with SERCA. Interestingly, the stronger densities in the pentamer are proximal to SERCA, and one appears next to transmembrane segment TM3 (*asterisk* in Figure 4.7a). An interaction between TM3 of SERCA and PLB was also suggested by our previous studies of the complex using electron cryo-microscopy of helical crystals (Figure 4 in ref Young et al[52]).

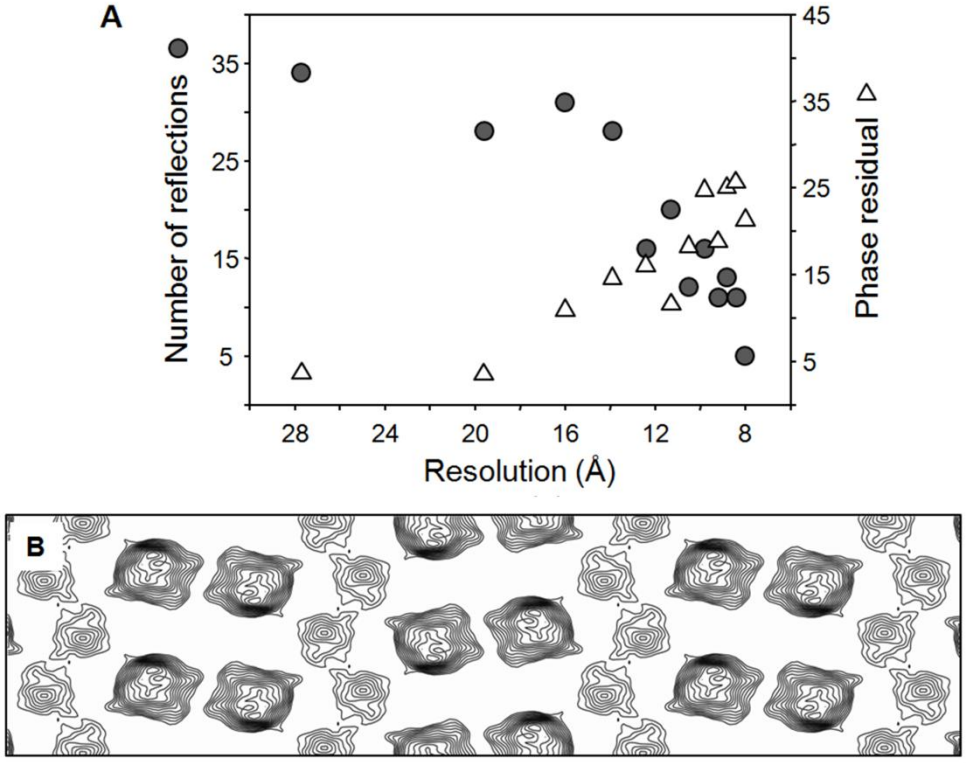

Figure 4.6. Projection map from frozen-hydrated co-crystals of SERCA in the presence of Lys27Ala PLB. Panel A, Statistics for merging fifteen crystal images indicate that phase residuals are <26° to a resolution of 8 Å. **Panel B,** Projection map generated for co-crystals of SERCA and Lys[27]Ala PLB. The region of the map shown is approximately 600 Å by 159 Å. The PLB densities are similar to those previously characterized for Ile[40]Ala PLB[41], reflecting an identical oligomeric state and mode of interaction with SERCA. The projection map is contoured showing only positive (solid lines) densities.

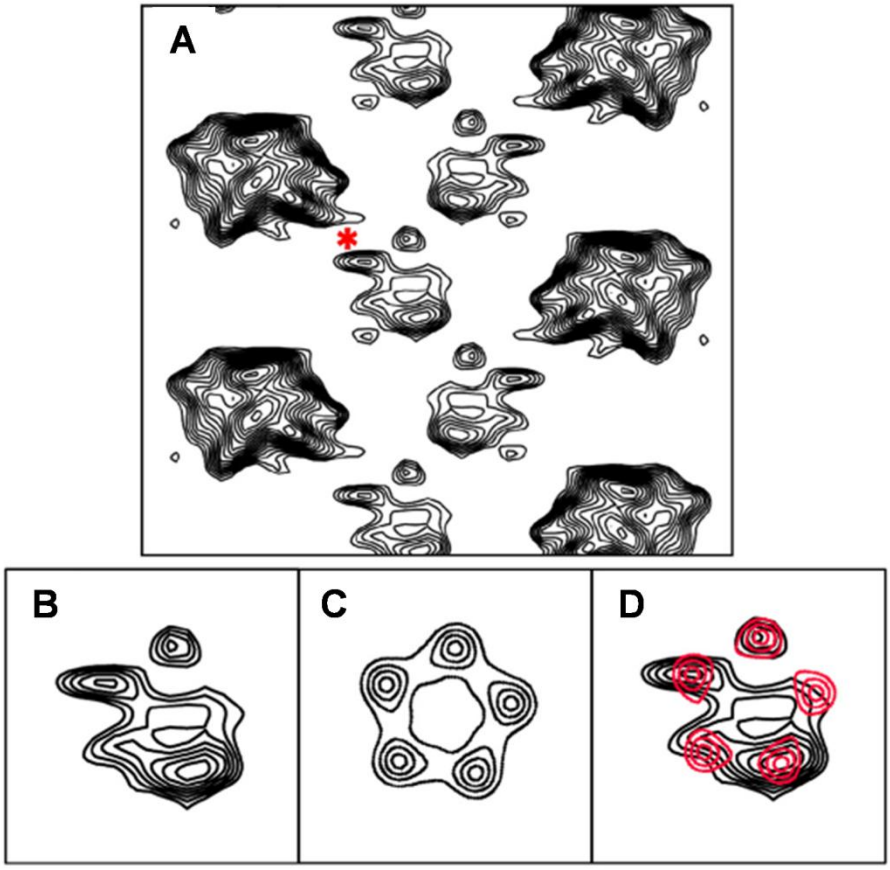

Figure 4.7. Projection map recalculated with an applied negative B-factor. Panel A, In the sharpened projection map, the contrast and level of detail is enhanced for both SERCA and PLB. The *asterisk* indicates the region of closest contact between the PLB pentamer and transmembrane segment TM3 of SERCA. **Panel B,** Close up view of the density associated with PLB. The size and shape of the PLB densities are now compatible with a pentamer. **Panel C,** For comparison, a simulated projection for a transmembrane pentamer is shown. **Panel D,** Superimposition of the maps shown in panel B and panel C indicating a slightly distorted pentameric arrangement.

4-2.7. Physical interactions between SERCA and PLB.

There is general consensus that the monomeric form of PLB interacts with TM2, TM4, and TM6 of SERCA[17, 19, 20, 24, 25, 47, 48], thus producing the inhibition that characterizes the resting state of cardiac muscle. However, oligomeric forms of PLB have been repeatedly observed both in detergent and membranous environments. While the pentamer appears to be the most stable oligomer, tetramers, trimers and dimers have all been observed and the balance between them can be influenced by single site mutations[17, 19]. Furthermore, there is dynamic exchange between oligomeric and monomeric forms of PLB and evidence that phosphorylation of PLB or increased cytosolic Ca^{2+} concentrations increase the proportion of the pentameric pool at the expense of the monomeric pool[15]. This evidence has led to the hypothesis that the monomer represents the "active" inhibitory form and that oligomeric forms represent an inactive reserve[20, 21]. While several congruent molecular models explaining the inhibitory properties of PLB have been described in the literature[46, 47, 60, 61], there are also a number of inconsistencies in published observations that are not fully explained. First, Kranias and colleagues demonstrated that a mutant form of PLB (Cys[41]-to-Phe) was insufficient for proper regulation of cardiac contractility in a mouse model [39]. Since this mutant was reported to be monomeric with the same inhibitory potency as the wild-type protein[62], the authors inferred a physiological role for the PLB pentamer. Despite the fact that the oligomeric state of the C41F mutant has not been directly demonstrated in a membrane environment, this notion is consistent with independent observations that SERCA may interact with oligomeric forms of PLB[40, 41, 63]. Thus, the existence of oligomers appears to offer a functional advantage for the SERCA-PLB interaction[42], and this advantage is not explained by current molecular models (i.e. PLB oligomers as inactive storage forms). Second, there are disparate observations on how the physical association between SERCA and PLB responds to phosphorylation. One group of studies postulate that PLB remains associated with SERCA and phosphorylation alters the structural interaction between the two proteins[29-32, 64]. Whereas contradictory cross-linking studies have led to the notion that intermolecular interactions at the TM2, TM4, and TM6 interface are lost following phosphorylation[27, 28] and PLB dissociates from SERCA.

More specifically, chemical cross-linking experiments[27, 28] indicate that PKA-mediated phosphorylation decreases the efficiency of cross-linking to SERCA at multiple sites distributed throughout both the cytoplasmic and transmembrane domains of PLB. The

inference then is that phosphorylation decreases PLB's binding affinity for SERCA and causes it to dissociate at sub-saturating Ca^{2+} concentrations. Contradictory evidence in favor of persistent association comes from the following literature. Antibodies recognizing PLB phosphorylated at Ser^{16} were shown to co-immunoprecipitate SERCA1a and SERCA2a after co-expression in HEK-293 cells[29]. Fluorescence, spin-label EPR spectroscopy and other biophysical studies demonstrated that SERCA restricts the motional freedom of PLB both before and after phosphorylation[30, 31]. More recent EPR studies also support persistent association and suggest that phosphorylation induces a dynamically disordered state in PLB's cytoplasmic domain[32]. This latter study supported the idea that phosphorylated PLB remains associated with SERCA in a non-inhibitory state. Despite this growing body of evidence, it is difficult to envision how PLB might remain bound to the TM2, TM4, and TM6 interface of SERCA, given the large conformational changes caused by Ca^{2+} binding that occlude this interaction interface.

These apparent contradictions can be reconciled by hypothesizing a physical interaction between SERCA and oligomeric PLB at a secondary, non-inhibitory site. Specifically, we have observed an interaction between TM3 of SERCA and the PLB pentamer in the two-dimensional co-crystals. Such an interaction could explain the mutual effects that SERCA and PLB have on spectroscopic analysis of each other's aggregation state[41, 63], and could provide a direct role for the PLB oligomer under physiological conditions [39]. In addition, distinct functional consequences and binding sites of the monomer and oligomer could explain the experimental discrepancy regarding the persistence of the interaction. While the PLB monomer may dissociate from the TM2, TM4, and TM6 inhibitory site under the appropriate physiological stimuli, there may be a high probability for interaction with the PLB oligomer at the secondary site on the other side of the SERCA molecule (e.g., M3). Compared to the dramatic movements of TM2, TM4 and TM6 during Ca^{2+} binding, transmembrane helix TM3 of SERCA is less mobile and may represent a stable interaction point for a PLB oligomer that is insensitive to phosphorylation or the level of cytosolic Ca^{2+}.

In the present work, our data support a functionally relevant interaction between SERCA and a PLB oligomer in two-dimensional co-crystals. In particular, the effects of PLB mutants on crystallization correlate with their effects on the inhibition of SERCA. Lys^{27}Ala and Asn^{34}Ala mutations were chosen for the similar stability of their pentameric form, yet widely different inhibitory behavior. Thus, it is significant that the gain-of-

function Lys[27]Ala mutation enhanced crystallization, whereas the loss-of-function Asn[34]Ala mutation interfered with crystallization. We conclude that the structural properties of PLB that govern the association of the monomer with the inhibitory site of SERCA are directly related to those used in the interaction of a PLB oligomer at the secondary, accessory site.

4-2.8. Effect of phosphorylation on physical interactions between SERCA and PLB.

In studies of the PLB monomer, there is some consistent evidence that phosphorylation of Ser[16] causes localized changes in the structure of its cytoplasmic domain[32, 33, 35, 65, 66]. These results provide a physical basis for disruption of the productive structural interaction between SERCA and PLB, which may or may not lead to dissociation of the complex. Early NMR and CD spectroscopy studies showed a continuous α-helix in the N-terminal portion of PLB (residues 1-16), which partially unwound upon phosphorylation (residues 12-16 were no longer helical)[35]. However, these studies utilized an N-terminal fragment of PLB (residues 1-25), rather than the full-length protein, and did not include SERCA. Since then, there have been many structural models for full-length PLB based on NMR measurements in the non-phosphorylated[40, 60, 67-71], phosphorylated[65] and pseudo-phosphorylated[72] state under a variety of experimental conditions. These models differ in the amount of secondary structure in the N-terminal cytoplasmic domain of PLB, suggesting that this domain can adopt a variety of conformational states. Furthermore, most studies agree that phosphorylation alters the dynamics of this domain, the NMR structure of a pseudo-phosphorylated form of PLB notwithstanding[72]. A variety of biophysical studies also indicate that PLB undergoes a conformational change upon phosphorylation[13, 34, 35, 73]. Many of these ideas coalesced in recent EPR[32] and NMR[33, 66] studies, which proposed an order-to-disorder transition in the cytoplasmic domain of PLB that disrupts intermolecular contacts and reverses SERCA inhibition, but does not dissociate the SERCA-PLB complex.

Consistent with this idea, we found that phosphorylation of wild-type PLB at Ser[16] selectively disordered the cytoplasmic domains of the pentamer (Figure 4.1) and reduced its ability to mediate two-dimensional crystallization with SERCA (Table 4.2). In maps from negatively stained crystals, densities attributable to the cytoplasmic domain disappeared when PLB was phosphorylated, whereas maps from frozen-hydrated crystals showed that the transmembrane helices of PLB were still clearly visible. We conclude that the transmembrane domain of phosphorylated PLB remains associated with SERCA

in the co-crystals, even though the cytoplasmic domain became disordered. This disordering did not occur for the Lys^{27}Ala gain-of-function mutant (Figure 4.2), yet it did occur for the Asn^{34}Ala loss-of-function mutant even in the non-phosphorylated state (Figure 4.4). Furthermore, the propensity to induce co-crystallization was retained by the Lys^{27}Ala after phosphorylation, whereas the Asn^{34}Ala mutant was marginal in co-crystallization even in the non-phosphorylated state (Table 4.2). It is interesting to consider where these three residues lie in the structure of PLB. Ser^{16} flanks the N-terminal end of domain Ib, Lys^{27} is found in the middle of this domain, and Asn^{34} flanks the C-terminal end. These residues also have two opposed functional effects – PLB function is lost when phosphorylated at Ser^{16} or mutated at Asn^{34}, and PLB function is enhanced when mutated at Lys^{27}. Thus, domain Ib may be the key structural element responsible for phosphorylation- or mutation-dependent conformational changes in PLB's cytoplasmic domain that impact SERCA inhibition. Indeed, many of the structural differences between existing PLB models involve domain Ib[40, 60, 65, 67-72], suggesting that this domain may be a less structured, more dynamic region of the protein. Therefore, it is reasonable to suppose that phosphorylation alters the dynamics of domain Ib, thereby controlling an order-to-disorder transition in PLB's cytoplasmic domain and reversing SERCA inhibition[29, 30, 32].

4-2.9. Model for the interaction of the PLB pentamer.

The major findings in this report are that the PLB pentamer is capable of a physical interaction with SERCA and that this interaction is sensitive to functional modification of PLB through phosphorylation or mutation. In particular, PKA-mediated phosphorylation of Ser^{16} caused the cytoplasmic domain of PLB to become disordered, yet the pentamer remained associated with SERCA through intramembrane interactions. This disordering also occurred for a well-characterized loss-of-function mutation, Asn^{34}-to-Ala, suggesting that the loss of inhibition might occur through a mechanism similar to phosphorylation. These data are consistent with a functional interaction between SERCA and PLB oligomers[42], and inconsistent with the notion of PLB oligomers as inactive storage forms[21]. The inhibitory site involving the PLB monomer and transmembrane helices TM2, TM4 and TM6 of SERCA[47, 49, 60] is distinct from the physical interactions that stabilize our 2D crystals, which center on TM3 of SERCA and involve the transmembrane domain of PLB. The inhibitory site of SERCA alternately opens and closes during the Ca^{2+} transport cycle, due to large movements of transmembrane helices

TM2, TM4, and TM6. This is not the case for the accessory site of SERCA, since TM3 is less mobile during the transport cycle. Thus, TM3 could act as an interaction point between SERCA and the PLB pentamer (and perhaps other oligomeric forms, as well). Interestingly, a primary structure comparison between SERCA and PLB reveals a region of sequence similarity that spans the C-terminal portion of PLB's transmembrane helix and TM3 of SERCA (Figure 4.8). Residues Leu^{266}, Val^{269} and Leu^{273} of SERCA face the lipid environment and adopt a side chain orientation similar to Leu^{44}, Ile^{47} and Leu^{51} of PLB. These residues form part of the Leu-Ile zipper that stabilizes the PLB pentamer[74].

Through its interaction with TM3 of SERCA, the PLB pentamer might play an active role in capturing monomeric or phosphorylated PLB species. Specifically, this SERCA-pentamer interaction may facilitate the exchange of PLB monomers with the SERCA inhibitory site in response to physiological cues (elevated cytosolic Ca^{2+} and/or phosphorylation). This interaction would explain how SERCA can influence the oligomeric state of PLB[63]. Based on their NMR structure of a PLB pentamer, Oxenoid and Chou[40] suggested that individual PLB monomers could initiate binding to SERCA without dissociation from the pentamer. We suggest a modification to this hypothesis, where a PLB pentamer interacts with the membrane domain of SERCA and serves as a reservoir for directed diffusion of monomers to and from the inhibitory site (Figure 4.8). This pathway may be important in efficiently delivering monomeric PLB to its binding site on SERCA, ensuring that the inhibited state is maintained following a cycle of Ca^{2+} release in cardiac muscle. Specifically, a site for the PLB pentamer on SERCA may position the monomer in a conformation compatible with formation of the inhibitory complex, as previously suggested[40]. The resultant depolymerization of the PLB pentamer would leave a tetramer that may remain associated with the pump. There is ample evidence of intermediate oligomers for PLB (e.g. Reddy et al[51]) and such intermediates could be poised to reacquire a PLB monomer once it dissociates from the SERCA. Finally, phosphorylation has been shown to increase the oligomeric propensity of PLB[15] and an interaction of these species with the pump could ensure a rapid return to the inhibited state upon dephosphorylation. Otherwise, if allowed to diffuse away during a period of β-adrenergic stimulation, there could be a substantial delay before SERCA randomly encounters a non-phosphorylated PLB molecule within the membrane plane.

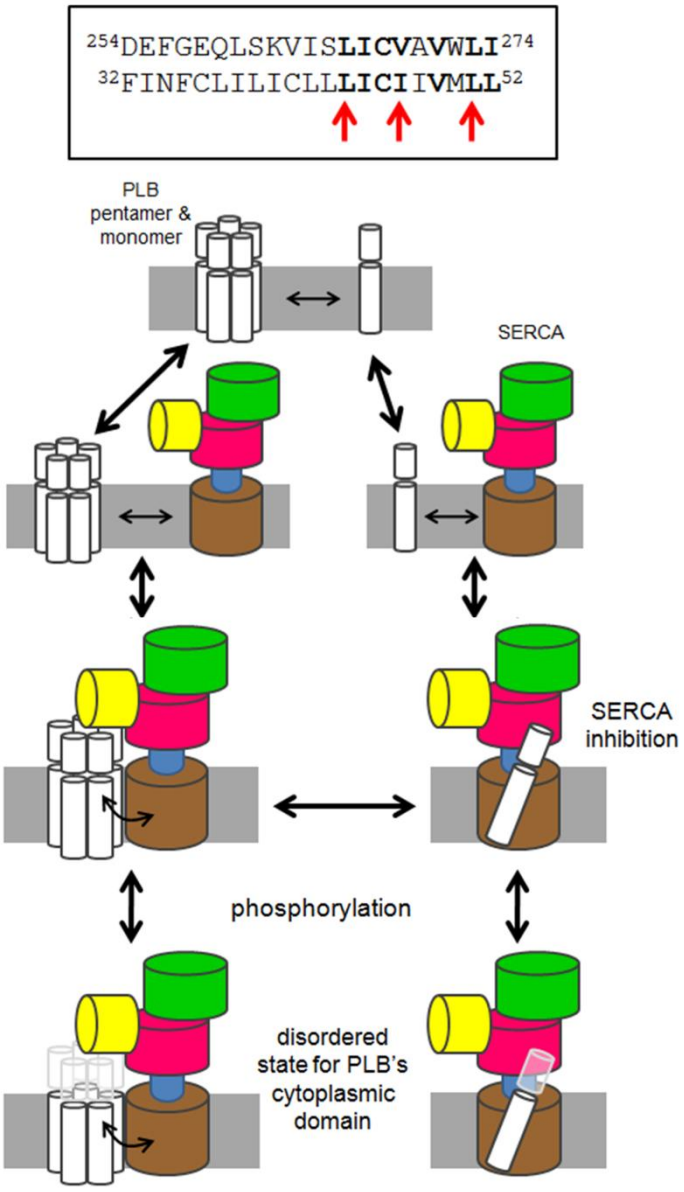

Figure 4.8. Partial sequence alignment and schematic diagram for the interaction of PLB with SERCA. Upper panel, Shown is the potential sequence similarity between the transmembrane domain of PLB (residues 32-52) and transmembrane segment TM3 of SERCA (residues 254-274). Leu^{44}, Ile^{47} and Leu^{51} make up part of the leucine-isoleucine zipper that stabilizes the pentameric state of PLB. **Lower panel,** The pentamer and monomer are in dynamic equilibrium, where the monomer is postulated to interact with and inhibit SERCA (*right side of figure*). We hypothesize that the pentamer also interacts with SERCA, which leads to the active association or dissociation of a monomer (*left side of figure*). The active dissociation of a monomer leads to a physical interaction with and inhibition of SERCA and this process is reversed by phosphorylation of PLB. These two pathways are not mutually exclusive, but may operate simultaneously or under disparate physiological conditions.

4-3. Materials and Methods.

4-3.1. Materials.

Octaethylene glycol monododecyl ether ($C_{12}E_8$) was obtained from Barnet Products (Englewood Cliff, NJ). SM-2 Biobeads were obtained from Bio-Rad (Hercules, CA). Egg yolk phosphatidylcholine (EYPC), egg yolk phosphatidylethanolamine (EYPE) and egg yolk phosphatidic acid (EYPA) were obtained from Avanti Polar Lipids (Alabaster, AL). All reagents used in the coupled enzyme assay for measuring ATPase activity[75] were of the highest purity available (Sigma-Aldrich, Oakville, ON Canada).

4-3.2. Reconstitution of SERCA with PLB.

SERCA was prepared from rabbit hind leg muscle[76] by affinity chromatography[10]. Recombinant human PLB was prepared as described[77]. The following proteins were made – wild-type PLB, a gain-of-function mutant Lys^{27}-to-Ala ($Lys^{27}Ala$), a partial loss-of-function mutant Arg^{14}-to-Ala ($Arg^{14}Ala$), and a loss-of-function mutant Asn^{34}-to-Ala ($Asn^{34}Ala$). Co-reconstitution of SERCA with PLB followed established methods for the formation of large two-dimensional co-crystals[41]. Briefly, 100 μg PLB and lipids (8:1:1 weight ratio of EYPC, EYPE and EYPA) were solubilized in a chloroform-trifluoroethanol mixture, dried to a thin film under nitrogen gas and lyophilized. Buffer (20 mM imidazole, pH 7.0, 100 mM KCl, 0.02% NaN_3) and detergent ($C_{12}E_8$) were added to solubilize the mixture, followed by the addition of 500 μg of detergent-solubilized, purified SERCA. It has been shown that this method of co-reconstitution yields complete recovery of SERCA transport activity and PLB inhibition[51, 78]. The final concentrations were adjusted to obtain weight ratios of 1 protein: 1 lipid: 2 detergents (final molar ratio of approximately1 SERCA: 3.5 PLB: 180 lipids). The detergent was removed by the slow addition of SM-2 Biobeads (25 milligrams of wet beads) over a 4-hour time course. For the best results, crystallization was performed immediately on the co-reconstituted proteoliposomes containing SERCA and PLB. Reconstituted proteoliposomes containing SERCA in the absence of PLB were prepared simultaneously under identical conditions. ATPase activity of the proteoliposomes was measured by a coupled-enzyme assay over a 0.1 μM to 10 μM range of Ca^{2+} concentrations[50, 75]. The K_{ca} (apparent Ca^{2+} affinity) was determined by fitting the data to the Hill equation using Sigma Plot software (SPSS Inc., Chicago, IL). The functional characterization of these mutants has been described by others[17, 54], as well as by our laboratory[50].

For studies of the effect of PLB phosphorylation, wild-type and $Lys^{27}Ala$ PLB were solubilized in detergent and phosphorylated with the catalytic subunit of protein kinase A (PKA; Sigma-Aldrich, St. Louis, MO) prior to co-reconstitution with SERCA into proteoliposomes. PKA was added to a concentration of 100 units/mg of detergent-solubilized PLB and the reaction was incubated at 30 °C for 3 hours. It was concluded that this treatment resulted in complete phosphorylation of PLB, since the unphosphorylated protein could not be detected either by MALDI-TOF mass spectrometry or SDS-PAGE and Western blotting (data not shown).

4-3.3. 2D Crystallization.

Co-reconstituted proteoliposomes were collected by centrifugation in crystallization buffer (20 mM imidazole, pH 7.4, 100 mM KCl, 35 mM $MgCl_2$, 0.5 mM EGTA, 0.25 mM Na_3VO_4, 30 μM thapsigargin)[79]. The pellet was subjected to two freeze-thaw cycles, resuspended with a micropipette, followed by two additional freeze-thaw cycles. Reconstituted samples were incubated at 4°C for several days to one week. Although crystallization occurred quickly, three to five days were optimal for the highest frequency and quality of two-dimensional crystals.

4-3.4. Electron microscopy.

Crystals were imaged in a Tecnai F20 electron microscope (FEI Company, Einhoven, Netherlands) in the Microscopy and Imaging Facility (University of Calgary) or a JEOL 2200FS electron microscope (JEOL Ltd., Tokyo, Japan) in the Electron Microscopy Facility (National Institute for Nanotechnology, University of Alberta and National Research Council of Canada). Both microscopes were operated at 200 kV. A standard room-temperature holder was used for negatively stained samples and a Gatan 626 cryoholder (Gatan Inc., Pleasanton, CA) was used for frozen-hydrated samples. Low-dose images were recorded either on film at 50,000x magnification (Tecnai F20) or image plates at 35,800x magnification (JEOL 2200FS). For film, the best images were digitized at 6.35 μm per pixel with a Nikon Super Coolscan 9000 followed by pixel averaging to achieve a final resolution of 2.54 Å per pixel. The image plates were scanned at 15 μm per pixel for a final resolution of 4.44 Å per pixel. All data were recorded with defocus levels between 0.5 and 2 μm, with an emphasis on low defocus images (0.5 and 1 μm) for the frozen-hydrated samples.

Projection maps were determined using the MRC image processing suite[80]. Two rounds of lattice unbending were performed prior to extracting amplitudes and phases from each image. Data from frozen-hydrated crystals were corrected for the contrast transfer function (CTF) after estimating defocus levels using the program PLTCTFX[81]. Data from negatively stained crystals were not corrected for the CTF. Common phase origins for merging were determined in the $p22_12_1$ plane group using the program ORIGTILT (considering reflections with IQ values <4). For averaging, data were weighted according to the signal-to-noise ratio (IQ) including data with IQ <7, and the corresponding phase residuals represent the inverse cosine of the Figure of Merit (FOM) from this averaging. Projection maps were determined by Fourier synthesis from the averaged data using the CCP4 software suite[82], followed by normalization of density levels to enable comparison of projection maps originating from different SERCA-PLB samples.

4-4. References.

1. Toyoshima C, Nakasako M, Nomura H, Ogawa H. Crystal structure of the calcium pump of sarcoplasmic reticulum at 2.6 angstrom resolution. Nature 2000 JUN 8;405(6787):647-55.

2. Toyoshima C, Nomura H. Structural changes in the calcium pump accompanying the dissociation of calcium. Nature 2002 AUG 8;418(6898):605-11.

3. Toyoshima C, Nomura H, Tsuda T. Lumenal gating mechanism revealed in calcium pump crystal structures with phosphate analogues. Nature 2004 NOV 18;432(7015):361-8.

4. Toyoshima C, Mizutani T. Crystal structure of the calcium pump with a bound ATP analogue. Nature 2004 JUL 29;430(6999):529-35.

5. Sorensen TLM, Moller JV, Nissen P. Phosphoryl transfer and calcium ion occlusion in the calcium pump. Science 2004 JUN 11;304(5677):1672-5.

6. Olesen C, Sorensen TLM, Nielsen RC, Moller JV, Nissen P. Dephosphorylation of the calcium pump coupled to counterion occlusion. Science 2004 DEC 24;306(5705):2251-5.

7. Toyoshima C, Norimatsu Y, Iwasawa S, Tsuda T, Ogawa H. How processing of aspartylphosphate is coupled to lumenal gating of the ion pathway in the calcium pump. Proc Natl Acad Sci U S A 2007 DEC 11;104(50):19831-6.

8. Olesen C, Picard M, Winther AL, Gyrup C, Morth JP, Oxvig C, Moller JV, Nissen P. The structural basis of calcium transport by the calcium pump. Nature 2007 DEC 13;450(7172):1036-U5.

9. Xu C, Rice WJ, He WZ, Stokes DL. A structural model for the catalytic cycle of Ca2+-ATPase. J Mol Biol 2002 FEB 8;316(1):201-11.

10. Stokes D, Green N. 3-dimensional crystals of Ca-ATPase from sarcoplasmic-reticulum - symmetry and molecular packing. Biophys J 1990 JAN;57(1):1-14.

11. Stokes D, Green N. Structure of Ca-ATPase - electron-microscopy of frozen-hydrated crystals at 6 a resolution in projection. J Mol Biol 1990 JUN 5;213(3):529-38.

12. Shi D, Hsiung H, Pace R, Stokes D. Preparation and analysis of large, flat crystals of Ca2+-ATPase for electron crystallography. Biophys J 1995 MAR;68(3):1152-62.

13. Li M, Cornea R, Autry J, Jones L, Thomas D. Phosphorylation-induced structural change in phospholamban and its mutants, detected by intrinsic fluorescence. Biochemistry (N Y) 1998 MAY 26;37(21):7869-77.

14. Ogawa H, Stokes D, Sasabe H, Toyoshima C. Structure of the Ca2+ pump of sarcoplasmic reticulum: A view along the lipid bilayer at 9-angstrom resolution. Biophys J 1998 JUL;75(1):41-52.

15. Cornea RL, Jones LR, Autry JM, Thomas DD. Mutation and phosphorylation change the oligomeric structure of phospholamban in lipid bilayers. Biochemistry (N Y) 1997 MAR 11;36(10):2960-7.

16. Jones L, Simmerman H, Wilson W, Gurd F, Wegener A. Purification and characterization of phospholamban from canine cardiac sarcoplasmic-reticulum. J Biol Chem 1985;260(12):7721-30.

17. Kimura Y, Kurzydlowski K, Tada M, MacLennan DH. Phospholamban inhibitory function is activated by depolymerization. J Biol Chem 1997 JUN 13;272(24):15061-4.

18. Cornea RL, Autry JM, Chen ZH, Jones LR. Reexamination of the role of the leucine/isoleucine zipper residues of phospholamban in inhibition of the Ca2+ pump of cardiac sarcoplasmic reticulum. J Biol Chem 2000 DEC 29;275(52):41487-94.

19. Autry J, Jones L. Functional co-expression of the canine cardiac Ca2+ pump and phospholamban in spodoptera frugiperda (Sf21) cells reveals new insights on ATPase regulation. J Biol Chem 1997 JUN 20;272(25):15872-80.

20. MacLennan DH, Kranias EG. Phospholamban: A crucial regulator of cardiac contractility. Nature Reviews Molecular Cell Biology 2003 JUL;4(7):566-77.

21. Becucci L, Cembran A, Karim CB, Thomas DD, Guidelli R, Gao J, Veglia G. On the function of pentameric phospholamban: Ion channel or storage form? Biophys J 2009 MAY 20;96(10):L60-2.

22. Wegener A, Simmerman H, Lindemann J, Jones L. Phospholamban phosphorylation in intact ventricles - phosphorylation of serine-16 and threonine-17 in response to beta-adrenergic stimulation. J Biol Chem 1989 JUL 5;264(19):11468-74.

23. Catalucci D, Latronico MVG, Ceci M, Rusconi F, Young HS, Gallo P, Santonastasi M, Bellacosa A, Brown JH, Condorelli G. At increases sarcoplasmic reticulum Ca2+ cycling by direct phosphorylation of phospholamban at thr(17). J Biol Chem 2009 OCT 9;284(41):28180-7.

24. Stokes D. Keeping calcium in its place: Ca2+-ATPase and phospholamban. Curr Opin Struct Biol 1997 AUG;7(4):550-6.

25. MacLennan D, Kimura Y, Toyofuku T. Sites of regulatory interaction between calcium ATPases and phospholamban. Cardiac Sarcoplasmic Reticulum Function and Regulation of Contractility 1998;853:31-42.

26. Thomas D, Reddy L, Karim C, Li M, Cornea R, Autry J, Jones L, Stamm J. Direct spectroscopic detection of molecular dynamics and interactions of the calcium pump and phospholamban. Cardiac Sarcoplasmic Reticulum Function and Regulation of Contractility 1998;853:186-94.

27. James P, Inui M, Tada M, Chiesi M, Carafoli E. Nature and site of phospholamban regulation of the Ca-2+ pump of sarcoplasmic-reticulum. Nature 1989 NOV 2;342(6245):90-2.

28. Chen Z, Akin BL, Jones LR. Mechanism of reversal of phospholamban inhibition of the cardiac Ca2+-ATPase by protein kinase a and by anti-phospholamban monoclonal antibody 2D12. J Biol Chem 2007 JUL 20;282(29):20968-76.

29. Asahi M, McKenna E, Kurzydlowski K, Tada M, MacLennan DH. Physical interactions between phospholamban and sarco(endo)plasmic reticulum Ca2+-ATPases are dissociated by elevated Ca2+, but not by phospholamban phosphorylation, vanadate, or thapsigargin, and are enhanced by ATP. J Biol Chem 2000 MAY 19;275(20):15034-8.

30. Negash S, Yao Q, Sun H, Li J, Bigelow D, Squier T. Phospholamban remains associated with the Ca2+- and Mg2+-dependent ATPase following phosphorylation by cAMP-dependent protein kinase. Biochem J 2000 OCT 1;351:195-205.

31. Fowler C, Huggins J, Hall C, Restall C, Chapman D. The effects of calcium, temperature and phospholamban phosphorylation on the dynamics of the calcium-stimulated atpase of canine cardiac sarcoplasmic-reticulum. Biochim Biophys Acta 1989 APR 28;980(3):348-56.

32. Karim CB, Zhang ZW, Howard EC, Torgersen KD, Thomas DD. Phosphorylation-dependent conformational switch in spin-labeled phospholamban bound to SERCA. J Mol Biol 2006 MAY 12;358(4):1032-40.

33. Metcalfe E, Traaseth N, Veglia G. Serine 16 phosphorylation induces an order-to-disorder transition in monomeric phospholamban RID B-4751-2010. Biochemistry (N Y) 2005 MAR 22;44(11):4386-96.

34. Terzi E, Poteur L, Trifilieff E. Evidence for a phosphorylation-induced conformational change in phospholamban cytoplasmic domain by cd analysis. FEBS Lett 1992 SEP 14;309(3):413-6.

35. Mortishire-Smith R, Pitzenberger S, Burke C, Middaugh C, Garsky V, Johnson R. Solution structure of the cytoplasmic domain of phospholamban - phosphorylation leads to a local perturbation in secondary structure. Biochemistry (N Y) 1995 JUN 13;34(23):7603-13.

36. Tatulian S, Jones L, Reddy L, Stokes D, Tamm L. Secondary structure and orientation of phospholamban reconstituted in supported bilayers from polarized attenuated total-reflection ftir spectroscopy. Biochemistry (N Y) 1995 APR 4;34(13):4448-56.

37. Pollesello P, Annila A. Structure of the 1-36 N-terminal fragment of human phospholamban phosphorylated at ser-16 and thr-17. Biophys J 2002 JUL;83(1):484-90.

38. Paterlini M, Thomas D. The alpha-helical propensity of the cytoplasmic domain of phospholamban: A molecular dynamics simulation of the effect of phosphorylation and mutation. Biophys J 2005 MAY;88(5):3243-51.

39. Chu GX, Li L, Sato Y, Harrer JM, Kadambi VJ, Hoit BD, Bers DM, Kranias EG. Pentameric assembly of phospholamban facilitates inhibition of cardiac function in vivo. J Biol Chem 1998 DEC 11;273(50):33674-80.

40. Oxenoid K, Chou JJ. The structure of phospholamban pentamer reveals a channel-like architecture in membranes. Proc Natl Acad Sci U S A 2005 AUG 2;102(31):10870-5.

41. Stokes DL, Pomfret AJ, Rice WJ, Glaves JP, Young HS. Interactions between Ca2+-ATPase and the pentameric form of phospholamban in two-dimensional co-crystals. Biophys J 2006 JUN;90(11):4213-23.

42. Colyer J. Control of the calcium-pump of cardiac sarcoplasmic-reticulum - a specific role for the pentameric structure of phospholamban. Cardiovasc Res 1993 OCT;27(10):1766-71.

43. Robia SL, Campbell KS, Kelly EM, Hou Z, Winters DL, Thomas DD. Forster transfer recovery reveals that phospholamban exchanges slowly from pentamers but rapidly from the SERCA regulatory complex. Circ Res 2007 NOV 26;101(11):1123-9.

44. Kelly EM, Hou Z, Bossuyt J, Bers DM, Robia SL. Phospholamban oligomerization, quaternary structure, and sarco(endo) plasmic reticulum calcium ATPase binding measured by fluorescence resonance energy transfer in living cells. J Biol Chem 2008 MAY 2;283(18):12202-11.

45. Chen ZH, Stokes DL, Jones LR. Role of leucine 31 of phospholamban in structural and functional interactions with the Ca2+ pump of cardiac sarcoplasmic reticulum. J Biol Chem 2005 MAR 18;280(11):10530-9.

46. Chen ZH, Stokes SL, Rice WJ, Jones LR. Spatial and dynamic interactions between phospholamban and the canine cardiac Ca2+ pump revealed with use of heterobifunctional cross-linking agents. J Biol Chem 2003 NOV 28;278(48):48348-56.

47. Toyoshima C, Asahi M, Sugita Y, Khanna R, Tsuda T, MacLennan DH. Modeling of the inhibitory interaction of phospholamban with the Ca2+ ATPase. Proc Natl Acad Sci U S A 2003 JAN 21;100(2):467-72.

48. Morita T, Hussain D, Asahi M, Tsuda T, Kurzydlowski K, Toyoshima C, MacLennan DH. Interaction sites among phospholamban, sarcolipin, and the sarco(endo)plasmic reticulum Ca2+-ATPase. Biochem Biophys Res Commun 2008 APR 25;369(1):188-94.

49. Chen Z, Akin B, Stokes D, Jones L. Cross-linking of C-terminal residues of phospholamban to the Ca2+ pump of cardiac sarcoplasmic reticulum to probe spatial and functional interactions within the transmembrane domain. J Biol Chem 2006 MAY 19;281(20):14163-72.

50. Trieber CA, Douglas JL, Afara M, Young HS. The effects of mutation on the regulatory properties of phospholamban in co-reconstituted membranes. Biochemistry (N Y) 2005 MAR 8;44(9):3289-97.

51. Reddy L, Jones L, Cala S, OBrian J, Tatulian S, Stokes D. Functional reconstitution of recombinant phospholamban with rabbit skeletal Ca2+-atpase. J Biol Chem 1995 APR 21;270(16):9390-7.

52. Young HS, Jones LR, Stokes DL. Locating phospholamban in co-crystals with Ca2+-ATPase by cryoelectron microscopy. Biophys J 2001 AUG;81(2):884-94.

53. Young H, Reddy L, Jones L, Stokes D. Co-reconstitution and co-crystallization of phospholamban and Ca2+-ATPase. Cardiac Sarcoplasmic Reticulum Function and Regulation of Contractility 1998;853:103-15.

54. Kimura Y, Asahi M, Kurzydlowski K, Tada M, MacLennan DH. Phospholamban domain ib mutations influence functional interactions with the Ca2+-ATPase isoform of cardiac sarcoplasmic reticulum. J Biol Chem 1998 JUN 5;273(23):14238-41.

55. Reddy L, Cornea R, Winters D, McKenna E, Thomas D. Defining the molecular components of calcium transport regulation in a reconstituted membrane system. Biochemistry (N Y) 2003 APR 22;42(15):4585-92.

56. Toyofuku T, Kurzydlowski K, Tada M, Maclennan DH. Amino-acids glu(2) to ile(18) in the cytoplasmic domain of phospholamban are essential for functional association with the Ca2+-atpase of sarcoplasmic-reticulum. J Biol Chem 1994 JAN 28;269(4):3088-94.

57. Robia SL, Flohr NC, Thomas DD. Phospholamban pentamer quaternary conformation determined by in-gel fluorescence anisotropy. Biochemistry (N Y) 2005 MAR 22;44(11):4302-11.

58. Traaseth NJ, Verardi R, Torgersen KD, Karim CB, Thomas DD, Veglia G. Spectroscopic validation of the pentameric structure of phospholarnban. Proc Natl Acad Sci U S A 2007 SEP 11;104(37):14676-81.

59. Auer M, Scarborough GA, Kuhlbrandt W. Three-dimensional map of the plasma membrane H+-ATPase in the open conformation. Nature 1998 APR 23;392(6678):840-3.

60. Seidel K, Andronesi OC, Krebs J, Griesinger C, Young HS, Becker S, Baldus M. Structural characterization of Ca2+-ATPase-bound phospholarnban in lipid bilayers by solid-state nuclear magnetic resonance (NMR) spectroscopy. Biochemistry (N Y) 2008 APR 15;47(15):4369-76.

61. Hutter M, Krebs J, Meiler J, Griesinger C, Carafoli E, Helms V. A structural model of the complex formed by phospholamban and the calcium pump of sarcoplasmic reticulum obtained by molecular mechanics. Chembiochem 2002 DEC 2;3(12):1200-8.

62. Fujii J, Maruyama K, Tada M, Maclennan DH. Expression and site-specific mutagenesis of phospholamban - studies of residues involved in phosphorylation and pentamer formation. J Biol Chem 1989 AUG 5;264(22):12950-5.

63. Reddy LG, Jones LR, Thomas DD. Depolymerization of phospholamban in the presence of calcium pump: A fluorescence energy transfer study. Biochemistry (N Y) 1999 MAR 30;38(13):3954-62.

64. Hou Z, Kelly EM, Robia SL. Phosphomimetic mutations increase phospholamban oligomerization and alter the structure of its regulatory complex. J Biol Chem 2008 OCT 24;283(43):28996-9003.

65. Chu S, Abu-Baker S, Lu J, Lorigan GA. N-15 solid-state NMR spectroscopic studies on phospholamban at its phosphorylated form at ser-16 in aligned phospholipid bilayers. Biochimica Et Biophysica Acta-Biomembranes 2010 MAR;1798(3):312-7.

66. Traaseth NJ, Thomas DD, Veglia G. Effects of Ser16 phosphorylation on the allosteric transitions of phospholamban/Ca2+-ATPase complex. J Mol Biol 2006 MAY 12;358(4):1041-50.

67. Lamberth S, Schmid H, Muenchbach M, Vorherr T, Krebs J, Carafoli E, Griesinger C. NMR solution structure of phospholamban. Helv Chim Acta 2000;83(9):2141-52.

68. Zamoon J, Mascioni A, Thomas DD, Veglia G. NMR solution structure and topological orientation of monomeric phospholamban in dodecylphosphocholine micelles. Biophys J 2003 OCT;85(4):2589-98.

69. Andronesi O, Becker S, Seidel K, Heise H, Young H, Baldus M. Determination of membrane protein structure and dynamics by magic-angle-spinning solid-state NMR spectroscopy RID A-7703-2010 RID C-2737-2009. J Am Chem Soc 2005 SEP 21;127(37):12965-74.

70. Potluri S, Yan AK, Chou JJ, Donald BR, Bailey-Kellogg C. Structure determination of symmetric homo-oligomers by a complete search of symmetry configuration space, using NMR restraints and van der waals packing. Proteins-Structure Function and Bioinformatics 2006 OCT 1;65(1):203-19.

71. Traaseth NJ, Shi L, Verardi R, Mullen DG, Barany G, Veglia G. Structure and topology of monomeric phospholamban in lipid membranes determined by a hybrid solution and solid-state NMR approach RID B-4751-2010. Proc Natl Acad Sci U S A 2009 JUN 23;106(25):10165-70.

72. Oxenoid K, Rice AJ, Chou JJ. Comparing the structure and dynamics of phospholamban pentamer in its unphosphorylated and pseudo-phosphorylated states. Protein Science 2007 SEP;16(9):1977-83.

73. Pollesello P, Annila A, Ovaska M. Structure of the 1-36 amino-terminal fragment of human phospholamban by nuclear magnetic resonance and modeling of the phospholamban pentamer. Biophys J 1999 APR;76(4):1784-95.

74. Simmerman HKB, Kobayashi YM, Autry JM, Jones LR. A leucine zipper stabilizes the pentameric membrane domain of phospholamban and forms a coiled-coil pore structure. J Biol Chem 1996 MAR 8;271(10):5941-6.

75. Warren GB, Toon PA, Birdsall NJ, Lee AG, Metcalfe JC. Reconstitution of a calcium-pump using defined membrane components. Proc Natl Acad Sci U S A 1974;71(3):622-6.

76. Eletr S, Inesi G. Phospholipid orientation in sarcoplasmic membranes - spin-label esr and proton nmr studies. Biochim Biophys Acta 1972;282(SEP1):174,&.

77. Douglas JL, Trieber CA, Afara M, Young HS. Rapid, high-yield expression and purification of Ca2+-ATPase regulatory proteins for high-resolution structural studies. Protein Expr Purif 2005 MAR;40(1):118-25.

78. Reddy L, Jones L, Pace R, Stokes D. Purified, reconstituted cardiac Ca2+-ATPase is regulated by phospholamban but not by direct phosphorylation with Ca2+/calmodulin-dependent protein kinase. J Biol Chem 1996 JUN 21;271(25):14964-70.

79. Dux L, Martonosi A. Two-dimensional arrays of proteins in sarcoplasmic-reticulum and purified Ca-2+-ATPase vesicles treated with vanadate. J Biol Chem 1983;258(4):2599-603.

80. Crowther RA, Henderson R, Smith JM. MRC image processing programs. J Struct Biol 1996 JAN-FEB;116(1):9-16.

81. Toyoshima C, Yonekura K, Sasabe H. Contrast transfer for frozen-hydrated specimens .2. amplitude contrast at very low-frequencies. Ultramicroscopy 1993 JAN;48(1-2):165-76.

82. Potterton E, McNicholas S, Krissinel E, Cowtan K, Noble M. The CCP4 molecular-graphics project. Acta Crystallographica Section D-Biological Crystallography 2002 NOV;58:1955-7.

Chapter 5.

Direct observation of SLN pentamers interacting with SERCA in two-dimensional crystals.

"Direct structural information has so far been limited because the crystals that had been obtained were useful only for electron microscopy."

-Chikashi Toyoshima et al. Nature 2000

Acknowledgements: J. Douglas cloned the human SLN gene and generated the MBP-SLN expression plasmid. Dr. C. Trieber purified SERCA for the co-reconstitutions. Images were recorded by Dr. H. Young and J.P. Glaves.

Chapter 5. Direct observation of SLN pentamers interacting with SERCA in two-dimensional crystals.

5-1. Introduction.

Activity of the sarco(endo)plasmic reticulum Ca^{2+}-ATPase (SERCA) is central to replenishing intracellular calcium (Ca^{2+}) stores following Ca^{2+} release and contraction in muscle cells. SERCA transports two cytoplasmic Ca^{2+} ions into the sarcoplasmic reticulum in exchange for two to three luminal protons. We currently have an excellent structural understanding of the SERCA transport cycle from high-resolution x-ray crystal structures, including seven different transport intermediates and three different SERCA-inhibitor complexes[1-9]. SERCA consists of three cytoplasmic domains (the nucleotide-binding, phosphorylation and actuator domains) connected by a two-helix stalk to a ten-helix transmembrane domain. ATP-binding and phosphoryl-transfer are mediated by the cytoplasmic domains, and the associated conformational changes are coupled to changes in the Ca^{2+} binding sites located in the transmembrane domain. Structures of SERCA in complex with small molecule inhibitors suggest the transport cycle can be inhibited using a variety of mechanisms[2, 6, 9].

Physiologically, SERCA activity is regulated by differential expression of SERCA isoforms and interactions between SERCA and small inhibitory transmembrane peptides. The SERCA2a isoform is predominantly expressed in cardiac muscle and is regulated by the expression of phospholamban (PLB), a 52 amino-acid transmembrane peptide that binds SERCA and lowers its apparent Ca^{2+} affinity. In fast-twitch skeletal muscle, SERCA1a is predominantly expressed and is regulated by the co-expression of sarcolipin (SLN), a 31 amino-acid transmembrane homolog of PLB. Although SLN has a much shorter cytoplasmic domain, PLB and SLN have homologous transmembrane domains with over 38% sequence identity between residues 29 to 49 of PLB and 6 to 26 of SLN[10]. With the exception that SLN reduces the apparent Ca^{2+} affinity to a lesser extent, SLN is thought to interact and inhibit SERCA in a similar manner as PLB[11]. The high degree of homology and similar inhibitory properties suggest PLB and SLN might use related

mechanisms to regulate SERCA, and potentially use overlapping sites of interaction[12, 13]. In support of these hypotheses, truncated variants of PLB, designed to mimic the transmembrane domain alone, are sufficient to inhibit SERCA with full-length PLB-like activity, albeit to a lesser extent[14-17].

Recently, we have shown that PLB pentamers interact with SERCA in two-dimensional (2D) co-crystals[18, 19]. The observed interaction was dependent on the functional state of PLB suggesting that binding of PLB pentamers is an active intermediate in the regulation of SERCA[19]. Given the similar inhibitory properties of SLN, and observations that SLN can form oligomers[16], we set out to determine if SLN could support co-crystallization with SERCA. Herein, we report a projection map to 8.4 Å resolution from 2D co-crystals of SERCA and SLN. The co-crystals contain ribbons of SERCA arranged in characteristic dimers, bordered by densities consistent with an oligomer of SLN. Temperature-factor sharpening of the projection maps revealed a five-lobed density for SLN supporting the oligomeric state of SLN as a pentamer in the crystal lattice. SLN pentamers interact with transmembrane helix 3 (TM3) of SERCA in a spatially-similar manner as the interaction between PLB pentamers and SERCA. However, an additional density in the projection map suggested the interaction of the SLN pentamer with SERCA may be mediated by a SLN monomer. The interaction of SERCA with pentameric SLN could be a common regulatory mechanism, shared with pentameric PLB, to deliver or remove inhibitory monomers from the enzyme.

5-2. Results and Discussion.

5-2.1 Reconstituted SLN inhibits SERCA in proteoliposomes.

SLN inhibits SERCA in our purified co-reconstitution system; the apparent Ca^{2+} affinity of SERCA is reduced from 0.39 μM in the absence of SLN to 0.72 μM in the presence of SLN (Figure 5.1). The observed inhibitory activity for SLN is consistent with earlier SLN and SERCA co-reconstitution studies[16, 20, 21] as well as SLN and SERCA heterologous co-expression studies[11, 22, 23].

We identified a novel gain-of-function mutant, SLN-Asn^{4}Ala, which reduces the apparent Ca^{2+} affinity of SERCA to 1.20 μM (Figure 5.1). Asparagine at position 4 in human SLN aligns with lysine at position 27 in human PLB. The mutation K27A in PLB also results in a gain-of-function[24].

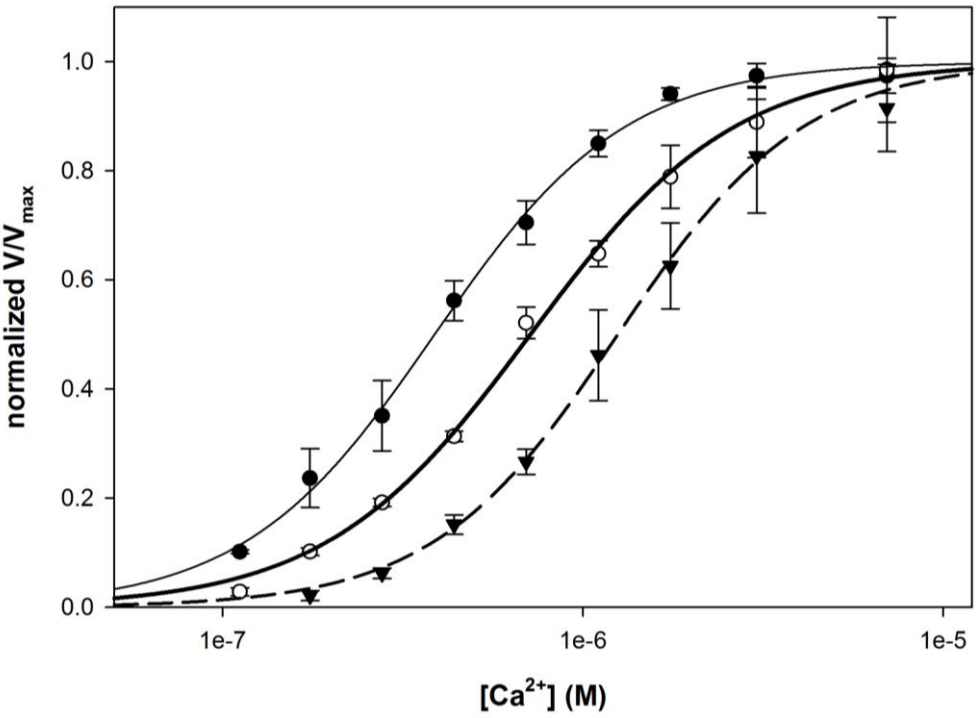

Figure 5.1. Ca^{2+}-dependent ATPase activity of SERCA co-reconstituted with recombinant SLN. ATPase activity of SERCA reconstituted in the absence (*gray line*) and in the presence of wild-type SLN (*solid black line*) and in the presence of SLN-Asn^{4}Ala (*dashed line*). The apparent Ca^{2+} affinity of SERCA is reduced by wild-type SLN from 0.39 μM to 0.72 μM. The gain-of-function mutant SLN-Asn^{4}Ala reduced the apparent Ca^{2+} affinity to 1.20 μM. All curves have been normalized to the maximal activity of SERCA control samples (in the absence of SLN).

5-2.2. Oligomers of SLN observed by glutaraldehyde cross-linking.

Detergent-solubilized SLN cross-links to itself in the presence of glutaraldehyde. Similar to earlier reports[16], the oligomerization of sarcolipin was concentration dependent with dimers of SLN visible at concentrations of 20 μM and above (Figure 5.2a). At higher concentrations, larger oligomeric assemblies such as SLN trimers are readily apparent by Western blot (Figure 5.2a), but only faintly observed in coomassie stained gels (Figure 5.2b).

5-2.3. Oligomers of SLN interact with SERCA in two-dimensional crystals.

We have studied the interaction between SERCA and SLN using cryo-electron microscopy of large two-dimensional crystals based on the co-crystallization of SERCA and PLB[18, 19]. Crystals were screened by negative-stain electron microscopy to identify samples suitable for freezing (Figure 5.3). Successful crystal trials were plunge-frozen in liquid ethane and imaged in the frozen-hydrated state. Similar to SERCA and PLB, the SERCA and SLN co-crystals are comprised of anti-parallel dimer ribbons of SERCA packed into a two-dimensional lattice with $p22_12_1$ symmetry (Table 1; Figure 5.4a). The 347 Å by 71 Å unit cell of SERCA-SLN co-crystals is almost identical to the 345 Å by 70 Å unit cell of SERCA-PLB co-crystals[19] (Table 5.1).

In crystals of SERCA and PLB, pentamers of PLB were found interspersed between SERCA dimer ribbons. In crystals of SERCA and SLN, a density consistent with an oligomer of SLN is observed in a similar location between SERCA dimer ribbons (Figure 5.4a). The relative size and position of the SLN oligomer density was not affected by co-crystals grown with the gain-of-function mutant SLN-Asn^{4}Ala (Figure 5.4b). However, the frequency of crystals was dramatically increased in co-crystals of SERCA with SLN-Asn^{4}Ala. An increase in co-crystals frequency was also observed for a second gain-of-function SLN mutant, Thr5Ala (the apparent Ca^{2+} affinity of SERCA is reduced from 0.39 μM to 0.90 μM). The correlation between increased co-crystallization and SLN gain-of-function parallels the co-crystallization behaviour of SERCA and PLB gain-of-function mutants, including PLB-Ile^{40}Ala and the (Asn^{4}Ala) homologous gain-of-function PLB-Lys^{27}Ala mutation[18, 19].

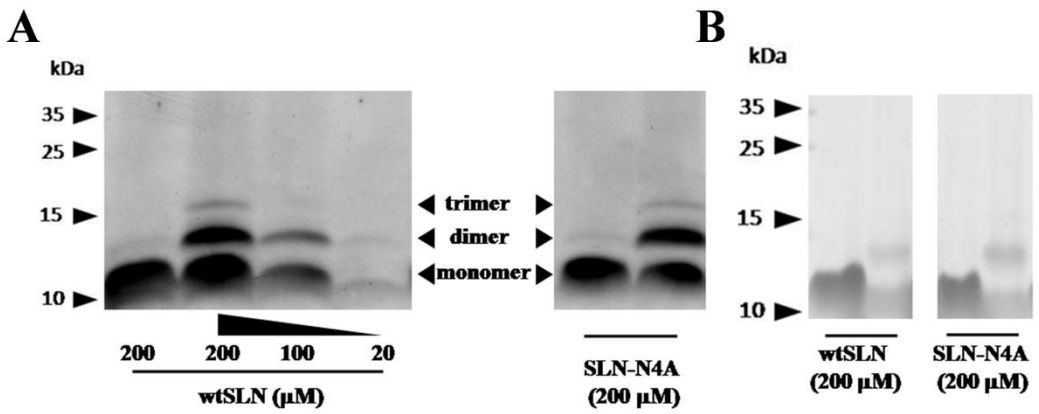

Figure 5.2. Glutaraldehyde cross-linking of recombinant SLN in detergent. Glutaraldehyde cross-linking of SLN was concentration dependent with dimers observed at 20 μM. **Panel A,** Western blot analysis of wild-type SLN and SLN-Asn^{4}Ala cross-linking reactions. The cross-linking profile of wild-type SLN and the gain-of-function mutant SLN-Asn^{4}Ala are identical at 200 μM. SLN dimers are faintly observed at 200 μM in the absence of glutaraldehyde. **Panel B,** Coomassie stained tris-tricine SDS-PAGE of SLN cross-linking reactions at 200 μM.

Table 5.1. Summary of crystallographic data for frozen-hydrated SLN co-crystals.

	Wild-type SLN	Asn^4Ala -SLN
Number of images	34	5
Cell parameters	a = 346.8 Å	a = 350.2 Å
	b = 70.5 Å	b = 70.5 Å
	$\gamma = 90.2°$	$\gamma = 90.4°$
Weighted phase residual	14.8°	20.4°

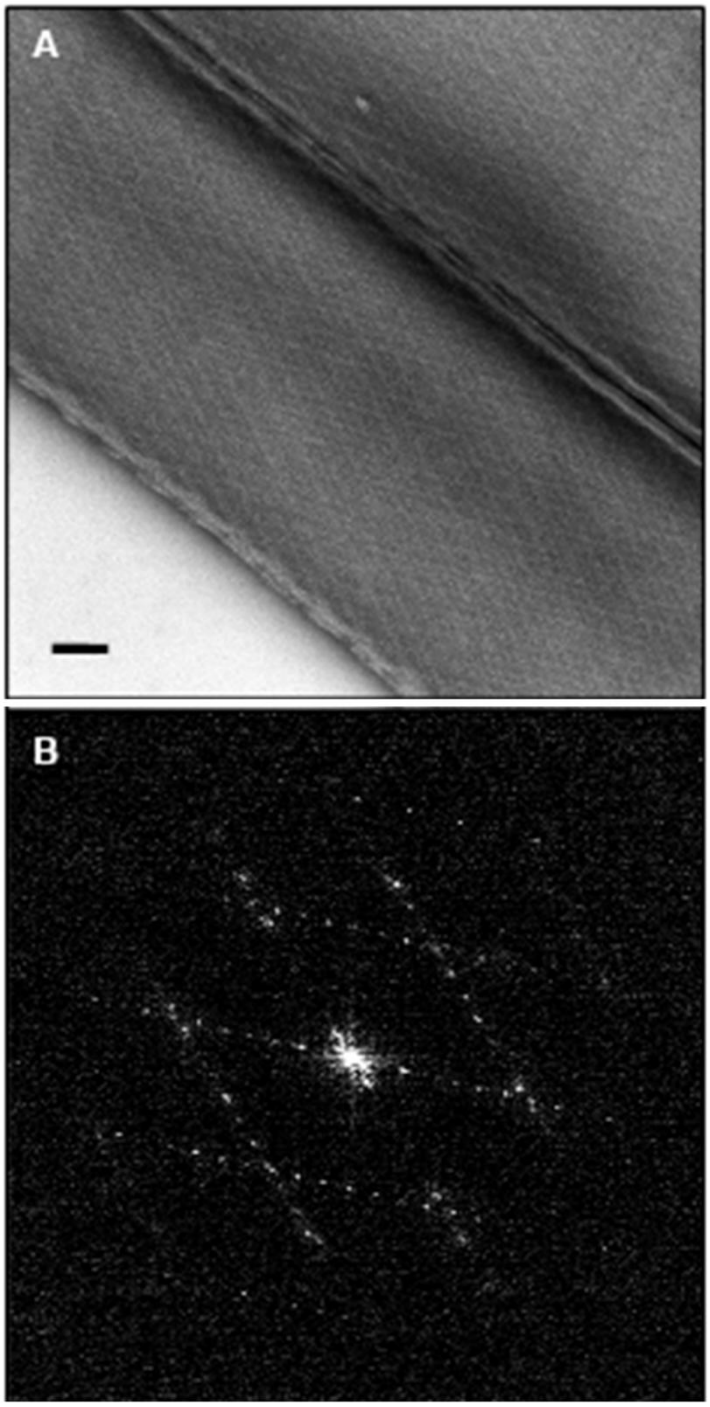

Figure 5.3. Negatively stained co-crystals of SERCA and wild-type SLN. Panel A, A high magnification image of two flattened tubular crystals lying side-by-side. The criss-cross appearance of each crystal is due to the projection of the two independent lattices from the near and far sides of the tube. Crystals were stained with 2% uranyl acetate. **Panel B**, The computed Fourier transform of a single crystal reveals the two independent lattices. The scale bar in panel A corresponds to 0.1 μm. In panel B, the corners of the diffraction pattern correspond to18 Å resolution.

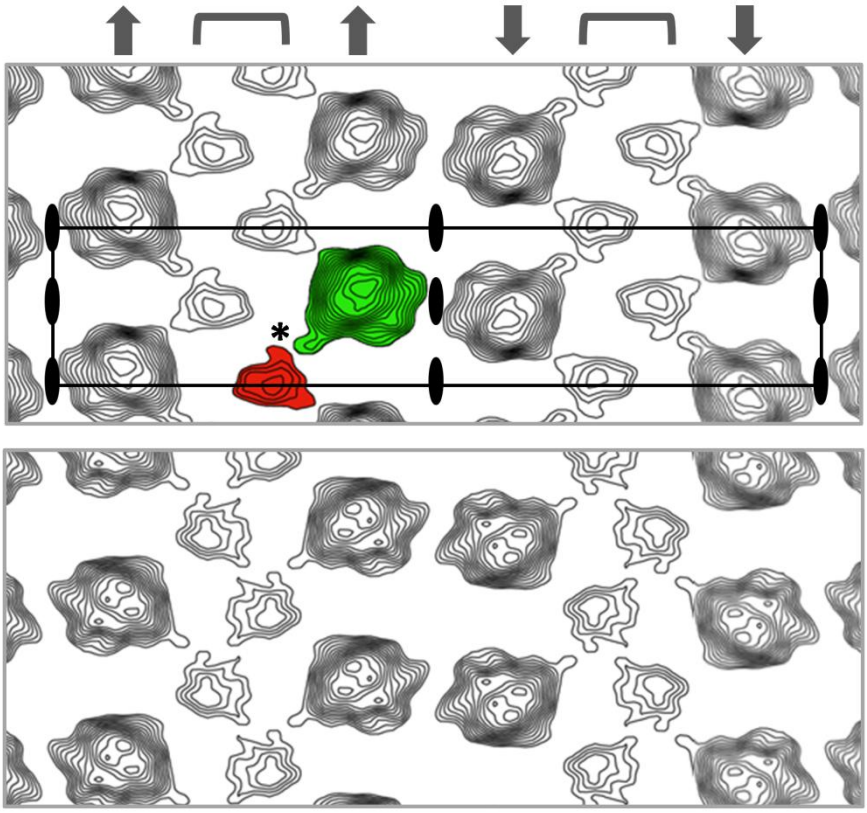

Figure 5.4. Projection maps from frozen-hydrated SERCA and SLN crystals at 10 Å resolution. Panel A, Projection map from co-crystals of SERCA and wild-type SLN with a single unit cell (a = 347 Å, b = 71 Å) and p2 symmetry operators indicated for the $p22_12_1$ plane group. The region of the map shown is approximately 400 Å by 150 Å. For clarity, only positive contours are shown. The relative locations and orientations of SERCA molecules are indicated by *arrows*, and the locations of the SLN densities are indicated by *brackets*. One proposed site of interaction between SLN oligomers (*red background*) and SERCA (*green background*) TM3 is indicated by an asterisk (*****). **Panel B,** Projection map from co-crystals of SERCA and the gain-of-function mutant SLN-Asn^4Ala. For clarity, only positive contours are shown.

From our 10 Å projection maps it was unclear how many SLN molecules were present in the oligomer density. To address this issue, we calculated higher resolution projection maps to 8.4 Å and applied a negative B-factor (or temperature factor) of 500 $Å^2$ during Fourier synthesis (Figure 5.5). The truncation of Fourier data at 8.4 Å resolution ensured minimal contribution from noise in our maps (Figure 5.5a). Temperature factor sharpening, used to enhance densities in projection maps[25], improved contrast and detail for the densities associated with both SERCA and SLN. In these projection maps, the SLN oligomer is observed as a five-lobed density that is most consistent with a pentamer of SLN (Figure 5.5b). Similar to wild-type SLN, the density for SLN-Asn^{4}Ala was also consistent with a pentamer following temperature-factor sharpening (data not shown).

5-2.4. Oligomers of recombinant SLN are consistent with previous synthetic SLN experiments.

Our cross-linking data clearly demonstrate the ability of recombinant SLN to form oligomers. The observed concentration-dependence was consistent with reports of synthetic SLN oligomers in detergent and lipid environments[16]. We attribute the observation of trimers as the largest SLN oligomer to a number of factors dependent on our cross-linking scheme. Two major contributing factors are the instability of SLN in SDS-PAGE and the limited number of amines present in the sequence of SLN available for glutaraldehyde cross-linking. The demonstration of SLN pentamers and higher oligomeric species has been convincingly shown using synthetic SLN in sedimentation equilibrium and hetero-bifunctional cross-linking experiments[16].

5-2.5. SLN pentamers bind to SERCA in a similar manner as PLB pentamers.

Our crystallographic data support a specific interaction between SLN pentamers and SERCA. The site of this interaction is very similar to that between PLB pentamers and TM3 of SERCA[18, 19]. The overall similarity suggests pentameric species of PLB and SLN interact with SERCA at a common site. We propose that, like PLB[19], the interaction of SLN pentamers with SERCA represents an active intermediate in the regulation of SERCA. This is supported by the observation that, compared to wild-type SLN, the gain-of-function mutant SLN-Asn^{4}Ala dramatically enhances co-crystallization with SERCA. Our current view is that oligomeric interactions with SERCA, centered on TM3,

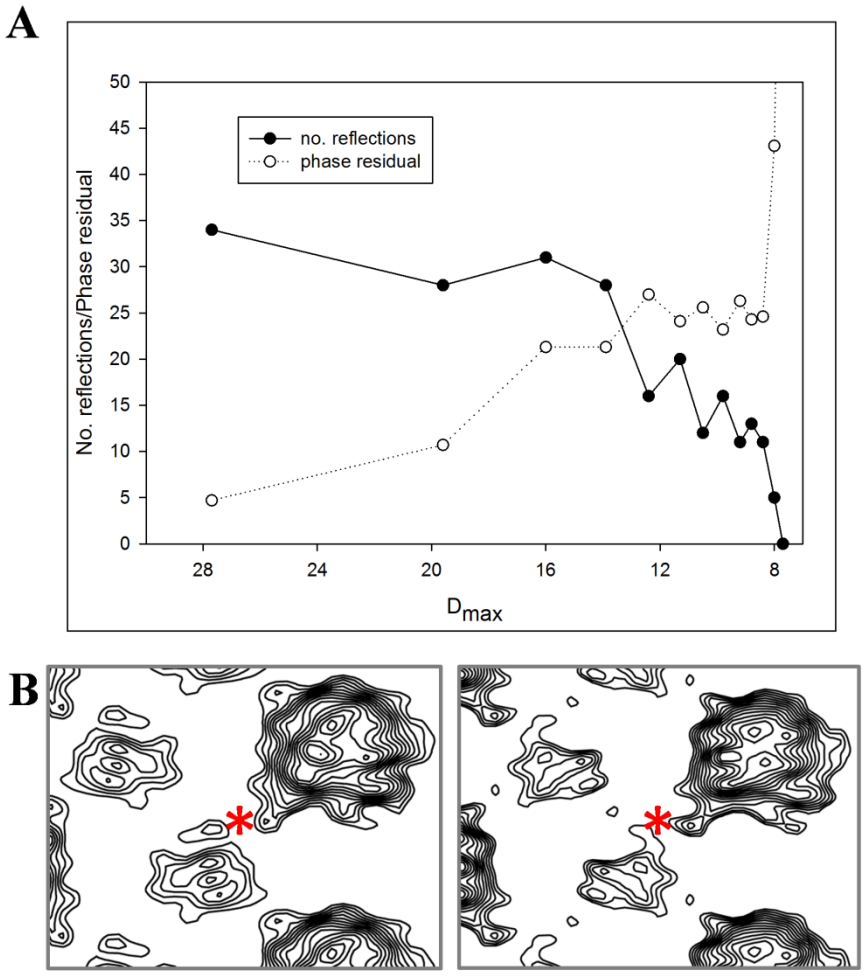

Figure 5.5. SLN pentamers are consistent with temperature-factor sharpened projection maps at 8.4 Å resolution. Panel A, Statistics for the merging of 34 images indicate that phase residuals are <26° to a resolution of 8.4 Å. **Panel B,** Temperature factor sharpened projection maps displays lobed SLN densities consistent with SLN pentamers. Projection maps were recalculated with an applied negative temperature factor (B-factor) of 500 A^2. Projection maps calculated from randomly merged co-crystal images (*left* panel) were similar to projection maps from the best co-crystal images (*right* panel). The interaction between TM3 and SLN (red asterisks) is different between than the interaction observed in SERCA and PLB co-crystals (see text for discussion).

influence the delivery or removal of inhibitory PLB or SLN monomers to their proposed binding pocket located on the opposite face of SERCA.

However, it is also interesting to note the differences between SLN and PLB projection maps from cryo-electron microscopy of co-crystals with SERCA. One difference occurs near the TM3 interaction site; the SLN projection maps show a stronger density between TM3 and the SLN pentamer (see the asterisk in Figure 5.4) than that observed between TM3 and PLB pentamers[19]. In the temperature-factor sharpened maps of SERCA and SLN, this additional density near TM3 could be attributed to a conformational change involving TM3 or it could be a SLN monomer moving between the SLN oligomer and SERCA. Thus, we could have trapped an intermediate in the delivery (or removal) of a SLN monomer to (from) SERCA. Interestingly, in previous cross-linking studies SLN was observed to form hexamers and higher-order species, whereas a PLB variant was limited to pentamers for its oligomeric size[16].

5-2.6. Transmembrane helix 3 of SERCA could serve as a docking site for SLN channels.

With respect to SLN, our identified interaction site between SERCA and SLN pentamers could have further implications. However, evidence is emerging that SLN has channel-like activity; SLN reconstituted in tethered bilayer lipid membranes demonstrated channel-like activity selective for small inorganic anions[26, 27] and a regulatory role for SLN channels was proposed involving SLN channels coming into close proximity to SERCA[26]. The authors propose the SLN channels might interact with SERCA using a binding site involving TM2, TM4, TM6, and TM9[26]. In our co-crystals, an oligomer of SLN would be physically excluded from this mode of binding as a result of crystal contacts between SERCA dimers. Not to exclude the earlier suggested binding site for SLN channels, our co-crystals point to an additional binding site for SLN oligomers at SERCA TM3. It would appear to us that the interaction of SLN pentamers with SERCA at TM3 would fulfill the proximity requirements for this hypothesis as well[26].

It is still very much debated whether PLB pentamers have channel-like activity. With this in mind, the same group that reported SLN activity did not observe channel-like activity using PLB under similar experimental conditions[28]. Thus, these results highlight a potential divergence in the regulatory mechanisms of SLN and PLB, if the channel-like activity can affect SERCA activity as proposed[26]. Unlike PLB, which has been observed

to oligomerize in the cell membrane[29, 30], it remains unclear if SLN behaves in a similar manner.

5-3. Materials and Methods.

5-3.1. Materials.

The following reagents were of the highest purity available: octaethylene glycol monododecyl ether ($C_{12}E_8$; Barnet Products, Englewood Cliff, NJ); egg yolk phosphatidylcholine (EYPC), phosphatidylethanolamine (EYPE) and phosphatidic acid (EYPA) (Avanti Polar Lipids, Alabaster, AL); reagents used in the coupled enzyme assay (Sigma-Aldrich, Oakville, ON Canada).

5-3.2. Expression and purification of recombinant SLN.

The wild-type SLN construct with a Gly-Ser-His_8 N-terminal extension was generated previously in our laboratory and inserted into the pMal-c2x plasmid[31]. Site-directed mutants of SLN were generated directly by PCR. Products were then cloned into the pMal-SLN plasmid with *Bam*HI and *Eco*RI, replacing the wild-type gene. All mutations were confirmed by DNA sequencing.

Recombinant SLN was expressed and purified as previously described[31] with an additional organic extraction step. *Escherichia coli* DH5α cells were transformed with MBP-SLN fusion expression plasmids. A 50 mL culture of LB growth media with 100 μg/mL ampicillin was inoculated with a single colony and incubated overnight at 37°C with shaking. The overnight culture was diluted into 1 L of minimal M9 media with 100 μg/mL ampicillin and grown at 37°C until OD_{600} ~0.6 (about 2-3 h). The incubation temperature was reduced to 22°C and following equilibration, expression of MBP-SLN was induced with 1 mM IPTG. Cells were harvested at 4°C after 48 h of induction and washed with 50 mM Tris HCl buffer (pH 8.0). Cell pellets were stored at -20°C.

Cell pellets from 1 L of culture were resuspended in 50 mL lysis buffer (20 mM phosphate, pH 8.0, 120 mM NaCl, 1 mM EDTA, 0.5% glycerol, 0.5% Triton X-100, 0.1 mM dithiothreitol). The resuspension was sonicated in a Branson digital sonifier 250 (Branson Ultrasonics, Danbury, CT, USA). The sonicated suspension was centrifuged at 50,000g for 25 min at 4°C in a Beckman Ti-45 rotor. The supernatant containing MBP-SLN fusion protein was subjected to amylose-affinity chromatography column. The column was washed with 5 column volumes of equilibration buffer (20 mM phosphate,

pH 8.0, 120 mM NaCl, 1 mM EDTA, and 0.02% azide). The MBP-SLN fusion protein was eluted with equilibration buffer containing 40 mM maltose. The purified MBP-SLN fusion protein was cleaved with AcTEV protease at 10U/mg with 1 mM dithiothreitol for 24 h in a 16°C water bath. A second addition of AcTEV protease was added with fresh dithiothreitol and incubated for an additional 24 h.

Following protease digestion of the maltose-binding protein and SLN fusion protein, trichloroacetic acid was added to a final concentration of 1% (check value). This mixture was incubated on ice for 20 minutes. The precipitate was collected by centrifugation at 4°C and subsequently homogenized in a mixture of chloroform : isopropanol : water (4 : 4 : 1) and incubated at room temperature for 3 hours. The organic phase, highly enriched in recombinant SLN, was removed, dried to a thin film under nitrogen gas and resuspended in 7 M GdnHCl. The addition of the organic extraction step to the purification of recombinant SLN was inspired by purifications of proteolipid from rabbit skeletal muscle[32, 33].

The extracted SLN in 7 M GdnHCl was centrifuged at 10,000g for 20 min at 4°C in a C0650 rotor to eliminate insoluble material. Reverse-phase HPLC was performed as described[31]. Solvent A was HPLC-grade distilled water and solvent B was HPLC-grade isopropanol with 0.05% TFA. The 7 M GdnHCl supernatant was applied to a Zorbax 300 SB-C8 column with a Zorbax C3 guard column (Agilent Technologies, Palo Alto, CA, USA) equilibrated at 20% solvent B. A gradient was run from 20% to 80% solvent B. Fractions were collected and analyzed by mass spectrometry and SDS-PAGE. Fractions containing pure SLN were combined and the protein concentration determined by the amido black protein assay. Aliquots of 75 μg were dried by speed-vac, lyophilized to dryness and stored at -80°C.

5-3.3. Co-reconstitution of SLN with SERCA.

Lyophilized SLN (75 μg) was resuspended in a 75 μL mixture of chloroform : trifluroethanol (2 : 1) and mixed with lipids (360 μg EYPC; 40 μg EYPA) from stock chloroform solutions. The peptide-lipid mixture was dried to a thin film under nitrogen gas and dried under vacuum overnight. The peptide-lipid mixture was hydrated in buffer (20 mM imidazole pH 7.0; 100 mM KCl; 0.02% NaN_3) at 37 °C for 10 min, cooled to room temperature, and detergent-solubilised by the addition of $C_{12}E_8$ (0.2 % final concentration) and vigorous vortexing. Detergent-solubilized SERCA was added (300

μg in a total volume of 200 μL) and the reconstitution was stirred gently at room temperature. Detergent was slowly removed by the addition of SM-2 biobeads (Bio-Rad, Hercules, CA) over a 4-hour time course (final ratio of 25 biobeads: 1 detergent w/w). Following detergent removal, the reconstitution was centrifuged over a sucrose-gradient for 1 h at 100,000g. The resultant layer of reconstituted proteoliposomes was removed, flash-frozen in liquid-nitrogen and stored at -80 °C. The final approximate molar ratios were 120 lipid : 5 SLN : 1 SERCA[24].

5-3.4. ATPase activity assays of SERCA reconstitutions.

ATPase activity of the co-reconstituted proteoliposomes was measured by a coupled-enzyme assay over a 0.1 μM to 10 μM range of Ca^{2+} concentrations[24, 34]. The K_{ca} (apparent Ca^{2+} affinity) was determined by fitting the data to the Hill equation (Sigma Plot software, SPSS Inc., Chicago, IL). Errors were calculated as the standard error of the mean for a minimum of three independent reconstitutions.

5-3.5. Glutaraldehyde cross-linking of recombinant SLN.

SLN was hydrated in water at 37 °C for 10 min, cooled to room temperature, and detergent-solubilised by the addition of $C_{12}E_8$ (0.75 % final concentration) followed by vigorous vortexing. Buffer was then added to a final concentration of 15 mM and the samples were cross-linked by the addition of glutaraldehyde to a final concentration of 0.05%. The cross-linking reaction was stopped after 5 min with tris-containing loading buffer and separated by tris-tricine SDS-PAGE[35].

Western blotting of SLN cross-linking reactions. Protein was transferred to PVDF membrane at 100 V (350 mAmp) for 1 hour. Washed with TBS before blocking, the membrane was blocked in 0.5 % skim milk TBS, washed three times with TBST (0.1% Tween 20), probed with anti-His HRP conjugate (1/5000 dilution; Qiagen), washed three times with TBST, and incubated for 5 min with Western Lightning® enhanced chemiluminescence reagents (Perkin Elmer).

5-3.6. Crystallization of SLN with SERCA.

SLN and SERCA were co-reconstituted in the presence of EYPE (final lipid ratio of 8 EYPC : 1 EYPA : 1 EYPE) to promote vesicle fusion and crystallization[18, 19]. Co-reconstituted proteoliposomes were collected by centrifugation in crystallization buffer (20 mM imidazole pH 7.0, 100 mM KCl, 35 mM $MgCl_2$, 0.5 mM EGTA, 0.25 mM Na_3VO_4, 30 μM thapsigargin). The samples were subjected to four freeze-thaw cycles, followed by incubation at 4°C for up to one week. Three to five days were optimal for the highest frequency and quality of two-dimensional crystals.

For initial screening of crystals by negative stain, crystals were adsorbed to carbon-coated grids and stained with 2% uranyl acetate. The grids were blotted with filter paper and air-dried.

5-3.7 Electron microscopy of frozen hydrated SERCA and SLN co-crystals.

Crystals were imaged in a Tecnai F20 electron microscope (FEI Company, Einhoven, Netherlands) at the Microscopy and Imaging Facility (University of Calgary) using a Gatan cryoholder (Gatan Inc., Pleasanton, CA). The microscope was operated at 200 kV and low-dose images were recorded at a magnification of 50,000x. The best films were digitized at 6.35 μm/pixel with a Nikon Super Coolscan 9000 followed by pixel averaging to achieve a final resolution of 2.54 Å/pixel. All data were recorded with defocus levels of 0.5-2 μm with an emphasis on low-defocus images (0.5 and 1.0 μm).

5-3.8. Data processing.

The MRC image processing suite was used for images of frozen-hydrated SERCA-SLN crystals[36]. Two rounds of unbending were performed prior to extracting amplitudes and phases from each image. Data was then corrected for the contrast transfer function using the program PLTCTFX[37]. Common phase origins for merging were determined in the $p22_12_1$ plane group using ORIGTILT with reflections of signal-to-noise ratio (IQ) <4. For averaging, data were weighted based on IQ including data with IQ <7, and the corresponding phase residuals represent the inverse cosine of the figure of merit from this averaging. Projection maps were calculated by Fourier synthesis from the averaged data using the CCP4 software suite[38].

5-4. References.

1. Toyoshima C, Nakasako M, Nomura H, Ogawa H. Crystal structure of the calcium pump of sarcoplasmic reticulum at 2.6 angstrom resolution. Nature 2000 JUN 8;405(6787):647-55.

2. Toyoshima C, Nomura H. Structural changes in the calcium pump accompanying the dissociation of calcium. Nature 2002 AUG 8;418(6898):605-11.

3. Toyoshima C, Nomura H, Tsuda T. Lumenal gating mechanism revealed in calcium pump crystal structures with phosphate analogues. Nature 2004 NOV 18;432(7015):361-8.

4. Toyoshima C, Mizutani T. Crystal structure of the calcium pump with a bound ATP analogue. Nature 2004 JUL 29;430(6999):529-35.

5. Olesen C, Sorensen TLM, Nielsen RC, Moller JV, Nissen P. Dephosphorylation of the calcium pump coupled to counterion occlusion. Science 2004 DEC 24;306(5705):2251-5.

6. Obara K, Miyashita N, Xu C, Toyoshima L, Sugita Y, Inesi G, Toyoshima C. Structural role of countertransport revealed in Ca2+ pump crystal structure in the absence of Ca2+. Proc Natl Acad Sci U S A 2005 OCT 11;102(41):14489-96.

7. Toyoshima C, Norimatsu Y, Iwasawa S, Tsuda T, Ogawa H. How processing of aspartylphosphate is coupled to lumenal gating of the ion pathway in the calcium pump. Proc Natl Acad Sci U S A 2007 DEC 11;104(50):19831-6.

8. Olesen C, Picard M, Winther AL, Gyrup C, Morth JP, Oxvig C, Moller JV, Nissen P. The structural basis of calcium transport by the calcium pump. Nature 2007 DEC 13;450(7172):1036-U5.

9. Moncoq K, Trieber CA, Young HS. The molecular basis for cyclopiazonic acid inhibition of the sarcoplasmic reticulum calcium pump. J Biol Chem 2007 MAR 30;282(13):9748-57.

10. Huang XQ, Miller W. A time-efficient, linear-space local similarity algorithm. Advances in Applied Mathematics 1991 SEP;12(3):337-57.

11. Odermatt A, Becker S, Khanna VK, Kurzydlowski K, Leisner E, Pette D, MacLennan DH. Sarcolipin regulates the activity of SERCA1, the fast-twitch skeletal muscle sarcoplasmic reticulum Ca2+-ATPase. J Biol Chem 1998 MAY 15;273(20):12360-9.

12. Asahi M, Sugita Y, Kurzydlowski K, De Leon S, Tada M, Toyoshima C, MacLennan DH. Sarcolipin regulates sarco(endo)plasmic reticulurn Ca2+-ATPase (SERCA) by binding to transmembrane helices alone or in association with phospholamban. Proc Natl Acad Sci U S A 2003 APR 29;100(9):5040-5.

13. Morita T, Hussain D, Asahi M, Tsuda T, Kurzydlowski K, Toyoshima C, MacLennan DH. Interaction sites among phospholamban, sarcolipin, and the sarco(endo)plasmic reticulum Ca2+-ATPase. Biochem Biophys Res Commun 2008 APR 25;369(1):188-94.

14. Kimura Y, Kurzydlowski K, Tada M, MacLennan DH. Phospholamban regulates the Ca2+-ATPase through intramembrane interactions. J Biol Chem 1996 SEP 6;271(36):21726-31.

15. Karim CB, Marquardt CG, Stamm JD, Barany G, Thomas DD. Synthetic null-cysteine phospholamban analogue and the corresponding transmembrane domain inhibit the Ca-ATPase. Biochemistry (N Y) 2000 SEP 5;39(35):10892-7.

16. Hellstern S, Pegoraro S, Karim CB, Lustig A, Thomas DD, Moroder L, Engel J. Sarcolipin, the shorter homologue of phospholamban, forms oligomeric structures in detergent micelles and in liposomes. J Biol Chem 2001 AUG 17;276(33):30845-52.

17. Afara MR, Trieber CA, Glaves JP, Young HS. Rational design of peptide inhibitors of the sarcoplasmic reticulum calcium pump. Biochemistry (N Y) 2006 JUL 18;45(28):8617-27.

18. Stokes DL, Pomfret AJ, Rice WJ, Glaves JP, Young HS. Interactions between Ca2+-ATPase and the pentameric form of phospholamban in two-dimensional co-crystals. Biophys J 2006 JUN;90(11):4213-23.

19. Glaves JP, Trieber CA, Ceholski DK, Stokes DL, Young HS. Phosphorylation and mutation of phospholamban alter physical interactions with the sarcoplasmic reticulum calcium pump. J Mol Biol 2011 JAN 21;405(3):707-23.

20. Buck B, Zamoon J, Kirby TL, DeSilva TM, Karim C, Thomas D, Veglia G. Overexpression, purification, and characterization of recombinant Ca-ATPase regulators for high-resolution solution and solid-state NMR studies. Protein Expr Purif 2003 AUG;30(2):253-61.

21. Douglas JA, Rice WJ, Stokes DL, Young HS. How to make two-dimensional crystals by core constitution of Ca2+-ATPase, phospholamban, and sarcolipin. J Gen Physiol 2005 JUL;126(1):128.

22. Asahi M, Kurzydlowski K, Tada M, MacLennan DH. Sarcolipin inhibits polymerization of phospholamban to induce superinhibition of sarco(endo)plasmic reticulum Ca2+-ATPases (SERCAs). J Biol Chem 2002 JUL 26;277(30):26725-8.

23. Asahi M, Nakayama H, Tada M, Otsu K. Regulation of sarco(endo)plasmic reticulum Ca2+ adenosine triphosphatase by phospholamban and sarcolipin: Implication for cardiac hypertrophy and failure. Trends Cardiovasc Med 2003 MAY;13(4):152-7.

24. Trieber CA, Douglas JL, Afara M, Young HS. The effects of mutation on the regulatory properties of phospholamban in co-reconstituted membranes. Biochemistry (N Y) 2005 MAR 8;44(9):3289-97.

25. Auer M, Scarborough GA, Kuhlbrandt W. Three-dimensional map of the plasma membrane H+-ATPase in the open conformation. Nature 1998 APR 23;392(6678):840-3.

26. Becucci L, Guidelli R, Karim CB, Thomas DD, Veglia G. An electrochemical investigation of sarcolipin reconstituted into a mercury-supported lipid bilayer. Biophys J 2007 OCT;93(8):2678-87.

27. Becucci L, Guidelli R, Karim CB, Thomas DD, Veglia G. The role of sarcolipin and ATP in the transport of phosphate ion into the sarcoplasmic reticulum. Biophys J 2009 Nov 18;97(10):2693-9.

28. Becucci L, Cembran A, Karim CB, Thomas DD, Guidelli R, Gao J, Veglia G. On the function of pentameric phospholamban: Ion channel or storage form? Biophys J 2009 MAY 20;96(10):L60-2.

29. Robia SL, Campbell KS, Kelly EM, Hou Z, Winters DL, Thomas DD. Forster transfer recovery reveals that phospholamban exchanges slowly from pentamers but rapidly from the SERCA regulatory complex. Circ Res 2007 NOV 26;101(11):1123-9.

30. Kelly EM, Hou Z, Bossuyt J, Bers DM, Robia SL. Phospholamban oligomerization, quaternary structure, and sarco(endo) plasmic reticulum calcium ATPase binding measured by fluorescence resonance energy transfer in living cells. J Biol Chem 2008 MAY 2;283(18):12202-11.

31. Douglas JL, Trieber CA, Afara M, Young HS. Rapid, high-yield expression and purification of Ca2+-ATPase regulatory proteins for high-resolution structural studies. Protein Expr Purif 2005 MAR;40(1):118-25.

32. Maclenna.Dh, Yip CC, Iles GH, Seeman P. Isolation of sarcoplasmic reticulum proteins. Cold Spring Harb Symp Quant Biol 1973;37:469-77.

33. Ohnoki S, Martonosi A. Purification and characterization of the proteolipid of rabbit sarcoplastic reticulum. Biochim Biophys Acta 1980;626(1):170-8.

34. Warren GB, Toon PA, Birdsall NJ, Lee AG, Metcalfe JC. Reconstitution of a calcium-pump using defined membrane components. Proc Natl Acad Sci U S A 1974;71(3):622-6.

35. Schagger H, Vonjagow G. Tricine sodium dodecyl-sulfate polyacrylamide-gel electrophoresis for the separation of proteins in the range from 1-kda to 100-kda. Anal Biochem 1987 NOV 1;166(2):368-79.

36. Crowther RA, Henderson R, Smith JM. MRC image processing programs. J Struct Biol 1996 JAN-FEB;116(1):9-16.

37. Toyoshima C, Yonekura K, Sasabe H. Contrast transfer for frozen-hydrated specimens .2. amplitude contrast at very low-frequencies. Ultramicroscopy 1993 JAN;48(1-2):165-76.

38. Potterton E, McNicholas S, Krissinel E, Cowtan K, Noble M. The CCP4 molecular-graphics project. Acta Crystallographica Section D-Biological Crystallography 2002 NOV;58:1955-7.

Chapter 6.

Re-examination of predicted PLB binding sites in the light of high-resolution SERCA structures.

"Action has meaning only in relationship, and without understanding relationship, action on any level will only breed conflict. The understanding of relationship is infinitely more important than the search for any plan of action".

-Jiddu Krishnamurti as quoted by Dr. Gabor Maté
in "In the Realm of Hungry Ghosts".

Chapter 6. Re-examination of predicted PLB binding sites in the light of high-resolution SERCA structures.

6-1. Summary of significant findings.

This thesis proposes a novel mode of interaction between SERCA and pentamers of PLB and between SERCA and pentamers of SLN based on cryo-electron microscopy of 2D co-crystals. The overall goal was to provide structural descriptions of SERCA regulatory interactions for the design of heart disease therapies. For clarity, we will begin our discussion focused on PLB and end with SLN.

The proposed site of interaction for the PLB pentamer involves TM3 of SERCA and is distinct from the modeled site of interaction for the PLB monomer (TM2, TM4, TM6, TM9). A critical question is: what does the PLB pentamer bound to the TM3 region of SERCA do? The frequency of co-crystallization points towards a functional role for the interaction between PLB pentamers and SERCA. However, defining this functional role has proven difficult. The primary obstacle is the oligomeric heterogeneity of PLB. To determine the function of the PLB pentamer only, without contributions from other oligomeric species, one would have to completely stabilize PLB pentamers without disturbing native structure and dynamics.

The dramatic increase in co-crystal frequency with certain PLB mutants was impressive. The clearest predictor of whether a PLB mutant would increase co-crystallization with SERCA was its inhibitory activity, such that gain-of-inhibition mutants increased co-crystal frequency relative to wild-type PLB and the opposite trend was observed for loss-of-inhibition mutants. Thus, the interactions observed in the SERCA-PLB co-crystals were favoured by mutations that had greater inhibitory activity. With respect to proposed mechanisms for PLB regulation of SERCA, this would be most consistent with an enhanced interaction between SERCA and PLB. The enhanced interaction mechanism, proposed by MacLennan and colleagues, was an alternative to the mass action mechanism to reconcile PLB mutants that had increased inhibition, but wild-type-like pentamer to monomer ratios in SDS-PAGE. One observation supporting the enhanced interaction model was the co-expression of SERCA with the gain-of-inhibition PLB mutant $Asn^{27}Ala$ (canine PLB numbering; Lys^{27} in human PLB). Indeed, PLB-$Lys^{27}Ala$

was among the best screened mutants for increasing co-crystallization with SERCA in our hands. An important distinction of our structural studies using PLB-Lys^{27}Ala was that we observed an enhanced interaction between the pentameric form of PLB and SERCA. Such a mechanism was never proposed with the enhanced interaction model, which was limited to interactions between monomeric PLB and SERCA. It is reasonable to consider this limitation in light of the prevalent "mass action" model at the time, however, our results suggest pentameric PLB could also enhance association (Figure 6.1). An important observation by MacLennan and colleagues was that the two PLB mechanisms, mass action and enhanced interaction, were additive. Thus, for our observations to agree with current models, our mode of enhanced interaction would have to be compatible with PLB mutants that motivated the mass action mechanism. Our observations with PLB-Ile^{40}Ala in SERCA co-crystals suggest that enhanced interaction between the PLB pentamer and SERCA is compatible with a "mass action" mutant. Our results might be interpreted further by suggesting that PLB-Ile^{40}Ala functions by enhancing both mechanisms, because Ile^{40}Ala also greatly increases co-crystal frequency relative to wild-type PLB. Irrespective of this interpretation, an enhanced mode of interaction between PLB pentamers and SERCA is compatible with proposed mechanisms of regulation by PLB (Figure 6.1).

PLB pentamers interacting with SERCA could provide a structural context to our current understanding of other aspects of PLB regulation as well. For example, a long debate has existed about whether PLB physically dissociates from SERCA when inhibition is relieved. More recent observations seem to be accumulating in favour of a stable complex that remains associated during SERCA activity and inhibition. The distinction of the TM3 as a site for pentamer-binding provides one explanation for how PLB could remain associated with SERCA without inhibiting the enzyme and without occupying the TM2, TM4, TM6, and TM9 groove. It has been suggested that the SERCA-PLB active complexes differ between inhibition relieved by micromolar Ca^{2+} and inhibition relieved by PLB phosphorylation. Chapter 4 highlighted the structural changes in SERCA-PLB co-crystals by PKA-phosphorylation of PLB-Ser^{16} that occur while the pentamer continued to interact with SERCA. Primarily, phosphorylation seemed to affect the cytoplasmic domain and was consistent with cytoplasmic disordering observed by others using phosphorylated PLB. Since the interaction between PLB pentamers and SERCA persisted in the absence of Ca^{2+} and following phosphorylation, we proposed that the

TM3 interaction is mediated primarily within the membrane. It is possible intra-membrane interactions could persist in the presence of Ca^{2+} with different cytoplasmic arrangements than the phosphorylated PLB and SERCA interaction, readily explaining how different active complexes could exist. However, this is speculation since our co-crystals required Ca^{2+}-free conditions. We have not directly investigated the effects of micromolar Ca^{2+} concentrations and whether such conditions permit interaction between PLB pentamers and SERCA.

This discussion will continue as a candid dialogue focused on some remaining questions about the regulation of SERCA by PLB in the context of this thesis. We will end the discussion with remaining questions pertaining to SLN.

6-2. Why do we not observe pentameric PLB cross-linked to SERCA?

A compelling question given our structural evidence for an interaction between pentameric PLB and SERCA is: why has pentameric PLB not been cross-linked to SERCA?

There are a number of key points with respect to previous SERCA-PLB cross-linking experiments that must first be discussed. The first initial SERCA-PLB cross-link was observed by James and coworkers, between PLB-Lys^{3} and SERCA-Lys^{397}/Lys^{400} in the N-domain, using native sources of PLB and SERCA[1]. However, this cross-link has been difficult to reproduce[2, 3] bringing to question the strength of the proposed interaction. Subsequent cross-linking experiments[2-4] used Cys-substitution of PLB residues, which required a Cys-less PLB background. It is worth recalling that mutation of the three transmembrane Cys residues in PLB destabilizes the pentamer and favours the monomeric form in SDS-PAGE. This disruption of oligomerization would inherently decrease the likelihood of cross-linking a PLB pentamer to SERCA.

As well, our experience with 2D co-crystals of SERCA and PLB has shown that the co-crystals are very sensitive to the lipid to protein ratio. The co-crystals require a low lipid to protein ratio, similar to the environment of the SR, for efficient crystallization. Co-crystallization occurs over a small range of lipid to protein ratios and was abolished by high lipid to protein ratios. Taken together, these observations suggest the interactions in the co-crystals, between pentameric PLB and SERCA, are also sensitive to the lipid to protein ratio. Previous cross-linking experiments used heterologous co-expression of

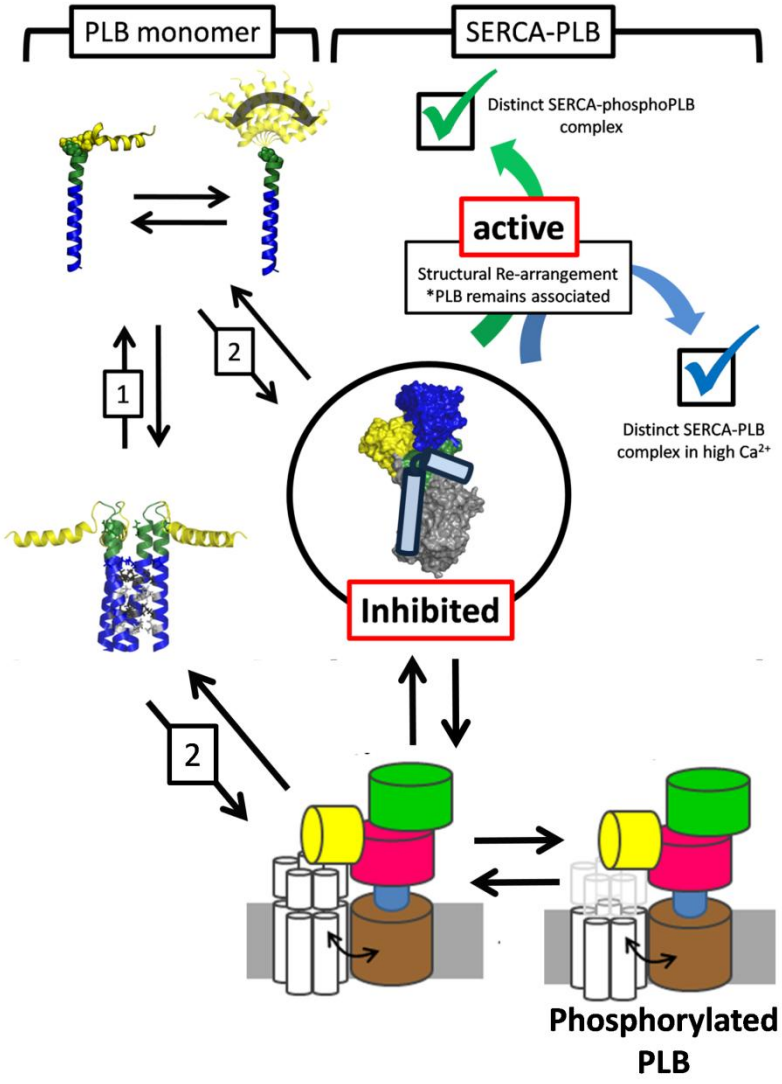

Figure 6.1. An expanded model of PLB regulation of SERCA including functional interaction between pentameric PLB and SERCA proposed in this thesis. Modifications have been made to the PLB regulation model presented in the Introduction (Figure 2.13) to include the interaction between the PLB pentamer and SERCA. At bottom, a schematic representation of the complexes formed between the PLB pentamer (*white cylinders*) and SERCA (*coloured cylinders*) based on 2D co-crystals. The interaction between pentameric PLB and SERCA was postulated to facilitate formation of the inhibitory SERCA-PLB complex (see Chapter 4). The disordered PLB cytoplasmic domain consistent with SERCA and phosphorylated-PLB co-crystals is shown as *dashed grey lines*. The arrow labelled 1 is the dissociation of the PLB pentamer associated with the "mass action" PLB mechanism. The arrow labelled 2 is the association of PLB with SERCA associated with the "enhanced interaction" PLB mechanism, which now includes association between the PLB pentamer and SERCA.

SERCA and PLB, which have inherently low protein expression levels and high lipid to protein ratios. With this in mind, the absence of an interaction between PLB pentamers and SERCA in heterologous co-expression would be expected, because the lipid to protein ratio is much higher than our co-reconstitutions.

However, with the question as to why PLB pentamers have not been cross-linked to SERCA permeating a review of previous cross-linking studies, one very interesting observation can be made. In some studies, a second band appears at a slightly higher molecular weight than the band assigned to the SERCA-PLB cross-link. This is most dramatic in the study by Jones and coworkers[3] where a prominent cross-link appears in the co-expression of PLB-Lys^{27}Cys with SERCA2a in insect cells (see Figure 2a in Chen et al. 2003[3]). The appearance of the second band varied among the different cross-linking reagents screened in the study, but nonetheless is strong under certain conditions. A faint higher molecular weight cross-link also occurs in the co-expression of PLB-Asn^{30}Cys and SERCA2a, although it is much less clear[3]. Unfortunately, the given molecular weight markers do not distinguish if the additional cross-link was between a PLB pentamer and SERCA or resulted from a different interaction, such as a SERCA dimer cross-linked to PLB. The apparent higher molecular weight cross-linked bands were not addressed by the authors. Regardless, the observations support the existence of higher-order interactions beyond SERCA with monomeric PLB. A similar observation can be made in the co-expression and cross-linking of PLB-Lys^{27}Cys and SERCA1a in HEK-293 cells by Toyoshima and coworkers (see Figure 1a in Toyoshima et al. 2003[4]).

We have preliminary cross-linking that supports the interaction of PLB oligomers with SERCA in non-crystallized co-reconstitutions. Figure 6.2a shows control (SERCA alone) and wild-type PLB co-reconstitutions in the absence of glutaraldehyde, and cross-linked with 0.01% and 0.1% glutaraldehyde. Glutaraldehyde will cross-link primary amines found within proteins and lipids (EYPE). Probed with an antibody against PLB, two bands are observed in the "high" wild-type PLB co-reconstitution in the absence of glutaraldehyde; the lower molecular weight band can be attributed to a homo-oligomer of PLB (likely the pentamer) and the higher molecular weight band to a complex between SERCA and PLB (upper panel in Figure 6.2a). Interestingly, the higher molecular weight band migrates at an apparent molecular weight that is greater than the expected molecular weight of a 1:1 SERCA-PLB. More specifically, the band is observed above the 126 kDa

marker, higher than where a 1:1 SERCA-PLB complex would be expected to migrate (SERCA ~110 kDa; PLB ~6 kDa; estimated molecular weight of 1:1 complex ~116 kDa). This band is also apparent at higher exposure times in the "low" wild-type PLB co-reconstitutions in the absence of glutaraldehyde (lower panel in Figure 6.2a). The signal in the region between 126 kDa and 208 kDa is increased by glutaraldehyde treatment (see "low" wild-type PLB in lower panel of Figure 6.2a). Unfortunately, the resolution of the bands in these initial cross-linking experiments was limited.

Figure 6.2b and 6.2c used 6% SDS-PAGE, allowing the dye front and low molecular weight species to migrate out of the gel, to resolve potential SERCA-PLB complexes. Control (SERCA only) and wild-type PLB co-reconstitutions have similar patterns when probed with an antibody against SERCA1a (IIH11; left panel of Figure 6.2b). The dashed lines in Figure 6.2b indicate the signal for SERCA monomers (long-dashed line) and SERCA dimers (short-dashed line). When probed with an antibody against PLB (2D12; middle and right panels of 6.2b), there is signal observed between SERCA monomers and SERCA dimers. Absent in the control reconstitutions, these signals can be attributed to SERCA-PLB complexes present in the wild-type PLB co-reconstitutions (middle panel in Figure 6.2b). The PLB signal in this region migrated as two distinct bands just above the migration for SERCA monomers (black arrowheads in Figure 6.2b). This was attributed to at least two species of SERCA-PLB complexes; a 1:1 complex between SERCA and monomeric PLB and a complex between SERCA and a PLB oligomer. The signal for the SERCA-PLB complexes increased upon glutaraldehyde treatment with a concomitant loss in the signal for the PLB homo-oligomer. As well, the band above the SERCA dimer migration distance that would be consistent with PLB interacting with dimeric or other oligomeric forms of SERCA.

Figure 6.2c shows a similar experiment with improved resolution of the complex bands that increased upon glutaraldehyde treatment. Along with an increased signal for the SERCA-PLB complexes that are observed in the absence of glutaraldehyde (closed black arrowheads in Figure 6.2c), there are two distinct bands that appeared upon glutaraldehyde treatment (open white arrowheads in Figure 6.2c). The stoichiometries of the observed SERCA-PLB complexes are currently unclear, but could represent transient complexes, such as two PLB pentamers with a SERCA monomer, that dissociate in SDS-PAGE without being cross-linked.

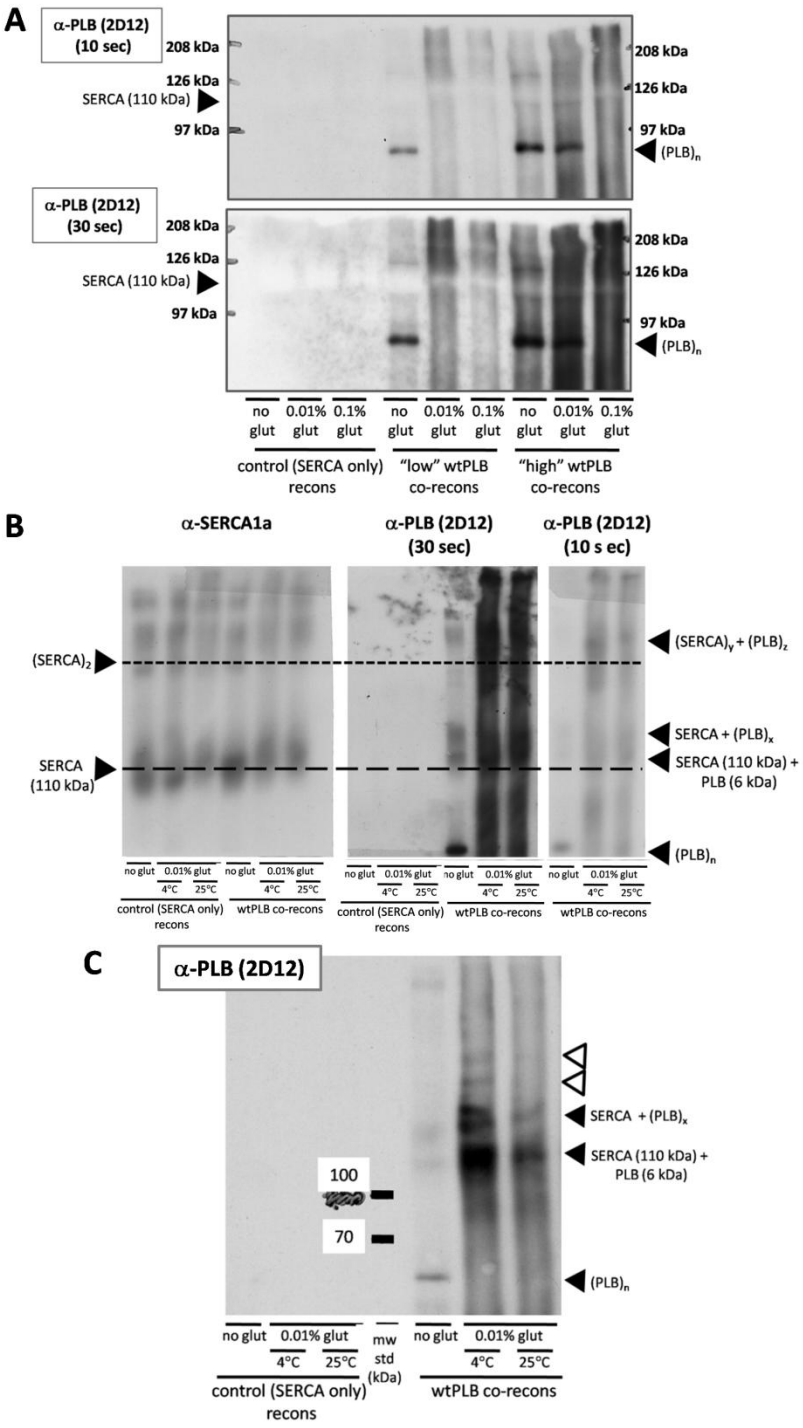

Figure 6.2. Cross-linking of SERCA co-reconstituted in the absence and presence of wild-type PLB. Panel A, 15% SDS-PAGE of control and wild-type PLB co-reconstitutions cross-linking reactions probed with α–PLB (2D12) antibody. "Low" wild-type PLB used 25 μg of PLB per reconstitution and "high" wild-type PLB used 200 μg per co-reconstitution. **Panels B and C,** 6% SDS-PAGE of control and wild-type PLB co-reconstitution reactions probed with the indicated antibody. See section 6-2 of the text for discussion and section 6-9 of the text for materials and methods.

6-3. Harnessing the boom: what SERCA transport intermediates interact with PLB?

Our structural understanding of SERCA has exploded in the last eleven years. Since Toyoshima's first high-resolution structure in 2000, there are now more than five SERCA structures representing four Ca^{2+}-bound E1 intermediates and ten SERCA structures representing five E2 intermediates. We will be using this group of fifteen structures for discussion. This group includes only structures with TG bound as an inhibitor and does not include SERCA bound to BHQ or CPA, primarily because BHQ and CPA were not included in the co-crystal conditions. As of today, there were 45 structures deposited in the Protein Data Bank (www.rcsb.org/pdb).

Even with an unprecedented amount of structural information about SERCA, a big question remains: how is energy transferred through SERCA during Ca^{2+}-transport? A mechanism was recently proposed by Nissen and coworkers[5] including a central core that acts as a communication mass between the phosphorylation site, Asp^{351}, and the gating residue of Ca^{2+}-binding, Glu^{309}. The central core[5] includes the cytosolic extension of TM4, the cytosolic extension of TM5 and part of the P-domain (Figure 6.3). Since the core remains closely associated in all available SERCA structures, Nissen and coworkers suggested that this region is important for bridging the distant phosphorylation site and the Ca^{2+}-binding sites[5]. SERCA activity can generally tolerate mutation to cytosolic extensions of the central core, except for residues near the cytosol-membrane border[5]. A second interesting aspect involved deeper membrane insertion of TM3 and TM4 in phosphorylated SERCA intermediates driving the enzyme to E2-like conformations[5]. This insertion mechanism could be influenced by the nature of the amino acids in the TM extensions near the cytosol-membrane border, explaining why mutations are detrimental in these regions of the central core.

Since we do not have a complete understanding of SERCA on its own, it is difficult to precisely describe how PLB regulates SERCA. Toyoshima proposed a regulatory mechanism for PLB paired with the modeled TM2, TM4, TM6, TM9 binding groove[4]. It was suggested that PLB favoured the E2 state by binding and tying TM groove helices

together in an E2-like conformation[4, 6]. Such a mechanism would be consistent with kinetic models that PLB increased the time SERCA spent in E2-like conformations[6, 7]. Toyoshima proposed PLB dissociated from the TM2, TM4, TM6, TM9 groove during transition to E1 states, being physically squeezed out by movement of TM2[4]. These assumptions were based on the comparison of the first two high-resolution SERCA structures: the Ca^{2+}-bound SERCA structure (pdb:1SU4)[8] and the Ca^{2+}-free TG-bound SERCA structure (pdb:1IWO)[9]. If such a mechanism were to exist, a second PLB-binding mode would be necessary to maintain association if a stable SERCA-PLB complex also existed. This thesis posits that TM3 of SERCA could act as an alternative mode of binding involving oligomeric PLB for maintaining association.

SERCA structural comparisons will be carried out with an important assumption: the analysis will involve high-resolution structures of SERCA alone that are related to states that interact with PLB. To visualize conformational changes, different SERCA structures have been aligned along TM5 to TM10. Regions including the TM7-TM10 platform are commonly used to visualize SERCA conformational changes between structures[5, 9]. PyMOL has been used to align all of the following discussion figures (The PyMOL Molecular Graphics System, Version 0.99, Schrödinger, LLC.). Figure 6.4 shows the excellent superimposition of TM5 to TM10 among ten SERCA structures representing five E2 states.

The comparison will focus on TM2 and TM3 as representative helices of the two proposed PLB binding sites. As an aside, we have highlighted residues based on intriguing observations from sequence alignments of SERCA with PLB and SLN. One example was highlighted in Chapter 4 between TM3 and PLB. Indeed, we suggested that this homology could be important for the interaction between SERCA and pentameric PLB. Linear sequence alignments are limited for membrane proteins given that the alignment generally proceeds linearly from the N-terminus to C-terminus. The interested reader can visit Appendix 2 before proceeding for further discussion. In brief, there was also homology between PLB and TM2 of SERCA, part of Toyoshima's proposed binding groove. We do not want to suggest that homology alone can support interaction between two transmembrane proteins, but these observations were striking in the context of other supporting data. Thus, we focused on select residues from the PLB-aligned regions of TM2 and TM3 to visualize conformational changes between SERCA structures.

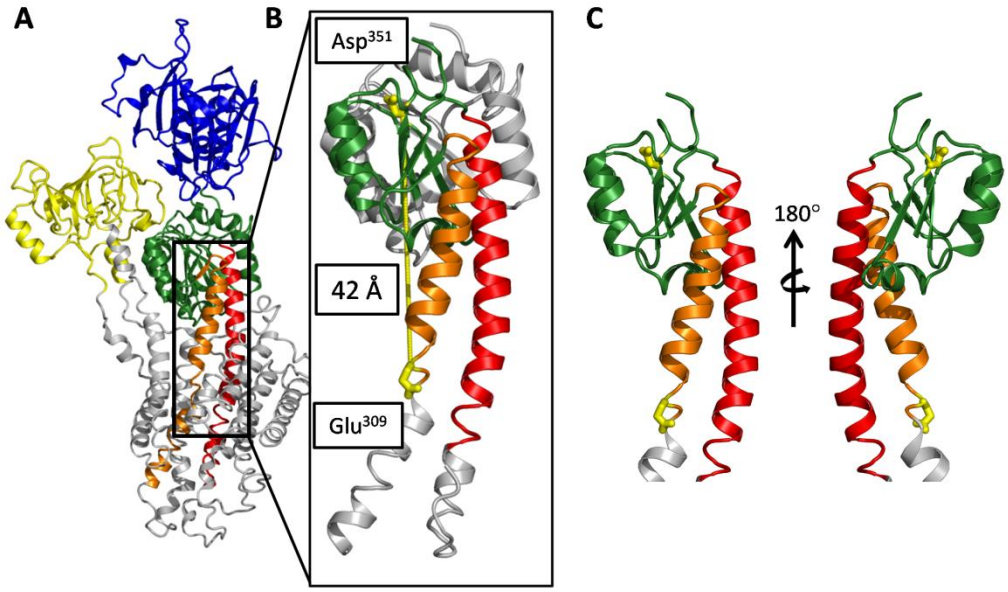

Figure 6.3. Visualizing the central core of SERCA proposed by Moller, Nissen and colleagues5. Panel A, a cartoon representation of SERCA (pdb: 3B9R)[10] is coloured to highlight the cytoplasmic domains (P-domain is green, N-domain is blue and the A-domain is yellow) and TM4 (orange) and TM5 (red). **Panel B,** the central core domain[5] is composed of the cytosolic parts of TM4 (orange) and TM5 (red) and part of the P-domain (green). The central core has been implicated in linking energy transfer between the residue of SERCA phosphorylated by ATP (Asp^{351}) and the distal gating residue (Glu^{309}) of the Ca^{2+} binding sites[5]. The distance between Asp^{351} and Glu^{309} is ~42 Å in this E2-P-ATP representation (pdb: 3B9R)[10].

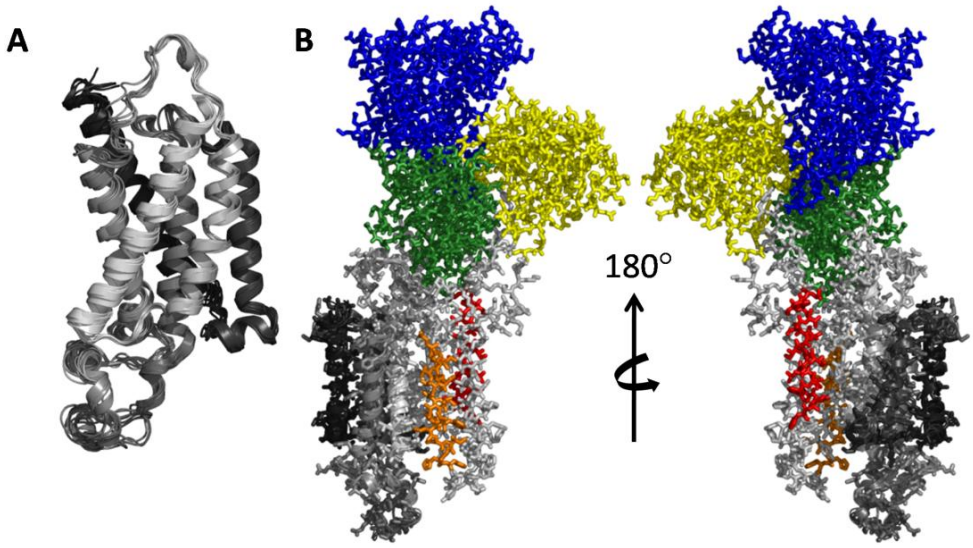

Figure 6.4. Superimposition of the platform region of ten SERCA structures representing five E2 intermediates. The superimposition of SERCA structures was performed using PyMol (The PyMOL Molecular Graphics System, Version 0.99, Schrödinger, LLC.). **Panel A,** the superimposition of TM5 to TM10 of ten SERCA structures representing E2-like states (pdb: 1IWO, 3B9B, 2ZBE, 2ZBF, 3B9R, 2ZBG, 1XP5, 1WPG, 2C88, 2C8K)[8-15]. The TM helices are coloured in grey from light (TM5 - foreground) to dark (TM10 – background). **Panel B,** the (H_2)E2P-ATP representative (pdb: 3B9R)[10] is shown in sticks. The cytoplasmic domains are green (P-domain), blue (N-domain) and yellow (A-domain). The TM helices proposed to be involved in two distinct PLB binding sites are coloured orange (TM3) and red (TM2). The right-side is a 180° rotation of the left-side along an axis parallel to the right edge of the page.

We can re-visit the TM2, TM4, TM6, TM9 PLB-binding groove with the greater number of SERCA E1 and E2 representatives now available. We can look to see if TM2 physically occupies the groove in more recent E1 structures that would physically prevent PLB from binding. Figure 6.5 shows the conformational changes between the first two high resolution Ca^{2+}-bound[8] and Ca^{2+}-free[9] (TG-bound) SERCA structures. The overall conformation of the TM2, TM4, TM6 and TM9 groove restricts when Ca^{2+} is bound as described by Toyoshima's model. We observed similar changes in the groove in other E1 and E2 states. For clarity, similar conformations are shown for two more recent SERCA structures, the nucleotide-bound E1 (pdb: 1T5S)[14] and E2 (pdb: 3B9R)[10] representatives (Figure 6.5).

The constriction of the TM2, TM4, TM6 and TM9 groove is most dramatic at the cytosolic-membrane border. In particular, TM2 approaches TM9 and closes off the PLB-binding groove. Thus, the mechanism for PLB dissociation between E1 and E2 states, proposed by Toyoshima, holds using more recent SERCA structures. It is interesting to highlight the access of the groove to the central core of SERCA proposed by Nissen and colleagues (Figure 6.5). For simplification, we will include the whole of TM4, TM5 and the P-domain to represent the central core. In E2 structures, the PLB binding groove had access to TM4 of the central core (Figure 6.5). This access was removed by TM2 in E1 structures. In contrast to E2 states, the surface of the central core was limited to extra-membrane regions from the TM2, TM4, TM6 and TM9 face of SERCA in E1 states.

We can also re-examine SERCA-PLB cross-linking. For example, the cross-linking of PLB to SERCA was favoured under Ca^{2+}-free conditions and required nucleotide (ATP or ADP). The consensus from cross-linking studies was that PLB bound SERCA in an E2 nucleotide-bound state. We can now compare differences between nucleotide-free and nucleotide-bound E2 representative states, with respect to changes in proposed PLB binding sites. We will assume that the nucleotide-bound E2 state binds to PLB consistent with positive cross-linking data. We will assume that PLB interacts differently with SERCA in the absence of nucleotide such that cross-linking is negative. Figure 6.6 aligns ten different SERCA high-resolution structures representing five different E2 states. If we focus on the reported fortuitous PLB cross-link to Val^{89} at the luminal end of TM2 in SERCA as a reporter landmark, we observe an upward lateral shift of TM2 in the absence of nucleotide in some of the nucleotide-free SERCA structures (Figure 6.6a). Careful examination of Figure 6.6c shows that in the absence of nucleotide Val^{89} of SERCA

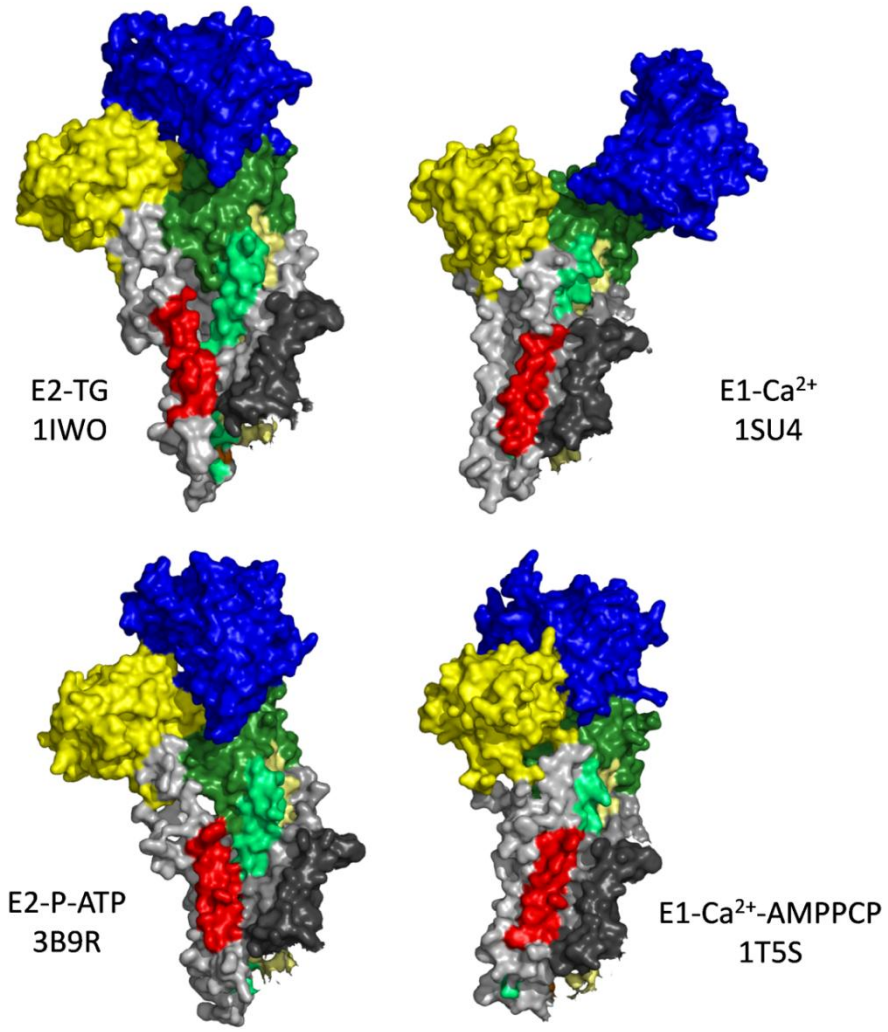

Figure 6.5. Comparison of the TM2, TM4, TM6, and TM9 groove proposed for PLB binding between SERCA E1 and E2 states. The representative states of SERCA and the corresponding Protein Data Bank identifiers (pdb) are indicated. For clarity, some of the platform domain (used for alignment) has been removed. The cytosolic extensions of TM4 (teal) and TM5 (beige) form the central core with part of the P-domain (green). The first two high-resolution SERCA structures (1IWO[8] and 1SU4[9]) were compared for changes in the TM2 (red), TM4 (teal), TM6 (light grey) and TM9 (dark grey) PLB-binding groove. PLB was proposed to dissociate because TM2 (red) physically closes the binding groove[4]. This agrees with more recent SERCA structures representing E1[14] and E2[10] states (bottom).

retracts approximately 5.1 Å from the nucleotide-bound conformation that cross-links to PLB. The exceptions to this observation include the E2 state (TG-bound)[9] and one of the three reported E2P structures (with BeF_3^- and TG bound)[12]. In these two cases, the structures in the absence of nucleotide have a similar position of TM2 as the six nucleotide-bound E2 structures. Given that SERCA-PLB cross-linking to TM2 was favoured by E2 nucleotide-bound states, PLB could interact with TM2 in its deeper inserted conformation.

It is worth reminding the reader that the difference between Nissen's and Toyoshima's E2P structures demonstrated that different high-resolution structures could be obtained using the same ligands (BeF_3^- to mimic the phosphorylation transition state in this case)[5]. More specifically, Nissen's E2P structure[10] had a proposed luminal opening that was not observed in Toyoshima's E2P structures[12]. With respect to the proposed TM2, TM4, TM6 and TM9 PLB-binding groove, Nissen's and Toyoshima's SERCA structures with only BeF_3^- bound have similar lateral positioning of TM2 that distinguishes them from the other eight E2 structures. In Toyoshima's unique E2P structure (BeF_3^- and TG bound), we observe TM2 in a similar lateral position as the six nucleotide-bound SERCA E2 structures and the E2 (TG-bound) structure.

6-4. Visualizing TM3 of SERCA as a PLB-binding site in the context of 2D co-crystals.

We have proposed that pentameric PLB interacts with the TM3 region of SERCA based on projection maps of 2D co-crystals. Before we investigate this potential binding in the context of high-resolution SERCA structures, we should discuss the co-crystals as a structural model.

First, the co-crystals were grown in Ca^{2+}-free conditions. Similar to PLB cross-linking, the interaction between PLB pentamers and SERCA can occur with an E2-like state of SERCA. In contrast to PLB cross-linking, the co-crystals do not require the addition of nucleotide, but do contain decavanadate which has been proposed to mimic E2P state[16]. As well, the co-crystals are grown in the presence of TG. Although TG has been proposed to minimally influence SERCA structure[5], as discussed bound TG may have subtle conformational effects (recall the difference in TM2 between Toyoshima's BeF_3^- with TG structure and Toyoshima's BeF_3^- only structure[12] in Figure 6.6). Although the particular co-crystal conditions favoured binding of the PLB pentamer to SERCA, as

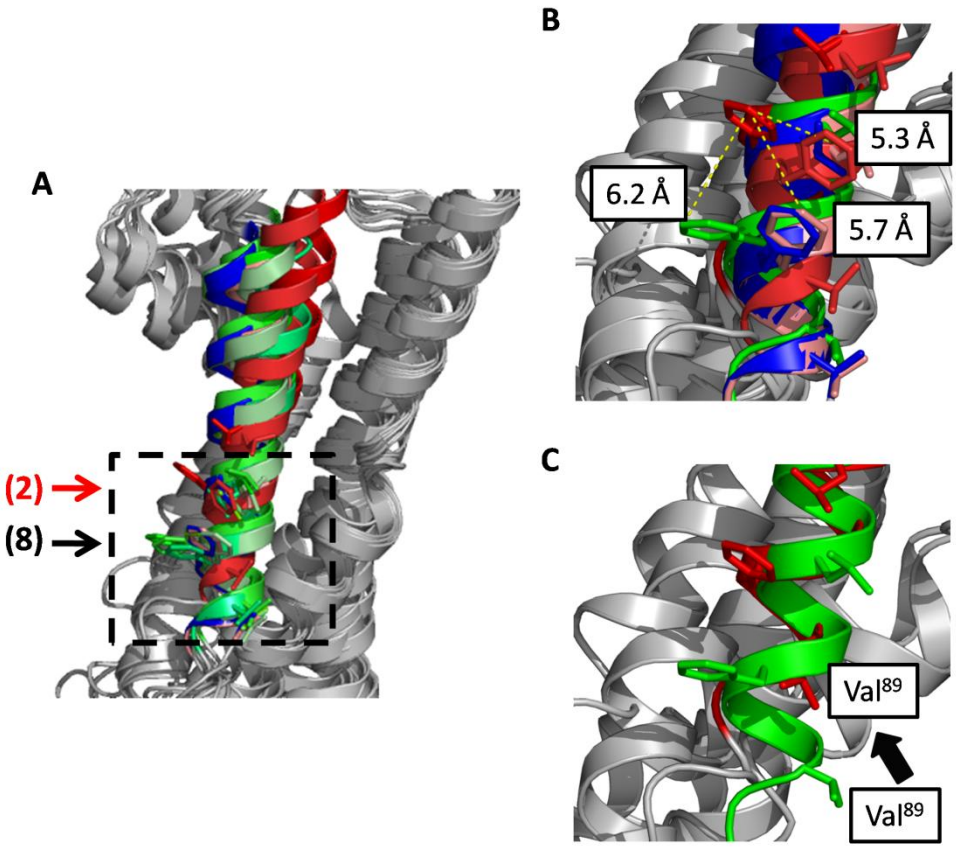

Figure 6.6. Superimposition of representative SERCA E2 structures centered on TM2. Panel A, superimposition of ten reported high-resolution SERCA structures representing five E2 states (pdb: 1IWO, 3B9B, 2ZBE, 2ZBF, 2ZBG, 3B9R, 2ZBG, 1WPG, 2C88, 2C8K)[8-15]. The lateral position of TM2 in *two* of the nucleotide-free E2 states (3B9B[10] and 2ZBE[12]) is shifted towards the cytoplasm relative to the other *eight* E2 representative structures. **Panel B,** distances are given between Phe[92] in different representative E2 structures. The upward shifted nucleotide-free E2 structures are coloured *red* (3B9B)[10] and *rust* (2ZBE)[12]. The downward shifted nucleotide-free E2 structures are *blue* and *pale-red*. One representative for the conformation of nucleotide-bound E2 structures (*green*) is shown for clarity. **Panel C,** Val[89], cross-links to PLB in E2 nucleotide-bound states (*green* as representation), retracts in some E2 nucleotide-free states (*red* as representation) ~5 Å away from the modeled PLB binding groove[4].

judged by crystal frequency, they do not rule out the binding of monomeric PLB simultaneously. As well, we do not want to imply that the PLB pentamer binds exclusively to the conformation of SERCA represented by the co-crystals. Indeed, our collaborators have produced 2D co-crystals in the absence of TG (David Stokes, unpublished data).

The types of lipid included in the co-reconstitution had a critical role in co-crystallization[17, 18]. We used a lipid ratio based on those that increased tubular crystallization of SERCA alone[17]. The switch from tubular co-crystals of SERCA and PLB to wide 2D co-crystals of SERCA and PLB required increased Mg^{2+} concentrations. The optimal Mg^{2+} concentration was 30 to 50 mM. This can be compared to the 5 mM Mg^{2+} concentrations used for tubular SERCA-PLB co-crystals[19]. At the higher Mg^{2+} concentrations sufficient for frequent wide 2D co-crystallization, a mixture of tubular and wide 2D co-crystals sometimes occurred. We then arrive at a personal favourite question, what is Mg^{2+} doing in the SERCA-PLB co-crystals?

We have discussed what higher Mg^{2+} concentrations do *to* the co-crystals, but we do not know what higher Mg^{2+} concentrations do *in* the co-crystals. We can speculate about how Mg^{2+} might influence the different components of the SERCA-PLB co-crystallization. We discussed in the introduction observations that Mg^{2+} influenced the order-to-disorder equilibrium of the PLB cytoplasmic domain[20]. Other groups have reported that monovalent and divalent cations influenced the ordering of lipid membranes[21, 22]. Unfortunately, Mg^{2+} has not been screened in these studies. We have some preliminary observations that Mg^{2+}, like Ca^{2+}, might influence lipid order (Grant Kemp, unpublished data). A lipid-dependent mechanism involving Mg^{2+} is consistent with our observations of the switch between tubular and wide 2D SERCA-PLB co-crystals[18].

In reference to the conformation of SERCA that interacts with pentameric PLB, a mechanism involving Mg^{2+} and negatively-charged lipids has been proposed to inhibit SERCA[23]. As well, the presence of high Mg^{2+} has been offered as an explanation for differences between the BeF_3^- E2P representative structures from Nissen[10] and Toyoshima[12]. More specifically, the higher Mg^{2+} in Nissen's co-crystals conditions stabilized an open luminal gate[5]. It is possible that a conformational effect of high Mg^{2+} could also occur in the presence of PLB in our co-crystals. Unfortunately, we do not know if higher Mg^{2+} influences the SERCA in the presence of TG and decavanadate.

6-5. Comparing SERCA conformational changes in the two proposed PLB binding sites.

Of the two proposed PLB-binding sites, TM3 had the largest divergence in conformation between Nissen's ("high Mg^{2+}") E2P structure[10] and Toyoshima's ("low Mg^{2+}") E2P structures[12] (Figure 6.7). In the region of TM2, the E2P structures with BeF_3^- alone were similar to each other and as a pair were distinct from the nucleotide-bound E2P conformations (Figure 6.6). For TM3, Toyoshima's E2P structure with BeF_3^- only was intermediate between Nissen's E2P structure and the nucleotide-bound E2P structures (Figure 6.7b). Similar to TM2, the nucleotide-free SERCA structures were in different lateral positions for TM3, shifted more towards the cytoplasmic side than the nucleotide-bound structures. Nissen's E2P representative SERCA structure, with BeF_3^- alone[10], was the most distinct from the other E2 states in accordance to its distinction as the only E2 structure with an open luminal gate (Figure 6.7).

In light of the insertion mechanism proposed by Nissen, it was intriguing that we observed differences in the lateral positioning of helices in both potential PLB binding sites dependent on the nucleotide-bound state of SERCA. The highlighted lateral shifts in TM2 and TM3 near the lumen-membrane border are paralleled by conformational changes in the helices near the cytoplasm-membrane border (Figures 6.6a and 6.7b). Our co-crystal conditions would be consistent with pentameric PLB binding TM3 in a less inserted conformation, in line with conformational changes in SERCA associated with

opening of its luminal gate. However, it is not clear what E2 conformation of SERCA interacts with pentameric PLB in our co-crystals and, as such, we cannot be sure if pentameric PLB favours a particular lateral position of TM3. This is unfortunate given that the lateral conformation of TM3 is intimately linked to larger conformational changes in the luminal end of TM4 (Figure 6.8). Recall that TM4 positioning and helix-unwinding is critical to co-ordination at Ca^{2+} binding site II. Also, the cytoplasmic end of TM4 is part of the central hydrophobic core of SERCA, proposed as an important domain for energy transduction through SERCA during transport[5]. The luminal positioning of TM4 would likely influence its cytoplasmic end and, in turn, its conformation as part of the central core. In the nucleotide-free E2 states, the luminal end of TM4 is very close to the luminal end of TM3 near our proposed site of interaction with pentameric PLB (Figure 6.8). In the nucleotide-bound E2 conformations, TM4 has shifted away from TM3 and is more closely aligned with the luminal end of TM4 in Ca^{2+}-bound E1 states (Figure 6.8). At this time, it is unclear if pentameric PLB influences the positioning of TM4 relative to TM3 in a similar manner as the influence of bound nucleotide.

It is interesting to note that TM3 undergoes a large conformational change between the E1 and E2 states. In all of the determined SERCA E1 structures, the conformation and lateral positioning of the luminal end of TM3 is identical (Figure 6.9). In the E1 structures, TM3 has rotated and moved closer to the face of SERCA containing the TM2 PLB-binding groove. In contrast to the E2 structures, the positioning of TM3 does not change in the E1 structures when nucleotide is bound or not. Recall that the TM2, TM4, TM6 and TM9 binding groove is closed off in E1 structures of SERCA. If PLB remains complexed with SERCA in E1 states when Ca^{2+} is bound, as has been proposed[24], this movement of TM3 could direct PLB towards or away from the TM2 binding groove. Indeed, we suggested in Chapter 4 that binding of pentameric PLB was involved in the delivery or removal of PLB from the inhibitory TM2, TM4, TM6 and TM9 binding groove. We cannot say if pentameric PLB remains bound to SERCA in the E1 states, or if some other oligomeric species is responsible for the SERCA-PLB complex[24] observed in the presence of Ca^{2+}.

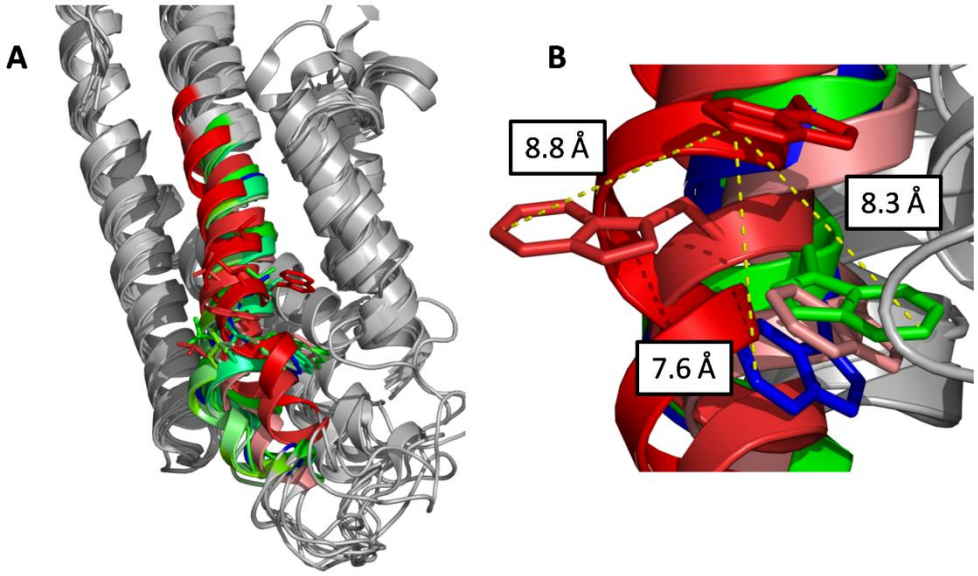

Figure 6.7. Superimposition of ten representative SERCA E2 structures centered on TM3. Panel A, superimposition of ten reported high-resolution SERCA structures representing five E2 states (pdb: 1IWO, 3B9B, 2ZBE, 2ZBF, 2ZBG, 3B9R, 2ZBG, 1WPG, 2C88, 2C8K)[8-15]. **Panel B,** distances are given between Trp^{272} in different representative E2 structures. The upward shifted nucleotide-free E2 structure is coloured *red* (3B9B)[10]. The nucleotide-free E2 structure intermediate between the upward and downward shifted TM3 conformations is coloured *rust* (2ZBE)[12]. The downward shifted nucleotide-free E2 structures are *blue* and *pale-red*. One representative for the conformation of nucleotide-bound E2 structures (*green*) is shown for clarity.

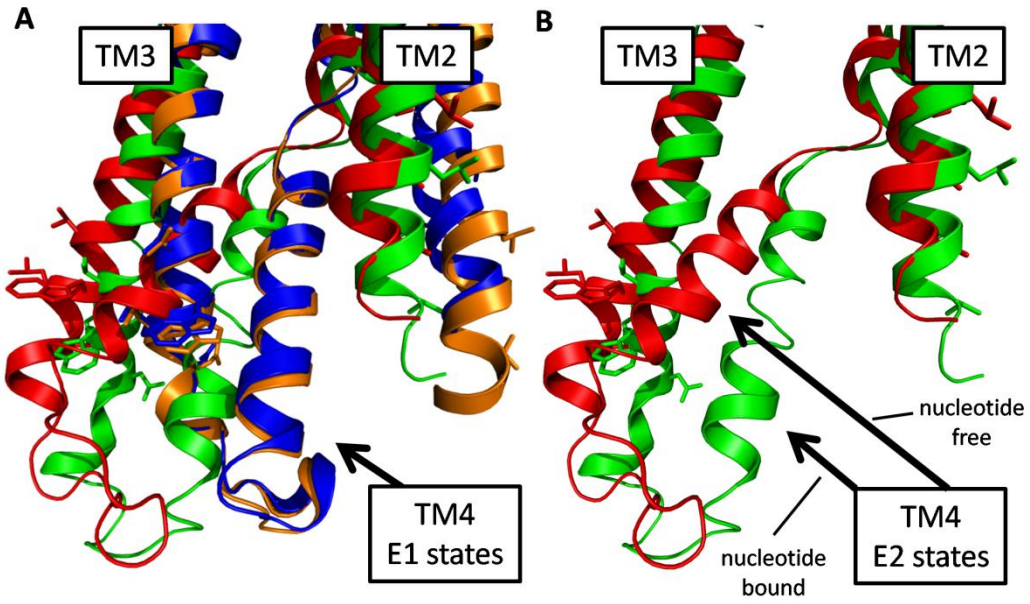

Figure 6.8. Positioning of TM4 relative to TM3 conformations in E1 and E2 representative SERCA structures. Panel A, representative SERCA structures for nucleotide-free (pdb: 1SU4 in *orange*)[8] and nucleotide-bound (pdb: 1T5S in *blue*)[14] E1 states are superimposed on representative SERCA structures for nucleotide-free (pdb: 3B9B in *red*) and nucleotide-bound (pdb: 3B9R in *green*). The positioning of TM3 and TM4 as a pair in similar in the E1 structures of SERCA. **Panel B,** the positioning of TM3 and TM4 is different between nucleotide-free (*red*) and nucleotide-bound (*green*) E2 structures of SERCA.

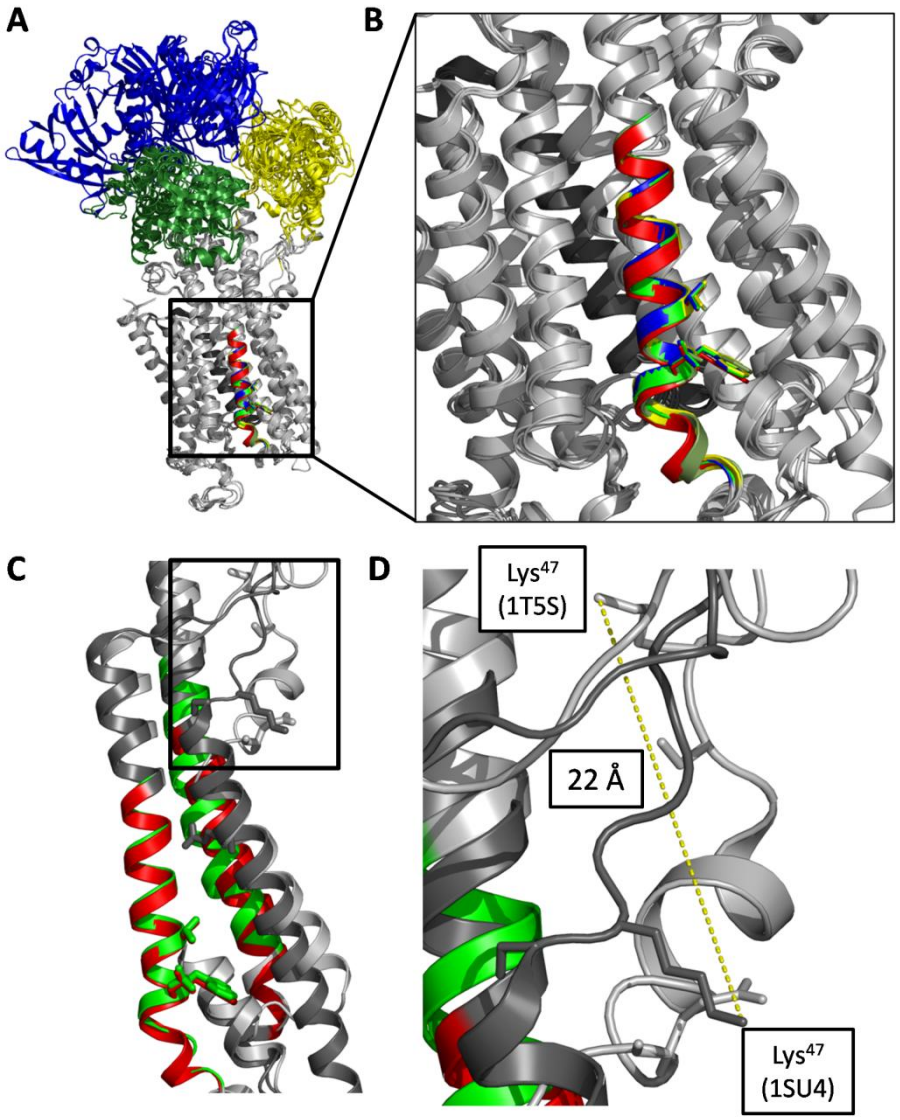

Figure 6.9. Superimposition of representative SERCA E1 structures centered on TM3. Panel A, superimposition of five reported high-resolution SERCA structures representing four E2 states (pdb: 1SU4, 1T5S, 1VFP, 1T5T, 3BA6)[8, 10, 14, 25]. **Panel A,** full enzyme cartoons of the superimposed E1 representative structures. **Panel B,** close-up view of TM3 region (box in panel A) to highlight the similar conformations within this region for all E1 representative structures.TM3 is coloured differently for each of the five reported E1 structures. **Panel C,** TM2 and TM3 are coloured red (1SU4)[8] or green (1T5S)[14] to highlight proposed PLB-binding sites relative to conformational changes in TM1 (*dark grey* – 1SU4[8]; *grey* – 1T5S[14]). **Panel D,** close-up view of the cytoplasmic ends of TM1 (box in panel C). Note the displacement of from this region is 22 between the nucleotide-free E1 structure (1SU4)[8] and the four nucleotide-bound E1 structures (represented by 1T5S)[14].

6-6. The role of SLN in the atria of the heart.

The consequences of SLN expression in the atria with PLB are of considerable interest. Co-expression of SERCA, PLB, and SLN in HEK-293 cells causes super-inhibition of SERCA, where the level of inhibition is greater than the sum of inhibition from separate SERCA-PLB and SERCA-SLN co-expression[26, 27]. The super-inhibitory mechanism was proposed to involve depolymerisation of PLB pentamers by SLN, increasing SERCA inhibition by increased mass action of PLB monomers [26, 27]. A common PLB and SLN binding site was proposed based on mutations in SERCA near TM6 that disrupted inhibition by both PLB and SLN[27]. However, co-immunoprecipitation data was consistent with a modified interaction in the super-inhibitory SERCA-PLB-SLN complex, primarily involving SLN[27].

The *in vitro* phosphorylation of SLN-Thr^{5} by CaMKII[28] has been difficult to reproduce. However, adenoviral transfer in rat myocytes suggests Thr^{5} of SLN could be an important target for phosphorylation[28]. It would be interesting to compare structural changes upon phosphorylation in SLN. The positioning of Thr^{5} in SLN aligns with Leu^{28} in PLB, which is located over 10 residues away from the PLB phosphorylation sites (Ser^{16} and Thr^{17}).

The expression of SLN in the atria also produces a novel regulatory complex that could form between SERCA, PLB and SLN simultaneously. In terms of heart disease therapies, little is known about the regulation of SERCA in the presence of both PLB and SLN, which occurs specifically in the atria. With respect to this, we have generated co-crystals from co-reconstitutions with SERCA, PLB and SLN. The SERCA-PLB-SLN co-crystals bear striking resemblance to SERCA-PLB co-crystals at low resolution and are sensitive to the presence of SLN. At current, the ~20 Å projection maps of SERCA-PLB-SLN co-crystals do not provide enough information to determine if the densities interspersed between the SERCA dimer ribbons belong to a PLB-SLN mixed oligomer or a PLB pentamer without SLN incorporated (data not shown). There is a predicted binding model for a SERCA-PLB-SLN complex based on Toyoshima's model of SERCA-PLB and co-immunoprecipitation in heterologous co-expression studies. We do not know how phosphorylation influences a potential SERCA-PLB-SLN complex.

6-7. The ultimate template: The SERCA-PLB complex as a drug target.

For the design of heart disease therapies that target SERCA, we have stressed the importance of understanding the relationship between SERCA and PLB. We have also alluded to the emerging importance of SLN in the atria. Thus, an important template for the structure-based design of small molecules or drugs targeting SERCA would be a high-resolution structure of SERCA in complex with PLB (as well as SERCA in complex with SLN and SERCA in complex with PLB and SLN). However, despite the large number of high-resolution structures of SERCA, there are no available high-resolution structures of SERCA in complex with its physiological binding partners.

We hope that our studies of SERCA-PLB and SERCA-SLN co-crystals will help fill this void. In collaboration with David Stokes, we have begun imaging tilt series of SERCA-PLB(Ile^{40}Ala) co-crystals for the 3D structure determination of pentameric PLB interacting with SERCA. A 3D structure would provide more details about TM3 as the modeled site of interaction than our current projection maps. As well, the first high-resolution structure of SERCA bound to Ca^{2+} was determined from crystal conditions that were "improved" from conditions for EM crystals[8]. We hope that our current studies might also lead to crystals suitable for high-resolution x-ray crystallography that have SERCA in complex with PLB, SLN or PLB and SLN. It is also exciting to consider the possibility of determining the structure of SERCA in complex with binding partners other than PLB and SLN. For example, it has been postulated that PKA can phosphorylate PLB while PLB is bound to SERCA[6]. In addition, it has been demonstrated that PLB can interact with A-kinase anchoring protein 18δ in rat heart SR and disruption of this interaction interfered with PLB phosphorylation[29]. Whether this interaction might also involve SERCA in unclear.

6-8. Closing perspectives.

The work in this thesis has provided a snapshot of SERCA in complex with its physiological regulators, PLB and SLN, in a previously unpredicted fashion. More specifically, we have identified an interaction between pentameric PLB and SERCA and between pentameric SLN and SERCA. The 3D structure determination of the complex between pentameric PLB and SERCA is currently underway and will provide important structural information for the therapeutic targeting of SERCA in failing hearts.

6-9. Materials and Methods.

6-9.1. Glutaraldehyde cross-linking of SERCA and PLB co-reconstitutions.

SERCA and PLB co-reconstitutions (50 to 75 μg total protein) were diluted to 5 x volumes with 20 mM imidazole, pH 7.0, 100 mM KCl and centrifuged at 40,000g for 30 min at 4°C. The supernatant was carefully aspirated away from the pellet. The pellet was resuspended in sodium acetate buffer to a final concentration of 10 mM and the samples were cross-linked by the addition of 0.01% or 0.1% glutaraldehyde at 4°C or 25°C. Cross-linking reactions were stopped after 5 min with tris-containing loading buffer and separated by SDS-PAGE.

Western blotting of cross-linking reactions. Co-reconstitutions were transferred to PVDF membrane at 100 V (350 mAmp) for 1 hour. Washed with TBS before blocking, the membrane was blocked in 0.5 % skim milk TBS, washed three times with TBST (0.1% Tween 20), probed with anti-PLB (2D12 - Abcam; 1:10,000 dilution) antibody or anti-SERCA1 antibody (IIH11 - Abcam; 1:5000 dilution), washed three times with TBST, probed with goat-anti-mouse secondary antibody (1:10,000 dilution) and rinsed with distilled water.

6-10. References.

1. James P, Inui M, Tada M, Chiesi M, Carafoli E. Nature and site of phospholamban regulation of the Ca-2+ pump of sarcoplasmic-reticulum. Nature 1989 NOV 2;342(6245):90-2.

2. Jones LR, Cornea RL, Chen ZH. Close proximity between residue 30 of phospholamban and cysteine 318 of the cardiac Ca2+ pump revealed by intermolecular thiol cross-linking. J Biol Chem 2002 AUG 2;277(31):28319-29.

3. Chen ZH, Stokes SL, Rice WJ, Jones LR. Spatial and dynamic interactions between phospholamban and the canine cardiac Ca2+ pump revealed with use of heterobifunctional cross-linking agents. J Biol Chem 2003 NOV 28;278(48):48348-56.

4. Toyoshima C, Asahi M, Sugita Y, Khanna R, Tsuda T, MacLennan DH. Modeling of the inhibitory interaction of phospholamban with the Ca2+ ATPase. Proc Natl Acad Sci U S A 2003 JAN 21;100(2):467-72.

5. Moller JV, Olesen C, Winther AL, Nissen P. The sarcoplasmic Ca2+-ATPase: Designof a perfect chemi-osmotic pump. Q Rev Biophys 2010 NOV;43(4):501-66.

6. MacLennan DH, Kranias EG. Phospholamban: A crucial regulator of cardiac contractility. Nature Reviews Molecular Cell Biology 2003 JUL;4(7):566-77.

7. Cantilina T, Sagara Y, Inesi G, Jones L. Comparative-studies of cardiac and skeletal sarcoplasmic-reticulum atpases - effect of a phospholamban antibody on enzyme activation by Ca2+. J Biol Chem 1993 AUG 15;268(23):17018-25.

8. Toyoshima C, Nakasako M, Nomura H, Ogawa H. Crystal structure of the calcium pump of sarcoplasmic reticulum at 2.6 angstrom resolution. Nature 2000 JUN 8;405(6787):647-55.

9. Toyoshima C, Nomura H. Structural changes in the calcium pump accompanying the dissociation of calcium. Nature 2002 AUG 8;418(6898):605-11.

10. Olesen C, Picard M, Winther AL, Gyrup C, Morth JP, Oxvig C, Moller JV, Nissen P. The structural basis of calcium transport by the calcium pump. Nature 2007 DEC 13;450(7172):1036-U5.

11. Toyoshima C, Nomura H, Tsuda T. Lumenal gating mechanism revealed in calcium pump crystal structures with phosphate analogues. Nature 2004 NOV 18;432(7015):361-8.

12. Toyoshima C, Norimatsu Y, Iwasawa S, Tsuda T, Ogawa H. How processing of aspartylphosphate is coupled to lumenal gating of the ion pathway in the calcium pump. Proc Natl Acad Sci U S A 2007 DEC 11;104(50):19831-6.

13. Olesen C, Sorensen TLM, Nielsen RC, Moller JV, Nissen P. Dephosphorylation of the calcium pump coupled to counterion occlusion. Science 2004 DEC 24;306(5705):2251-5.

14. Sorensen TLM, Moller JV, Nissen P. Phosphoryl transfer and calcium ion occlusion in the calcium pump. Science 2004 JUN 11;304(5677):1672-5.

15. Jensen AL, Sorensen TL, Olesen C, Moller JV, Nissen P. Modulatory and catalytic modes of ATP binding by the calcium pump. EMBO J 2006 JUN 7;25(11):2305-14.

16. Xu C, Rice WJ, He WZ, Stokes DL. A structural model for the catalytic cycle of Ca2+-ATPase. J Mol Biol 2002 FEB 8;316(1):201-11.

17. Young HS, Rigaud JL, Lacapere JJ, Reddy LG, Stokes DL. How to make tubular crystals by reconstitution of detergent-solubilized Ca2+-ATPase. Biophys J 1997 JUN;72(6):2545-58.

18. Glaves JP, Fisher L, Ward A, Young HS. Helical crystallization of two example membrane proteins: Msba and the Ca(2+)-ATPase. Methods in Enzymology, Vol 483: Cryo-Em, Part C: Analyses, Interpretation, and Case Studies 2010;483:143-59.

19. Young HS, Jones LR, Stokes DL. Locating phospholamban in co-crystals with Ca2+-ATPase by cryoelectron microscopy. Biophys J 2001 AUG;81(2):884-94.

20. Karim CB, Kirby TL, Zhang ZW, Nesmelov Y, Thomas DD. Phospholamban structural dynamics in lipid bilayers probed by a spin label rigidly coupled to the peptide backbone. Proc Natl Acad Sci U S A 2004 OCT 5;101(40):14437-42.

21. Cambrea LR, Haque F, Schieler JL, Rochet J, Hovis JS. Effect of ions on the organization of Phosphatidylcholine/Phosphatidic acid bilayers. Biophys J 2007 SEP;93(5):1630-8.

22. Lamberson ER, Cambrea LR, Hovis JS. Controlling the charge and organization of anionic lipid bilayers: Effect of monovalent and divalent ions. J Phys Chem B 2007 DEC 13;111(49):13664-7.

23. Warren G, Metcalfe J, Lee A, Birdsall N. Mg2+ regulates atpase activity of a calcium-transport protein by interacting with bound phosphatidic-acid. FEBS Lett 1975;50(2):261-4.

24. Mueller B, Karim CB, Negrashov IV, Kutchai H, Thomas DD. Direct detection of phospholamban and sarcoplasmic reticulum Ca-ATPase interaction in membranes using fluorescence resonance energy transfers. Biochemistry (N Y) 2004 JUL 13;43(27):8754-65.

25. Toyoshima C, Mizutani T. Crystal structure of the calcium pump with a bound ATP analogue. Nature 2004 JUL 29;430(6999):529-35.

26. Asahi M, Kurzydlowski K, Tada M, MacLennan DH. Sarcolipin inhibits polymerization of phospholamban to induce superinhibition of sarco(endo)plasmic reticulum Ca2+-ATPases (SERCAs). J Biol Chem 2002 JUL 26;277(30):26725-8.

27. MacLennan D, Asahi M, Tupling A. The regulation of SERCA-type pumps by phospholamban and sarcolipin. Na,k-Atpase and Related Cation Pumps: Structure, Function, and Regulatory Mechanisms 2003;986:472-80.

28. Bhupathy P, Babu GJ, Ito M, Periasamy M. Threonine-5 at the N-terminus can modulate sarcolipin function in cardiac myocytes. J Mol Cell Cardiol 2009 NOV;47(5):723-9.

29. Lygren B, Carlson CR, Santamaria K, Lissandron V, McSorley T, Litzenberg J, Lorenz D, Wiesner B, Rosenthal W, Zaccolo M, Tasken K, Klussmann E. AKAP complex regulates Ca2+ re-uptake into heart sarcoplasmic reticulum. EMBO Rep 2007 NOV;8(11):1061-7.

Appendix 1.

Prion fragments as models of disease: The beta-strand 1 region of the prion protein self assembles into fibrils in a species-dependent manner.

Acknowledgements: Dr. K. Alier kindly performed the electrophysiology experiments and D. MacTavish kindly performed the toxicity experiments. The three-dimensional reconstruction of the fibrils was developed and performed by Dr. H. Young.

Appendix 1. Prion fragments as models of disease: The beta-strand 1 region of the prion protein self assembles into fibrils in a species-dependent manner.

I-1. Introduction.

Misfolding of the prion protein (PrP) is central to the transmission and pathobiology of transmissible spongiform encephalopathies (TSEs), including Creutzfeldt-Jakob disease (CJD) in humans, bovine spongiform encephalopathy (BSE; or mad cow disease) in cattle, and chronic wasting disease (CWD) in deer, elk, and moose. All TSEs primarily target the brain, causing a sponge-like appearance associated with neuronal loss, and inevitably result in death. The TSE infectious agent has been postulated to be PrP alone, in the absence of any nucleic acids. This is better known as the "protein-only hypothesis", first proposed by Alper[1] and Griffith[2] in the late 1960's, and strongly promoted by the Nobel Laureate Stanley Prusiner[3] in the 1980's and 90's. To date, there is no cure for TSEs and death occurs rapidly following clinical diagnosis (usually within 8 months for CJD).

PrP misfolding converts the cellular form of PrP (PrP^{c}) to the disease-associated scrapie form (PrP^{Sc}). PrP^{c} is a glycosylated, α-helical protein with two short β-strands linked by a glycophosphatidylinositol anchor to the cell membrane. The physiological function of PrP^{c} is not known and likely involves a multitude of functions (a very large number of functions for PrP^{c} have been proposed that are currently the center of ongoing debates in the field). In contrast to PrP^{c}, the disease-associated PrP^{Sc} form is rich in β-sheet structure

and prone to aggregation[4], forming protease-resistant amyloid fibrils and plaques in diseased tissue. The conversion and transmission mechanisms relating PrP^{c} and PrP^{Sc} remain unclear.

If we subscribe to the "protein-only hypothesis", there exist two baffling characteristics of TSEs: prion "strains" and species transmission barriers. Prion "strains" are distinguishable TSE pathology profiles within a species. For example, two individuals of the same species can present different amounts and localization of PrP^{Sc} in the brain. Prion "strains" are also distinguished by variable levels of protease-resistance and incubation times (the time-course from exposure to clinical diagnosis and death). Species transmission barriers are naturally and experimentally observed variations in the transmission of TSEs between species. While one species is susceptible to transmission from a different species, a second species is not. For example, variable CJD results from the transmission of BSE to humans[5, 6], but BSE cannot be transmitted to rabbits. Thus, there exists a species barrier protecting some species from transmission. The species barrier concept is best exemplified in rabbits and guinea pigs which are considered "resistant" to TSE transmission[7].

The sequence of PrP between species is very similar and begs the question as to how differences that lead to prion "strains" and species barriers might arise? The determination of PrP^{c} structures from a wide range of species[8-13] has shown that, in addition to sequence homology, the structure of PrP^{c} is also very similar. The similarity of PrP^{c} within and between species suggests a common starting point for PrP^{Sc} conversion. From this standpoint, distinguishing features of "strains" and species barriers would culminate in the misfolding of PrP^{c} and resulting PrP^{Sc} structures. Thus, it is of great interest to study PrP^{c} to PrP^{Sc} conversion and PrP^{Sc} structures from different species. Unfortunately, the heterogeneous and aggregation-prone nature of PrP^{Sc} has complicated the study of its structure. Fortunately, small fragments of PrP that form amyloid-like fibrils and cause toxicity in cultured neurons have been identified that serve as simplified models of prion disease[14, 15]. Although still prone to aggregation, these smaller PrP fragments generate more homogeneous populations of PrP^{Sc}–like structures that are subsequently more amenable to high-resolution structural studies. Importantly, two of the PrP fragments, PrP(106-126) and PrP(127-147), formed fibrils that were similar in size to fibrils observed in diseased tissue. By studying the mechanisms and consequences of PrP misfolding using smaller fragments, we can reconstruct events in the misfolding of full-

length PrP. Understanding these molecular mechanisms on a species-to-species basis could provide insight into prion "strains" and species barrier phenomena.

In May 2003, a case of BSE was identified in the province of Alberta which led to a shutdown of cattle trade with the United States and Mexico to prevent potential BSE outbreaks. The Alberta cattle sector was devastated at all levels, from the feedlot to farm to meat processing centers. The introduction of rigorous testing and prevention measures has since re-opened trading and, for the time being, the Alberta cattle industry has recovered. Unfortunately, another PrP disease has since afflicted animals in the province of Alberta. The spread of CWD recently reached natural populations of deer, elk, and moose in Alberta and Saskatchewan. Since our understanding of TSE transmission within and between species is not complete, the presence of CWD in Alberta and Saskatchewan poses a serious threat. The inter-species transfer of CWD could provide a source of PrP disease that could transmit to other animals and potentially pose a risk towards the human population as well.

Herein, we have screened PrP peptides homologous to the (127-147) region (*human numbering*) of different species to study the resulting PrP^{Sc} structures. We chose this region for two key reasons: first, of the two PrP fragments that recapitulate PrP^{Sc}-like properties and serve as models of disease[14, 15], PrP(127-147) displays more sequence variability between species than PrP(106-126), and second, PrP(127-147) has been much less experimentally characterized than PrP(106-126). The PrP(127-147) peptides in this study were based on sequences of elk and bovine PrP, as these two species are central to TSE issues in Alberta (CWD in elk and BSE in bovine). We also studied the PrP(127-147) peptide based on hamster PrP, which has been an important prion research model for over three decades[16] and hamsters have relatively high susceptibility to TSE transmission among different species[17]. More importantly, we chose to study hamster PrP(127-147) because fibrils formed by a longer hamster PrP peptide have been structurally characterized by atomic force microscopy (AFM)[18-20] and provide a comparison for our studies by electron microscopy. Our results demonstrate that, structurally, the PrP(127-147) peptides adopt distinct populations of fibrils. The majority of elk PrP(127-147) and bovine PrP(127-147) fibrils are distinctly periodic, whereas hamster PrP(127-147) fibrils are primarily smooth and non-periodic. We generated three-dimensional (3D) reconstructions from negative stain electron microscope (EM) images of PrP(127-147) fibrils to highlight the structural differences between species. Compared to bovine

PrP(127-147) and hamster PrP(127-147), elk PrP(127-147) is distinct in its ability to enhance thioflavin T (ThT) fluorescence and its ability to reduce whole cell currents of rat basal forebrain neurons. We propose that PrP(127-147) would serve as an excellent model for understanding species-dependent variability in PrP^{Sc} structure at an atomic level.

I-2. Results and Discussion.

I-2.1. Sequence variability of PrP(106-126) and PrP(127-147) between species.

PrP(127-147) is naturally more variable than PrP(106-126) with respect to amino acid sequence between species (Figure I.1a). The sequences of elk PrP(106-126) and bovine PrP(106-126) are identical, and there is only one amino acid change in the hamster sequence at the equivalent position of 112 (Val in elk and bovine, Met in hamster). Although not a species studied herein, the human PrP(106-126) sequence is identical to hamster PrP(106-126). In terms of PrP misfolding, the region of (106-126) is unlikely to contribute differences between species given its high degree of similarity. The region of (127-147) in PrP, on the other hand, is variable between all three species of interest (Figure I.1b).

I-2.2. PrP(127-147) peptides have variable ThT-binding properties.

The misfolding of PrP can lead to the formation of amyloid fibrils, which are deposited in the diseased neuronal tissue. As a standard for the detection of amyloid fibril formation, the fluorescent dye ThT selectively binds amyloid fibrils *in vivo* and *in vitro*, resulting in a large increase in the ThT fluorescence emission. ThT has been used previously as a standard to detect *in vitro* formation of amyloid fibrils using PrP peptides[18]. We used ThT-binding to detect amyloid fibril formation using elk PrP(127-147), bovine PrP(127-147) and hamster PrP(127-147).

At millimolar concentrations, elk PrP(127-147) significantly increases ThT-fluorescence relative to bovine PrP(127-147) and hamster PrP(127-147) (Figure I.2). A control peptide, reverse-elk PrP(127-147), had no effect on ThT-fluorescence (data not shown). The increase in ThT-fluorescence occurs within minutes of resuspending lyophilized elk PrP(127-147) peptides and mixing with buffered ThT. At the highest screened concentrations (3 mM), hamster PrP(127-147) and bovine PrP(127-147) did not increase ThT-fluorescence relative to buffered ThT (data not shown).

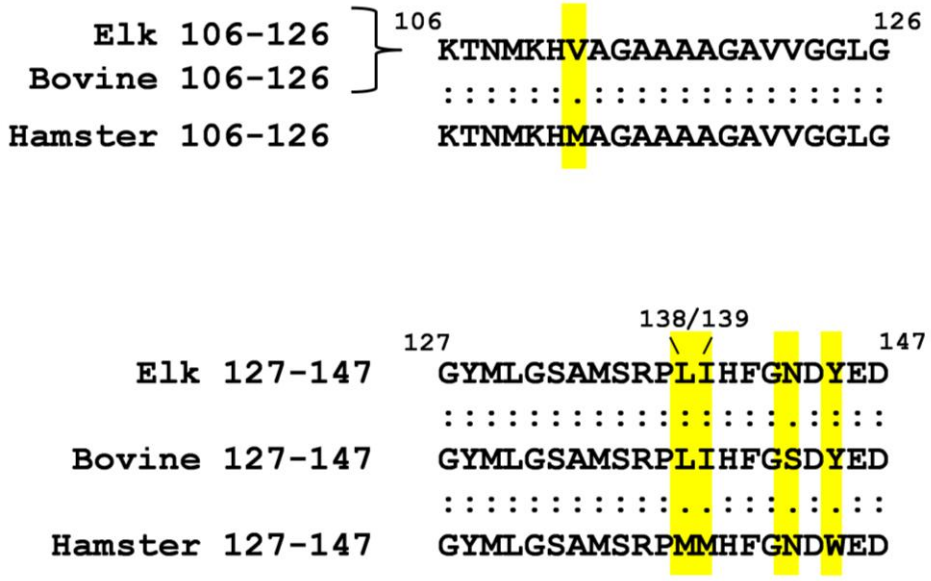

Figure I.1. Sequence variability in neurotoxic fragments PrP(106-126) and PrP(127-147) between elk, bovine and hamster. Alignment of amino acid sequences from the regions homologous to (106-126) and PrP(127-147) for elk (*Cervus elaphus* - GenBank: CAA70902.1), bovine (*Bos taurus* - GenBank: BAA01467.1) and hamster PrP (*Mesocricetus auratus* - GenBank: ABL75504.1). Conservative mutations between species are highlighted in yellow. Residues 138 and 139 have been identified to be involved in variable PrP(23-144) fibril structure and *in vitro* seeding characteristics between species[18-20].

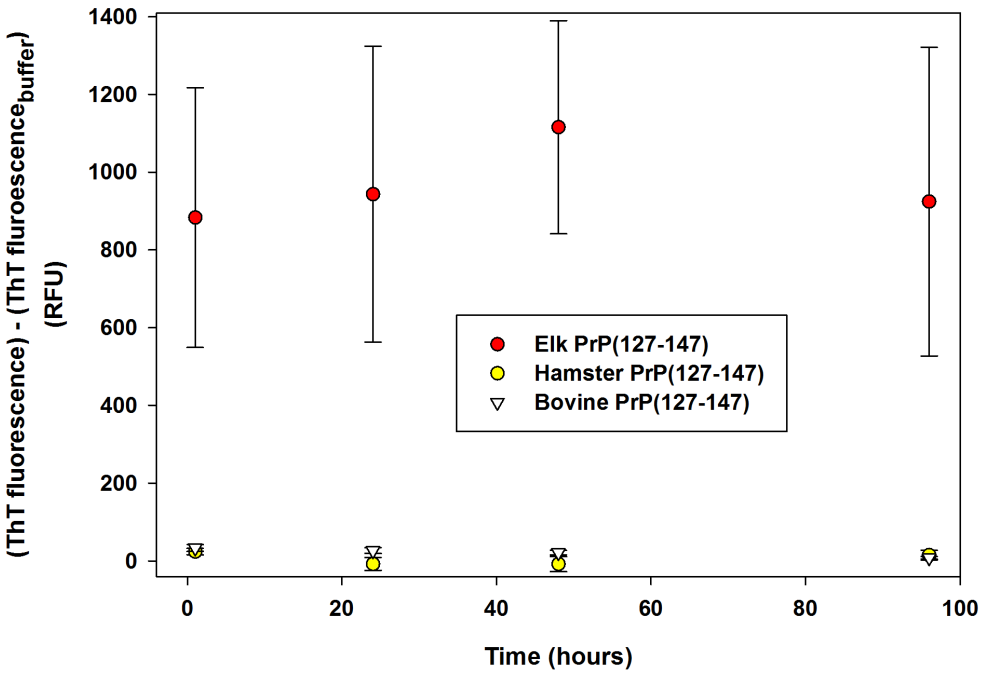

Figure I.2. ThT-fluorescence in the presence of PrP(127-147) peptides. Elk PrP(127-147) (*red circles*), bovine PrP(127-147) (*open triangles*) and hamster PrP(127-147) peptides (*yellow circles*) were resuspended at 1 mM in deionized water and incubated at 4°C. Samples were mixed with buffered ThT at various time-points to a final ThT concentration of 4 μM. ThT fluorescence emission between 450 and 600 nm was measured with 445 nm excitation on a M5 SpectraMax™ spectrofluorometer (Molecular Devices). The maximum ThT fluorescence (~480 nm) was plotted. Data represent the average of a minimum of three independent experiments +/- standard error of the mean (SEM).

I-2.3. PrP(127-147) fibril parameters show species-dependent populated states.

In addition to differences in ThT-binding properties, the elk, bovine and hamster PrP(127-147) peptides displayed variable fibril morphologies by negative-stain EM. The reverse elk PrP(127-147) peptide did not form any fibrils under identical conditions (data not shown). The elk PrP(127-147) peptide formed a very high frequency of fibrils following resuspension in deionized water (see inset Figure I.3a). The elk PrP(127-147) peptide formed a much larger number of fibrils relative to bovine PrP(127-147) and hamster PrP(127-147). The large number of fibrils and relatively high efficiency of fibril formation provides a possible explanation for the unique ability of elk PrP(127-147) to enhance ThT fluorescence. In terms of fibril width, elk PrP(127-147) fibrils were the thinnest overall (~14.1 nm), followed by bovine PrP(127-147) fibrils (~17.0 nm) and hamster PrP(127-147) fibrils (~18.4 nm) (Table I.1). Despite somewhat similar fibril widths, the PrP(127-147) peptides formed different fibril morphologies.

To quantify the different fibril morphologies, we measured fibril parameters from negative-stain EM images of elk PrP(127-147), bovine PrP(127-147) and hamster PrP(127-147) (Table I.1). The fibril parameters represent a minimum of three separate experiments for each PrP(127-147) peptide and 100 fibrils were surveyed for each species of interest. The parameters suggest the PrP(127-147) peptides adopt species-dependent fibril morphologies.

Elk PrP(127-147) formed homogeneous fibril populations dominated by helical periodic fibrils. The majority of elk PrP(127-147) fibrils were periodic (71%) with an average repeat distance of ~69.0 nm (Table I.1). The periodic fibril width and repeat distance were very similar between elk PrP(127-147) fibrils, and much more homogeneous compared to bovine PrP(127-147) and hamster PrP(127-147) fibrils.

Bovine PrP(127-147) also formed fibril populations dominated by periodic fibrils. The majority of bovine PrP(127-147) fibrils were periodic (57%) with a repeat distance of ~77.2 nm, larger than the repeat distance of elk PrP(127-147) fibrils (Table I.1). The periodic fibril width and repeat distance were more variable than elk PrP(127-147), but more homogeneous than hamster PrP(127-147) fibrils.

Hamster PrP(127-147) formed the most heterogeneous fibril population, which was dominated by smooth, non-periodic fibrils with a flat, ribbon-like appearance. Only a

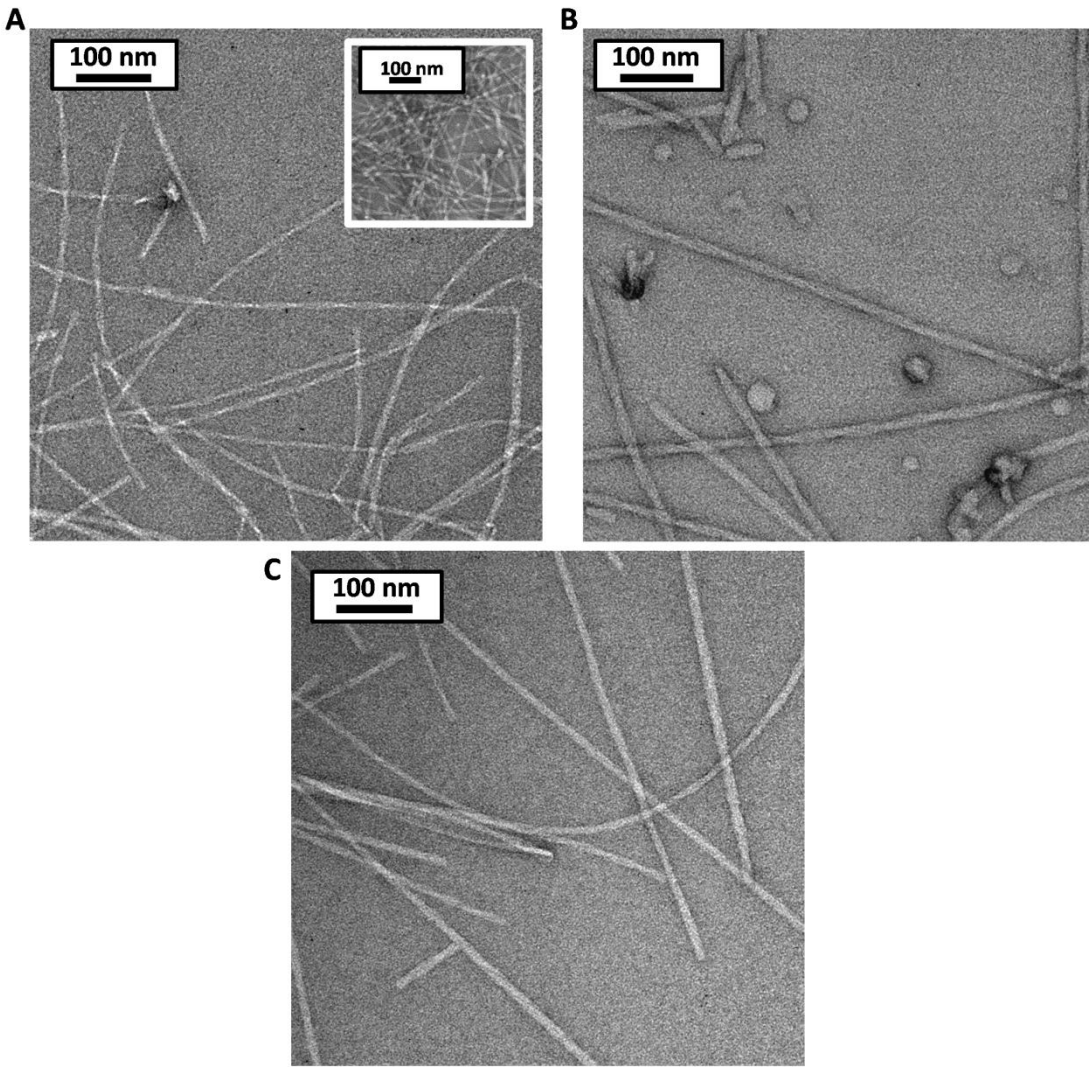

Figure I.3. Representative negative-stain electron microscope images of PrP(127-147) fibrils. Elk PrP(127-147) (inset panel A), bovine PrP(127-147) (panel B) and hamster PrP(127-147) peptides (panel C) resuspended at 1 mM in deionized water. Following 3 to 14 days of incubation at 4°C, samples were adsorbed to glow-discharged solid carbon grids and imaged. Elk PrP(127-147) formed a large number of fibrils (inset panel A). Following 1:10 dilution, the elk PrP(127-147) fibrils were of similar frequency as 1 mM resuspensions of bovine PrP(127-147) and hamster PrP(127-147). Scale bars are 100 nm. For detailed fibril parameters see Table I.1.

Table I.1. Fibril parameters of elk, bovine, and hamster PrP(127-147) by negative-stain electron microscopy. Fibril parameters were measured from negative-stain EM images (at a final resolution of 3.275 Å/pixel) using EMAN – boxer image software[21].

		Elk PrP (127-147)	Bovine PrP (127-147)	Hamster PrP (127-147)
All Fibrils				
n		100	100	100
Fibril width +/- SEM (nm)		14.1 +/- 0.4	17.0 +/- 0.3	18.4 +/- 0.4
range		8.5 – 22.7	7.3 – 23.0	11.1 – 26.9
(% included)		(98.0)	(99.0)	(97.0)
	Periodic			
	n	71	57	35
	Period +/- SEM (nm)	69.0 +/- 4.2	77.2 +/- 3.5	191.4 +/- 13.4
	range	47.9 – 78.2	32.7 – 124.0	53.2 – 338.0
	(% included)	(95.8)	(96.5)	(94.3)
	Min. fibril width +/- SEM (nm)	8.2 +/- 0.3	11.2 +/- 0.2	12.1 +/- 0.4
	range	5.5 – 13.4	7.7 – 14.0	7.5 – 15.9
	(% included)	(97.2)	(96.5)	(91.4)
	Max. fibril width +/- SEM (nm)	13.7 +/- 0.3	17.4 +/- 0.3	18.7 +/- 0.7
	Non-periodic			
	n	29	43	65
	Fibril width +/- SEM (nm)	15.1 +/- 0.9	16.2 +/- 0.6	18.7 +/- 0.7

minority of hamster PrP(127-147) fibrils formed periodic structures (35%) with an average repeat distance of ~191.4 nm, much larger than elk and bovine periodic fibrils (Table I.1). The periodic hamster PrP(127-147) fibrils were the most variable in terms of both fibril width and repeat distance, with no apparent homogeneity.

To visualize the relative homogeneity of periodic fibrils between elk, bovine and hamster PrP(127-147), a 3D plot of measured parameters on a per-fibril basis is shown in Figure I.4. The elk PrP(127-147) periodic fibrils are clustered tightly in all three dimensions reflecting their homogeneity. The bovine PrP(127-147) periodic fibrils are less homogeneous than elk PrP(127-147), but are relatively well clustered between two groups of periodic repeat distances (26% have smaller repeats between 30 and 60 nm, and 63% have larger repeats between 60 and 100 nm). The hamster PrP(127-147) fibrils are heterogeneous with highly variable repeat distances and do not cluster.

The non-periodic fibrils, overall, were similar between elk, bovine and hamster PrP(127-147). The trend of non-periodic fibril widths followed the trend of all fibrils in that elk fibrils were the thinnest (~15 nm), followed by bovine (~16 nm) and hamster fibrils (~19 nm) (Table I.1).

I-2.4. 3D reconstructions of elk PrP(127-147), hamster PrP(127-147), and bovine PrP(127-147) highlight differences in fibril morphologies.

To visualize the different fibril morphologies, we generated 3D reconstructions from representative fibril images for elk PrP(127-147), bovine PrP(127-147) and hamster (127-147). Periodic fibrils were selected because the inherent periodicity of the fibrils aided in the reconstruction process (see Materials and Methods). The final 3D reconstructions for representative elk PrP(127-147), bovine PrP(127-147) and hamster PrP(127-147) fibrils are shown with the average fibril parameters from surveyed EM images (Figure I.5).

I-2.5. Variable effects of PrP(127-147) peptides on whole cell currents of isolated rat basal forebrain neurons.

Recently, PrP(106-126) was observed to influence the whole cell currents of rat basal forebrain neurons at nanomolar concentrations[22]. At concentrations of 50 nm, human PrP(106-126) significantly decreased whole cell currents compared to control neurons in

the absence of PrP(106-126) treatment [22]. Because of the similar properties of PrP(106-126) and PrP(127-147), we investigated the effects of PrP(127-147) peptides on isolated rat basal forebrain neurons.

At concentrations of 100 nm, the elk PrP(127-147) peptide was able to significantly reduce the whole cell current of isolated rat basal forebrain neurons (n=11; Figure I.6a) compared to control neurons not treated with PrP(127-147) peptide. Preliminary observations of hamster PrP(127-147) (Figure I.6b) and bovine PrP(127-147) (data not shown) suggest these two peptides have no effect on the whole cell currents of rat basal forebrain neurons. It remains to be determined if the effects of elk PrP(127-147) on the whole cell currents results from its distinct fibrillar structure, its distinct ThT-positive amyloid properties, or some other characteristic that is not found in the hamster PrP(127-147) nor bovine PrP(127-147) peptides.

I-2.6. Visualizing PrP(127-147) in the context of cellular PrP structures.

The mouse PrP(121-231) structure determined by NMR[8] was the first structural view of PrP^c. As predicted[23], the PrP(121-231) structure was mainly α–helical, with three α-helices, but also contained two short unpredicted β–strands[9]. Overall, the mouse PrP(121-231) structure is representative of the mature full-length mouse PrP(23-231) structure, determined the following year, because the additional N-terminal region is unstructured[9]. As discussed previously, PrP^c structures have been determined for a wide range of species and overall these structures are very similar. To visualize this, we have aligned the (127-147) region from mouse, human, elk, hamster, and bovine PrP^c structures (Fig I-7a). The PrP(127-147) region is an extended structure, aside from the short β-strand 1 (residues 128-131), sandwiched between helix-1 (residues 144 to 154) and helix-3 (residues 200 to 217) with a solvent exposed surface[8]. Residues 134, 137, 139, and 141 contribute to the "stabilizing" hydrophobic core of the protein, composed of residues from all three alpha-helices, the second beta-strand and two other loops[8].

The interactions that occur in PrP^c will ultimately contribute to PrP misfolding as these interactions become altered during conversion to PrP^{Sc}, and minor variations in PrP^c between species will be important during conversion processes. As such, we do not want to overstate the similarity of PrP^c structure between species, since there is evidence that

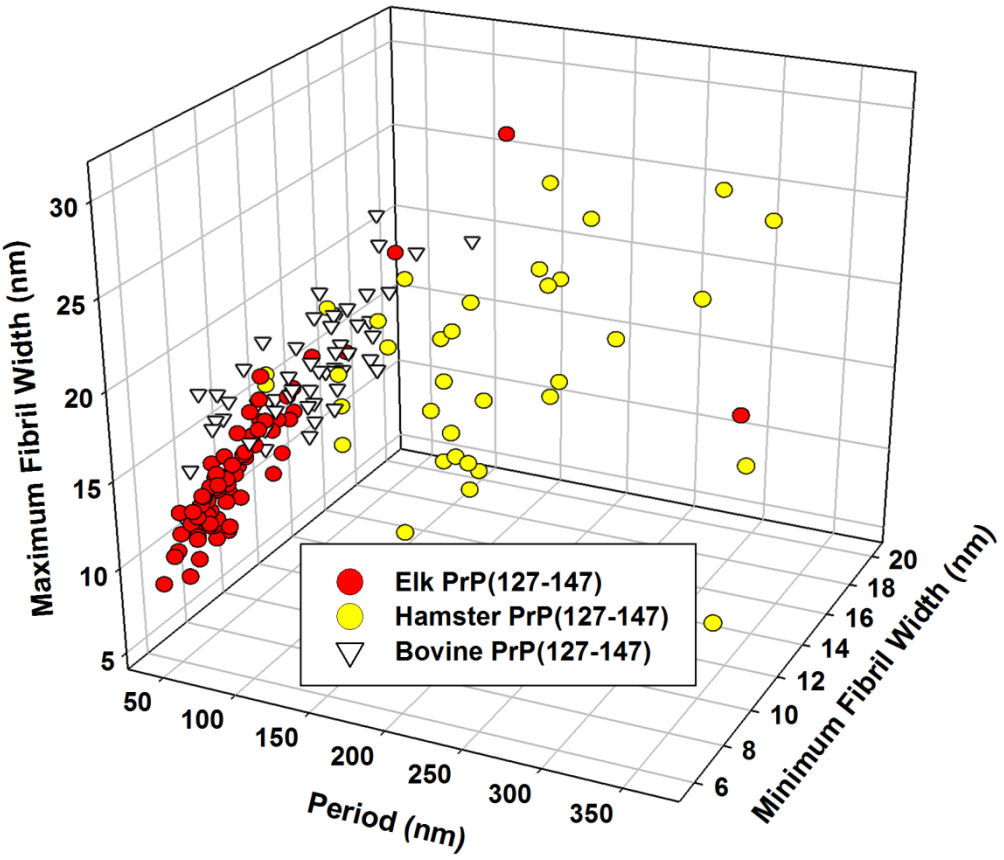

Figure I.4. Periodic fibril parameters of PrP(127-147) from different species in a 3D plot. Fibril parameters were measured from negative-stain EM images of elk, bovine, and hamster PrP(127-147) using EMAN - boxer[21]. Minimum and maximum fibril widths represent the average of three measurements per fibril. Period represents the average distance between neighbouring fibril width minimums for three measurements per fibril.

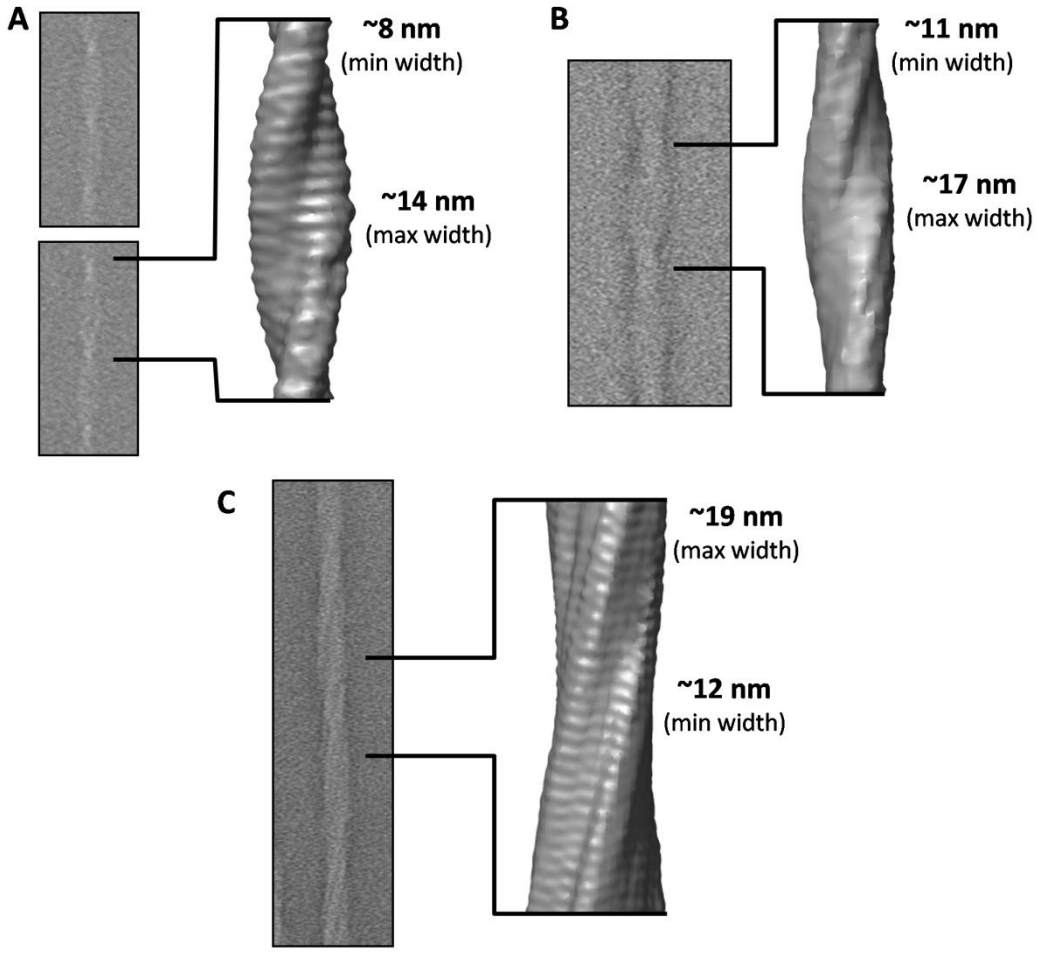

Figure I.5. Three-dimensional reconstructions of elk, bovine, and hamster PrP(127-147) periodic fibrils. Representative periodic fibrils were selected for elk PrP(127-147) (panel A), bovine PrP(127-147) (panel B) and hamster PrP(127-147) peptides (panel C). The 3D reconstructions were generated by digital boxing of periodic fibrils (see section I-3.4 in Materials and Methods). The presented 3D reconstructions were low-pass filtered to 20 Å resolution and are displayed with average fibril parameters from negative-stain EM images (Table I.1).

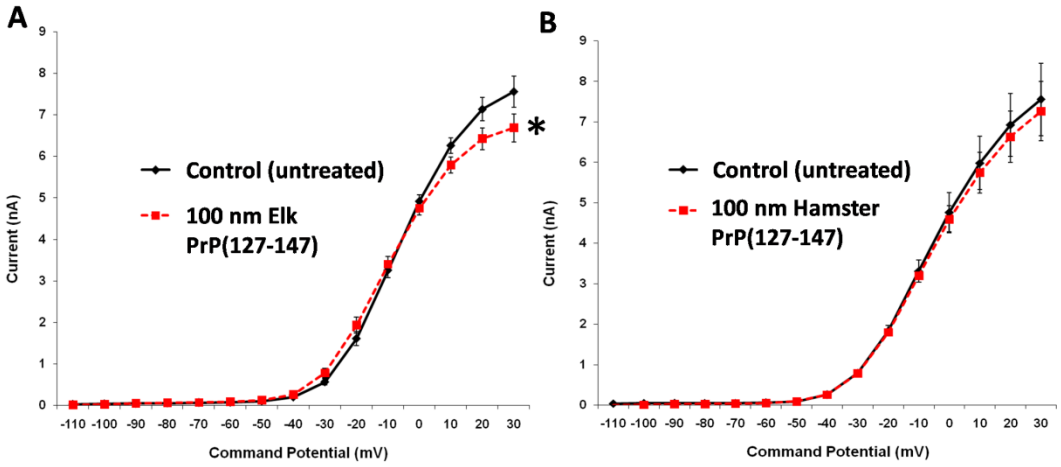

Figure I.6. Effects of elk and hamster PrP(127-147) peptides on the whole cell currents of rat basal forebrain neurons. Whole cell potassium currents were investigated in isolated rat basal forebrain neurons. Experiments were performed in the presence of PrP(127-147) and compared to controls performed in the absence of peptide application. **Panel A**, the current-voltage plot of reduction in whole cell current following elk PrP(127-147) treatment (100 nm, n = 9, *p <0.05). **Panel B**, the application of hamster PrP(127-147) had no effect on whole cell current (100 nm, n = 4). Error bars represent SEM.

species-to-species variability in PrP^c structures contributes to species transmission barriers (for a review see Sweeting et al. 2010)[17]. However, since our results suggest the sequence of PrP(127-147) alone can lead to variable fibril morphology, we will focus on the role of PrP(127-147) in oligomeric structures of PrP to see how PrP(127-147)-mediated variability might occur in PrP^{Sc} structures. Our hypothesis would require PrP(127-147) to come into contact with PrP(127-147) in an inter-molecular interaction.

Direct evidence that PrP(127-147) from different PrP molecules can interact comes from the structure of the sheep PrP^c crystal dimer[24]. Formation of the crystal dyad in the sheep PrP structure is mediated by β–strand 1 (residues 129-131) (Figure I.7b) and the dimer conformation presents a second β–strand region that was modeled by the authors as a locus for PrP tetramerization[24]. In this way, initial dimerization at β–strand 1 perpetuates PrP oligomerization. It is worth noting that other dimers have been observed in crystallized human[25] and rabbit PrP[26] that do not involve the PrP(127-147) region in the dimer interface. Such observations support more than one determinant for PrP oligomerization and suggest more than one interface could be involved.

I-2.7. The importance of PrP(127-147) in the GSS-associated peptide.

Potential roles of PrP(127-147) in PrP^{Sc} formation and structure come from studies of the Gertsmann-Straussler-Schienker syndrome (GSS) associated peptide. GSS is a rare, familial human TSE, and like other TSEs does not have a cure and inevitably results in death. The core PrP peptide in diseased GSS tissue is a truncated 7 kDa peptide from residue ~80 to ~145[27, 28]. In studies of a synthetic PrP(82-146) peptide, the PrP(127-146) region was critical to fibril morphology and amyloid-like properties[29]. If the (127-146) region was scrambled, the variant peptide had decreased aggregation and did not form fibrils. In contrast, scrambling of the (106-126) region did not prevent fibril formation. The authors suggested the charge distribution in the PrP(127-147) region might be important for the assembly of β–structures through electrostatic interactions[29]. Interestingly, the authors observed two distinct PrP(82-146) fibril populations; thin (5.5 nm) fibrils and wider (9.8 nm) fibrils. The dimensions of the PrP(82-146) fibril populations were in close agreement with the elk PrP(127-147) periodic fibrils, which had a 5.5 nm minimum fibril width and an average of 8.2 nm (Table I.1). The amyloid-positive ThT-binding of the elk PrP(127-147) peptide also mimicked the PrP(82-146)

peptide supporting the study of the PrP(127-147) peptide as a model of GSS disease. However, the authors made no mention of periodicity observed in the PrP(82-146) fibrils.

In another study of GSS-associated PrP peptides, Surewicz and coworkers demonstrated that residues 138 and 139 confer different fibril morphologies and *in vitro* seeding characteristics to human, mouse, and hamster PrP(23-144) variants[18-20]. Similar to the predominant hamster PrP(127-147) fibril morphology observed in this study, hamster PrP(23-144) characterized by AFM formed smooth, featureless fibrils with no apparent repeat. Both human and mouse PrP(23-144) formed periodic fibrils with repeat distances of 30 nm[20]. Overall, the study of PrP(23-144) from different species (human, mouse and hamster) correlated fibril morphology with *in vitro* seeding capabilities and identified that residues 138 and 139 within the (127-147) region provided variability to PrP^{Sc} structure[20]. In this study, both the elk and bovine PrP(127-147) peptides formed periodic fibrils with repeat distances of 69 nm and 77 nm, respectively. In terms of sequence, the elk and bovine contain $Leu^{138}Ile^{139}$ which is similar to the human $Ile^{138}Ile^{139}$ sequence that

formed periodic PrP(23-144) fibrils by AFM[20]. Interestingly, studies of recombinant human PrP(91-231) by cryo-EM also characterized periodic fibrils with variable repeat distances between 85 and 120 nm[30]. Our results suggest PrP(127-147) peptides resemble PrP^{Sc} structures formed by larger fragments of PrP, and thus recapitulate species-dependent differences in a simpler model for high resolution structural studies.

I-2.8. Towards high-resolution structures of PrP fibrils.

Studying PrP^{Sc} structure between species on a per-residue basis will aid in our understanding of species transmission barriers. As mentioned previously, PrP^{Sc} from diseased tissue is heterogeneous which subsequently limits the resolution of structural studies. As we advance towards higher resolution PrP^{Sc} models[31-33], it would be worthwhile to characterize smaller fragments of PrP in PrP^{Sc}-like structures. On this front, there is a structural model of human PrP(106-126) fibrils from solid-state NMR that reveals side-chain interactions[34]. Each protofibril in the PrP(106-126) fibril is a stack of in-register, parallel β–strands, and each in-register protofibril faces a second protofibril in an anti-parallel fashion[34] (Figure I.8a). The PrP(106-126) fibrils are stabilized by hydrophobic interactions between the corresponding middle regions of β–strands between protofibrils, His^{111} – His^{111} ring stacking between stacked β-strands, and an electrostatic

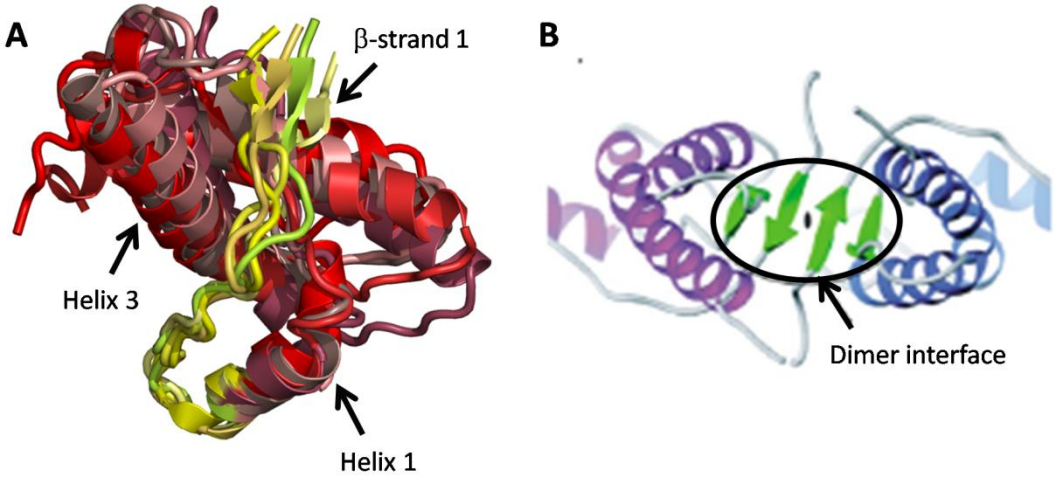

Figure I.7. Superimposition of the PrP(127-147) regions from PrPc structures from different species. Panel A, elk, bovine, and hamster PrP^c structures are aligned with the mouse and human PrP^c structures to highlight global similarity. The elk PrP^c is in red with a yellow (127-147) region. The other structures are coloured in gradations of red with their respective (127-147) regions in gradations of yellow. The backbone α–carbons between residues 137 to 147 have been aligned using PyMOL (The PyMOL Molecular Graphics System, Version 0.99, Schrödinger, LLC.). The PDB accession codes for the structures used in the superimposition were: elk–1XYW, bovine-1DX1, hamster-1B10, mouse-1AG1, human-1QM3. **Panel B**, the dimer interface of sheep PrP^c is mediated by β–strand 1. The sheep PrP^c crystals dimer is shown with one monomer in purple and the other monomer in blue. β–strand 1 and β–strand 2 are shown in green for both monomers. β–strand 1 (residues 129-131) mediates the crystal dyad (indicated by black oval). Figure adapted from Haire et al. 2004[24].

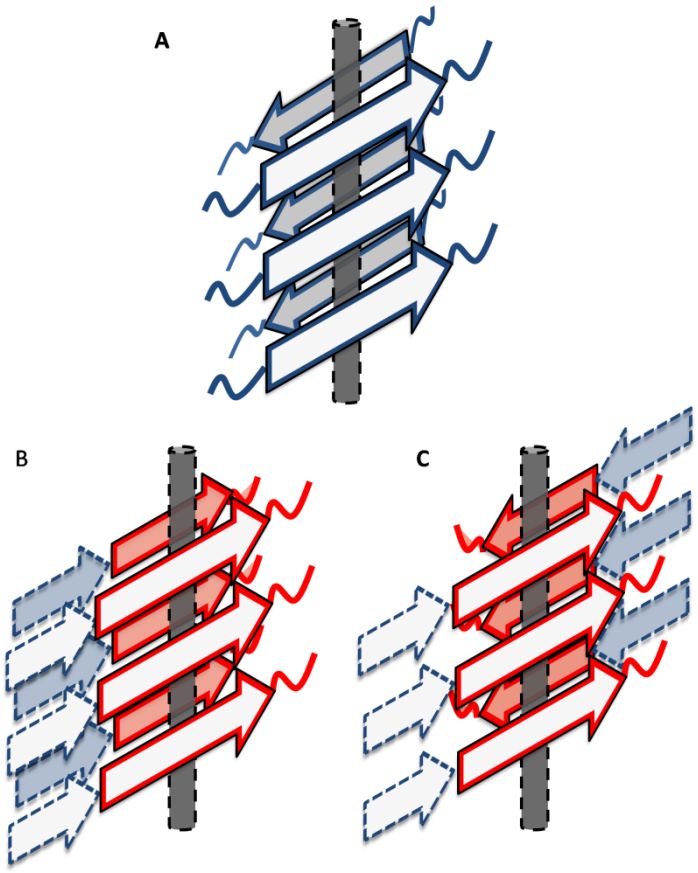

Figure I.8. The consequences of parallel and anti-parallel arrangements in the PrP(127-147) fibrils on the arrangement of the PrP(106-126) interface. Panel A, schematic representation of the anti-parallel protofibril arrangement in the PrP(106-126) fibril model[34]. One protofibril (white arrows) interacts in an anti-parallel fashion with a second protofibril (light blue) across the long PrP(106-126) fibril axis (dashed cylinder). **Panels B and C**, schematic representations of possible parallel (panel B) and anti-parallel (panel C) protofibril arrangements in PrP(127-147) fibrils (red arrows). Given the anti-parallel arrangement in PrP(106-126) fibrils, the co-existence of PrP(106-126) and PrP(127-147) interfaces cannot be satisfied by a single interface in either PrP(127-147) protofibril arrangement (dashed blue arrows in panels B and C do not satisfy the arrangement in panel A).

interaction between K^{110} and the C-terminus of anti-parallel β-strands between protofibrils[34].

We also have a structural model of human PrP(127-147) protofibrils[35], but not of PrP(127-147) fibrils. The PrP(127-147) protofibril is also a stack of in-register, parallel β–strands similar to the PrP(106-126) protofibrils. However, the PrP(127-147) protofibrils are not continuous β–strands, but are disrupted at Pro^{137} into two short β–strands[35]. In order to satisfy close β–strand interaction, the authors "arbitrarily twisted" the stacked β–strands by 2.8°, which was reduced to 2.4° in the final model[35]. Given a inter-β-strand distance of 5.5 Å parallel to the long protofibril axis[35], each protofibril would turn 180° over a distance of ~41 nm (~75 β-strands). This is comparable to the periodic distances we have characterized for elk PrP(127-147) and bovine PrP(127-147) fibrils (~69 nm and ~77 nm, respectively). The disruption at Pro^{137} could provide different degrees of protofibril twist if Pro^{137} influences, or is influenced by, the nature of its neighbouring amino acids such as residues 138 and 139. In the PrP(127-147) fibril model the authors support multiple protofibrils in each fibril based on the width of fibrils measured by EM in their preparations[35]. The degree of protofibril twist likely influences inter-protofibril interactions in PrP(127-147) fibrils.

Unfortunately, we do not know if PrP(127-147) protofibrils are arranged in an anti-parallel fashion like PrP(106-126) fibrils, or interact in a parallel fashion. Despite the parallel or antiparallel arrangement of PrP(127-147) protofibrils, the interface will not comply with the anti-parallel interface observed between PrP(106-126) protofibrils in the context of a single, homogeneous interface in full-length PrP fibril formation (Figure I.8b and Figure I.8c). As such, there may be competing fibril interfaces during the formation of full-length PrP^{Sc} structure, which could result in a heterogeneous mixture of fibril interfaces. In terms of the elk PrP(106-126) and PrP(127-147) regions acting as competing interfaces, it is interesting that elk PrP(106-147) peptides form periodic fibrils similar to the elk PrP(127-147) peptide alone (data not shown). We discussed the possibility of multiple determinants for PrP oligomerization and multiple oligomerization interfaces based on high-resolution crystallized dimers of PrP^{c} structures. Determining the nature and interplay of these interfaces will be important for understanding PrP misfolding in disease.

Consistent with our results with PrP(127-147), PrP(138-143) crystals have variable β-structures between species mediated by different inter-residue interactions, and these differences result in different inter-strand orientations[36]. Specifically, human and mouse PrP(138-143) crystallize in a parallel-stacked arrangement, whereas hamster PrP(138-143) stacks in an anti-parallel fashion[36]. Worth noting is that crystals of PrP(170-175) also display species-dependent structures at atomic resolution[36-38] and, in addition to PrP(127-147), could also lead to variability between PrP^{Sc} structures from different species. Competing fibril interfaces could help explain the heterogeneous nature of PrP^{Sc} in diseased tissue. We suggest the PrP(127-147) interface plays a critical role in PrP misfolding, because the fibril morphology of PrP(127-147) peptides is similar to the variable fibril morphologies between species observed in longer fragments, such as the human, mouse and hamster GSS-model PrP peptides[18-20].

Understanding species-dependent mechanisms of PrP^{Sc} formation and structure at a molecular level will benefit our understanding of TSE transmission in natural populations. To this point, we have discussed species barriers in a linear manner between two species. However, in natural populations, different species do not interact in a strictly linear manner and there is a complex web of species interactions. With respect to CWD, which is currently affecting natural populations of deer, elk and moose in Alberta and Saskatchewan, the implications of inter-species interactions could potentially alter the host range of CWD and provide means for bypassing linear species barriers. An example of the host range of CWD being altered upon passage through different species has been shown experimentally[39]. It had been difficult to passage CWD to hamsters[39], despite the relatively high susceptibility of hamsters to TSE transmission among different species[17] and thus, there was a strong species barrier protecting hamsters from CWD. However, if the CWD was first passaged to ferrets, the ferret-passaged CWD could then transmit more readily to hamsters, altering the apparent host range of CWD[39]. Such implications underscore the importance for furthering our understanding of species barriers to control the spread of TSEs in natural populations.

I-3. Materials and Methods.

I-3.1. Sequence of elk, bovine and hamster PrP(127-147) peptides.

Peptides used in this study are as follows:

Elk PrP(127-147) NH_2-GYMLGSAMSRPLIHFGSDYED-COOH,

Bovine PrP(127-147) NH_2-GYMLGSAMSRPLIHFGNDYED-COOH,

Hamster PrP(127-147) NH_2-GYMLGSAMSRPMMGSDWED-COOH,

Reverse elk PrP(127-147) NH_2-DEYDSGFHILPRSMASGLMYG-COOH,

Human PrP(106-126) NH_2-KTNMKHMAGAAAAGAVVGGLG-COOH.

All peptides were purchased from Biomatik Corp. (Toronto, Canada), except human PrP(106-126) which was purchased from Bachem (California, USA). All peptides were of greater than 95% purity as confirmed by HPLC and mass spectrometry.

I-3.2. ThT fluorescence assays.

Binding of ThT (Sigma) to PrP(127-147) peptides was assayed by adding freshly prepared ThT in PBS to PrP(127-147) peptides resuspended in deionized water. The final concentration of ThT was 4 μM. Fluorescence emission spectra were measured between 450 to 600 nm with 445 nm excitation using a M5 SpectraMax™ spectrofluorometer (Molecular Devices). Background ThT fluorescence was measured using a control sample containing only buffered ThT and water. ThT fluorescent values represent the fluorescence maximum at ~490 nm for a minimum of three independent experiments.

I-3.3. Electron microscopy.

Fibrils were imaged in a JEOL 2200FS electron microscope (JEOL Ltd., Tokyo, Japan) in the Electron Microscopy Facility (National Institute for Nanotechnology, University of Alberta and National Research Council of Canada) operated at 200 kV. A standard room temperature holder was used for negatively-stained samples. Images were recorded on image plates at a magnification of 45,800x. The image plates were scanned at 15 μm/pixel for a final resolution of 3.28 Å/pixel. All data were recorded with defocus levels of 1-2 μm.

I-3.4. Three-dimensional fibril reconstruction from negative-stain electron microscope images.

Representative periodic fibrils were selected from a set of at least 80 images for each PrP(127-147) peptide. Individual fibrils were many microns in length and could be segmented along the helical axis into (typically) 300 pixels by 300 pixels sized boxes, with the boxes spaced 2-5 pixels apart. For each individual fibril, a set of boxes covering at least one helical turn was obtained in this manner. By measuring the repeat distance of the helical fibril, we could estimate the angular orientation of each box in the set. The underlying assumption here was that each box represents an identical view of the fibril, where each view is rotated according to the helical twist. By assigning these angles to each image in the set, we could generate a preliminary 3D reconstruction by back projection of the 2D images into a 3D volume. The preliminary 3D reconstruction could then be refined against a larger set of image boxes from multiple similar fibrils to obtain the final 3D reconstruction. The image processing software SPIDER[40] was used for the reconstruction process.

I-3.5. Toxicity assay of PrP(127-147) peptides using rat primary fetal cortical neurons.

Rat primary fetal cortical neurons were grown in 96-well plates and cell viability was measured using the MTT (3-(4,5-Dimethylthiazol-2-yl)-2,5-diphenyltetrazolium bromide) assay. MTT was dissolved in DMSO, applied for 90 min. MTT absorbance was measured at 545 nm. Cell viability was measured following 48 hr exposure to PrP(127-147) peptides at various concentrations. Cell viability was measured as a percentage of control cell viability with no peptide application (set at 100% cell viability).

We also screened the PrP(127-147) peptides for toxicity using cultured rat primary fetal cortical neurons. All of the peptides displayed low levels of toxicity, achieving ~60% toxicity after 48 hr exposure regimes at 150 μM concentrations (Figure I.9). This toxicity was comparable to human PrP(106-126) peptide used as a positive control (~50% toxicity at 150 μM). Interestingly, the level of toxicity was similar between elk and hamster PrP(127-147) peptides suggesting that, under the experimental conditions, toxicity is not influenced by differences in their respective fibrillar structures. The bovine PrP(127-147) peptide was slightly less toxic than the elk and hamster PrP(127-147) peptides (Figure I.9). The reverse-elk PrP(127-147) peptide had a very small effect on neuron viability at these concentrations (Figure I.9).

I-3.6. Whole cell current recordings of PrP(127-147) treated rat basal forebrain neurons.

Whole cell current recordings were performed as described previously[22]. Briefly, rat basal forebrain neurons were isolated from the diagonal band of Broca and identified by visual inspection. Diagonal band of Broca neurons have been reported to be involved in learning and memory[41-43]. Whole-cell patch recording were measure at room temperature using an Axopatch-1D amplifier. Series resistance compensation was adjusted to 80% during the course of each experiment. The internal patch pipette solution contained: 140 mM K-methylsulfate, 10 mM EGTA, 5 mM $MgCl_2$, 1 mM $CaCl_2$, 10 mM HEPES pH 7.2, 2.2 mM Na_2-ATP, and 0.3 mM Na-GTP. After whole-cell configuration was established, the cells were allowed to stabilize for 5 min. Cells were held in voltage clamp at -80 mV, then hyper-polarized for 1 sec by changing the command potential to -110 mV to remove potassium channel inactivation. Subsequently, a slow voltage ramp to +30 mV was applied (20 mV/sec). No tail currents were observed at the end of the ramp when the voltage was returned to -80 mV suggesting the ramp excited primarily steady-state currents. Membrane currents were recorded and analyzed using pCLAMP software (version 10.1).

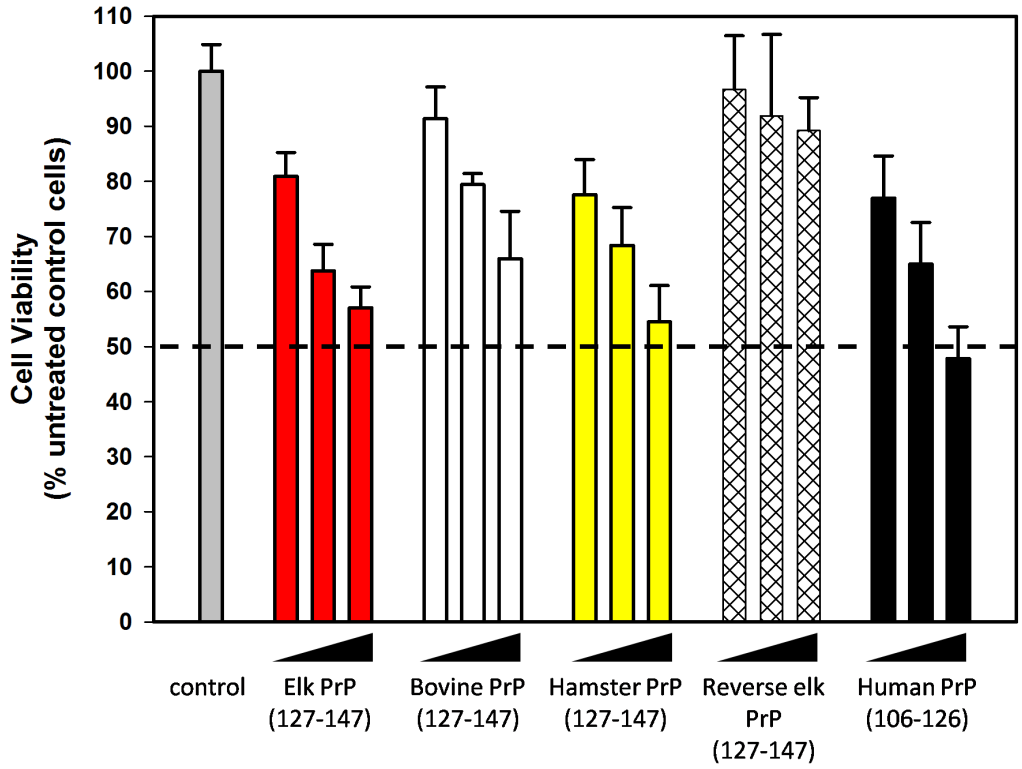

Figure I.9. Toxicity of PrP(127-147) peptides on viability of rat fetal primary cortical neurons. Rat primary fetal cortical neurons were grown in 96-well plates and cell viability was determined using the MTT assay. Neurons were treated with 50, 100, and 150 μM concentrations of PrP(127-147) peptide in the media. Neurons were assayed for viability following a 48 hr growth period after PrP(127-147) treatment. MTT was incubated with the neurons at a concentration of 5 mg mL^{-1} for 90 min and MTT absorbance was measured at 545 nm. Values are expressed as the percentage of control cell viability (no peptide treatment; set as 100% cell viability). Error bars represent SEM for a minimum of three technical replicates.

I-4. References.

1. Alper T, Cramp WA, Haig DA, Clarke MC. Does agent of scrapie replicate without nucleic acid. Nature 1967;214(5090):764,&.

2. Griffith JS. Self-replication and scrapie. Nature 1967;215(5105):1043,&.

3. Prusiner SB. Prions. Proc Natl Acad Sci U S A 1998 NOV 10;95(23):13363-83.

4. Pan KM, Baldwin M, Nguyen J, Gasset M, Serban A, Groth D, Mehlhorn I, Huang ZW, Fletterick RJ, Cohen FE, Prusiner SB. Conversion of alpha-helices into beta-sheets features in the formation of the scrapie prion proteins. Proc Natl Acad Sci U S A 1993 DEC 1;90(23):10962-6.

5. Hill AF, Desbruslais M, Joiner S, Sidle KCL, Gowland I, Collinge J, Doey LJ, Lantos P. The same prion strain causes vCJD and BSE. Nature 1997 OCT 2;389(6650):448-50.

6. Bruce ME, Will RG, Ironside JW, McConnell I, Drummond D, Suttie A, McCardle L, Chree A, Hope J, Birkett C, Cousens S, Fraser H, Bostock CJ. Transmissions to mice indicate that 'new variant' CJD is caused by the BSE agent. Nature 1997 OCT 2;389(6650):498-501.

7. Gibbs CJ, Gajdusek DC. Experimental subacute spongiform virus encephalopathies in primates and other laboratory-animals. Science 1973;182(4107):67-8.

8. Riek R, Hornemann S, Wider G, Billeter M, Glockshuber R, Wuthrich K. NMR structure of the mouse prion protein domain PrP(121-231). Nature 1996 JUL 11;382(6587):180-2.

9. Riek R, Hornemann S, Wider G, Glockshuber R, Wuthrich K. NMR characterization of the full-length recombinant murine prion protein, mPrP(23-231). FEBS Lett 1997 AUG 18;413(2):282-8.

10. Zahn R, Liu AZ, Luhrs T, Riek R, von Schroetter C, Garcia FL, Billeter M, Calzolai L, Wider G, Wuthrich K. NMR solution structure of the human prion protein. Proc Natl Acad Sci U S A 2000 JAN 4;97(1):145-50.

11. Garcia FL, Zahn R, Riek R, Wuthrich K. NMR structure of the bovine prion protein. Proc Natl Acad Sci U S A 2000 JUL 18;97(15):8334-9.

12. Gossert AD, Bonjour S, Lysek DA, Fiorito F, Wuthrich K. Prion protein NMR structures of elk and of mouse/elk hybrids. Proc Natl Acad Sci U S A 2005 JAN 18;102(3):646-50.

13. James TL, Liu H, Ulyanov NB, FarrJones S, Zhang H, Donne DG, Kaneko K, Groth D, Mehlhorn I, Prusiner SB, Cohen FE. Solution structure of a 142-residue recombinant prion protein corresponding to the infectious fragment of the scrapie isoform. Proc Natl Acad Sci U S A 1997 SEP 16;94(19):10086-91.

14. Forloni G, Angeretti N, Chiesa R, Monzani E, Salmona M, Bugiani O, Tagliavini F. Neurotoxicity of a prion protein-fragment. Nature 1993 APR 8;362(6420):543-6.

15. Tagliavini F, Prelli F, Verga L, Giaccone G, Sarma R, Gorevic P, Ghetti B, Passerini F, Ghibaudi E, Forloni G, Salmona M, Bugiani O, Frangione B. Synthetic peptides homologous to prion protein residues 106-147 form amyloid-like fibrils in-vitro. Proc Natl Acad Sci U S A 1993 OCT 15;90(20):9678-82.

16. Prusiner SB, Groth DF, Cochran SP, Masiarz FR, Mckinley MP, Martinez HM. Molecular-properties, partial-purification, and assay by incubation period measurements of the hamster scrapie agent. Biochemistry (N Y) 1980;19(21):4883-91.

17. Sweeting B, Khan MQ, Chakrabartty A, Pai EF. Structural factors underlying the species barrier and susceptibility to infection in prion disease. Biochemistry and Cell Biology-Biochimie Et Biologie Cellulaire 2010 APR;88(2):195-202.

18. Kundu B, Maiti NR, Jones EM, Surewicz KA, Vanik DL, Surewicz WK. Nucleation-dependent conformational conversion of the Y145Stop variant of human prion protein: Structural clues for prion propagation. Proc Natl Acad Sci U S A 2003 OCT 14;100(21):12069-74.

19. Vanik DL, Surewicz KA, Surewicz WK. Molecular basis of barriers for interspecies transmissibility of mammalian prions. Mol Cell 2004 APR 9;14(1):139-45.

20. Jones EM, Surewicz WK. Fibril conformation as the basis of species- and strain-dependent seeding specificity of mammalian prion amyloids. Cell 2005 APR 8;121(1):63-72.

21. Ludtke SJ, Baldwin PR, Chiu W. EMAN: Semiautomated software for high-resolution single-particle reconstructions. J Struct Biol 1999 DEC 1;128(1):82-97.

22. Alier K, Li Z, MacTavish D, Westaway D, Jhamandas JH. Ionic mechanisms of action of prion protein fragment PrP(106-126) in rat basal forebrain neurons. J Neurosci Res 2010 AUG 1;88(10):2217-27.

23. Hornemann S, Glockshuber R. Autonomous and reversible folding of a soluble amino-terminally truncated segment of the mouse prion protein. J Mol Biol 1996 SEP 6;261(5):614-9.

24. Haire LF, Whyte SM, Vasisht N, Gill AC, Verma C, Dodson EJ, Dodson GG, Bayley PM. The crystal structure of the globular domain of sheep prion protein. J Mol Biol 2004 MAR 5;336(5):1175-83.

25. Knaus KJ, Morillas M, Swietnicki W, Malone M, Surewicz WK, Yee VC. Crystal structure of the human prion protein reveals a mechanism for oligomerization. Nat Struct Biol 2001 SEP;8(9):770-4.

26. Khan MQ, Sweeting B, Mulligan VK, Arslan PE, Cashman NR, Pai EF, Chakrabartty A. Prion disease susceptibility is affected by beta-structure folding propensity and local side-chain interactions in PrP. Proc Natl Acad Sci U S A 2010 NOV 16;107(46):19808-13.

27. Tagliavini F, Prelli F, Porro M, Rossi G, Giaccone G, Farlow MR, Dlouhy SR, Ghetti B, Bugiani O, Frangione B. Amyloid fibrils in gerstmann-straussler-scheinker disease (indiana and swedish kindreds) express only prp peptides encoded by the mutant allele. Cell 1994 NOV 18;79(4):695-703.

28. Tagliavini F, Lievens PMJ, Tranchant C, Warter JM, Mohr M, Giaccone G, Perini F, Rossi G, Salmona M, Piccardo P, Ghetti B, Beavis RC, Bugiani O, Frangione B, Prelli F. A 7-kDa prion protein (PrP) fragment, an integral component of the PrP region required for infectivity, is the major amyloid protein in gerstmann-straussler-scheinker disease A117V. J Biol Chem 2001 FEB 23;276(8):6009-15.

29. Salmona M, Morbin M, Massignan T, Colombo L, Mazzoleni G, Capobianco R, Diomede L, Thaler F, Mollica L, Musco G, Kourie JJ, Bugiani O, Sharma D, Inouye H, Kirschner DA, Forloni G, Tagliavini F. Structural properties of gerstmann-straussler-scheinker disease amyloid protein. J Biol Chem 2003 NOV 28;278(48):48146-53.

30. Tattum MH, Cohen-Krausz S, Khalili-Shirazi A, Jackson GS, Orlova EV, Collinge J, Clarke AR, Saibil HR. Elongated oligomers assemble into mammalian PrP amyloid fibrils. J Mol Biol 2006 MAR 31;357(3):975-85.

31. Wille H, Prusiner SB. Ultrastructural studies on scrapie prion protein crystals obtained from reverse micellar solutions. Biophys J 1999 FEB;76(2):1048-62.

32. Leffers KW, Wille H, Stohr J, Junger E, Prusiner SB, Riesner D. Assembly of natural and recombinant prion protein into fibrils. Biol Chem 2005 JUN;386(6):569-80.

33. Wille H, Bian W, McDonald M, Kendall A, Colby DW, Bloch L, Ollesch J, Borovinskiy AL, Cohen FE, Prusiner SB, Stubbs G. Natural and synthetic prion structure from X-ray fiber diffraction. Proc Natl Acad Sci U S A 2009 OCT 6;106(40):16990-5.

34. Walsh P, Simonetti K, Sharpe S. Core structure of amyloid fibrils formed by residues 106-126 of the human prion protein. Structure 2009 MAR 11;17(3):417-26.

35. Lin N, Chao JC, Cheng H, Chou F, Chang C, Chen Y, Chang Y, Huang S, Chan JCC. Molecular structure of amyloid fibrils formed by residues 127 to 147 of the human prion protein. Chemistry-a European Journal 2010;16(18):5492-9.

36. Apostol MI, Wiltzius JJW, Sawaya MR, Cascio D, Eisenberg D. Atomic structures suggest determinants of transmission barriers in mammalian prion disease. Biochemistry (N Y) 2011 APR 5;50(13):2456-63.

37. Sawaya MR, Sambashivan S, Nelson R, Ivanova MI, Sievers SA, Apostol MI, Thompson MJ, Balbirnie M, Wiltzius JJW, McFarlane HT, Madsen AO, Riekel C, Eisenberg D. Atomic structures of amyloid cross-beta spines reveal varied steric zippers. Nature 2007 MAY 24;447(7143):453-7.

38. Wiltzius JJW, Landau M, Nelson R, Sawaya MR, Apostol MI, Goldschmidt L, Soriaga AB, Cascio D, Rajashankar K, Eisenberg D. Molecular mechanisms for protein-encoded inheritance. Nature Structural & Molecular Biology 2009 SEP;16(9):973-U98.

39. Bartz JC, Marsh RF, McKenzie DI, Aiken JM. The host range of chronic wasting disease is altered on passage in ferrets. Virology 1998 NOV 25;251(2):297-301.

40. Frank J, Radermacher M, Penczek P, Zhu J, Li Y, Ladjadj M, Leith A. SPIDER and WEB: Processing and visualization of images in 3D electron microscopy and related fields. J Struct Biol 1996 JAN-FEB;116(1):190-9.

41. Paolini AG, Mckenzie JS. Effects of lesions in the horizontal diagonal band nucleus on olfactory habituation in the rat. Neuroscience 1993 DEC;57(3):717-24.

42. Roman FS, Simonetto I, Soumireumourat B. Learning and memory of odor-reward association - selective impairment following horizontal diagonal band lesions. Behav Neurosci 1993 FEB;107(1):72-81.

43. Wilson DA, Fletcher ML, Sullivan RM. Acetylcholine and olfactory perceptual learning. Learning & Memory 2004 JAN-FEB;11(1):28-34.

Appendix 2.

Topology corrected sequence alignments: PLB and SLN share homology with SERCA binding sites proposed from cross-linking and structural studies.

Appendix 2. Topology corrected sequence alignments: PLB and SLN share homology with SERCA binding sites proposed from cross-linking and structural studies.

II-1. Introduction.

Membrane proteins can have complex topologies with multiple transmembrane helices and intervening extensions, loops and domains protruding from different sides of the membrane. SERCA provides an excellent example: the ten transmembrane helices are interspersed with three large cytoplasmic domains (see Introduction). The P-domain and N-domain of SERCA are formed by the cytoplasmic extension between TM4 and TM5, and the A-domain is formed by the cytoplasmic N-terminus (leading to TM1) and the cytoplasmic extension between TM2 and TM3.

The simplest example of different membrane topologies would single-pass Type I and Type II transmembrane proteins. Type I transmembrane proteins have an exterior (or luminal) N-terminus and a cytoplasmic C-terminus. Type II proteins are oppositely oriented in the membrane, with a cytoplasmic N-terminus and an exterior (or luminal) C-terminus. PLB and SLN are both examples of Type II proteins.

In Chapter 4, we proposed TM3 as an interaction site between PLB pentamers and SERCA based on cryo-electron microscopy of co-crystals[1, 2]. Our results suggested that PLB pentamers can remain anchored to SERCA via intra-membrane interactions that can withstand cytoplasmic disordering of PLB by phosphorylation at Ser[16]. In Chapter 5, we proposed that SLN pentamers also bound SERCA at TM3 in a similar position as PLB pentamers. The TM3 pentameric PLB and SLN binding site[1, 2] was distinct from the TM2, TM4, TM6, TM9 binding groove proposed for monomeric PLB based on cross-linking and modelling[3]. The TM2, TM4, TM6 and TM9 groove has also been proposed to bind SLN[4, 5] and to bind PLB and SLN simultaneously[4-7].

If we take into account the nature of the TM3 binding site, we can observe homology between SERCA, PLB and SLN. We made first mention of this in Chapter 4 (see Figure 4.8) where we indicated the homology observed between the C-terminal luminal region of the PLB transmembrane domain and the luminal end of TM3 of SERCA. Briefly, in the Discussion we mentioned that there is also homology between PLB and the TM2 region of SERCA, which is consistent with the proposed monomeric PLB binding groove. This appendix will cover these statements in more depth. We do not want to convey that homology between transmembrane proteins determines interaction, but in light of supporting data, the results are intriguing.

II-2. Results and Discussion.

II-2.1. Limitations of general linear protein sequence alignments with multi-pass transmembrane proteins.

A protein sequence alignment generally proceeds from the N-terminus of proteins and compares windows of residues, producing homology scores for the compared windows. The search windows then shift along the protein sequences from the N-terminus toward the C-terminus some distance, the newly positioned windows again compared and scored (Figure II.2.1a). This process is re-iterated for the entire sequences of the proteins and the best scored search window comparisons are reported for the input sequences.

We are going to consider how a sequence alignment would compare a single-pass transmembrane protein to a multiple pass transmembrane protein (Figure II.2.1). As an example we are going to consider SERCA, PLB and SLN which were the major focus of the chapters of this thesis. The special consideration would be that the two proteins are going to interact within a membrane. We consider this because we have proposed that the PLB pentamer can interact with SERCA in a functional manner whereby the PLB pentamer interacting with SERCA is linked to the inhibitory interaction with the PLB monomer. For this to occur, the PLB pentamer would need to dissociate. However, the PLB pentamer is considered to be very stable and does not dissociate in SDS-PAGE. There is evidence that SERCA can interact with oligomers of PLB and disrupt PLB oligomerization[8]. It seems reasonable that disruption of stable PLB homo-pentamers might involve a homologous region of SERCA that could compete for homo-oligomeric interfaces, such as the PLB Leu/Ile zipper (see Introduction). In such a way, a homologous region of SERCA would disrupt homo-oligomeric interactions between PLB monomers by mimicking the monomer itself. The reverse would also be possible.

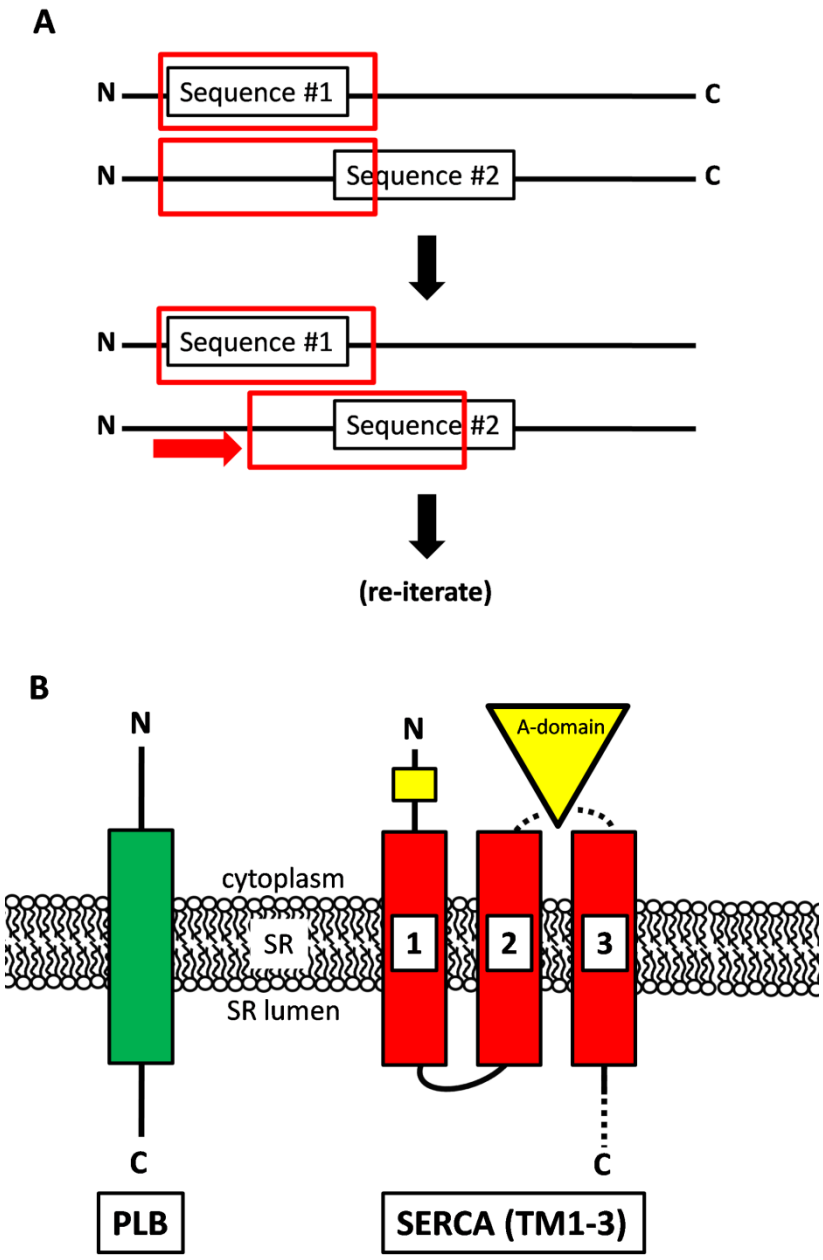

Figure II.1. Linear sequence homology alignments and membrane protein topology considerations. Panel A, general scheme for protein sequences alignments using a search window (red box). Two search windows are compared and scored based on search criteria. The search boxes are shifted by some distance (red arrow) in the subsequent search step. These steps are re-iterated until the sequences of both proteins have been covered by the search windows. The best score will be aligned and reported. **Panel B,** schematics are shown for PLB and the three N-terminal transmembrane helices of SERCA. If PLB and SERCA were aligned using a general scheme for protein sequence alignment, an alignment between PLB and TM2 of SERCA would not agree with their topologies.

We will focus primarily on the transmembrane domains, because Chapter 4 proposed the interaction between pentameric PLB and SERCA is anchored within the membrane and can accommodate disordering of the PLB cytoplasmic domain. We will also include PLB and SLN in the alignments because both proposed sites of interaction with SERCA have been proposed for both PLB and SLN.

If we input the sequences of SERCA, PLB and SLN we need to consider the topology of the proteins (Figure II.1). Given we are looking for potential inter-protein interactions, it is not logical to use a general alignment procedure, as described above, for SERCA, PLB and SLN. The primary reason is the sequence alignment proceeds in a linear manner from the N-terminus to the C-terminus. To visualize why this is so, see Figure II.1b. In the special case of transmembrane proteins, alignment between two linear regions of sequence that do not agree with the topology would not make logical sense. This would occur, as an example, between PLB and TM2 of SERCA. A stretch of amino acids that align between PLB and TM2 of SERCA would not agree with their membrane topology, because the N-terminus of PLB is cytoplasmic and the N-terminus region of TM2 is luminal (Figure II.1b).

Figure II.2a shows the results of an alignment where homology is observed between PLB and TM5 and TM6 of SERCA. The alignment in Figure II.2a would not support interaction because of conflicting topology between the aligned regions (Figure II.2b). All alignments are the output of ClustalW hosted on the European Bioinformatics Institute (EBI) website (www.ebi.ac.uk)[9, 10]. A sequence alignment of the transmembrane domains of PLB (PLB-tm; residues 34 to 52) and SLN (SLN-tm; residues 11 to 31) with the entire sequence of SERCA1a is shown in Figure II.2a. The alignment in Figure II.2a is the result from aligning the input PLB-tm, SLN-tm and SERCA1a sequences with the default user settings.

The transmembrane domain of PLB would only agree with the sequence alignment in Figure II.2a if the C-terminus of PLB re-inserted into the membrane in the opposite direction of the rest of the PLB transmembrane domain. This is possible, but the alignment itself has other limitations that we can address by changing the default search criteria. For example, there are large gaps between the clusters of aligned residues (Figure II.2). Although residues far away in sequence can be close in 3D space, there is a limit to the distance between sequential residues. If we also consider that PLB, SLN and TM5 are

helical in structure through the membrane, then the alignment gap between transmembrane regions 2 and 3 in Figure II.2 is too distant in sequence to interact simultaneously with another homologous transmembrane helix. To interact simultaneously, one of the transmembrane helices would have to lose its helical structure and there is no structural evidence for this in PLB, SLN or TM5 of SERCA. Even if helix unwinding occurred, the gap between transmembrane region 1 and 2 in Figure II.2 is even larger and would require more extensive re-arrangement to accommodate an interaction.

II-2.2. Special considerations for interacting, homologous transmembrane helices in protein sequence alignments.

Based on the results of our initial (default criteria) alignment (Figure II.2a), we can address our concerns with a single changed criterion and re-align the sequences of SERCA, PLB and SLN. The new criterion will address the gaps observed between the clusters of aligned residues that would have to unwind the respective transmembrane helix to accommodate interaction. We can limit gaps in the sequence alignment by increasing the gap extension penalty (the default setting is 0.2 for multiple sequence alignments). Since we are particularly invested in intra-membrane interactions between two transmembrane helices, we increased the gap extension penalty of the alignment of PLB-tm, SLN-tm, and SERCA1a. A gap extension penalty of 0.5 produced similar gaps as the 0.2 default setting. A gap penalty of 1.0 reduced the observed gaps to a maximum of 2 sequential residues in most of the alignments. Figure II.3 shows the resulting alignment of PLB-tm, SLN-tm and SERCA1a with the increased gap extension penalty.

Our best scored alignment with the increased gap extension penalty is between PLB-tm, SLN-tm and TM1 of SERCA. Indeed, the ends of the transmembrane helices align very well, both in terms of their respective topology and for maintaining transmembrane helical structures (Figure II.3). However, TM1 of SERCA has not been implicated otherwise in interaction with PLB and SLN. To look for other homologous regions, that have a lower score than the aligned regions in Figure II.3, we next removed TM1 of SERCA1a from the alignment. The removal of TM1 was performed because ClustalW reports only one best fit. If we remove the best fit region from the input sequence of the larger protein, we can get the second best fit by re-aligning the altered sequences using ClustalW.

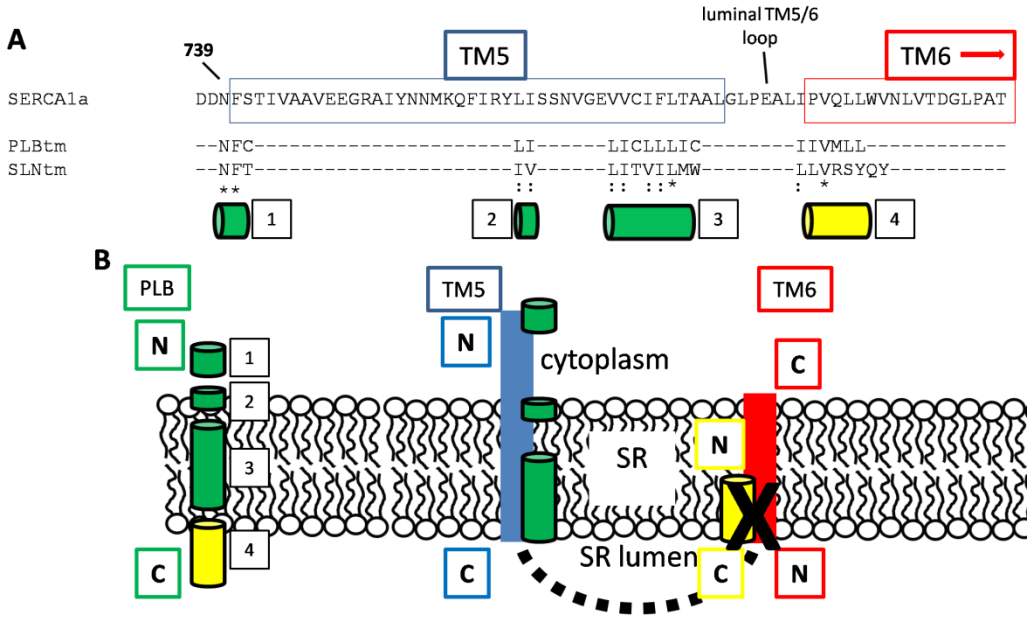

Figure II.2. An example of a sequence alignment between SERCA, PLB and SLN that would not be compatible with inter-protein interaction between two transmembrane helices. Sequence alignments of the transmembrane domains of PLB (PLB-tm; residues 34 to 52) and SLN (SLN-tm; residues 11 to 31) with the entire sequence of SERCA1a. Alignment was performed using ClustalW at the European Bioinformatics Institute (EBI) website (www.ebi.ac.uk)[9, 10]. **Panel A,** alignment between PLB-tm, SLN-tm and SERCA1a. Asterisks (*) indicate fully conserved residues and colons (:) indicate strong conservation between residues. **Panel B,** schematic interpretation of the PLB-tm and SERCA aligned regions based on topology. The interaction between PLB regions 1 to 3 (*green cylinders*) with TM5 (*blue rectangle*) agree with the topology of the aligned regions. However, the interaction between PLB transmembrane region 4 (*yellow cylinder*) and TM6 of SERCA (*red rectangle*) would not be possible in the general topology of PLB (shown by the "X" between PLB region 4 and TM6). The alignment would agree with an interaction if the C-terminus of PLB re-inserted in an opposite direction as the rest of it transmembrane helix (see section II-2.1 of the text for discussion). The gaps in the alignment between PLB regions 1 and 2, and between PLB regions 2 and 3, would require disruption of the helical structure of PLB, SLN or TM5. There is no structural evidence for such extensive unwinding.

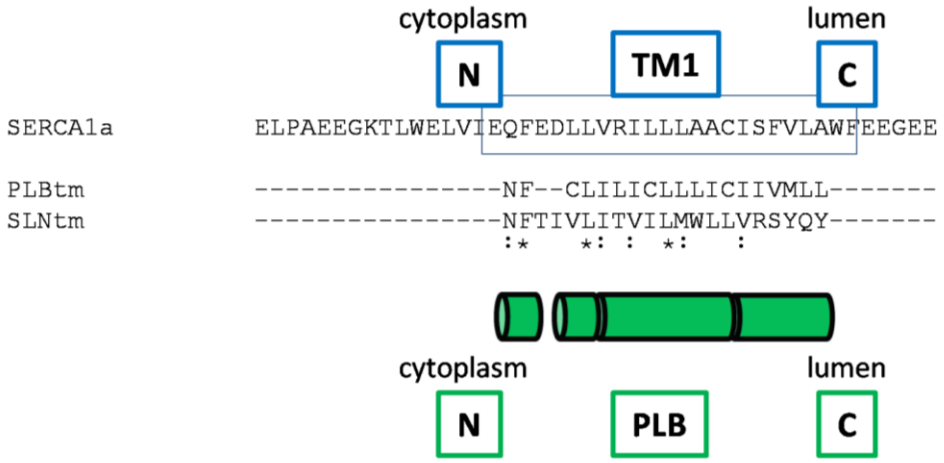

Figure II.3. An example of a sequence alignment between SERCA, PLB and SLN compatible with inter-protein interaction between two transmembrane helices. The sequence alignment was performed as described in Figure II.2 (also see section II-3 of the text) with the gap extension penalty increased to 1.0 from the default of 0.2. The aligned regions between PLB-tm, SLN-tm and SERCA1a are now compatible with interaction in terms of topology and transmembrane helical structures.

The second best score, following the removal of TM1, is shown in Figure II.4a. The aligned regions are primarily between PLB-tm, SLN-tm and TM9 of SERCA1a. Although TM9 has also been implicated in the binding of PLB and SLN (in the TM2, TM4, TM6 and TM9 groove), the topology is not a good fit with the aligned regions. More specifically, the cytoplasmic end of PLB-tm aligns with the luminal end of TM9. Although the directions of the aligning termini are in agreement, the topology is not. To continue, we next removed the TM9 and TM9/10 luminal loop regions. The third best score, following removal of TM1 and TM9, is shown in Figure II.4b. The aligned regions are consistent with the proposed interaction site for PLB and SLN pentamers centered on TM3 of SERCA based on co-crystals. The ends of the transmembrane helices align very well, both in terms of their respective topology and for maintaining transmembrane helical structures (Figure II.4b).

II-2.3. Correcting the topology of transmembrane proteins for multiple sequence alignments: SERCA, PLB and SLN as an example.

Our third alignment provided our first good fit between homologous regions and proposed interaction sites between PLB, SLN and SERCA1a. We did observe homology between PLB and SLN with the TM2, TM4, TM6 and TM9 groove, but the topology was not a good fit for interaction between transmembrane helices. To this point, we have disregarded alignments based on topology of PLB, SLN and SERCA1a. However, we can address the limitations of linear sequence alignments in two simple ways.

The first would be to create a SERCA1a sequence that reads linearly in a manner that is coherent to how PLB or SLN could interact with SERCA in the membrane. For example, the sequence for TM2 would be reversed, such that a positive alignment would necessarily agree with topology. This would be repeated for the other transmembrane helices with a similar topology as TM2, including TM4, TM6, TM8 and TM10. With ten transmembrane helices in SERCA this becomes somewhat difficult, however, in determining the alignment of intervening loops and extensions between transmembrane helices. Since we are fortunate to be aligning relatively short sequences (PLB-tm and SLN-tm) with SERCA1a, we can choose a second approach. We can bridge the problem by simply reversing the PLB-tm and SLN-tm sequences, and performing an alignment of the reversed sequences with SERCA1a (Figure II.5).

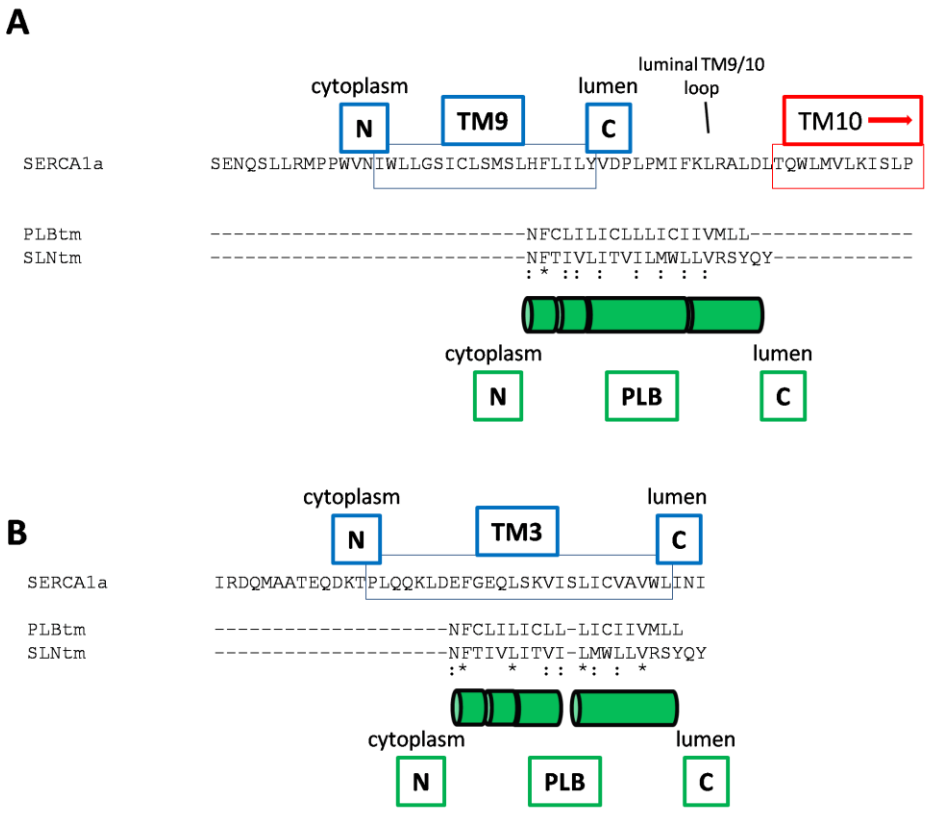

Figure II.4. Examples of sequence alignments between SERCA, PLB and SLN compatible with identified PLB-binding sites. The sequence alignment was performed as described in Figure II.2 (also see section II-3 of the text) with the gap extension penalty increased to 1.0 from the default of 0.2. **Panel A,** the aligned regions are compatible with transmembrane helical structure, but not a good fit in terms of topology. **Panel B,** the aligned regions are compatible with interaction in terms of topology and transmembrane helical structures. This sequence alignment was reported in Chapter 4 and is consistent with the proposed interaction site for pentameric PLB with TM3 of SERCA.

Figure II.5 uses this latter approach and the results align PLB-tm (backwards), SLN-tm (backwards) and TM2 of SERCA1a (Figure II.5a). The aligned regions are consistent with the proposed TM2, TM4, TM6 and TM9 interaction site for PLB monomers based on cross-linking and modelling[3]. In fact, the aligned regions place Val^{49} of PLB close to Val^{89} of SERCA, which was a strong reported cross-link[3]. The ends of the transmembrane helices align very well, both in terms of their respective topology and for maintaining transmembrane helical structures (Figure II.5a). If we continue a similar approach as before, removing the top scored regions and re-aligning the adjusted sequences, we can observe homology between PLB-tm (backwards), SLN-tm (backwards) and TM6 of SERCA1a (Figure II.5b). The ends of the transmembrane helices align very well in terms of their respective topology and a good fit is made for maintaining transmembrane helical structures (Figure II.5b). Again, this would be consistent with the proposed TM2, TM4, TM6 and TM9 binding groove for the PLB monomer[3]. The alignment with TM6 of SERCA represents the sixth best scored alignment using the reverse PLB-tm and SLN-tm sequences. The second and fourth best scores were disregarded because of topology conflicts (the aligned regions were TM1 and TM3, which were the first and third best scored alignments using the forward PLB-tm and SLN-tm sequences – see Figures II.3 and II.4). The third best scored alignment involved TM10 of SERCA, which could also interact with pentameric PLB in our co-crystals[2].

II-2.4. TM1 of SERCA as a region of homology with the transmembrane domains of PLB and SLN.

It is interesting that TM1 of SERCA was identified as the best region of homology with the forward sequences of PLB-tm and SLN-tm (Figure II.3). We have proposed that binding of the PLB pentamer, centered on TM3, could deliver PLB to its monomeric binding site in the TM2, TM4, TM6 and TM9 groove (see Chapter 4). In the Discussion, we highlighted the movement of TM3 towards the face of SERCA containing the monomer-binding groove in E1 states of SERCA with Ca^{2+} bound (see Figure 6.9 in Discussion). However, to move the shortest distance between the proposed TM3 and the TM2, TM4, TM6 and TM9 binding sites, PLB would have to navigate around TM1. In the simplest delivery mechanism, SERCA would begin with a PLB pentamer bound to TM3. By mimicking each other, the homology between the PLB transmembrane domain and TM3 of SERCA (Figure II.4b) would promote dissociation of a PLB monomer from

a PLB pentamer. The dissociated monomer would then interact with the homologous TM1 region (Figure II.3) and, subsequently, be delivered to the TM2, TM4, TM6 and TM9 binding groove, where PLB shares homology with TM2 (Figure II.5a). In this groove, bound PLB monomers would inhibit SERCA. The monomeric PLB would be squeezed out of the groove when Ca^{2+} binds, as proposed[3], and a reverse sequence of events could remove PLB and return it to the PLB oligomer bound to TM3.

We aligned for homology between PLB and SERCA1a using a different alignment procedure. LALIGN[12] is an alignment program for binary sequences (hosted at the EMBnet website - www.ch.embnet.org/). PLB-tm and PLB-tm(backwards) served as control sequences aligned with SERCA. The stringency of LALIGN was set to BLOSUM 35 (search matrix)[13], otherwise the settings were the given default values. Without showing more alignments, the overall summary of the LALIGN results are given with those from ClustalW in Table II.1. Both of the discussed proposed PLB-binding sites TM2 and TM3 are again aligned with excellent fits for topology and membrane helix interactions. The rankings of the alignments differ between ClustalW and LALIGN, but TM2 and TM3 alignments are found among the highest ranks using both alignment programs.

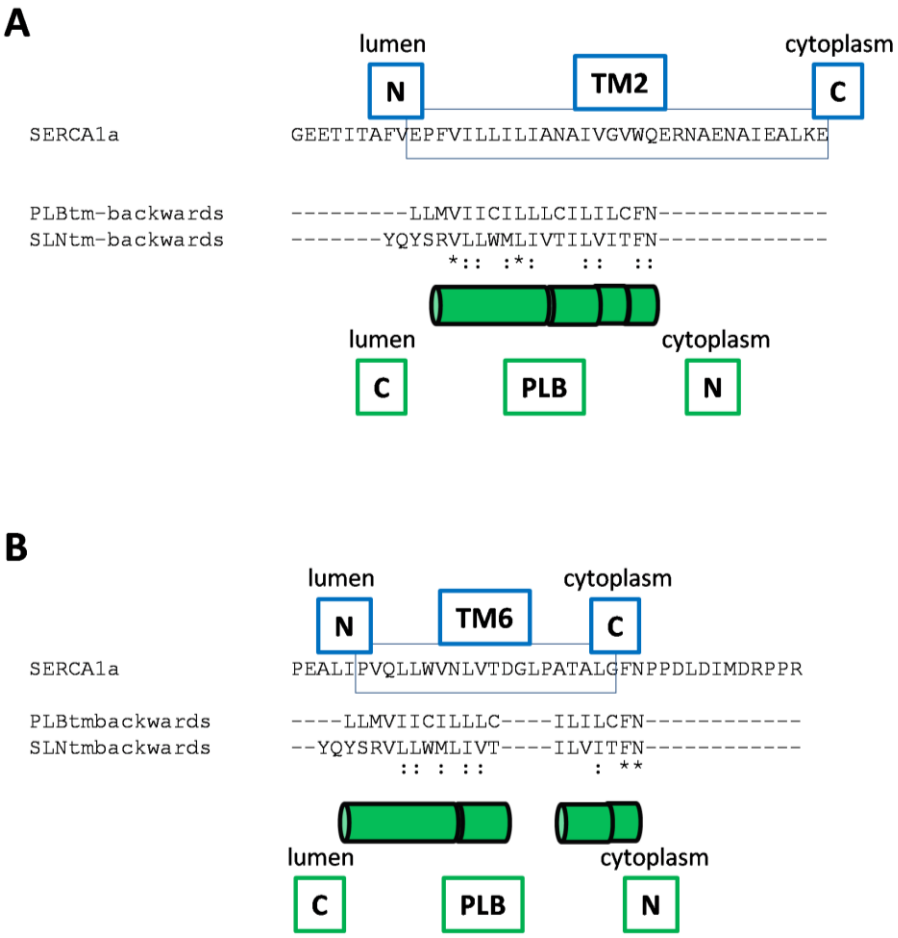

Figure II.5. Examples of topology corrected sequence alignments between SERCA, PLB and SLN compatible with identified PLB-binding sites. The sequence alignment was performed as described in Figure II.2 (also see section II-3 of the text) with the gap extension penalty increased to 1.0 from the default of 0.2. The reverse sequences of PLB-tm and SLN-tm were aligned with SERCA1a. Both alignments are consistent with the proposed TM2, TM4, TM6 and TM9 binding groove for the PLB monomer[3]. **Panel A,** the aligned regions are compatible with interaction in terms of topology and transmembrane helical structures. **Panel B,** the aligned regions are compatible with interaction in terms of topology and a good fit for maintaining transmembrane helical structures.

Table II.1. Comparison of ClustalW and LALIGN output for SERCA1a and PLB with topology correction.

	Description	Proposed PLB-binding site (method)	Topology-correct	ClustalW rank	LALIGN rank
PLB-tm [SERCA1a]					
	TM1	N	**Y**	1	2
	TM3	Y (co-crystals)	**Y**	3	1
	TM9	Y (cross-link/model)	**N**	2	-
PLB-tm (backwards) [SERCA1a]					
	TM2	Y (cross-link/model)	**Y**	1	5
	TM1	N	**N**	2	3
	TM3	Y (co-crystals)	**N**	3	2
	TM10	Y (co-crystals)	**Y**	4	-
	TM9	Y (cross-link/ model)	**N**	5	-
	TM6	Y (cross-link/ model)	**Y**	6	-
	TM5	N	**N**	-	1

II-3. Materials and Methods.

All sequence alignments were performed using ClustalW version 2 at the European Bioinformatics Institute website (www.ebi.ac.uk)[9, 10]. The sequence alignments were performed with the default settings unless otherwise described (only the gap extension penalty was changed). The TM regions of SERCA were defined by the residues given in Kuhlbrandt 2004[11].

II-4. References.

1. Glaves JP, Trieber CA, Ceholski DK, Stokes DL, Young HS. Phosphorylation and mutation of phospholamban alter physical interactions with the sarcoplasmic reticulum calcium pump. J Mol Biol 2011 JAN 21;405(3):707-23.

2. Stokes DL, Pomfret AJ, Rice WJ, Glaves JP, Young HS. Interactions between Ca2+-ATPase and the pentameric form of phospholamban in two-dimensional co-crystals. Biophys J 2006 JUN;90(11):4213-23.

3. Toyoshima C, Asahi M, Sugita Y, Khanna R, Tsuda T, MacLennan DH. Modeling of the inhibitory interaction of phospholamban with the Ca2+ ATPase. Proc Natl Acad Sci U S A 2003 JAN 21;100(2):467-72.

4. Asahi M, Sugita Y, Kurzydlowski K, De Leon S, Tada M, Toyoshima C, MacLennan DH. Sarcolipin regulates sarco(endo)plasmic reticulurn Ca2+-ATPase (SERCA) by binding to transmembrane helices alone or in association with phospholamban. Proc Natl Acad Sci U S A 2003 APR 29;100(9):5040-5.

5. Buffy JJ, Buck-Koehntop BA, Porcelli F, Traaseth NJ, Thomas DD, Veglia G. Defining the intramembrane binding mechanism of sarcolipin to calcium ATPase using solution NMR spectroscopy. J Mol Biol 2006 APR 28;358(2):420-9.

6. Morita T, Hussain D, Asahi M, Tsuda T, Kurzydlowski K, Toyoshima C, MacLennan DH. Interaction sites among phospholamban, sarcolipin, and the sarco(endo)plasmic reticulum Ca2+-ATPase. Biochem Biophys Res Commun 2008 APR 25;369(1):188-94.

7. MacLennan D, Asahi M, Tupling A. The regulation of SERCA-type pumps by phospholamban and sarcolipin. Na,k-Atpase and Related Cation Pumps: Structure, Function, and Regulatory Mechanisms 2003;986:472-80.

8. Thomas D, Reddy L, Karim C, Li M, Cornea R, Autry J, Jones L, Stamm J. Direct spectroscopic detection of molecular dynamics and interactions of the calcium pump and phospholamban. Cardiac Sarcoplasmic Reticulum Function and Regulation of Contractility 1998;853:186-94.

9. Larkin MA, Blackshields G, Brown NP, Chenna R, McGettigan PA, McWilliam H, Valentin F, Wallace IM, Wilm A, Lopez R, Thompson JD, Gibson TJ, Higgins DG. Clustal W and clustal X version 2.0 RID B-9464-2009 RID D-3997-2009. Bioinformatics 2007 NOV 1;23(21):2947-8.

10. Goujon M, McWilliam H, Li W, Valentin F, Squizzato S, Paern J, Lopez R. A new bioinformatics analysis tools framework at EMBL-EBI. Nucleic Acids Res 2010 JUL;38:W695-9.

11. Kuhlbrandt W. Biology, structure and mechanism of P-type ATPases. Nature Reviews Molecular Cell Biology 2004 APR;5(4):282-95.

12. Huang, X.Q. and Miller, W. A time-efficient, linear-space local similarity algorithm. Advances in Applied Mathematics 1991 SEP; 12(3) 337-357.

13. Henikoff, S. and Henikoff, J.G. Amino Acid Substitution Matrices from Protein Blocks. PNAS 1992 89(22): 10915–10919.